

Novel Chemosensors for Biologically Important Analytes

THÈSE N° 6792 (2015)

PRÉSENTÉE LE 25 SEPTEMBRE 2015

À LA FACULTÉ DES SCIENCES DE BASE

LABORATOIRE DE CHIMIE SUPRAMOLÉCULAIRE

PROGRAMME DOCTORAL EN CHIMIE ET GÉNIE CHIMIQUE

ÉCOLE POLYTECHNIQUE FÉDÉRALE DE LAUSANNE

POUR L'OBTENTION DU GRADE DE DOCTEUR ÈS SCIENCES

PAR

Ziya KÖSTERELI

acceptée sur proposition du jury:

Dr A.-S. Chauvin, présidente du jury

Prof. K. Severin, directeur de thèse

Prof. A. D. Cort, rapporteuse

Dr D. C. Magri, rapporteur

Prof. F. Stellacci, rapporteur



ÉCOLE POLYTECHNIQUE
FÉDÉRALE DE LAUSANNE

Suisse
2015

ACKNOWLEDGEMENT

Fisrt of all, I would like to thank my supervisor, Profesor Kay Severin for giving me a PhD position in his group. He always motivated and encouraged me in project discussions. It would not have been possible to do this work without his guidance, and support. It was very nice to work under his supervision.

I would like to thank my jury members (Prof. Francesco Stellacci and Docteur Anne-Sophie Chauvin from EPFL, Prof. Antonella Dalla Cort from Università di Roma La Sapienza, and Dr. David C. Magri from University of Malta) for their time and effort to read and evaluate my thesis. Furthermore, I also want to acknowledge Mathew Wise and Bilal Ozen for proof reading of my thesis.

Special thanks to Anne Lene Odegaard and Christina Zamanos-Empreman for helping all administrative staff, Euro Solari for helping and finding solutions to all technical problems in the lab and Rosario Scopelliti for X-ray analysis. I thank to Dr. Pascal Mieville for his support in NMR and magasin staffs: Annelise Carrupt, Gladys Pasche, and Benjamin Kronenberg for their help.

I would like to express my gratitude to our former and current group members Erin, Burcak, Matt, Bo, Benan, Kai, Loic, Leonard, Giacomo, Gregor, Suzanne, Florian, Clement, Justus, Alex T, Alex D, Kevin, Abdusalom, Marcus, Nicolas, Mathieu, Mirela, Albert, Julie, Bassam for their friendship , and great ambiance in the laboratory. It was wonderful to work with them. Special thanks to Stéphanie for tea breaks and French translation and Nicolas for helping me in all electronic-related problems. Thank you very much. I am particularly thankful to Marie Curie actions for funding my PhD studies under the name of ITN ReAd Network. I would like to thank all PIs in the network and all fellows: Sergio, Rakesh, Giulia, Artem, Ivica, Yousef, Elena, Julia, Leonardo and Elnaz. We had great time in the meetings.

I would like to thank my friends outside of EPFL for their valuable friendship. I spent great time with them in different organizations.

Finally, I want to express my gratitude to my wife for her patience and support during my PhD. She was very helpful and it would not have been possible without her support. I also

want to thank my family members for their love, support, and understanding. I owe them a lot.

ABSTRACT

In this work, fluorescent-based chemosensors for the detection of important analytes in aqueous solution are described. The sensors are based on different detection concepts, including analyte-induced aggregation/de-aggregation, pattern-based sensing and micelle-based sensing.

In chapter 2, we present an analyte-induced aggregation-type chemosensor for the sensing of spermine. A charge-frustrated amphiphile composed of a highly fluorescent pyrene-1,3,6-trisulfonate head group and an eicosane side chain was used as a fluorescence chemosensor. Analyte-induced aggregation of the dye upon addition of spermine results in pronounced fluorescence quenching. The sensor enables the detection of spermine down to the nanomolar concentration range with good selectivity over closely related biogenic amines such as spermidine.

In chapter 3, we describe a conceptually new ‘one-cuvette’ sensing system for the pattern-based analysis of seven aminoglycoside antibiotics. The antibiotics include amikacin, apramycin, gentamicin, kanamycin A and B, neomycin, and paromomycin. A mixture of two amphiphiles with fluorescent head groups was used as a sensing ensemble. In buffered aqueous solution, the amphiphiles form a dynamic mixture of micellar aggregates. In the presence of aminoglycosides, the relative amount and the composition of the micelles is modified. The re-equilibration of the system is analyte-specific, and characteristic fluorescence spectra are obtained for different aminoglycosides. Accurate differentiation in the low micromolar concentration range is achieved by a principal component analysis of the spectral data. Also, the sensing system allows the differentiation of pure aminoglycosides from their mixtures.

In chapter 4, a fluorescent chemosensor based on analyte-induced aggregation/de-aggregation is described for the sensing of Al^{3+} and citric acid. An amphiphilic dye with a disulfonated BODIPY head group and a heptadecane side chain was used as an Al^{3+} sensor. In buffered aqueous solution, the amphiphile can form aggregates and the aggregation of the dye is associated with a strong quenching of its fluorescence. Al^{3+} promotes aggregation, whereas other metal ions have a much smaller effect, in particular when histidine is added as masking agent. The Al^{3+} -induced aggregation is used to sense Al^{3+} in the low micromolar

concentration range with high selectivity. Furthermore, we demonstrate that the non-fluorescent dye- Al^{3+} complex can be used as a sensing ensemble for the detection of citric acid. The assay is able to quantify the citric acid content of commercial beverages such as energy drinks.

A simple micelle-based assay for the fluorescence sensing of vitamin K_1 is described in the following chapter 5. The assay enables the detection of vitamin K_1 in the low micromolar concentration range. As a sensing ensemble, a mixture of the surfactant triton X-100 and 1-aminopyrene in buffered aqueous solution is employed. Vitamin K_1 co-localizes with the fluorescent aminopyrene dye in the micelle, resulting in fluorescence attenuation by dynamic quenching. The assay displays good selectivity and can be used to determine the concentration of vitamin K_1 in a commercial preparation.

In chapter 6, a fluorescent-based sensor array for the optical analysis of purine derivatives is described. The array is composed of four polysulfonated fluorescent dyes, all of which can bind purines via π -stacking interactions. The complexation of the analytes results in partial quenching of the fluorescence. The fluorescence response of the four dyes provides a characteristic signal pattern, enabling the identification of thirteen purine derivatives including caffeine, theophylline, theobromine, purine, hypoxanthine, paraxanthine, 8-chlorotheophylline, 6-mercaptopurine, cladribine and penciclovir at low millimolar concentration. Furthermore, it is possible to use the array for obtaining information about the quantity and the purity of samples. This point was demonstrated by the analysis of samples containing different amounts of caffeine and/or theophylline.

Key Words

Chemosensors, Fluorescent Chemosensors, Analyte-Induced Aggregation/De-Aggregation, Pattern-Based Sensing, Sensor Array, Micelle-Based sensing, Surfactants, Fluorescent Amphiphiles, Spermine, Biogenic Amines, Aminoglycosides, Aluminum, Citric Acid, Purine Alkaloids, Caffeine, Fluorescence, Supramolecular Chemistry

RÉSUMÉ

Dans ce travail, des senseurs chimiques basés sur la fluorescence sont décrits pour la détection d'importants analytes dans des solutions aqueuses. Les senseurs sont basés sur différents concepts de détection, comprenant l'agrégation / de-agrégation induite par l'analyte, la détection basée sur différents modèles et la détection à base de micelles.

Dans le chapitre 2, nous présenterons un senseur chimique basé sur l'agrégation induite par l'analyte pour la détection de spermine. Un amphiphile à charges frustré composé d'une tête pyrène-1,3,6-trisulfonate fortement fluorescente et une chaîne latérale eicosane a été utilisé comme senseur chimique fluorescent. L'agrégation du colorant, induite par l'addition de l'analyte, la spermine, suscite une diminution de la fluorescence. Le capteur permet la détection de spermine jusqu'à la plage de concentration nanomolaire avec une bonne sélectivité sur les amines biogènes étroitement liées, tels que la spermidine.

Dans le chapitre 3, nous décrivons conceptuellement un nouveau système de détection appelée 'one-cuvette' pour l'analyse de sept aminosides antibiotiques. Les antibiotiques comprennent l'amikacine, l'apramycine, la gentamicine, la kanamycine A et B, la néomycine, et paromomycine. Un mélange de deux amphiphiles avec des têtes fluorescentes a été utilisé comme un ensemble de détection. Dans la solution tamponnée, les amphiphiles forment un mélange dynamique d'agrégats micellaires. En présence d'aminoglycosides, la quantité relative et la composition de micelles est modifiée. La remise à l'équilibre du système est spécifique à l'analyte, et les spectres de fluorescences caractéristiques sont obtenus pour différents aminoglycosides. La séparation précise des analytes dans la plage de concentration micromolaire peut être effectuée par une analyse des données du spectre. En outre, le système de détection permet la différenciation des aminoglycosides purs à partir de leurs mélanges.

Dans le chapitre 4, un senseur chimique fluorescent, sur la base de l'agrégation ou de la de-agrégation induite par l'analyte, est décrit pour la détection de Al^{3+} et de l'acide citrique dans la solution tampon. Un colorant amphiphile avec une tête de BODIPY disulfonée et une chaîne latérale heptadécane a été utilisé en tant que senseur Al^{3+} . Dans une solution tampon, l'amphiphile peut former des agrégats et l'agrégation du colorant est associée à une forte diminution de sa fluorescence. Al^{3+} favorise l'agrégation, alors que d'autres ions métalliques ont un effet beaucoup plus faible, en particulier lorsque l'histidine est ajoutée comme agent de masquage. L'agrégation, induite par Al^{3+} , est utilisée pour détecter Al^{3+} dans la concentration

micromolaire avec une grande sélectivité. De plus, nous démontrons que le complexe non-fluorescent, formé par le colorant et Al^{3+} , peut être utilisé comme un senseur pour la détection de l'acide citrique. Le senseur est capable de quantifier la teneur en acide citrique de boissons commerciales telles que les boissons énergisantes.

Un simple senseur, basé sur des micelles, est exploité pour la détection de la fluorescence de la vitamine K1 dans le chapitre 5. Le senseur permet la détection de la vitamine K1 dans la concentration micromolaire. Comme ensemble de détection, un mélange de l'agent tensioactif Triton X-100 et d'un aminopyrène en solution aqueuse tamponnée est utilisé. La vitamine K1 et le colorant fluorescent pyrène coexistent dans la micelle, ce qui entraîne une atténuation de la fluorescence par disparition dynamique. Le senseur présente une bonne sélectivité, et peut être utilisée pour déterminer la concentration de vitamine K₁ dans une préparation commerciale.

Dans le chapitre 6, une série de senseurs basés sur la fluorescence est décrit afin d'analyser optiquement des dérivés de purine. Le réseau est composé de quatre colorants fluorescents. Ces derniers peuvent se lier avec les purines via des interactions d'empilement π . La complexation des analytes se traduit par une baisse partielle de la fluorescence. La réponse des quatre colorants fournit un signal caractéristique, ce qui permet l'identification de treize dérivés de purine à faible concentration millimolaire, y compris la caféine, la théophylline, la théobromine, la purine, l'hypoxanthine, la paraxanthine, la 8-chlorothéophylline, 6-mercaptopurine, la cladribine et la penciclovir. En outre, il est possible d'utiliser le senseur pour obtenir des informations sur la quantité et la pureté des échantillons. Ce point a été démontré par l'analyse d'échantillons contenant différentes quantités de caféine et / ou de théophylline.

Mots Clés

Senseurs Chimiques, Senseurs Chimiques Fluorescents, Agrégation / De-Agrégation Induite par un Analyte, Détection par Motifs, Détection Basée sur des Micelles, Tensioactifs, Amphiphiles Fluorescents, Spermine, Amines Biogènes, Aminoglycosides, Aluminium, Acide Citrique, Purine Alcaloïdes, Fluorescence, Chimie Supramoléculaire

Table of Contents

1	General Introduction.....	1
1.1	Fluorescent Chemosensors	3
1.2	Chemosensors Based on Analyte-Induced Aggregation	9
1.3	Chemosensors Based on Analyte-Induced De-Aggregation.....	15
1.4	Micelle-Based Chemosensors.....	20
1.5	Pattern-Based Sensing Systems	23
1.5.1	Pattern Recognition Tools	24
1.5.2	Sensor Arrays	25
1.5.3	Single Sensing Systems.....	29
2	Fluorescence Sensing of Spermine with a Frustrated Amphiphile.....	33
2.1	Introduction.....	35
2.2	Results and Discussion	37
2.3	Conclusion	45
2.4	Experimental.....	46
3	Pattern-Based Sensing of Aminoglycosides with Fluorescent Amphiphiles	51
3.1	Introduction.....	53
3.2	Results and Discussion	55
3.3	Conclusion	68
3.4	Experimental.....	69
4	Selective Detection of Al ³⁺ and Citric Acid with a Fluorescent Amphiphile	75
4.1	Introduction.....	77
4.2	Results and Discussion	79
4.3	Conclusion	89

4.4	Experimental.....	90
5	Fluorescence Sensing of Vitamin K ₁ using a Simple Micelle-Based Assay..	95
5.1	Introduction.....	97
5.2	Results and Discussion	97
5.3	Conclusion	107
5.4	Experimental.....	107
6	Array-Based Sensing of Purine Derivatives with Fluorescent Dyes.....	111
6.1	Introduction.....	113
6.2	Results and Discussion	115
6.3	Conclusion	122
6.4	Experimental.....	123
7	General Conclusion	125
8	Annex	129
8.1	UV and Fluorescence Spectra.....	129
8.2	LDA Plots	143
8.3	TEM and DLS images	146
8.4	NMR Data.....	148
8.5	Crystallographic data	158
	References	161
	Curriculum Vitae	177

LIST of ABBREVIATIONS AND SYMBOLS

A	absorbance
A	acceptor
AIA	analyte-induced aggregation
ANS	8-Anilinonaphthalene-1-sulfonic acid
AP	1-aminopyrene
APTS	trisodium 8-aminopyrene-1,3,6-trisulfonate
ATP	adenosine triphosphate
a.u.	arbitrary units
BODIPY	4,4-difluoro-4-bora-3a,4a-diaza-s-indacene (boron-dipyrromethene)
°C	degree Celcius
calcd	calculated
CBT	2-cyano-6-methoxybenzothiazole
CHES	<i>N</i> -Cyclohexyl-2-aminoethanesulfonic acid
cmc	critical micelle concentration
CNS	central nervous system
CR	cryptand
CTAB	hexadecyl trimethyl ammonium bromide
CV	cyclic voltammetry
d	doublet
D	donor
δ	chemical shift
DCL	dynamic combinatorial chemistry
dd	doublet of doublets
DIPEA	<i>N,N</i> -Diisopropylethylamine
DLS	dynamic light scattering
DMF	<i>N,N</i> -dimethylformamide
DMSO	dimethyl sulfoxide

EET	electronic energy transfer
<i>e.g.</i>	exempli gratia, for example
E. I.	emission intensity
ems	emission
EtOH	ethanol
ESI	electrospray ionization
<i>et al.</i>	et alia, and others
E. Q.	emission quenching
exc	excitation
FRET	fluorescence resonance energy transfer
G	gentamicin
g	gram
GC	gas chromatography
GFP	green fluorescent protein
h	hour
HCA	hierarchical cluster analysis
HCl	hydrochloric acid
HEPES	4-(2-hydroxyethyl)piperazine-1-ethanesulfonic acid
HOMO	highest-occupied molecular orbital
HPLC	high performance liquid chromatography
HPTS	8-hydroxy-1,3,6-pyrenetrisulfonic acid
Hz	Hertz (s ⁻¹)
ICT	internal charge transfer
IDLH	immediately dangerous to life or health
IPA	isopropyl alcohol
<i>i.e.</i>	id est, that is
IDA	indicator displacement assay
IUPAC	the international union of pure and applied chemistry
<i>J</i>	coupling constant
K _a	association constant
KB	kanamycin B
λ	frequency (nm)

LC-MS	liquid chromatography-mass spectrometry
LDA	linear discriminant analysis
LUMO	lowest-occupied molecular orbital
m	multiplet
M	molar ($\text{mol} \cdot \text{L}^{-1}$)
m/z	mass-to-charge ratio
Me	methyl
mg	milligram
MHz	megahertz
min	minutes
mL	milliliter
mm	millimeter
mM	millimolar ($\text{mmol} \cdot \text{L}^{-1}$)
mmol	millimole
MOPS	3-(<i>N</i> -morpholino)propanesulfonic acid
MPTS	8-methoxypyrene-1,3,6-trisulfonate
MS	mass spectrometry
μm	micrometer
μM	micromolar ($\mu\text{mol} \cdot \text{L}^{-1}$)
μmol	micromole
NaCl	sodium chloride
NaOH	sodium hydroxide
NH_4OH	ammonium hydroxide
nm	nanometer
NMR	nuclear magnetic resonance
NP	nanoparticle
P	paromomycin
p	pentet
PCA	principal component analysis
PCT	photo-induced charge transfer
PD	podand
PET	photo-induced electron transfer

ppb	parts per billion
ppm	parts per million
PTFE	polytetrafluoroethylene
PTS	pyrene-1,3,6,8-tetrasulfonate
ref	reference
s	singlet
SDS	sodium dodecyl sulfate
SQ	squaraine
t	triplet
TEM	transmission electron microscopy
TDS	disodium 3,4:3',4'-bibenzo[<i>b</i>]thiophene-2,2'-disulfonate
TFA	trifluoroacetic acid
THF	tetrahydrofuran
TIC	toxic industrial chemical
Triton X-100	polyoxyethylene octyl phenyl ether
Tween 20	polyoxyethylene (20) sorbitan monolaurate
UV	ultraviolet
UV-vis	UV-visible
vol	volume
vs.	versus, against
wt	weight
2D	two dimensional

Note: usual abbreviations are used for amino acids

1 General Introduction

In the opening chapter, a general introduction about fluorescent-based chemosensors is given, followed by a description of different sensing approaches. Selected literature examples are discussed for each type.

1.1 Fluorescent Chemosensors

There are many definitions of a chemosensor in the literature.¹⁻³ Simply, it can be defined as a chemical species that can report the presence of an analyte with a measurable change. A more informative and approved IUPAC definition is ‘a chemical sensor is a device that transforms chemical information, ranging from the concentration of a specific sample component to total composition analysis, into an analytically useful signal’.⁴ From this definition, it is clear that a chemosensor should ideally be selective for one analyte molecule over other potential analyte molecules and also it should allow the concentration of the analyte to be monitored.¹

Over the last decades, sensor designs have been reported in the literature, ranging from simple receptor-based systems to complex multi-fluorophore sensing ensembles.^{1-2, 5-7} However, in general, chemosensors can be divided into two major classes; electrochemical sensors and optical sensors. In electrochemical sensors, a redox active unit is attached to the receptor. Binding of the guest molecule causes a change in the redox properties of the receptor and this change is measured by electrochemical techniques such as cyclic voltammetry (CV).⁸⁻¹² In optical sensors, the photophysical properties of the reporter change upon binding of the guest molecule to the receptor. UV-vis and fluorescence instruments are used to characterize this change depending on the type of sensor. Optical sensors have been extensively studied and reviewed for different classes of analytes including metal ions,¹³⁻¹⁶ anions,¹⁷⁻²⁶ thiols,²⁷⁻²⁸ nucleotides,²⁹ aminoacids,³⁰ and gases.³¹ Here, the types and design principles of fluorescent-based optical sensors will be discussed and selected examples will be presented.

Fluorescent chemosensors are amongst the most common types of optical sensors because they are simple, cheap, highly sensitive and easy to use. Fluorescent chemosensors based on different types^{24, 32-45} have been extensively used to detect the various classes of analytes including organic analytes,^{32, 43, 46-48} metal cations,^{14-15, 33, 35, 49-53} anions,^{19-21, 24-25, 54} explosives,⁵⁵ thiols,^{27-28, 34} and gases.^{31, 34} In the design of a fluorescent chemosensor, there are two main units, the recognition (receptor) and signaling moieties (fluorophore).^{1, 4, 33, 40, 45, 56} Generally, they are covalently connected to each other. The target analyte selectively binds to the receptor and the fluorophore converts this binding event into a fluorescence signal. The binding of the analyte can occur *via* a covalent bond^{43, 46-47, 52, 57-59} or

via a non-covalent reversible interaction.^{40, 56, 60-61} The non-covalent interactions between receptor and analyte include hydrogen bonding, electrostatic interactions, metal chelation, π - π or cation- π interactions, or reversible covalent bond formation including boronic acid-boronate and imine bonds. The type of the change in the fluorophore signal upon binding process can be predicted. These changes could be quenching or enhancement of the fluorescence signal, as well as red or blue shift in the emission wavelength of the fluorophore.⁴⁰

There are generally two types of design in fluorescent chemosensors which are the fluorophore-spacer-receptor type and the integrated fluorescent type probes.^{1, 40, 45, 56} In the fluorophore-spacer-receptor chemosensors (Figure 1.1), there is a spacer between the receptor and the fluorophore which interrupts the electronic communication between receptor and signaling unit. As a result, photo-induced electron transfer (PET) occurs between the units. Thus, there is either amplification or quenching of the fluorescence signal upon binding of analyte to the receptor. In the mechanism of PET (Scheme 1.1), there are two different energy levels belonging to the fluorophore and receptor units in the system. Upon excitation of the fluorophore, one electron is promoted from the HOMO to the LUMO. This enables electron transfer from the HOMO of the receptor to that of the fluorophore resulting in fluorescence quenching. However, upon binding of an analyte to the receptor, the bound-receptor HOMO becomes lower in energy and electron transfer is inhibited, resulting in the restoration of fluorescent emission.^{33, 62}

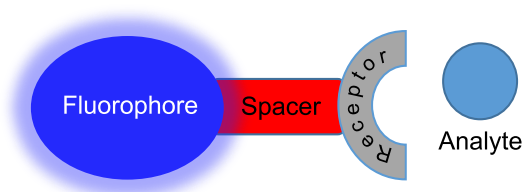
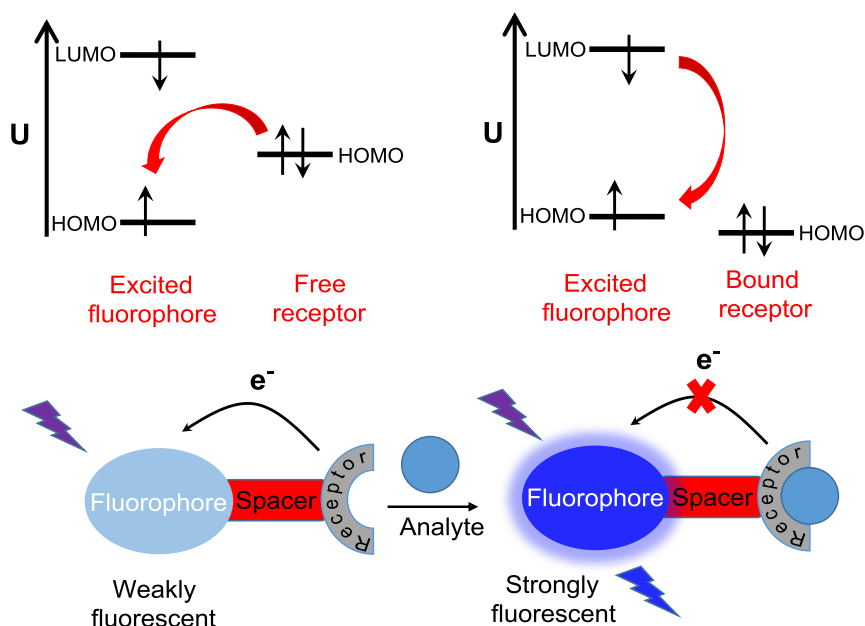


Figure 1.1 Schematic representation of a fluorophore-spacer-receptor type chemosensor.



Scheme 1.1 Photo-induced electron transfer (PET) mechanism.

One of the first examples of a PET-type chemosensor was published by A. P. de Silva who contributed greatly to this area.⁵⁶ This molecular sensor contains an aza-crown receptor which is attached to an anthracene dye by a methylene bridge (**AC** in Figure 1.2). In the absence of an analyte (K^+ cation), fluorescence of the dye is quenched because of electron transfer (PET) from nitrogen atom to the anthracene moiety. Binding of the potassium cation to the receptor inhibits PET, resulting in a fluorescence emission enhancement. In this example, an aza-crown receptor was used but there are also PET-type sensors which contain different receptors (Figure 1.2) such as podands (**PD**),⁵⁰ cryptands (**CR**),⁶³ crown ethers,^{40, 56} and dipicolylamine.⁶⁴

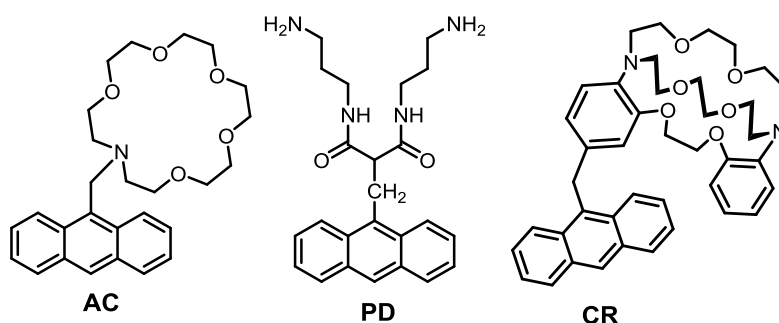
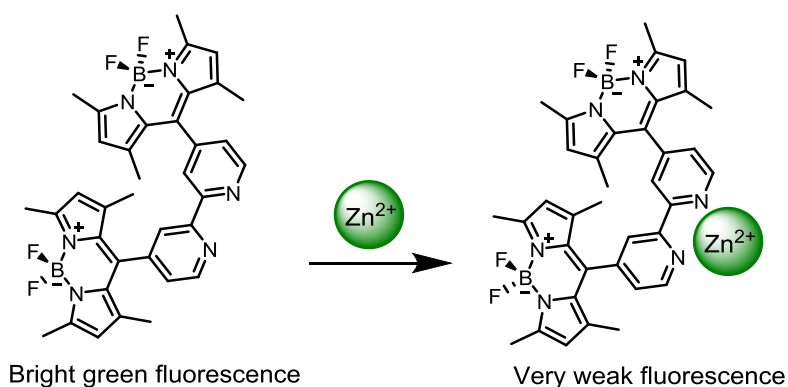


Figure 1.2 Examples of PET-type fluorescent chemosensors.

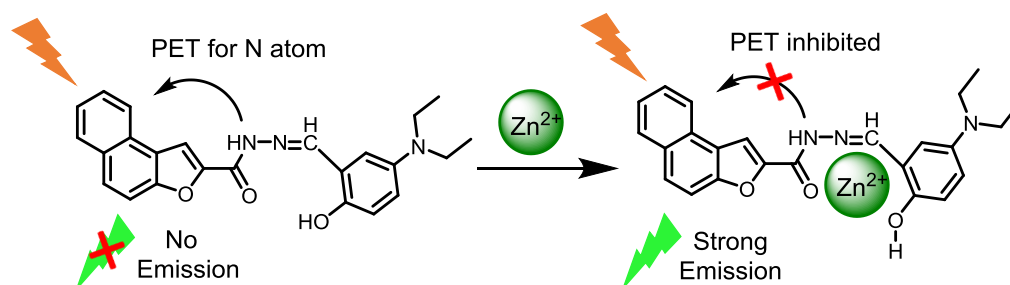
In another example, published by Akkaya *et. al.*, two BODIPY dyes are connected to each other through a bipyridyl receptor to sense phosphate ion.⁶⁵ In an organic solvent, the

fluorophore has a bright green fluorescence. Addition of a Zn(II) cation quenches the fluorescence *via* a PET mechanism, resulting in a non-fluorescent BODIPY-Zinc(II) complex (Scheme 1.2). Addition of phosphate anion to the non-fluorescent complex restores the fluorescence by a 25-fold enhancement. Phosphate does not remove the Zn(II) ion, but partially neutralizes the charge on the metal center *via* simple electrostatic interactions.



Scheme 1.2 A BODIPY-based PET-type fluorescent chemosensor.

The Zhang group has recently described a PET-type chemosensor for the selective detection of Zn(II) and Cu(II) cations using the fluorophore shown in Scheme 1.3.⁶⁶ In this sensor, they used acylhydrazone as a Zn(II) receptor. The molecule did not show any fluorescence emission in the absence of analyte because of PET from the N atom to the core. Upon binding of Zn(II) to the receptor, PET is inhibited resulting in a turn-on fluorescent response. When they added Cu(II) to the fluorescent dye-Zn(II) complex, there was a turn-off response, allowing the detection of Cu(II) at micromolar concentrations. As a result, they were able to detect Zn(II) and Cu(II) using the same chemosensor.



Scheme 1.3 A PET type of fluorescent chemosensor for Zn (II) and Cu (II).

In the integrated fluorescent probe design, there is an electronic conjugation between the fluorophore and the receptor (Figure 1.3). Therefore, the receptor is a part of a π -electron system of the fluorophore and there is only one HOMO-LUMO level of the system (Figure 1.4). They are also called ICT (internal charge transfer)-type chemosensors.

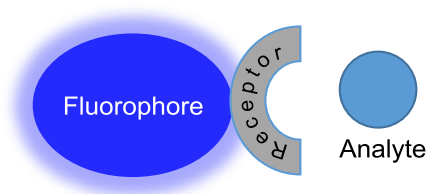


Figure 1.3 Schematic representation of an integrated fluorescence chemosensor.

In ICT-type designs, the sensor has an electron rich (electron donor) or electron poor (electron acceptor) receptor site. When the system is excited, a dipole is created because of re-distribution of electron density enabling internal charge transfer (ICT) from donor to acceptor.^{4, 67} Upon binding of an analyte, photo-induced charge transfer (PCT) occurs, which causes either a red shift or a blue shift of the bands in the UV-vis and/or fluorescence spectra (Figure 1.4). Upon binding of a cation to the fluorophore that has an electron donating group conjugated to it, there will be a decrease in the electron donating ability of that group, causing a reduction in electronic conjugation. As a result, a blue shift will be observed. Conversely, upon binding of a cation to the side of the fluorophore that has an electron accepting group, interaction of a cation with that group will enhance its electron withdrawing ability (Figure 1.4). This will stabilize the system resulting in a red shift in the spectrum.

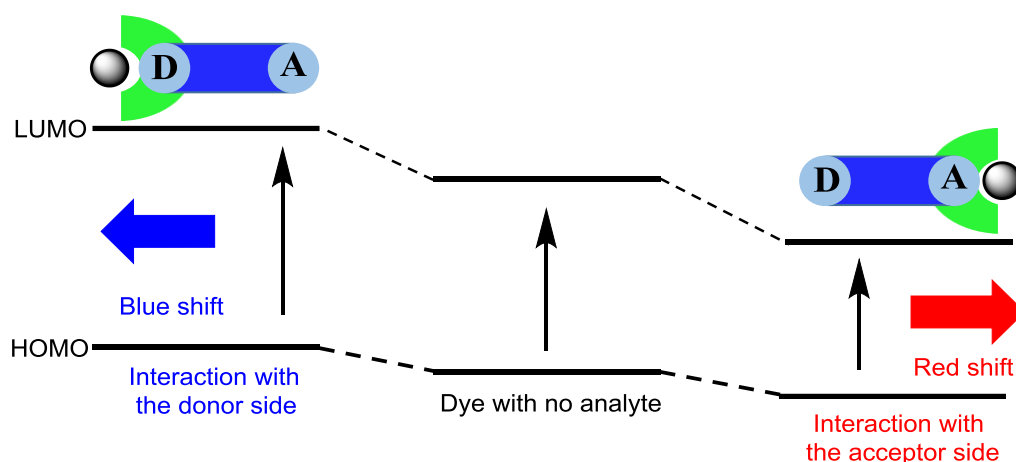


Figure 1.4 Mechanism of ICT.

A simple and clear example of an ICT type sensor was published by Akkaya and co-workers as an inspiring approach for the design of novel NIR fluorescent ratiometric pH probes.⁶⁸ In this study, they synthesized two structurally similar BODIPY dyes (Figure 1.5). The first was modified with electron donating dimethyl amino groups and the other was modified with electron accepting pyridyl groups as receptor parts. These kinds of systems are also called ‘Push-Pull’ systems because they contain electron donor (D) and electron acceptor (A) groups which permit intramolecular charge transfer (ICT) through the π -conjugated bridge (D- π -A systems). Both dyes exhibited green emission in chloroform. When they added trifluoroacetic acid (TFA) to the solution of the first dye in order to protonate the dimethyl amino groups, they observed a blue shift in both the absorption and emission spectra. The reason for this blue shift was that protonation made the donor dimethyl amino groups less effective π -donors, resulting in an increase in the energy gap change between ground and excited states. However, protonation of pyridyl units in the second dye resulted in a different response. As expected, addition of TFA caused a red shift in the UV-vis and fluorescence spectra for the second dye. Pyridyl groups are electron withdrawing groups and protonation makes them better electron acceptors, resulting in a decrease in the energy gap between ground and excited states.

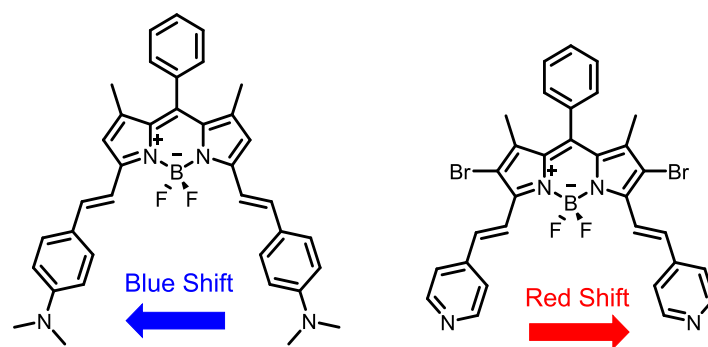
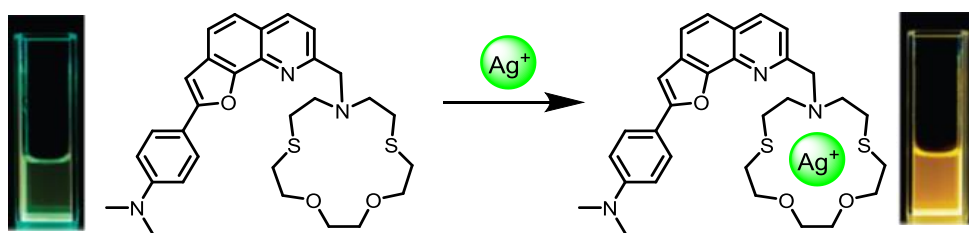


Figure 1.5 Blue and red shift of the dyes upon addition of TFA in ICT based chemosensors.

The Jiang group has published an ICT-based ratiometric fluorescent sensor for Ag^+ ions (Scheme 1.4).⁵³ In this study, a furoquinoline fluorophore was modified with an azacrown to give a ratiometric fluorescent silver chemosensor. They observed a 50 nm red shift upon addition of silver cations in ethanol. They also undertook an NMR study to find the binding position of the silver cation. They concluded that silver coordination involved both the furoquinoline fluorophore and the crown ether moiety.



Scheme 1.4 An ICT-type fluorescent chemosensor. Adapted with permission from ref [53]. Copyright 2010 American Chemical Society.

Recently, an ICT-based chemosensor was published by the Xiong group for ratiometric fluorescence imaging of cellular activity (Figure 1.6).⁶⁹ They described the first mitochondrial molecular polarity probe based on an ICT mechanism. In this probe, so called BOB, they used a donor- π -acceptor (D- π -A) system with coumarin as a donor and benzothiazene as an acceptor group. The BOB probe emits strongly in the green and weakly in the red region. The green emission band is sensitive to polarity changes and this allowed them to follow changes in polarity inside the mitochondria. They successfully distinguished cancer cells from normal cells by detecting the mitochondrial polarity differences between the two.

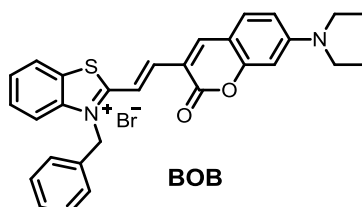
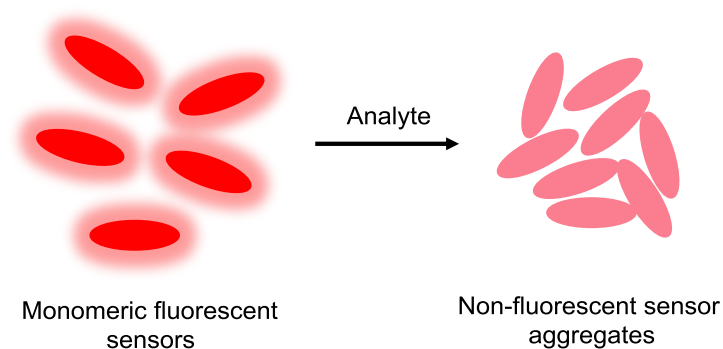


Figure 1.6 Structure of the BOB chemosensor.

1.2 Chemosensors Based on Analyte-Induced Aggregation

The analyte-induced aggregation (AIA) concept is based on aggregation of sensor molecules upon addition of the analyte to the sensor containing solution (Scheme 1.5). The interaction between analyte and sensor plays an important role in the aggregation process. In

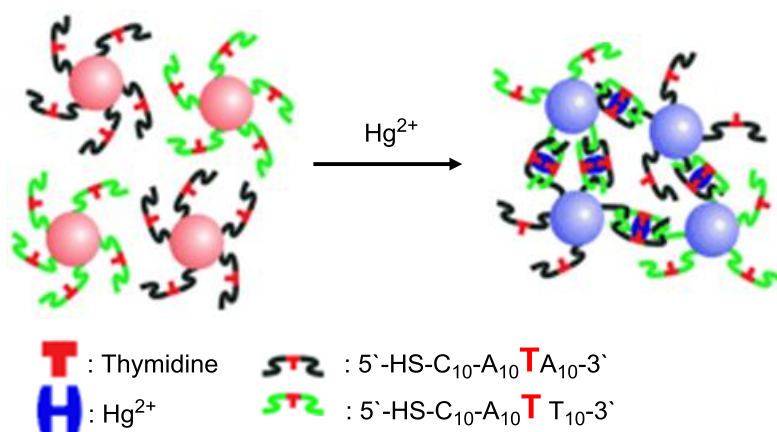
this context, conjugated polymers⁷⁰⁻⁷⁵ and calorimetric nanoparticles^{74, 76-82} have been used as calorimetric sensors. For optical sensors, mainly, luminescent polymers^{74, 83-87} have been employed, but there are also some other compounds⁷⁴ used for this purpose such as metal complexes,⁸⁸⁻⁸⁹ fluorescent dyes⁹⁰⁻⁹¹ and amphiphiles,⁹²⁻⁹⁴ quantum dots,^{82, 95} and polypyridyl ligands.⁹⁶



Scheme 1.5 Aggregation of sensor molecules upon analyte addition.

Metallic nanoparticles are particularly useful in this context.^{76, 81-82, 97} Gold and silver nanoparticles are the most common type of metallic nanoparticles and they have an absorption in the visible region because of localized surface plasmons. This absorption originally arises due to the oscillation of conduction band electrons upon irradiation of the nanoparticle with a light frequency that can induce resonance. For example, gold nanoparticles absorb at 520 nm, but upon aggregation of the particles, a red-shift in the UV-vis spectrum is observed. By considering this effect, different chemosensors have been designed based on assembly or disassembly of nanoparticles. There are different parameters that can affect the resonance oscillation of the nanoparticles, including nanoparticle shape, size and the environment of the particle.

The surface of the nanoparticles was modified with functionalities that can have an interaction with the desired analytes. In an example published by the Mirkin group, gold nanoparticles (Au-NPs) were modified with DNA to sense the toxic and carcinogenic mercury cation (Hg^{2+}).⁹⁸ They prepared two Au-NPs functionalized with a complementary DNA sequence with the exception of a thymidine-thymidine mismatch. Hg^{2+} binds selectively to the bases making up the mismatch. As a result, two different Au-NPs form stable colored aggregates. They could selectively detect Hg^{2+} using absorbance spectroscopy.



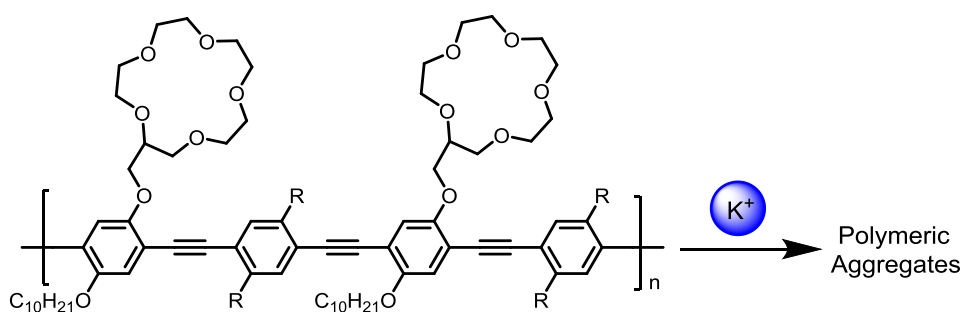
Scheme 1.6 Aggregation of DNA-modified nanoparticles in the presence of Hg^{2+} (II) cation. Adapted with permission from ref [98]. Copyright 2007, WILEY-VCH Verlag GmbH & Co. KGaA, Weinheim.

In another study, melamine, which is an illegal additive for milk-based products, was visually detected using modified gold nanoparticles.⁹⁹ The Lu group synthesized stable thiol functionalized cyanuric acid derivative-modified Au-NPs. The color of the well dispersed NPs were wine red in water. However, upon addition of melamine, the color changed to blue indicating melamine-NPs aggregate formation. The system was quite sensitive. They were able to detect melamine at ppb level.

Conjugated polymers have also been used for the analyte-induced aggregation concept in sensing applications. In the design of such polymers, there is at least one backbone chain that has alternating single and double bonds.⁷¹ They may commonly contain π -electron rich aromatic systems such as polythiophene, or polypyrrole. A receptor unit that is specific to a desired analyte is attached to the side chain of the polymer. Upon addition of an analyte to the conjugated polymer solution, polymer aggregates form, resulting in polymer chain twisting, interchain aggregation, or π - π stacking. This behaviour leads to an alteration of π -conjugation of the system that modulates the bandgap of the polymer electronic system. As a result, some photophysical changes occur in the spectrum. The interaction between the analyte and the side chain determines the final optical response.

The Swager group is amongst the most active groups in this field. In one study, they were able to selectively sense K^+ using a conjugated polymer (Scheme 1.7).⁷⁰ The side chain of the polymer has a crown ether as a receptor for the potassium ion, which forms a 1:2 complex with the crown ether, resulting in aggregation of the polymers. There is an

interpolymer π -stacking aggregation which leads to a red shift in the spectrum. Their system had selectivity over other potential analytes such as Na^+ and Li^+ .



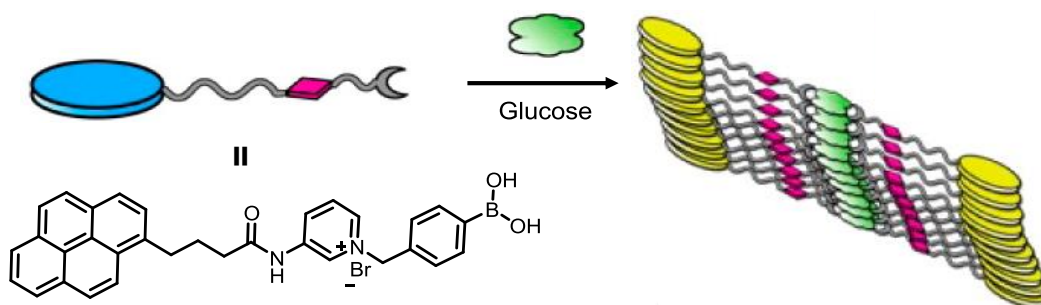
Scheme 1.7 Addition of potassium cation induces aggregation of polymers.

In another study published by the Swager group, an anthryl-doped conjugated polymer was used to sense biogenic amines including spermine, spermidine and putrescine.⁸⁵ Addition of amines to the polymer induced aggregate formation between the polymer chains. Aggregation resulted in different color responses for different amines. However, the overall system was not very selective because of non-specific electrostatic interactions between the amine and the negatively charged polymer.

Fluorescent amphiphiles have also been used for the analyte-induced aggregation concept. Commercial fluorescent dyes can be modified according to the desired properties for the analyte. Generally, fluorescent amphiphiles contain two units which are hydrophobic and hydrophilic. The analyte interacts with the amphiphile, resulting in aggregation. Different aggregation products could be obtained depending on the system.⁹⁴ Upon aggregation, aromatic units interact and results in different changes such as emission enhancement,⁹² emission quenching,⁷⁴ red and blue shifts, or excimer formation.⁹³⁻⁹⁴

An example of this approach was published by the Yang group.⁹² They reported an ATP imaging system. The system is based on analyte-induced aggregation which results in fluorescence enhancement. The probe molecule was synthesized and it had a weak emission in polar media. In this molecule, they have one fluorescent part, a unit for the differentiation of mono-, di-, and triphosphate groups, and ethylene glycol units for water solubility. ATP and the probe formed a charge-neutral complex. This complex aggregates. As a result, the fluorescence of the probe increased *via* a positive solvakinetic effect. They selectively identified and quantified the amount of ATP *in vivo* and *in vitro* at low concentrations.

In a paper published by James, Jiang and coworkers, a monoboronic acid amphiphile was used to sense glucose (Scheme 1.8).⁹³ In the design of the amphiphile, there is a pyrene unit which provides the formation of a long wavelength excimer, allowing a ratiometric response. Addition of glucose and fructose resulted in two different responses; glucose caused an enhancement only in excimer emission not in monomer emission, and fructose caused only monomer emission enhancement. The reason behind this was that there were different kinds of aggregation products upon addition of glucose and fructose. Glucose addition caused the formation of 1:2 complexes which resulted in the ordered aggregates, because glucose binds two boronic acid units at the same time, enabling two sensor molecules to come together. As a result, the 1:2 complexes started to aggregate and aggregation led to excimer emission. However, in fructose, there was only 1:1 complex formation which caused the de-stabilization of the aggregates causing the monomer emission. Their ratiometric fluorescent sensor was quite selective and sensitive for glucose.



Scheme 1.8 Aggregation of sensor molecules upon addition of glucose. Adapted with permission from ref [93]. Copyright 2007 American Chemical Society.

In addition to the examples mentioned above, the analyte-induced aggregation concept has been used for the detection of metal ions (Hg^{2+} ,^{87, 100} K^+ ,⁷⁰ Mg^{2+} ,⁹⁶ Al^{3+} ,¹⁰¹⁻¹⁰²), pyrophosphate,⁸⁴ chloride,¹⁰³ biogenic amines,^{85, 104} oxalic acid,⁸⁶ DNA,⁸³ ATP,^{80, 89, 92, 105} heparin,¹⁰⁶ pH,⁸⁸ glucose,⁹³ explosives,¹⁰⁷ citric acid,¹⁰⁸ cysteine and homocysteine.⁹⁰

Chemosensors based on aggregation-induced emission (AIE) can also be classified as analyte-induced aggregation type chemosensors. Fluorescent molecules show different emission properties at different concentration.¹⁰⁹ Generally, they quench themselves at high concentration because of aggregation caused quenching (self quenching). However, there are some fluorescent molecules that do not show any fluorescence emission when they are well solubilized (present as monomers in solution). Upon changing the type and/or composition of

the solvent, they become poorly soluble and start to aggregate as fluorescent clusters (Figure 1.7).¹¹⁰ This phenomenon is called aggregation-induced emission. It is a photophysical process at molecular level. The mechanism of AIE is related to intramolecular restriction of rotations in molecule.¹⁰⁹ There are intramolecular rotations in the molecule which causes non-radiative relaxation of the excited state forming non-emissive (non-fluorescent) molecules. Upon aggregation, the intramolecular rotations are restricted blocking the non-radiative emissions. As a result, the molecules become emissive (fluorescent).

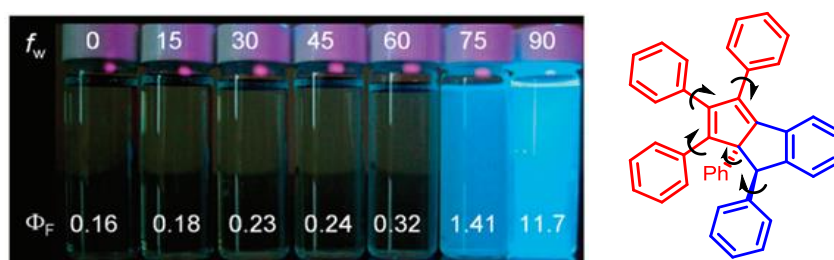


Figure 1.7 The photographs of the solutions of the dye under UV-vis light in THF/water mixtures with at different composition ratio of water (f_w , vol%) and the fluorescence quantum yields (Φ_F , %) of the dye. Adapted with permission from ref [94]. Copyright 2008, WILEY-VCH Verlag GmbH & Co. KGaA, Weinheim.

The AIE approach has been used for the detection of ions,¹¹¹⁻¹¹² DNA,¹¹³ cancer cells,¹¹⁴⁻¹¹⁵ proteins,¹¹⁶⁻¹¹⁷ thiols,¹¹⁸ ATP,¹¹⁹ carbon dioxide,¹²⁰ explosives,¹²¹ and environmental pollutants.¹²² Selected examples of chemosensors based on AIE will be discussed below.

The Tang group published a cysteine sensor using the AIE concept.¹¹⁸ They synthesized the non-fluorescent maleimide modified tetraphenylethene probe for this purpose (Figure 1.8). When the molecule is exposed to the cysteine, it reacts with the cysteine and transformed into a species which shows AIE behavior. They could be able to detect the cysteine at about 1 ppb by naked eye.

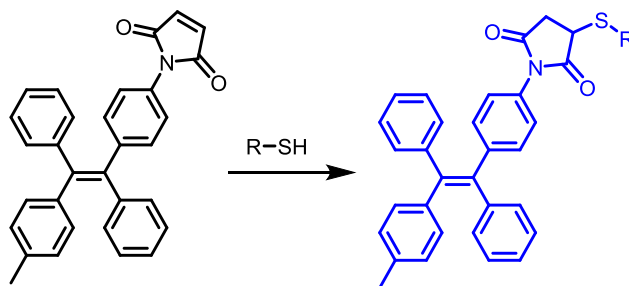


Figure 1.8 An AIE sensor for cysteine.

Picric acid detection was achieved by the Kumar group using hexabenzocoronene-based probes.¹²³ The probes include rotors at the corners of the coronones which enables the aggregation-induced emission enhancement to occur (Figure 1.9). At a certain ratio of mixed aqueous solvent (THF:H₂O), the probes start to aggregate with an enhancement in fluorescence emission. They were able to selectively detect picric acid in mixed aqueous solvents as well as in the vapor phase. In addition to this, they achieved the detection of picric acid using fluorescent test strips with a detection limit in the attograms range.

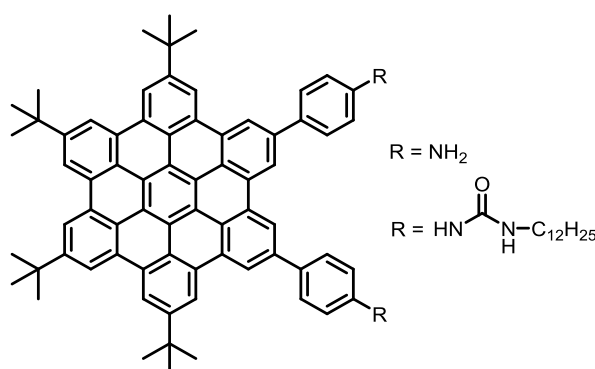
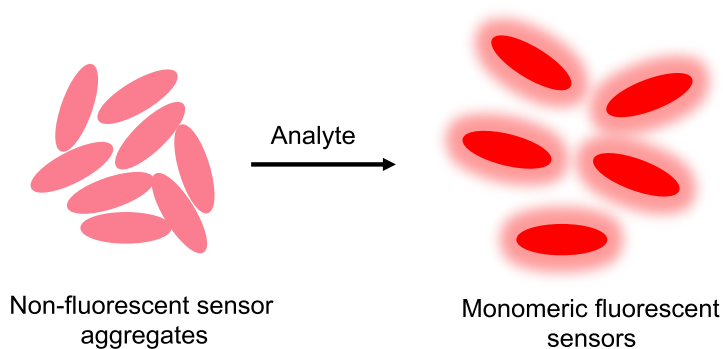


Figure 1.9 The structure of coronene-based picric acid probes

1.3 Chemosensors Based on Analyte-Induced De-Aggregation

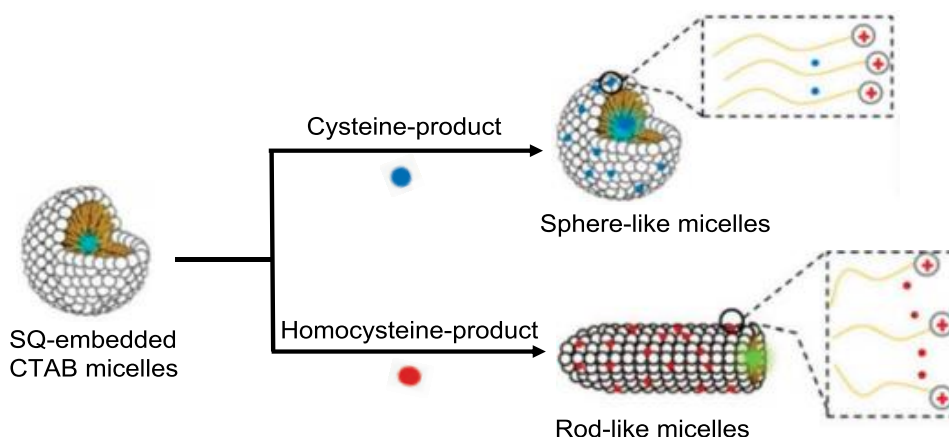
The analyte-induced de-aggregation approach is complementary to the analyte-induced aggregation approach. In this approach, sensor molecules aggregate without analyte.^{91, 124-125} Upon binding of an analyte to the sensor molecule, pre-assembled sensor molecules start to de-aggregate, resulting in sensor-analyte complex formation. A sensor molecule has already the ability to interact with an analyte molecule which requires no additional receptor. As a result of binding, the photophysical properties of the sensor molecules change, such as fluorescent quenching or enhancement. Information about the analyte is obtained by the measurement of the sensor response.



Scheme 1.9 De-aggregation of the sensor molecules upon analyte addition.

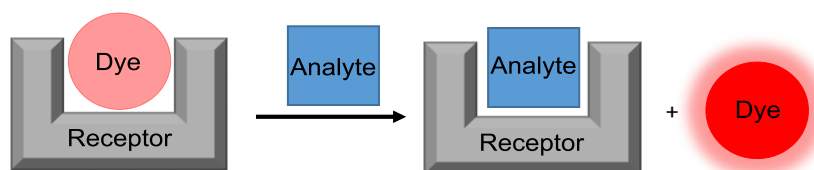
This approach was successfully used by the Chang group.⁹¹ They used a modified fluorescent BODIPY dye to sense the drug GBL (Gamma-butyrolactone). The dye showed poor solubility in water, resulting in aggregation in polar solvents. Addition of GBL disassembled the aggregates and resulted in a turn-on response of the dye. They used this fluorescence response to quantify the concentration of the drug.

A different strategy of analyte-induced de-aggregation was used by the Pang group to sense cysteine and homocysteine.¹²⁶ In this approach, they did not observe de-aggregation but rather a change in the shape of aggregates (Scheme 1.10). They used squaraine (SQ) and 2-cyano-6-methoxybenzothiazole (CBT) dyes and the cationic surfactant hexadecyl trimethyl ammonium bromide (CTAB). Cysteine and homocysteine reacted with CBT and interact with the CTAB micelles *via* electrostatic interactions. However, the products have differences in amphiphilicity, resulting in different aggregation types. Upon interaction of homocysteine products with spherical micelles, there was a transition from spherical to rod-like micelles which was not the case for cysteine. The SQ dye gave a different response, allowing selective detection of cysteine and homocysteine from the other potential analytes.



Scheme 1.10 Analyte-dependent shape change of the aggregates for the sensing of cysteine and homocysteine. Adapted with permission from ref [126]. Copyright 2013, Royal Society of Chemistry (RSC).

The analyte-induced de-aggregation approach is also related to indicator displacement assays (IDAs). Indicator displacement assays are sensing systems which keep receptor and signaling unit together *via* self-assembly.¹²⁷ This approach has different design principles compared to fluorescent chemosensors, which have covalently attached receptor and signaling units (dye).¹²⁸ An IDA allows a synthetic receptor to be converted into a powerful optical sensor.¹²⁷ In an IDA, there is no covalent bond between the units, and a dye reversibly binds to the receptor *via* non-covalent interactions such as electrostatic interactions, or hydrogen-bonding. The sensing mechanism is based on a competition between dye and analyte for binding to the receptor (Scheme 1.10). Upon addition of an analyte to a dye-receptor complex, some of the bound dyes are exchanged for analyte and this displacement causes modulation of the optical properties of the dye. The signal change can be used to obtain information about the analyte qualitatively and quantitatively. The signal modulation could be based on different mechanisms including photo-induced electron transfer (PET), fluorescence resonance energy transfer (FRET), and electronic energy transfer (EET).¹²⁸⁻¹²⁹



Scheme 1.11 Basic concept of an indicator displacement assay (IDA).

There are some basic design requirements for IDA-type sensors. The dye and the analyte should not have very different binding affinities towards a receptor.^{127, 129} If the dye has a much higher binding affinity than the analyte for the receptor, it will not be able to exchange with the analyte. Therefore, no information can be obtained about the analyte. On the contrary, if the analyte has much higher binding affinity than the dye to the receptor, all the dyes will be exchanged with the analyte at even very low concentrations of the analyte.

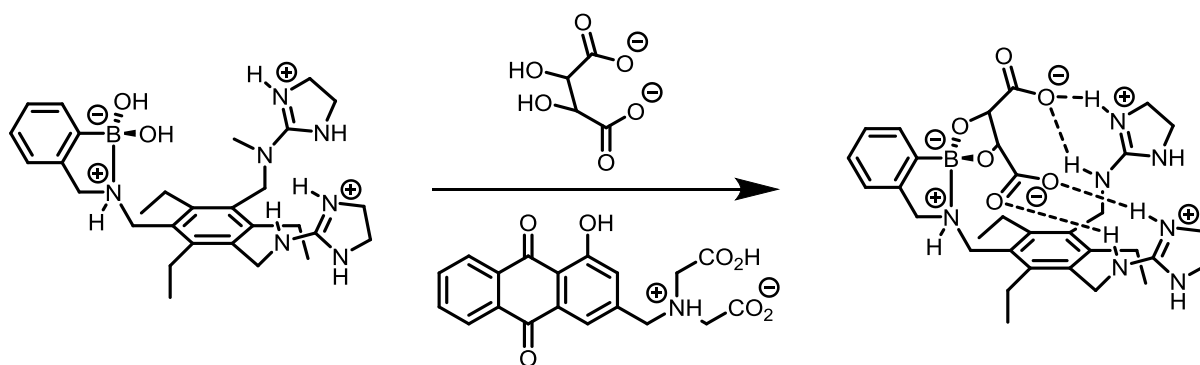
IDAs have some advantages compared to classical chemosensors. From a synthetic point of view, these systems are easier to make because one does not have to couple dye and receptor together covalently. A sensing system is obtained by mixing the dye and receptor. In general, commercial dyes are used as reporters in IDAs. Different species can be used as a receptor including nanoparticles,^{82, 130-137} synthetic receptors,^{129, 138-143} and metal complexes.¹⁴⁴⁻¹⁴⁹ It is important to design and synthesize a selective receptor for the analyte. Also, one can use different indicators with same receptor.¹⁴² It is also easy to optimize the sensing system for the selectivity and sensitivity by modulating the concentration ratio of dye/receptor.

Nanoparticles have been used extensively for IDA-type chemosensors.^{82, 130-137} NPs are decorated with a binding unit (receptor) and reporter unit (fluorescent dyes) *via* different interactions. Upon assembly, the fluorescence of the indicator is quenched. When the analyte is added, it forms a complex with the NPs, removing dyes from the surface of the NPs and causing fluorescent enhancement in the signal. The receptor is designed according to the analyte. As indicators, fluorescent dyes, fluorescent conjugated polymers and green fluorescent proteins can be used.

IDA-type chemosensors have been extensively studied and reviewed.^{127, 129} Such systems have been used for the detection of different analytes including anions,^{128, 134, 148} aminoacids,^{137, 149} chemical warfare agents,¹⁴⁷ citrate,¹³⁹ the dicarboxylate anion,¹⁴⁶ malate,¹⁵⁰ metal cations (Cu^{2+} ,¹³² Hg^{2+} ,^{131, 133} Pb^{2+130}), nitric oxide,¹⁴⁵ oxalate,¹⁴³ phosphate¹⁵¹ pyrophosphate,¹³⁵ peptides,¹⁴⁴ and proteins.¹²⁴⁻¹²⁵ Below, we will discuss some selected examples.

Eric Anslyn, one of the pioneers of this field, made IDA-based chemosensors to sense the tartrate anion, which is a natural product found in grape juice and wines (Scheme 1.11).¹⁴² The receptor contains a boronic acid and positively-charged guanidinium groups, and the indicator alizarin has two carboxylate groups providing negative charges. The analyte tartrate

has a diol and two carboxylate groups. In the design of the receptor, they anticipated that the boronic acid would bind to this diol and the guanidinium groups could interact with the carboxylate groups of the analyte electrostatically. Upon addition of the receptor to the dye solution, the color of Alizarin changed from yellow to orange, with a 1:1 binding constant of $K_a = 2.7 \times 10^4 \text{ M}^{-1}$. Addition of a tartrate solution to the sensing ensemble changed the color of the solution from orange to yellow, showing that tartrate formed a complex with the receptor. They also tested structurally similar analytes including lactate, succinate, ascorbate, L-malate and sugars. They observed good selectivity over potential competitors except for malate ($5.5 \times 10^4 \text{ M}^{-1}$ for tartrate, 150 M^{-1} for glucose, 350 M^{-1} for succinate, $4.8 \times 10^4 \text{ M}^{-1}$ for malate). As an application of their sensing ensemble, they quantified the amount of tartrate/malate in some grape derived beverages. They also used NMR experiments to quantify the amount of tartrate/malate. The results showed that it was possible to quantify the amount of tartrate/malate correctly (difference is less than 10 %).



Scheme 1.12 IDA-type chemosensor for the detection of tartrate.

The use of indicator displacement assays inside living cells is an attractive application for these types of chemosensor. In one example of this approach, Nau *et. al.* detected the uptake efficiencies of bioorganic analytes by living cells.¹⁵² Initially, different receptor/dye combinations were tested to see whether they had the compatibility to be uptaken into the cells (Chinese hamster ovary and fibroblast cells). They found that the *p*-sulfonatocalixarene lucigenin pair had a good uptake into cells. This pair also possesses biocompatibility and low toxicity, having no adverse effect on the cells upon incubation, which is an important issue for cell studies. The receptor and the dye formed a stable complex in pure water ($K_a = 2.8 \times 10^7 \text{ M}^{-1}$), resulting in fluorescence quenching of the dye lucigenin. The pair was taken into cell

and gave no emission. Analyte addition to the cell caused fluorescence to be recovered depending on the type of analyte and incubation time. They selected choline and protamine as analytes because of their efficient cellular uptake and strong binding affinity to the receptor. Control experiments, which were done using betaine, showed that the sensor was analyte-selective. This IDA allowed them monitoring the uptake efficiencies of choline and protamine into the cell.

1.4 Micelle-Based Chemosensors

Micelles are aggregates of surfactant molecules in aqueous media. A typical surfactant molecule contains a hydrophilic ‘head group’ and a covalently linked hydrophobic ‘tail group’.¹⁵³ Some surfactants can contain more than one head group, they are called bolaamphiphiles.¹⁵⁴ The shape and size of a micelle depends on the structure of the surfactant molecule and on different parameters such as concentration, temperature, pH and ionic strength. Micelles have a size of 3 to 6 nm and can adopt different shapes (e.g. ellipsoids, cylinders, bilayers). The concentration of the surfactant at which micelles start to form in solution is defined as critical micelle concentration (cmc). In water, the hydrophobic effect is the driving force for micelle formation

Chemosensors are often used to detect and quantify analytes in organic solvents. However, the preparation of chemosensors which work in water is a challenging task. There are two major problems. The first one is about the dye that is used for sensing. Many of the fluorescent dyes are hydrophobic and they are poorly soluble in water. Therefore, one has to modify the dye to make it water soluble and this requires synthetic effort. The second problem is about binding: there is competition between receptor and water for binding to the analyte. For instance, it is difficult to sense carbohydrates in water due to hydrogen bonding of sugars with water.

Micelles can be used to solve some of the problems mentioned above and to sense analytes in water. The advantage of using micelles is that one can form hydrophobic pockets in water. Forming such pockets in water is highly important for sensors because they allow

sensing unit and/or the analyte to be solubilized in case they are poorly soluble in water. Solubilizing the fluorophore and the analyte inside a micelle or at a micelle-water interface can increase the binding constant between the fluorophore and the analyte (e.g by increased static or dynamic quenching).¹⁵⁵⁻¹⁶⁰ Also, in reaction-based chemosensors, the reaction rate can be increased, resulting in a shorter response time.¹⁶¹⁻¹⁶³ The selectivity of the sensor can also be changed by using different surfactants.¹⁶⁴⁻¹⁶⁶ Furthermore, by changing the surfactant, the size of the micelle can be adjusted to dye and analyte. For example, if a cationic dye is used, anionic micelles can be used to facilitate the interaction. There are many examples of micelle-based fluorescent chemosensors in the literature.¹⁶⁷⁻¹⁶⁸

The Akashi group, for example, published a Ba^{2+} sensor that works in water (Figure 1.10).¹⁶⁶ They synthesized a PET type hydrophobic chemosensor. In the absence of Ba^{2+} , the sensor does not show fluorescence emission because of electron transfer from the nitrogen atom to pyrene. When Ba^{2+} is coordinated to the sensor, it blocks the PET and fluorescence intensity is enhanced. First, they examined the sensor in water and they did not see any response upon addition of Ba^{2+} . However, when they used triton X-100, they obtained a strong fluorescence signal upon addition of Ba^{2+} . Complex formation between the sensor and Ba^{2+} is improved by using the micellar environment.

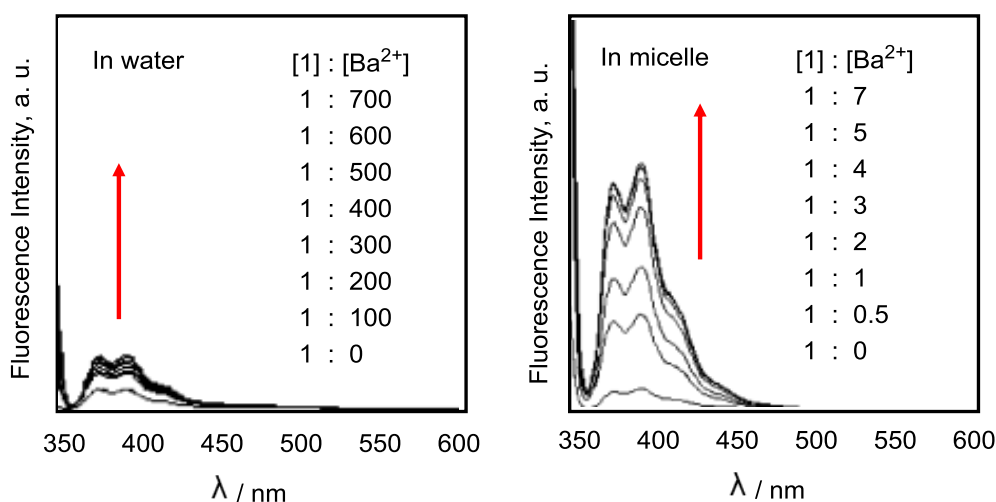
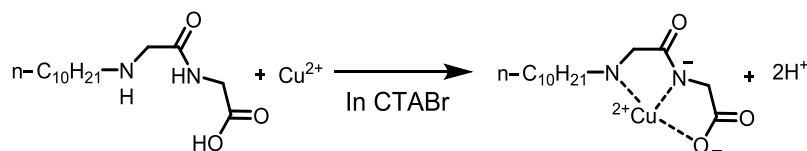


Figure 1.10 Fluorescence spectral changes in the absence/presence of Triton X-100 micelles. Adapted with permission from ref [166]. Copyright 2003, Royal Society of Chemistry (RSC).

The Pallavicini group published a fluorescent sensor for lipophilicity.¹⁵⁷ They were able to sense the lipophilicity of molecular fatty acids $\text{CH}_3(\text{CH}_2)_x\text{COOH}$ ($x=0-16$) in water.

They used 1-pyrenecarboxylic acid as a reporter and a lipophilic cyclen ligand as a receptor that can bind to Zn^{2+} . 1-Pyrenecarboxylic acid forms a complex with cyclen in the presence of Zn^{2+} inside triton X-100 micelles, and this complex is fluorescent. When they added fatty acids to the solution, depending on the chain length (hydrophobicity), they participated in the micelle formation or remained in water. Fatty acids that entered the micelles made a stable complex with the receptor and resulted in fluorescence quenching of the dye. They successfully characterized the lipophilicity of the fatty acids using this fluorescence response.

Amphiphiles with a long alkyl chain tail and a specific recognition group have also been used in the presence of commercial surfactants and hydrophobic dyes to detect metal cations.¹⁶⁷⁻¹⁷⁵ In these studies, the hydrophobic dye is encapsulated inside the micelles which are formed by the chelating amphiphile and the surfactant. Upon complexation of a metal to the receptor, there is fluorescence emission quenching of the dye. In an example published by the Tonellato group, they were able to sense the Cu(II) ion selectively in aqueous solutions in the presence of CTAB micelles.¹⁷⁰ They synthesized a lipophilic ligand containing a long alkyl chain and a dipeptide-based head group (Scheme 1.13). Mixing of the ligand and the surfactant gave co-micellar aggregates in water. The commercial ANS dye, which is negatively charged, was added to the micellar solution and it binds strongly to the micellar aggregates resulting in strong fluorescence emission due to solubilization of the dye in the less polar environment of the micelle. The mixture of the ligand, dye and surfactant was used as a sensing system for the Cu(II) ion. The addition of Cu(II) to the micellar solution caused the formation of a complex and the binding resulted in the quenching of the ANS dye. There was no quenching of the dye in the absence of ligand upon addition of Cu(II) . They achieved very selective binding because of Cu(II) -mediated deprotonation of the amido nitrogen at slightly acidic or neutral pH. In this study, they also changed the components of the sensing system to optimize the properties of the sensor. They tested different surfactants and different commercial dyes.



Scheme 1.13 Complexation of amphiphile receptor to Cu^{2+} in the presence of CTABr.

There is another approach for preparing micelle-based fluorescence sensors. An amphiphile which aggregates in the presence of the analyte is used to create micellar aggregates.^{89, 92-93, 176} Fluorescent amphiphiles or lipophilic fluorophores are used to get information about the aggregation as a fluorescence signal. This approach is quite similar to the approach discussed in section 1.2. The opposite approach has also been studied: addition of the analyte de-aggregates the micelles resulting in a fluorescence response.¹⁷⁶⁻¹⁷⁷ This approach was discussed in section 1.3.

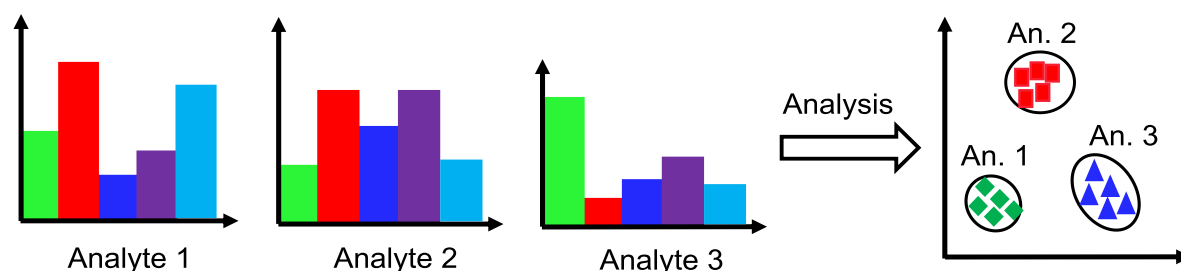
1.5 Pattern-Based Sensing Systems

So far, the discussion has been limited to chemical sensors for individual analytes. These types of systems are based on a lock and key principle. Generally, there is one receptor (lock) which selectively and strongly binds a target analyte (key) resulting in an optical change in the reporter unit. Rational design and synthetic effort is required to get a good receptor. As we have mentioned in the previous sections, there are numerous applications of such chemosensors.^{1, 4} In these studies, the analytes are typically small molecules such as organic compounds, metals ions, biogenic amines, and amino acids. However, there are some other classes of analytes in nature which have large and complex structures such as antibiotics, nucleic acids, and proteins. Also, there are some samples containing a mixture of analytes that must be analyzed together such as beverages, and perfumes. In such cases, classical chemosensors or IDAs are not very useful because it is not easy to design and synthesize a receptor for complex molecules such as proteins. Also, it is not possible to sense more than one analyte using one selective receptor. Sensing of complex analytes or analyzing mixture of analytes requires different approaches to sensing. One possibility is to use pattern-based sensing systems. Pattern-based sensing systems convert non-selective chemosensors into powerful sensing systems. There are mainly two different approaches to pattern-based sensing systems in the literature, which are sensor arrays and single sensing systems (dynamic combinatorial library sensors) approaches which will be explained with the examples in the

following sections. However, before going into detail, data treatment methods for pattern-based systems will be discussed.

1.5.1 Pattern Recognition Tools

Sensor arrays often give multidimensional data sets which are difficult to interpret. Multivariate analysis techniques are used to analyze data of such systems. These techniques provide classification of the multidimensional data by using the similarities in the data sets (Scheme 1.14).¹⁷⁸⁻¹⁸⁰ As a result, the dimensionality of the data is reduced and useful information is extracted from the multidimensional data sets. We use three different analysis in our studies, namely linear discriminant analysis (LDA), principal component analysis (PCA), and hierarchical cluster analysis (HCA).



Scheme 1.14 Multivariate analysis of the data for PBS systems.

Linear discriminant analysis is a statistical method used to classify data according to their similarities. It reduces the dimensionality of the data set for classification.¹⁸⁰ LDA is a supervised method because a prior knowledge is given to the system showing which data belong together. Because of this reason, LDA often gives over-optimistic results compared to principal component analysis (PCA). The quality of the LDA analysis can be evaluated by using a jack-knife validation routine. In a jack-knife validation routine, one sample is left out randomly and the remaining data is used for classification. Discrimination success is evaluated by the proportion of the correct classification of the omitted sample.

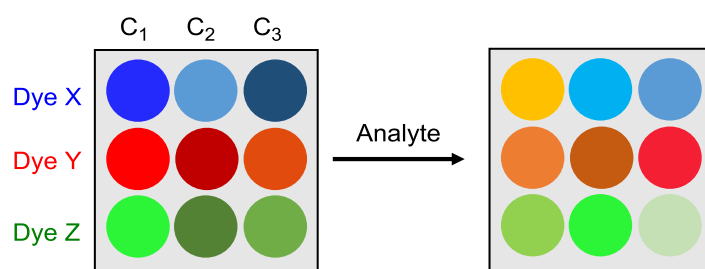
PCA is similar to LDA as it tries to classify the ungrouped data set according to their similarities.¹⁸⁰ However, PCA is a non-supervised statistical method because the program does not recognize which data belong to the same cluster. As a result, it allows the separation of one sample from the other qualitatively. The data analysis uses orthogonal transformation (orthogonal eigenvectors) for the conversion of a set of correlated variables into a set of linearly uncorrelated variables (principal components). The number of components should be equal to or less than the original variables. This can be defined such that the first principal component has the highest degree of possible variance and each succeeding component has the order of decreasing variance. Mostly, dimensionality of the data set is reduced to two or three principal components which are enough to get information with minimal lost because they contain at least 95% of the total variance.

Hierarchical cluster analysis (HCA) is different from PCA and LDA analysis. It tries to build a hierarchy of clusters according to their origin and family.¹⁸¹ There are two types of strategies for this type of clustering which are agglomerative and divisive. In the agglomerative type, a "bottom up" approach is used in such a way that each sample starts to build its own cluster, and different clusters start to pair with each other, moving up a hierarchy. However in the divisive type, the approach is "top down". All samples are in one cluster at the beginning and start to split into different clusters as moving down the hierarchy.

1.5.2 Sensor Arrays

Inspired by the nature, sensor arrays are powerful sensing systems for complex analytes and analyte mixtures.¹⁸²⁻¹⁸⁴ Odor detection of the nose in humans and other mammals uses a similar mechanism.¹⁸⁵⁻¹⁸⁶ In the biological olfactory system for odor detection, a limited number of non-selective receptors can detect and distinguish many different analytes and analyte mixtures. The olfactory systems of different species in nature have different sensitivity and discriminatory power.¹⁸² For example, mice can differentiate between pairs of enantiomers¹⁸⁷ and honeybees are able to detect structurally similar odorant pairs.¹⁸⁸ Similarly, a sensor array is composed of different non-selective and separated chemosensors in an array format. Sensors of the array interact with analytes to a different degree. The

interaction could be covalent or non-covalent depending on the type of the sensors in the array. As a result, the combination of the array gives a characteristic signal pattern or so called “fingerprint” for each analyte. Individual data of a sensor in the array do not provide too much information about the analyte, but when a combination of all data is analyzed using pattern recognition tools, qualitative as well as quantitative information about the analytes can be obtained. A sensor in the array does not have to be selective for a specific analyte, which is one advantage of the arrays because one can obtain a very selective sensing system using different non-selective chemosensors in an array format. Individual sensors in the array can be IDA type sensors, organic dyes or metal-dye complexes. Scheme 1.15 shows schematically a small sensor array. It contains nine different sensors. For example, one could use nine different dyes or IDAs in the array, or there could be three different dyes **X**, **Y**, and **Z** at three different conditions C_1 , C_2 , C_3 . C could be anything that modulates the interaction with the analytes such as pH, solvent, temperature etc..



Scheme 1.15 A sensor array that contains nine separated sensors.

The sensor array field is expanding very fast because of its applicability for different classes of analytes and analyte mixtures which are difficult to sense using classical chemosensors. For example, sensor arrays were used to analyze anions,¹⁸⁹⁻¹⁹⁶ metal ions,¹⁹⁷⁻²⁰⁸ heavy metals,^{198, 200} neutral molecules,¹⁹¹ amines,^{72, 75, 209-214} amino acids,²¹⁵⁻²¹⁸ carboxylates,²¹⁹⁻²²³ chemical and biological hazards,²²⁴ drugs,²²⁵⁻²²⁶ explosives,²²⁷⁻²²⁹ carbohydrates,²³⁰⁻²³⁸ organophosphates,²³⁹ peptides,²⁴⁰⁻²⁴⁶ proteins,²⁴⁷⁻²⁵⁹ toxic chemicals,²⁶⁰⁻²⁶³ toxic gases,^{261-262, 264-266} samples containing complex mixtures (beer,²⁶⁷ coffee,²⁶⁸ soft drinks,²⁶⁹ odorants²⁷⁰), bacteria,²⁷¹ and fungi.²⁷² Selected examples will be discussed below.

The Severin group has employed sensor arrays to sense different analyte classes including amino acids,²¹⁶ short oligodeoxynucleotides,²⁷³ and different peptides.²⁴²⁻²⁴³ For

example, they have used an IDA-based sensor array for the discrimination 20 natural amino acids in buffer solutions using UV-vis spectroscopy.²¹⁶ In the array, a water soluble organometallic Cp*Rh complex was used as a receptor in combination with three different dyes, which are gallocyanine, xylenol orange, and calcein blue (Figure 1.11). The sensor array is formed by mixing the dyes and the metal complex at different ratios and different pH. Upon binding of the dyes to the receptor, there is a strong color change in the UV-vis spectra of the dyes. The Rh complex also forms stable complexes with amino acids. There is competition between amino acids and dyes for binding to the Cp*Rh complex. The array is tested with the amino acids. The data was analyzed using the pattern recognition tools linear discriminant analysis (LDA) and principal component analysis (PCA). The sensor arrays enabled very good separation of 20 different amino acids in aqueous solution. There was only overlap for valine and isoleucine.

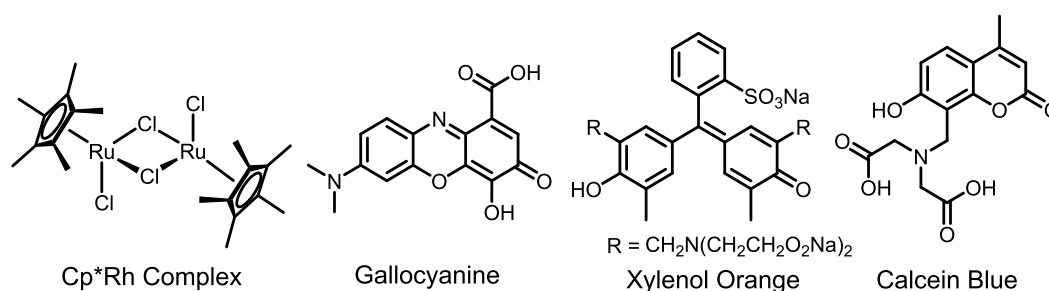


Figure 1.11 Ligand and dyes used in the sensor array.

Another powerful sensor array was published by Sslick.²⁶³ In this study, they were able to detect 19 different volatile toxic industrial gases using a calorimetric cross-reactive nanoporous sensor array at low gas concentrations. This is an important study, because it is difficult to sense gaseous samples at low concentration. In the array, there are four classes of chemically responsive dyes (Figure 1.12), containing overall 36 dyes (6×6). The first class is metalloporphyrins which are responsive to Lewis basicity. The second class is pH indicators responding to Bronsted acidity/basicity. The third class is composed of vapochromic or solvatochromic dyes which respond to local polarity, and the last class is metal salts responding to redox reactions. They tested the sensor array with 19 toxic industrial chemicals (TICs) at their IDLH (immediately dangerous to life or health) dose. The sensor array was exposed to a diluted gas mixture for two minutes. It gave characteristic pattern for a given TCI resulting in good separation between 19 different analytes. They also examined quantitative analysis using their sensor array. They used principle component analysis (PCA)

and hierarchical cluster analysis (HCA). HCA resulted in very good separation of 19 TCIs with no misclassification or error out of 140 cases.

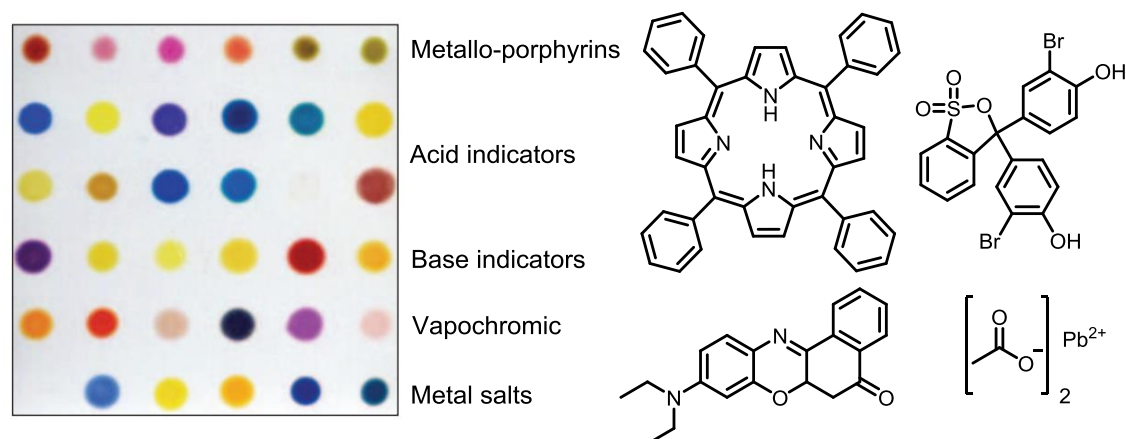


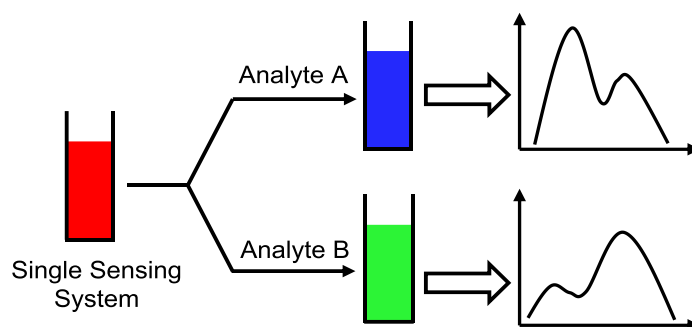
Figure 1.12 Dyes used in the sensor array. Adapted with permission from ref [263]. Copyright 2009, Nature Publishing Group.

Rotella and coworkers published a sensor array which was able to differentiate proteins in human serum using nanoparticles and green fluorescent proteins.²⁵⁸ It is a challenging task to differentiate proteins in human serum because it contains more than 20000 proteins. The sensor array is composed of green fluorescent proteins (GFP) and nanoparticles (NPs). It was able to detect the concentration of proteins in buffered solution and human serum. They selected five serum proteins including human serum albumin, immunoglobulin G, transferrin, fibrinogen and α -antitrypsin. The sensor array is based on the electrostatic interaction between GFP and NPs. They had 5 positively charged nanoparticles with different functionalities (NP1-NP5). Each modification has a specific capability in such a way that NP1 has a cationic charge featuring electrostatic interaction, NP2 and NP4 have the ability of hydrophobic interaction, NP3 can form hydrogen bonds, and NP5 has the ability of π - π interaction. GFP binds to nanoparticles with different binding constants and upon addition of a target protein to the solution, there is a competition between GFP and the target analyte for binding to NP. The binding modulates the fluorescence signal. The modulation depends on the binding constant of the target protein to the GFP and NP complex. The system was able to identify five of the serum proteins. And also it can distinguish a mixture of proteins and a single protein at different concentrations.

1.5.3 Single Sensing Systems

A sensor array contains multiple sensors in an array format. However, pattern-based sensing can also be achieved by using a single sensing system. The requirement is to have a characteristic pattern output upon addition of different analytes to the single sensing system. In this context, there are two approaches which are dynamic combinatorial library (DCL) sensors and single molecular probes.^{243, 274}

A DCL is a library of different building blocks that interact with each other resulting in the formation of thermodynamically controlled aggregates.^{243, 274-280} The interaction between the building blocks can have covalent character, such as metal-ligand bonds, or non-covalent character. The library products are sensitive to some external factors such as temperature, pH, and solvent. This kind of library (DCL) can be used as a pattern-based sensing system. Addition of an analyte to an equilibrated DCL-sensor solution disturbs the equilibrium resulting in a re-equilibration process. Each analyte causes different re-equilibrated products, which gives a characteristic spectral pattern for each analyte (Scheme 1.16). The data is analyzed using pattern recognition tools and analytes can be distinguished from each other qualitatively and quantitatively. DCL sensors are also used to differentiate pure analytes from their mixtures.

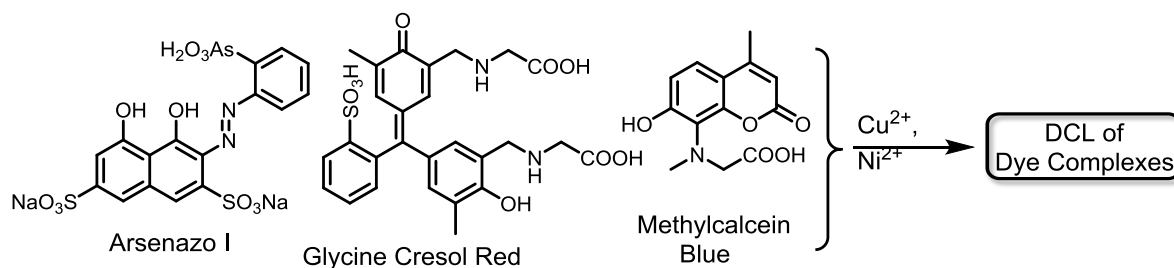


Scheme 1.16 Single sensing system for different analytes.

There are some advantages of DCL sensors over sensor arrays. First of all, there is no need to prepare many different solutions containing individual sensors (dyes, IDAs). There is only one solution in which all sensors are added and the same solution is used for all analytes.

Also, it is easy to prepare and optimize the DCL sensors in terms of selectivity and sensitivity by varying the building blocks or by changing the ratio of building blocks of the library.

Our group has published different studies about DCL sensors.^{240, 243, 246, 274, 281} The first study about a DCL sensor was published in 2005.²⁴⁰ A DCL of a metal-dye complex was used as a sensor to discriminate between closely related dipeptides. A library was formed by mixing the commercially available dyes arsenazo I, methylcalcein blue, and cresol red with CuCl_2 and NiCl_2 in CHES buffer solution at pH 8.4 (Scheme 1.17).



Scheme 1.17 Building blocks of the DCL sensor.

In buffered aqueous solution, stable complexes were formed between dyes and metals. They gave a characteristic UV-vis spectrum at different conditions indicating that a ground state complex was formed between dyes and metals. There is a dynamic equilibrium between the free dyes and metal ions in the DCL. Addition of an analyte disturbed the equilibrium, resulting a characteristic change of the UV-vis spectrum. This change was used to obtain information about the analyte. The system was able to distinguish between dipeptides including Val-Phe, Gly-Ala, His-Ala, Ala/His, Phe/Pro and Pro/Gly. The system also achieved a more challenging task: the differentiation of the very similar dipeptides Gly-Ala, Val-Phe, Ala-Phe, Phe-Ala and D-Phe-Ala, as well as dipeptides at different concentrations. The UV-vis data was analyzed with a pattern recognition tools. The resulting data showed that the DCL sensor was able to clearly separate these very closely related dipeptides.

In the second approach towards a single sensing system, there is one molecular probe that gives a characteristic pattern response upon addition of different analytes. The origin of the pattern for different analytes could come from different mechanisms such as energy transfer efficiencies between the units of the molecules,²⁸² or different aggregation products (change of conformation)^{72, 75, 283} for different analytes depending on the type of molecular probe.

Margulies' group has published a DCL-type molecular probe ('combinatorial fluorescent sensor') which has several recognition units containing four emission channels.²⁸² This molecular probe was able to identify many pharmaceuticals including the macrolide, cardiac glycoside, rifamycin and aminoglycoside drug families as well as drug concentrations and different drug compositions in urine samples. The molecular sensor has four different fluorophores (naphthalene, anthracene, dansyl and fluorenyl) with three boronic acid functionalities.

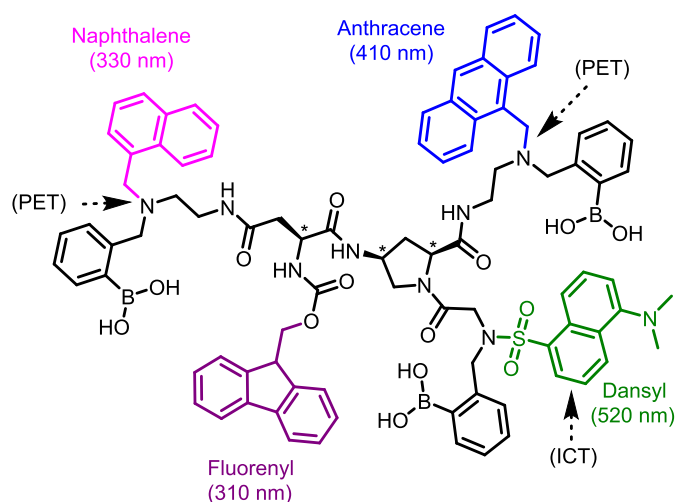
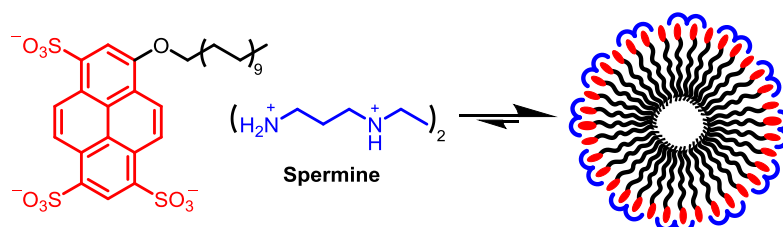


Figure 1.13 The structure of the 'combinatorial fluorescent sensor'.

The recognition system is based on different photophysical processes in the molecule. Boronic acids interact with the diol and four fluorescent molecules behave as receptors. They also transform the binding into a measurable optical signal. Binding of each analyte affected the photophysical communication between the fluorophores which are photo-induced electron transfer (PET), internal charge transfer (ICT) and fluorescence resonance energy transfer (FRET) processes. These processes created a characteristic pattern for each analyte. The system provides very good differentiation between analytes. The system was also tested to identify and quantify unknown drug samples (D-xylose and rifampycin) in urine. The molecular sensor was able to clearly identify and distinguish unknown drug samples at different concentrations with 97 % success.

Single sensing systems were used to analyze amines,^{72, 75, 209} drugs,²⁸² heavy metals,²⁸⁴ nucleotides,²⁸³ peptides,^{240, 243, 246} organic molecules,²⁸⁵ and thiols.²⁸⁶

2 Fluorescence Sensing of Spermine with a Frustrated Amphiphile



In this chapter, a fluorescence-based chemosensor is presented for the sensing of spermine. A charge-frustrated amphiphile composed of a pyrene-1,3,6-trisulfonate head group and an eicosane side chain was used as a fluorescence chemosensor. The sensor allows the detection of spermine down to the nanomolar concentration range with good selectivity over closely related biogenic amines such as spermidine.

This study was published in:²⁸⁷ “Fluorescence Sensing of Spermine with a Frustrated Amphiphile” Ziya Köstereli and Kay Severin, *Chem. Commun.*, **2012**, 48, 5841-5843.

2.1 Introduction

Spermine is a natural polyamine that is found in eukaryotic cells and body fluids (Figure 2.1).²⁸⁸⁻²⁹¹ It plays an important role in basic genetic processes such as DNA synthesis.²⁹² It also has a key role in cell migration, proliferation and differentiation in plants and animals.²⁹³ Elevated spermine concentrations in urine may be indicative of the presence of malignant tumors, and monitoring spermine in urine was proposed as a tool for early diagnosis and to evaluate the effectiveness of cancer therapy.²⁹⁴⁻²⁹⁶ Table 2.1 shows the spermine and spermidine concentrations in normal tissues, solid tumors and blood tumors.²⁹³

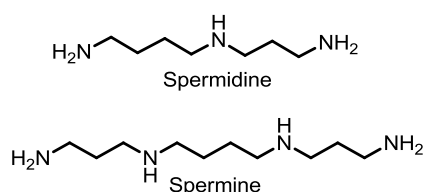


Figure 2.1 Molecular structures of spermine and spermidine.

Table 2.1 Spermine and spermidine concentrations in normal tissues, solid tumors and blood tumors

	[spermine]		[spermidine]	
	mg/g creatinine	μmol/L	mg/g creatinine	μmol/L
Normal	0.18±0.04	1.2	1.32±0.05	11.9
Solid tumors	1.23±0.24	7.93	2.90±0.40	26.0
Blood tumors	1.47±0.50	9.47	4.77±0.91	42.8

Spermine concentrations are typically determined by immunoassays, electrophoresis, or by chromatographic techniques.²⁹⁷⁻³⁰⁰ Optical methods based on fluorescence or UV-vis spectroscopy are interesting alternatives because measurements are fast and easy to perform. A number of studies on optical spermine chemosensors have been reported in recent decades.^{75, 85, 209, 301-305} Among these studies, the most sensitive systems described so far are BODIPY-decorated gold nanoparticles,³⁰² a montmorillonite-hydrogel composite material,³⁰⁴ a coumarin-based molecular probe,³⁰¹ and anthranyl-doped conjugated polyelectrolytes.⁸⁵

These sensors allow the detection of spermine in the micromolar concentration range. In all cases, a moderate selectivity for spermine over the closely related biogenic amine spermidine was observed. Selected examples will be discussed below.

A turn-on fluorescent chemosensor for polyamines was published by the Kim group.³⁰² In this study, gold nanoparticles were modified with citrate to give negatively charged nanoparticles. As pairs to the negatively charged nanoparticles, positively charged water soluble fluorescent BODIPY dyes were synthesized (Figure 2.2). Upon addition of Au-Nps to the BODIPY containing solution, there is a transition in the color of the particles from blue to red due to aggregation of Au-NPs with BODIPY dyes. As a result, the fluorescence of the dyes was completely quenched. Upon addition of spermine, the aggregates recovered the fluorescence of the BODIPY dyes as spermine binds to the NPs stronger than the dyes, and consequently, exchanges with the dyes on the surface of the NPs. As a result, dyes become free in solution with a fluorescent emission. This system enables selective detection of the spermine and spermidine over other structurally similar polyamines. Their system was also quite sensitive: they were able to detect low micromolar concentrations of spermine and spermidine.

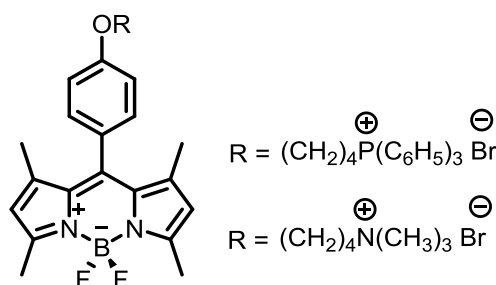


Figure 2.2 Cationic BODIPY derivatives for the sensing of spermine and spermidine.

Our group published a reaction-based probe for the sensing of biogenic amines in aqueous media (AP 1, Figure 2.3).³⁰¹ The probe was used in the presence of SDS micelles due to poor solubility. Addition of an amine to a solution containing AP 1 and SDS caused changes in the UV-vis and fluorescence spectra. Different responses were observed for five different amines including spermine, spermidine, cadaverine, putrescine, and histamine, among many other biogenic amines and amino acids. The most pronounced effect was observed for spermine and cadaverine. Further analysis gave information about possible products of the reaction between amines and the probe. It was concluded that the products A,

B, and C was formed by the reaction of the probe and the primary amines (Figure 2.3). The probe was found to be very sensitive: it was possible to detect biogenic amines in a micromolar concentration range.

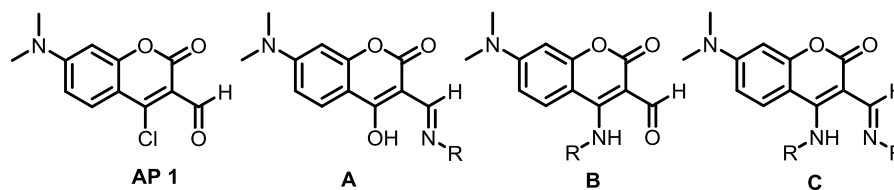


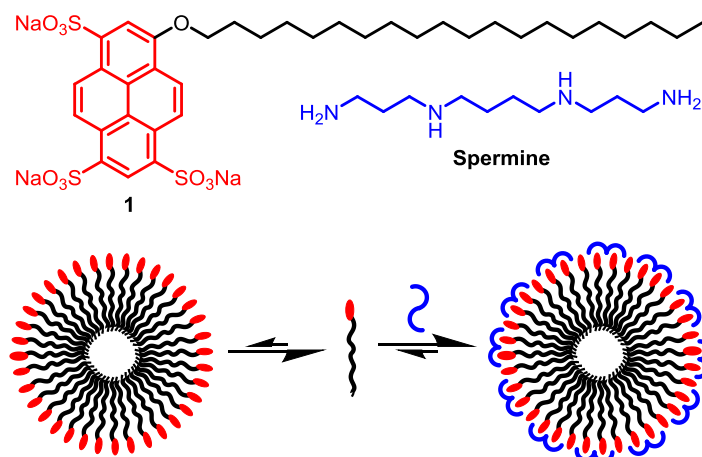
Figure 2.3 The amine probe (AP 1) and the reaction products: imine (A), enamine (B) and double condensation product (C).

Below, we describe a conceptually novel fluorescent sensor for spermine-based on a charge-frustrated amphiphile. The sensing system relies on the analyte-induced aggregation concept. The sensor allows the detection of spermine in the nanomolar concentration range with very good selectivity over other biologically relevant amines. In our system, we have used amphiphile **1** which was synthesized from the commercially available dye trisodium-8-hydroxypyrene-1,3,6-trisulfonate (HPTS). HPTS is a fluorescent dye with a high quantum yield (nearly one).³⁰⁶ By alkylation with 1-bromoeicosane, it can be converted into the amphiphile **1** (Scheme 2.1).³⁰⁷⁻³⁰⁹

2.2 Results and Discussion

The photophysical properties and the aggregation behavior of **1** have been studied by Sasaki and Murata.³⁰⁹ Despite its very long alkyl chain, **1** displays a rather large critical micelle concentration (cmc ~ 3 mM). The high cmc can be attributed to the electrostatic repulsion of the highly charged pyrene head group.³⁰⁹ Dye **1** can thus be regarded as a charge-frustrated amphiphile. Interestingly, the cmc of **1** can be reduced dramatically by addition of methylviologen, which forms a complex with the sulfonated pyrene.³⁰⁹ We hypothesized that a related substrate-induced aggregation of **1** could be used for sensing purposes, because

micellization of **1** results in pronounced attenuation of its fluorescence. Spermine appeared to be a suitable analyte to test this hypothesis. Under physiological conditions, spermine exists predominantly as a tetracation. It therefore has the potential to act as ‘charge-neutralizing glue’ facilitating the aggregation of **1** (Scheme 2.1).



Scheme 2.1 The presence of spermine promotes the micellization of the fluorescent amphiphile **1**.

When spermine was added to a buffered aqueous solutions (0.8 mM MOPS, pH 7.0) of dye **1**, the fluorescence emission at 430 nm ($\lambda_{\text{ex}} = 350$ nm) was reduced. Screening of different concentrations revealed that fluorescence quenching can be observed down to the nanomolar concentration range. The relative fluorescence intensity of solutions containing **1** (250 nM) and different amounts of spermine (0-400 nM) are depicted in Figure 2.4 and 2.5. Only 93 nM of spermine are required to induce a 50% reduction of the emission signal. The dynamic range of the sensing system can easily be adjusted by variation of the amphiphile concentration. Using 2.0 μM of dye **1**, it is possible to sense spermine in the high nanomolar concentration range, whereas 5.0 μM and 8.0 μM allow the detection of spermine in the low micromolar concentration range (Figure 2.6, see also Annex, Figures A1 - A6).

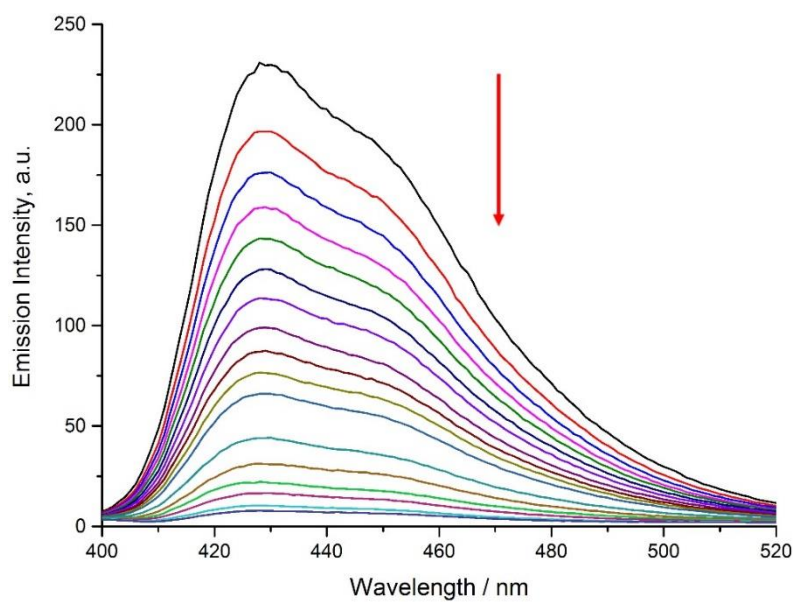


Figure 2.4 Fluorescence emission spectra (λ_{ex} : 350 nm) of buffered aqueous solutions (0.8 mM MOPS, pH 7) containing dye **1** (250 nM) and different amounts of spermine (0-400 nM).

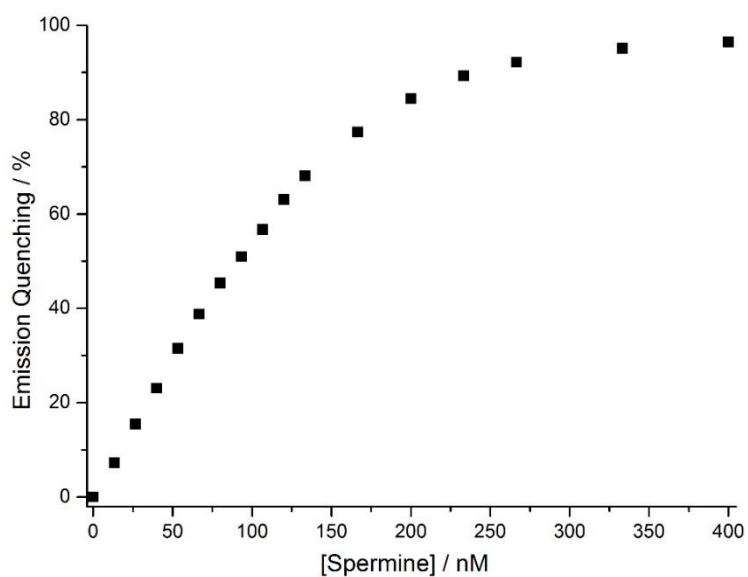


Figure 2.5 Fluorescence emission quenching ($\lambda_{\text{ex}} = 350$ nm, $\lambda_{\text{em}} = 430$ nm) of buffered aqueous solutions (0.8 mM MOPS, pH 7.0) containing dye **1** (250 nM) and different amounts of spermine (0-400 nM).

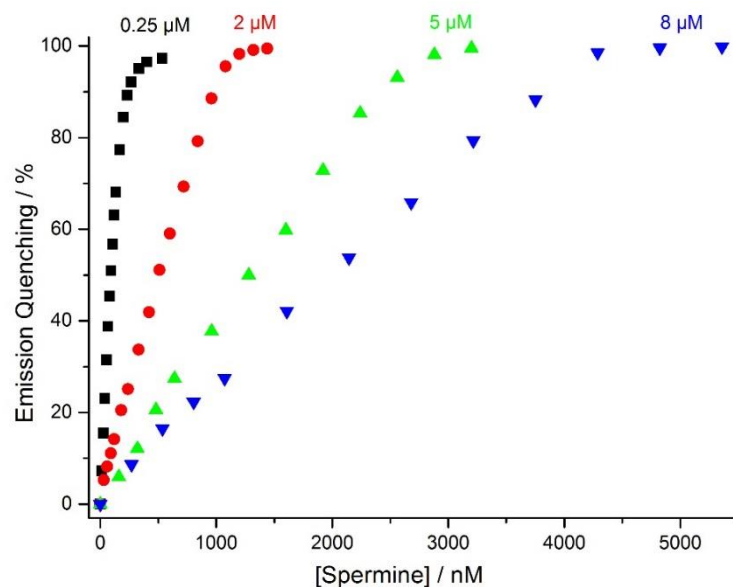


Figure 2.6 Fluorescence emission quenching ($\lambda_{\text{ex}} = 350 \text{ nm}$, $\lambda_{\text{em}} = 430 \text{ nm}$) of buffered aqueous solutions (0.8 mM MOPS, pH 7.0) containing dye **1** (black: 250 nM; red: 2.0 μM ; green: 5.0 μM ; blue: 8.0 μM) and different amounts of spermine.

There is 2:1 binding in this system because nearly complete fluorescence quenching is achieved at a dye **1** to spermine ratio of 2:1. This observation indicates that at saturation, each analyte molecule is bound to two dye molecules. Fitting of the fluorescence titration data obtained with dye **1** at 250 nM to an equation describing a 2:1 binding model³¹⁰ gave apparent binding constants of $K_1 = 2.1 \times 10^6 \text{ M}^{-1}$ and $K_2 = 5.1 \times 10^6 \text{ M}^{-1}$ (Figure 2.7).

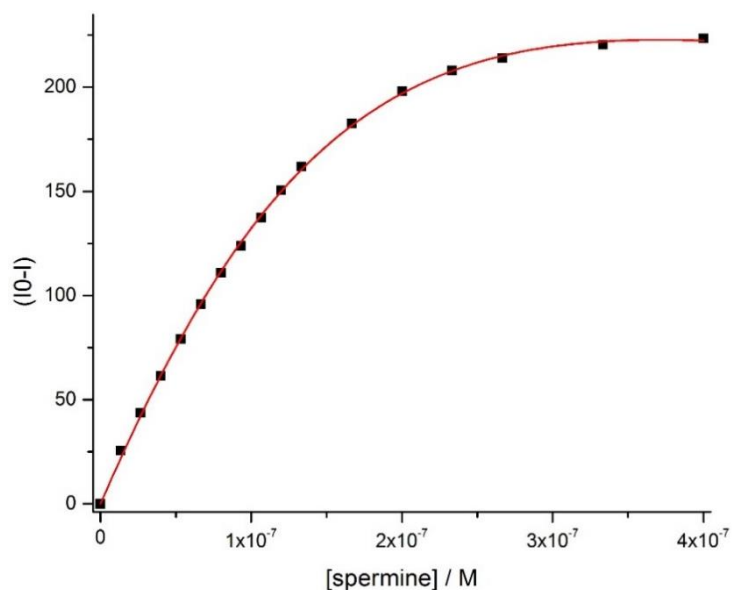


Figure 2.7 Fluorescence titration data of dye **1** (black) and the calculated binding isotherm (red). (I_0-I) is the difference in emission intensity.

The effect of ionic strength was investigated using buffered solutions containing dye **1** (8.0 μM), NaCl (0, 50 or 100 mM) and spermine (0 or 3.75 μM). Increasing the salt concentration from 0 to 100 mM led to an overall decrease of the fluorescence intensity. However, the spermine-induced fluorescence quenching was nearly constant with values between 88 and 97% (Table 2.2). Changing the pH of the solution from 7.0 to 8.0 had a small effect on the sensor response (Table 2.2).

Table 2.2 Fluorescence emission quenching ($\lambda_{\text{ex}} = 350 \text{ nm}$, $\lambda_{\text{em}} = 430 \text{ nm}$) under different conditions (E.Q. is Emission Quenching)

Solutions	I [a.u.] (no spermine/plus spermine)	E.Q. [%]
dye 1 (8 μM) + spermine (0 or 3.75 μM)	436/52	88
dye 1 (8 μM) + NaCl (50mM) + spermine (0 or 3.75 μM)	318/11	97
dye 1 (8 μM) + NaCl (100mM) + spermine (0 or 3.75 μM)	161/8	95
dye 1 (8 μM) + spermine (0 or 3.75 μM), pH 8	461/48	90

To verify that the amphiphilic nature of dye **1** is crucial for the sensor, we performed control experiments with the dye trisodium-8-methoxypyrene-1,3,6-trisulfonate containing a methyl group instead of an eicosane side chain. Even high concentrations of spermine (15 μM or 68 μM) resulted in only minor quenching of the fluorescence ($\leq 5\%$ or 12%). Furthermore, solutions containing **1** (66 μM) with and without spermine (0 or 66 μM) were analyzed by ^1H NMR spectroscopy (D_2O , phosphate buffer, $\text{pD} = 7.0$). In the presence of spermine, the signals of the aromatic protons of the pyrene head group vanished in line with aggregation-induced line broadening (Figure 2.8).

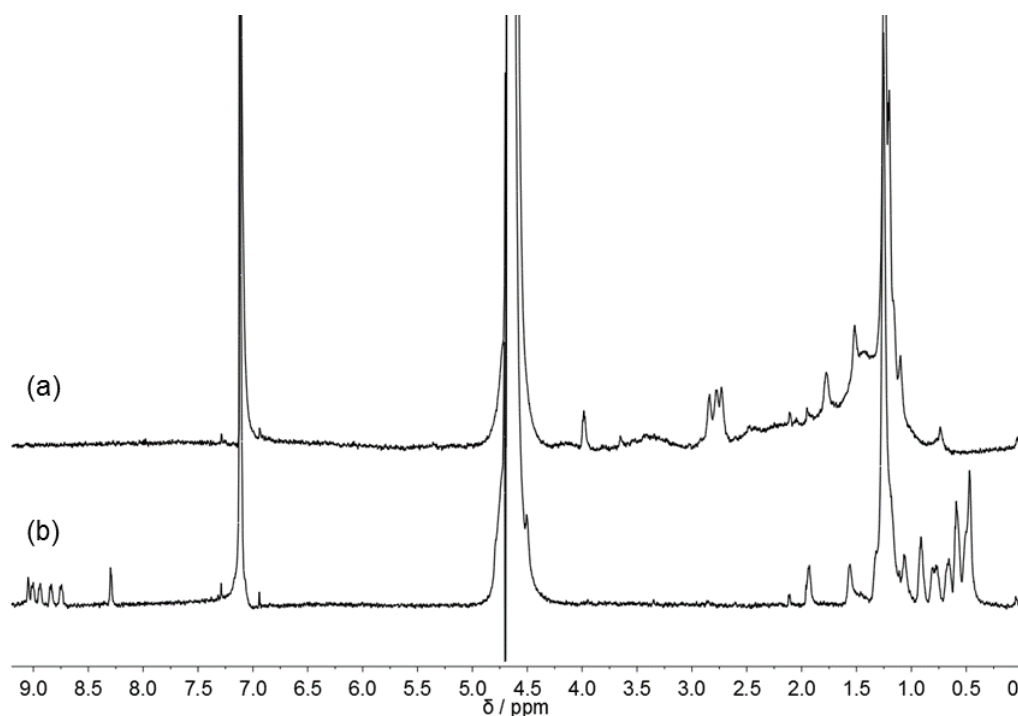


Figure 2.8 ^1H NMR spectra (600 MHz) of solutions (D_2O) containing: (a) dye **1** (66 μM) in the presence of equimolar amounts of spermine, or (b) only dye **1** (66 μM). The intense peaks at 4.7 and 7.2 ppm are due to water and chloroform (CDCl_3 was used as reference in a shigemi tube which was inserted). The spectra were acquired using a pulse sequence for suppression of the water peak.

We attempted to use dynamic light scattering (DLS) to observe spermine-induced aggregation of **1** but the measurements were not successful. Only data of poor quality were obtained, presumably due to the low solubility of spermine/**1** mixtures ($< 80 \mu\text{M}$). However, transmission electron microscopy images of stained samples on a carbon-coated copper grid revealed inhomogeneous aggregates with a size of $\sim 15 \text{ nm}$ and larger (see Annex, Figure A32).

Spermine-induced aggregation of **1** was further evidenced by using the hydrophobic dye Nile Red, which can be used as an indicator for micellation. In the presence of spermine (3.75 μM), the fluorescence emission intensity of solutions containing dye **1** (8.0 μM) and Nile Red was enhanced by 298 % (Figure 2.9).

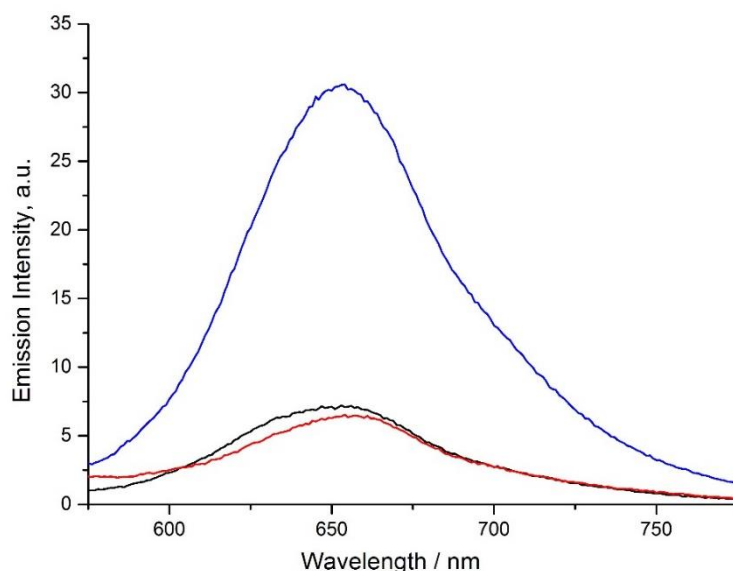


Figure 2.9 Fluorescence emission spectra (λ_{ex} : 520 nm) of buffered aqueous solutions (0.8 mM MOPS, pH 7) of Nile Red in the presence of dye **1** (red, 8.0 μM) and spermine (black, 0 μM and blue, 3.75 μM).

The selectivity of the sensor was examined using a variety of biologically relevant amines including the biogenic amines spermidine, tyramine, cadaverine, putrescine, and histamine, the amino acids histidine, cysteine, lysine, and phenylalanine, the neuroactive amines ephedrine and serotonin, as well as the simple diamines 1,3-diaminopropane and 1,2-diaminoethane. Solution containing dye **1** (250 nM) and the respective amine (200 nM) were analyzed by fluorescence spectroscopy. In all cases, the analyte-induced fluorescence quenching was small compared to what was observed for spermine (Figure 2.10). The largest response was found for spermidine. However, the selectivity for tetramine spermine (84% quenching) over the closely related triamine spermidine (16% quenching) is still very good. Due to the high quantum yield of **1**, it is even possible to distinguish solutions containing 200 nM spermine or spermidine by the naked eye. It is worthwhile to note that methylviologen lead to a rather low fluorescence quenching (17%). The selectivity of the sensing system was also examined at a higher concentration of dye **1** (2.0 μM). The sensor maintained a very

good selectivity over all amines except spermidine, which resulted in 48% fluorescence quenching (Figure 2.11).

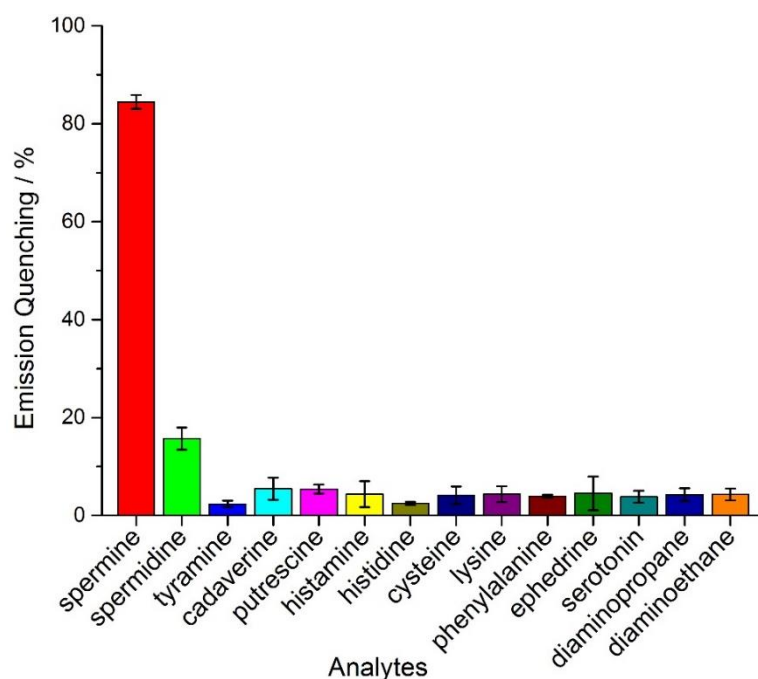


Figure 2.10 Fluorescence emission quenching ($\lambda_{\text{ex}} = 350 \text{ nm}$, $\lambda_{\text{em}} = 430 \text{ nm}$) of buffered aqueous solutions (0.8 mM MOPS, pH 7.0) containing dye **1** (250 nM) and different amines (200 nM). The values are averages from three independent measurements.

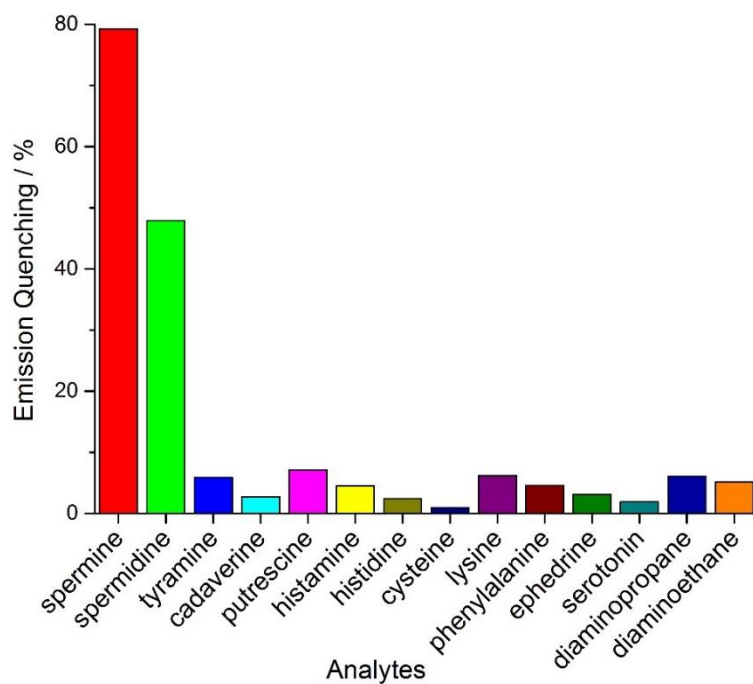


Figure 2.11 % Fluorescence emission quenching ($\lambda_{\text{ex}} = 350 \text{ nm}$, $\lambda_{\text{em}} = 430 \text{ nm}$) of buffered aqueous solutions (0.8 mM MOPS, pH 7.0) containing dye **1** (2.0 μM) and different amines (840 nM).

At the end, we have examined if we can use our system for the sensing of spermine in artificial urine. For this purpose, we prepared two solutions of artificial urine containing either 2.24 or 3.26 μM of spermine. For comparison, we made solutions of MOPS buffer containing the same concentrations of the analyte. The solutions were mixed with amphiphile **1** and fluorescence spectra were recorded. The values obtained for artificial urine were in good agreement with the values obtained for MOPS buffer solutions (difference < 8%, Figure 2.12). These results demonstrate that sensor **1** allows the sensing of spermine in a complex matrix.

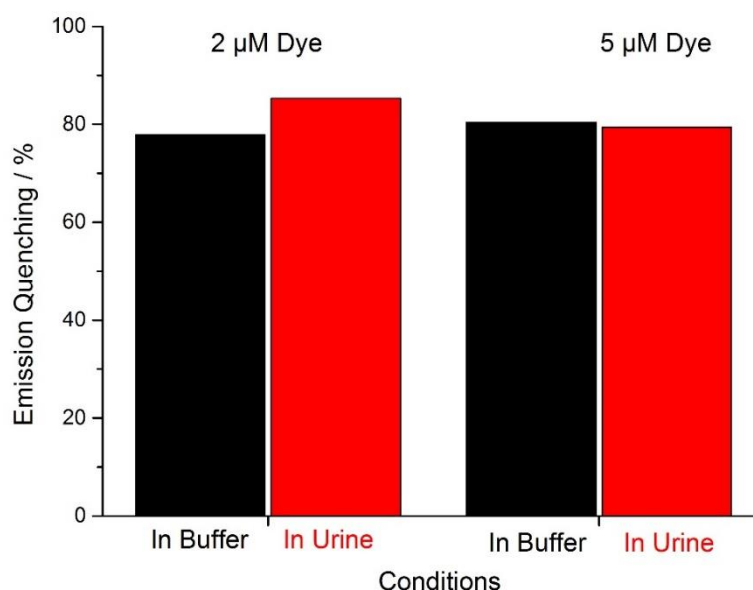


Figure 2.12 Fluorescence emission quenching ($\lambda_{\text{ex}} = 350 \text{ nm}$, $\lambda_{\text{em}} = 430 \text{ nm}$) of solutions containing dye **1** (2.0 μM and 5.0 μM) and spermine (2.24 μM and 3.26 mM) in artificial urine or buffer (0.8 mM MOPS, pH 7.0).

2.3 Conclusion

In summary, we have described a conceptually new chemosensor for the biogenic amine spermine. The sensor is based on a charge-frustrated amphiphile with a highly fluorescent head group. There is analyte-induced aggregation upon addition of spermine and it results in pronounced fluorescence quenching. The sensor displays remarkable sensitivity: the

detection of spermine is possible down to the low nanomolar concentration range. Furthermore, it displays a very good selectivity over spermidine and other biological relevant amines. Preliminary tests with artificial urine are evidence that sensing is also possible in a complex matrix.

2.4 Experimental

All chemicals and solvents were purchased from standard suppliers and used without further purification. Stock solutions were prepared with bidistilled water and were stored at 4 °C. For phosphate buffer solutions (100 mM phosphate buffer, pD 7.0), appropriate amounts of K_2HPO_4 and KH_2PO_4 were dissolved in D_2O . MOPS buffer (0.8 mM MOPS buffer, pH 7.0) was prepared by dissolving 3-(N-morpholino)propanesulfonic acid in water. HCl, DCl and NaOH solutions were used to adjust the pH of the buffers. Fluorescence measurements were performed on a Varian Cary Eclipse fluorescence spectrophotometer at room temperature. ^1H NMR spectra were recorded on a Bruker Advance DPX 400 instrument or a Bruker Advance DRX 600 instrument at 25 °C. TEM imaging was performed with a FEI Tecnai G2 F30. High resolution mass spectra were recorded with a waters Q - TOF Ultima (ESI-TOF) instrument.

Stock solutions of dye **1** (trisodium 8-eicosyloxyppyrene-1,3,6-trisulfonate), MPTS (trisodium 8-methoxyppyrene-1,3,6-trisulfonate) and the analytes were prepared in MOPS buffer (0.8 mM, pH 7) and kept at 4 °C. For the fluorescence titration experiments, solutions containing different concentration of dye **1** (0.25, 2, 5, 8 μM) were prepared in quartz cuvettes by mixing aliquots of a stock solution of dye **1** with buffer (final volume of 1.5 mL). The solutions were equilibrated for 2 h before starting the titration. For each titration, different stock solutions of the analyte spermine were used (10 μM for 0.250 nM dye, 45 μM for 2 μM dye, 120 μM for 5 μM dye, 201 μM for 8 μM dye). Appropriate amounts of analyte were added to the solution of dye **1** and a fluorescence spectrum was recorded after 5 min (λ_{ex} : 350 nm, λ_{em} : 430 nm). Dilution effects were neglected as the total volume of analyte solution that was added did not exceed 50 μL . It should be noted that plastic cuvettes should be avoided

when using low dye concentrations. We encountered problems of reproducibility when using plastic cuvettes, probably because the dye sticks to the walls.

Binding constants were calculated using fluorescence titration data obtained with dye **1** (0.25 μM) and different amounts of spermine. The data was fitted to an equation describing a 2:1 binding model (Figure 2.7).³¹⁰ The resulting binding constants were $K_1 = 2.1 \times 10^6 \text{ M}^{-1}$ and $K_2 = 5.1 \times 10^6 \text{ M}^{-1}$.

For selectivity tests, stock solutions (10 μM) of the analytes were prepared in MOPS buffer (0.8 mM, pH 7). An aliquot of analyte stock solution (30 μL) was added to a solution of dye **1** (200 nM, $V_{\text{total}} = 1.5 \text{ mL}$) in a quartz cuvette. A fluorescence spectrum was recorded 5 min after addition of the analyte (λ_{ex} : 350 nm, λ_{em} : 430 nm). Selectivity was also tested at higher concentration of dye **1** (2.0 μM) and analytes (840 nM). The results are depicted in Figure 2.9 and Figure 8.8.

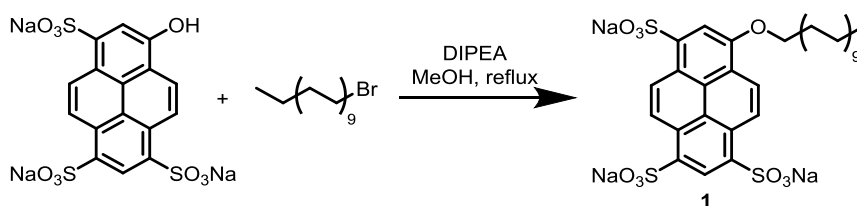
Sensitivity of the system was also tested in artificial urine. For this purpose, artificial urine was prepared as described in the literature.³⁰⁴ It contained potassium dihydrogen phosphate (7.0 mM), dipotassium hydrogen phosphate (7.0 mM), sodium sulfate (10 mM), magnesium sulfate (2.0 mM), lactic acid (1.1 mM), citric acid (2.0 mM), calcium chloride (2.5 mM), sodium chloride (90 mM), urea (170 mM), sodium bicarbonate (25 mM), and ammonium chloride (25 mM). All compounds were dissolved in bi-distilled water. The pH of the solution was 6.8. Stock solutions of dye **1** (50 μM) and spermine (120 μM) in MOPS buffer (0.8 mM, pH 7) were employed. An aliquot of the dye stock solution (60 μL) was added to artificial urine ($[\text{1}]_{\text{final}} = 2.0 \text{ }\mu\text{M}$, $V_{\text{total}} = 1.5 \text{ mL}$) in a quartz cuvette, and a fluorescence spectrum was recorded after equilibration for 20 min. Subsequently, an aliquot of the spermine stock solution was added (28 μL , $[\text{spermine}]_{\text{final}} = 2.24 \text{ }\mu\text{M}$), and a fluorescence spectrum was recorded after equilibration for 5 min (λ_{ex} : 350 nm, λ_{em} : 430 nm). For measurements with a total dye concentration of 5 μM , the amounts of added dye and spermine were increased accordingly. For comparison, measurements with identical dye and spermine concentrations were performed in MOPS buffer instead of artificial urine. The results are depicted in Figure 2.12.

Control experiments with trisodium 8-methoxypyrene-1,3,6-trisulfonate (MPTS): an aliquot of a stock solution of spermine was added to a solution of MPTS in MOPS buffer (0.8 mM MOPS, pH 7, $[\text{spermine}]_{\text{final}} = 80 \text{ }\mu\text{M}$, $[\text{MPTS}]_{\text{final}} = 8 \text{ }\mu\text{M}$). A fluorescence spectrum was recorded after 5 min (λ_{ex} : 370 nm, λ_{em} : 430 nm).

Characterization of the aggregates were studied using different methods including Nile Red, TEM and NMR. For the Nile Red study, a stock solution of the dye Nile Red (1.0 mM) was prepared in ethanol. An aliquot of this stock solution ($[\text{Nile Red}]_{\text{final}} = \sim 8 \mu\text{M}$, 12 μL) was pipetted in a vial. The ethanol was removed by evaporation. Subsequently, aliquots of stocks solutions of dye **1** ($[\mathbf{1}]_{\text{final}} = 8 \mu\text{M}$, 240 μL in 0.8 mM MOPS, pH 7) and spermine ($[\text{spermine}]_{\text{final}} = 0$ or 3.75 μM , 0 or 28 μL in 0.8 mM MOPS, pH 7) were added and the volume was completed to 1.5 mL with MOPS buffer (0.8 mM, pH 7). The vial was sonicated for 10 min and the resulting mixture was filtered. A fluorescence spectrum of the clear solution was recorded (λ_{ex} : 520 nm). The results are depicted in figure 2.9. The increased fluorescence emission in the presence of spermine is indicative of micelle formation.

Diluted sample were placed on a Lacey carbon coated 300 mesh copper grid for the TEM measurement. Uranyl acetate solution (2 wt%) was used for staining. 20 μL of a solution containing dye **1** and spermine ($[\mathbf{1}] = [\text{spermine}] = 66 \mu\text{M}$, 0.8 mM MOPS, pH 7) was put on a parafilm sheet. The grid was placed on the top of the drop with its upper side down and kept there for 2 min. Then, 20 μL of a uranyl acetate solution (2 wt%) was put on a parafilm sheet. The grid was placed on the top of the drop with its upper side down and kept there for 5 min. Stained grids were dried in the fume hood at room temperature.

The effect of aggregation was also seen in NMR. A ^1H NMR spectrum (600 MHz) of a solution of dye **1** (66 μM) in D_2O was recorded. A second spectrum was recorded shortly after addition of an aliquot of a spermine stock solution ($[\text{spermine}]_{\text{final}} = 66 \mu\text{M}$). The results are depicted in figure 2.8.

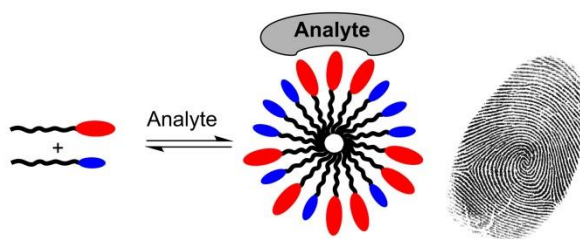


Trisodium 8-eicosyloxy pyrene-1,3,6-trisulfonate (**1**) was synthesized in a similar fashion as described in the literature:³⁰⁹ 1-bromoeicosane (2.21 g, 6.11 mmol) and *N,N*-diisopropylethylamine (630 μL , 3.81 mmol) were added to a refluxing solution of trisodium 8-hydroxypyrene-1,3,6-trisulfonate (400 mg, 763 μmol) in MeOH (50.0 mL). The reaction mixture was heated under reflux with stirring for 6 days. The mixture was then cooled to room temperature, filtered, and concentrated under reduced pressure. The resulting solid was

washed several times with diethyl ether. Further purification was achieved by column chromatography (SiO₂; eluent: NH₄OH : IPA - 1 : 2) to give dye **1** as a yellow solid (184 mg, 0.229 mmol, 30%).

¹H-NMR (400 MHz, CD₃OD): δ = 0.92 (t, J = 6.8 Hz, 3 H, CH₃), 1.20-1.48 (m, 30 H, CH₂), 1.52 (m, 2 H, CH₂), 1.70 (p, J = 7.5 Hz, 2 H, CH₂), 2.08 (p, J = 7.0 Hz, 2 H, CH₂), 4.47 (t, J = 6.4 Hz, 2 H, CH₂), 8.42 (s, 1 H, CH_{arom}), 8.68 (d, J = 9.6 Hz, 1 H, CH_{arom}), 9.12 (d, J = 9.6 Hz, 1 H, CH_{arom}), 9.20 (d, J = 9.6 Hz, 1 H, CH_{arom}), 9.26 (d, J = 9.6 Hz, 1 H, CH_{arom}), 9.40 (s, 1 H, CH_{arom}); ESI-MS calcd. for C₃₆H₄₈S₃O₁₀ [(M-3Na+H)⁻²] m/z = 368.1210 found 368.1205.

3 Pattern-Based Sensing of Aminoglycosides with Fluorescent Amphiphiles



In this chapter, we describe a conceptually new ‘one-cuvette’ sensing system for the pattern-based analysis of aminoglycoside antibiotics. A mixture of two amphiphiles with fluorescent head groups was used as a sensing ensemble. In buffered aqueous solution, the amphiphiles form a dynamic mixture of micellar aggregates. In the presence of aminoglycosides, the relative amount and the composition of the micelles is modified. The re-equilibration of the system is analyte-specific, and characteristic fluorescence spectra are obtained for different aminoglycosides. Accurate differentiation in the low micromolar concentration range can be achieved by a principal component analysis of the spectral data.

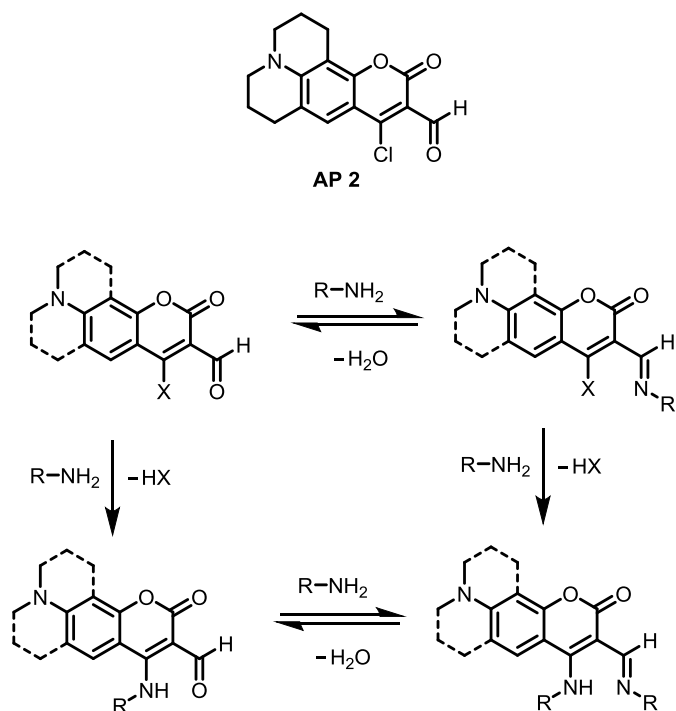
This work was published in:³¹¹ “Pattern-based sensing of aminoglycosides with fluorescent amphiphiles” Ziya Köstereli, Rosario Scopelliti and Kay Severin, *Chem. Sci.*, **2014**, 5, 2456-2460.

3.1 Introduction

Aminoglycosides are organic molecules which possess amino-modified sugars in their structure. They have biological significance because they are antibacterial agents and they play an important role in the inhibition of protein synthesis in bacteria.³¹² They are polycationic compounds at neutral pH. Sensing of such analytes is still a challenging task because of their complex structures. Pattern-based sensing systems can be used to sense these kinds of complex analytes.

As we have mentioned in general introduction chapter, pattern recognition tools allows an ensemble of differential but non-selective chemosensors to be converted into remarkably powerful sensing systems.³¹³⁻³¹⁸ Our group has used sensor arrays and single sensing systems in this context to sense different classes of analytes and analyte mixtures.

In one of the studies published by our group, a coumarin-based molecular probe (AP **2**, Scheme 3.1) was used for the pattern-based sensing of the aminoglycosides antibiotics paromomycin, kanamycin A and B, gentamicin, neomycin, and apramycin.³¹⁹ The reaction of the probe AP **2** with antibiotics gave different covalent products. Each product has a characteristic color, resulting in a complex UV-vis spectrum. The PCA analysis of the UV-vis data enabled identification of the closely related antibiotics. The system also enabled quantitative and purity information about analytes to be obtained.



Scheme 3.1 The structure of probe AP 2, and different covalent adducts with amine containing analytes.

In this chapter, we describe a conceptually new 'one-cuvette' sensing system (single sensing system) for the pattern-based analysis of aminoglycosides. We use an analyte-induced micellization process to form a pattern-based sensing system. Characteristic fluorescence spectra are obtained by analyte-induced aggregation of fluorescent amphiphiles. We selected seven aminoglycosides as analytes for this study (Figure 3.1).

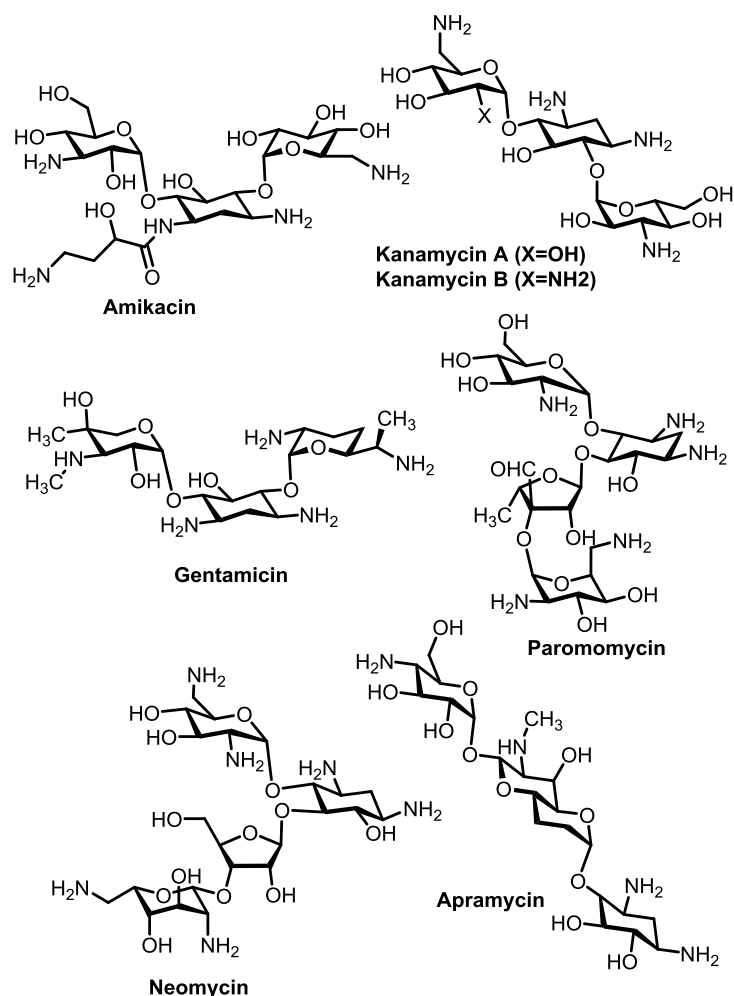
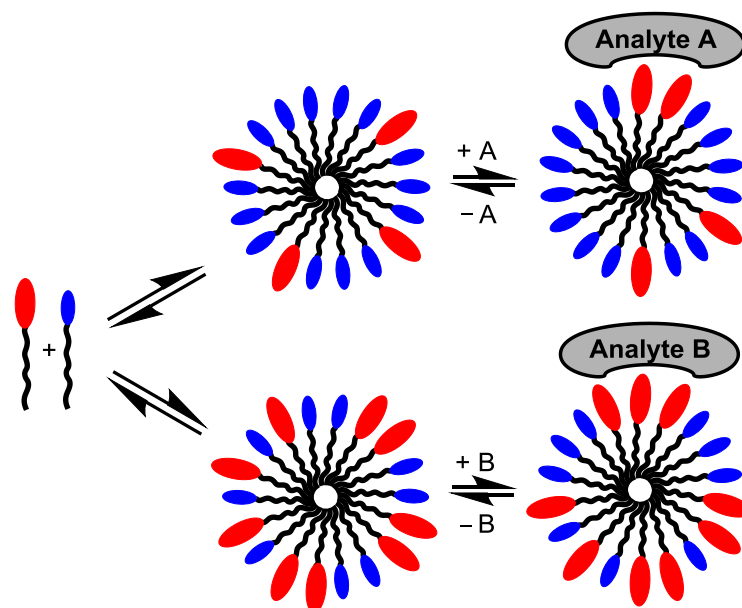


Figure 3.1 The aminoglycoside analytes used in this study.

3.2 Results and Discussion

In chapter 2, we have shown that a fluorescent amphiphile with a sulfonated pyrene head group can be used as a sensitive sensor for the biogenic amine spermine.²⁸⁷ Interaction of the negatively charged dye with the polycation spermine results in charge compensation and micelle formation. The latter is associated with fluorescence quenching, which allows the quantification of spermine down to the nanomolar concentration range.²⁸⁷ We hypothesized that an analyte-induced micellization process could also be used for the creation of a pattern-based sensing system (Scheme 3.2).



Scheme 3.2 Two amphiphilic dyes can form micellar aggregates. The relative amount and the composition of the micelles is influenced by the nature of the analyte. The different equilibrium distribution for each analyte is reflected by a characteristic fluorescence spectrum.

In order to obtain a complex, information-rich spectrum, two or more amphiphiles with distinct fluorescent properties would be required. We expected that a mixture of these dyes could result in the formation of a dynamic combinatorial library (DCL)^{278, 280, 320-323} of micellar aggregates. Therefore, we could observe a characteristic fluorescence spectrum, if the total amount and/or the composition of these micelles is affected by an analyte.

To examine the feasibility of such an approach, we synthesized the amphiphilic dyes **2** and **3** (Figure 3.2). Dye **2** contains a disulfonated naphthalene head group and a hexadecane side chain. It was obtained in two steps by alkylation of naphthalene-2-ol, followed by sulfonation. Dye **3** has a monosulfonated BODIPY head group and an heptadecane side chain. We achieved its synthesis in two steps following standard procedures.³²⁴⁻³²⁵

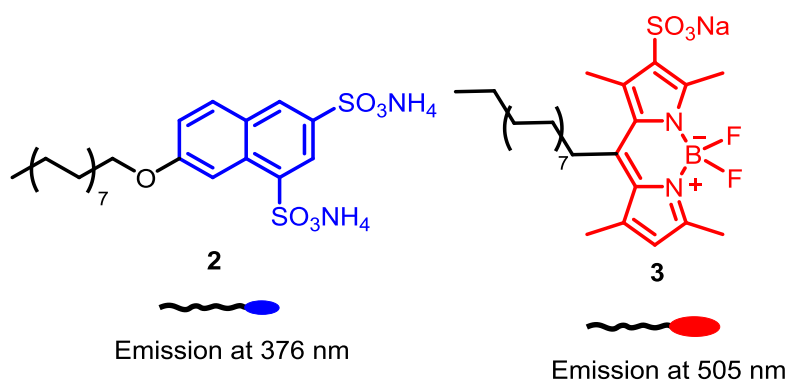


Figure 3.2 Structures and optical properties of the dyes **2** and **3**.

The amphiphiles **2** and **3** were characterized by NMR spectroscopy, mass spectrometry and fluorescence spectroscopy. In addition, dye **2** was characterized by single crystal X-ray diffraction (Figure 3.3). In the solid state, the hexadecane side chains show a regular zig-zag conformation, pointing away from the naphthalene chromophore (Figure A58). As expected, one can observe hydrogen bonds between the ammonium ions and the sulfonate groups.

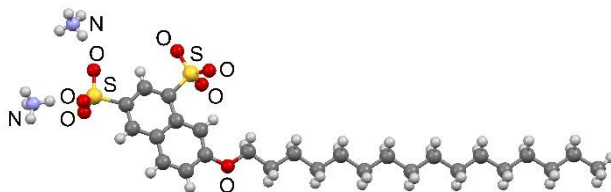


Figure 3.3 Molecular structure of dye **2** in the crystal.

Dye **2** displays good solubility (~ 2.4 mM) in water (10 mM MOPS, pH 7.0). The solutions are fluorescent, with an emission maximum at 376 nm ($\lambda_{\text{ex}} = 335$ nm, Figure A7). Dye **3** is less soluble than **2**, but low micromolar concentrations, as required for sensing applications, can be achieved without problems. Buffered aqueous solutions of **3** show a broad emission with a maximum at 505 nm ($\lambda_{\text{ex}} = 460$ nm, (Figure A8). Under a UV-vis light, solutions of **2** appear blue, whereas solutions of **3** are yellow. Using two dyes with distinct fluorescence properties was part of our design strategy, because the sensing ensemble would show emission over a broader spectral range. One should also note that there is some overlap between the emission spectrum of **2** and the absorption spectrum of **3** (Figure 3.4). As a consequence, fluorescence resonance energy transfer (FRET) from **2** to **3** is possible. The efficiency of a FRET process is strongly distance dependent. Analyte-induced micellization and/or compositional re-organization of a micelle (as schematically depicted in Scheme 3.2) would alter the FRET efficiency. The resulting spectral changes can potentially contribute to the differentiation of analytes.

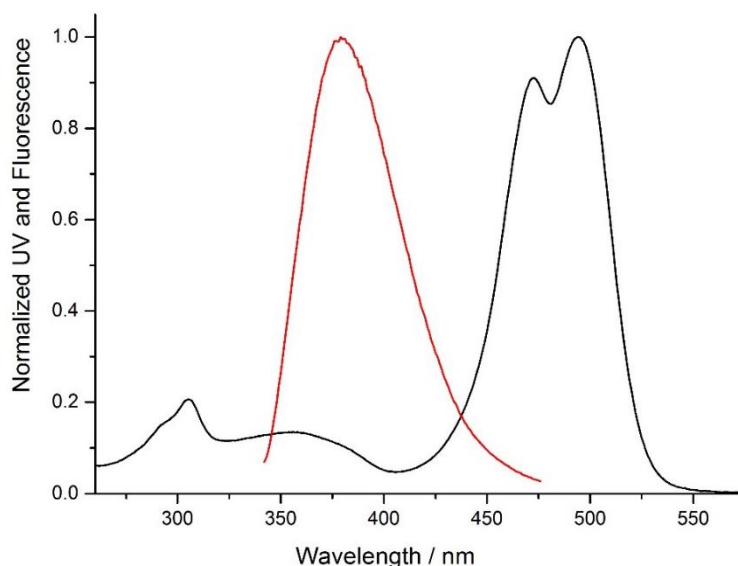


Figure 3.4 Normalized UV-vis spectrum of a buffered aqueous solution (10 mM MOPS, pH 7.0) containing dye **3** (black line, $[3] = 10 \mu\text{M}$), and normalized fluorescence spectrum of a solution containing dye **2** (red line, $[2] = 10 \mu\text{M}$, λ_{ex} : 335 nm).

The aggregation of dye **2** and **3** in buffered aqueous solution (10 mM MOPS, pH 7.0) was investigated using fluorescence spectroscopy, transmission electron microscopy (TEM) and dynamic light scattering (DLS). We observed a red shift for the emission maxima of **2** and **3** upon increasing the concentration (Figure 3.5). Using this shift, a critical micelle concentration (cmc) of 13 μM was determined for dye **2**, whereas a value of 5 μM was observed for dye **3** (Figure 3.6). The lower cmc of **3** (5 μM) as compared to that of **2** (13 μM) can be explained by the reduced negative charge of the head group and longer alkyl side chain. We observed spherical inhomogeneous aggregates with a size of 8-30 nm in TEM images of stained samples of dye **2** on a carbon-coated copper grid (Figure A35). Unfortunately, we could not observe aggregation of dye **3** by TEM due to low solubility of dye **3** in water. DLS measurements of buffered aqueous solutions revealed the presence of polydisperse aggregates with a size of ~ 6 nm for dye **2** (1.0 mM) and a size of ~ 12 nm for dye **3** (50 μM) (Figure A 36 and A 37).

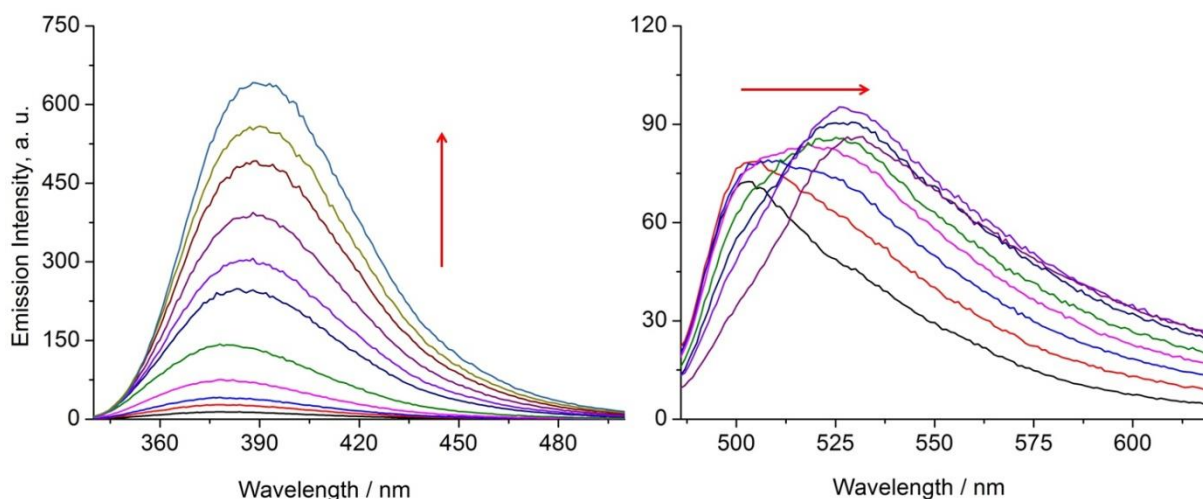


Figure 3.5 Fluorescence emission spectra of buffered aqueous solutions (10 mM MOPS, pH 7.0) containing dye **2** (left, λ_{ex} : 335 nm, 1-256 μM) and **3** (right, λ_{ex} : 460 nm, 1-45 μM). The red arrows indicate the changes with increasing concentration.

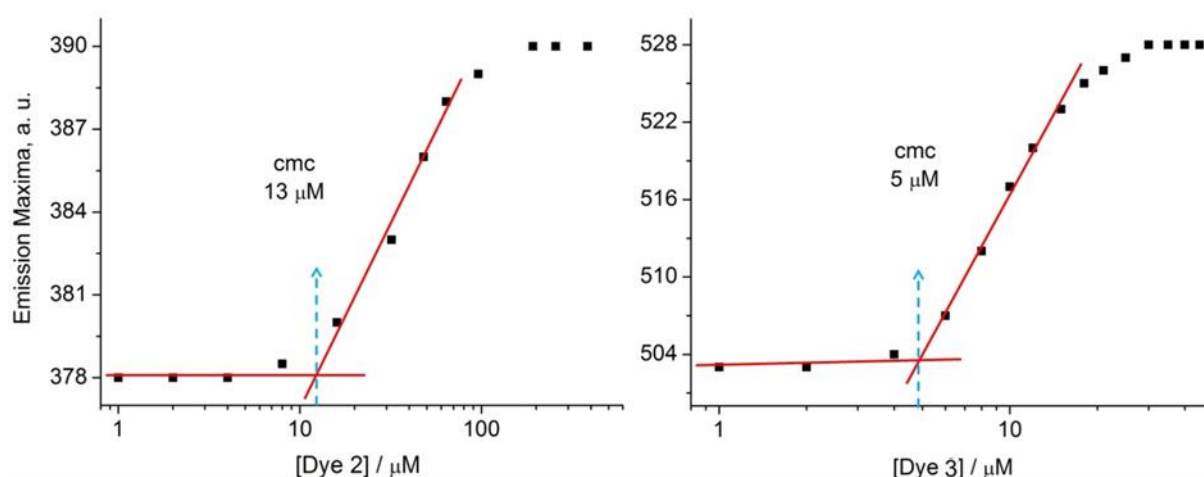


Figure 3.6 Fluorescence emission maxima of buffered aqueous solutions (10 mM MOPS, pH 7.0) containing increasing amounts of dye **2** (λ_{ex} : 335 nm, 1-512 μM) or **3** (λ_{ex} : 460 nm, 1-45 μM) and critical micelle concentration (cmc) of dye **2** and **3**. The graphs are plotted on a logarithmic scale.

We have also recorded the UV-vis spectra of solutions containing dye **3** (30 μM) and different amounts of dye **2** (0-30 μM). The absorption of the BODIPY chromophore was found to depend on the concentration of dye **2** (Figure 3.7), indicating an interaction between the two dyes in solution. Taken together, these data show that both dyes form micellar aggregates in the low micromolar concentration range. Importantly, micellization is associated with a change of the optical properties, which is of importance for sensing applications.

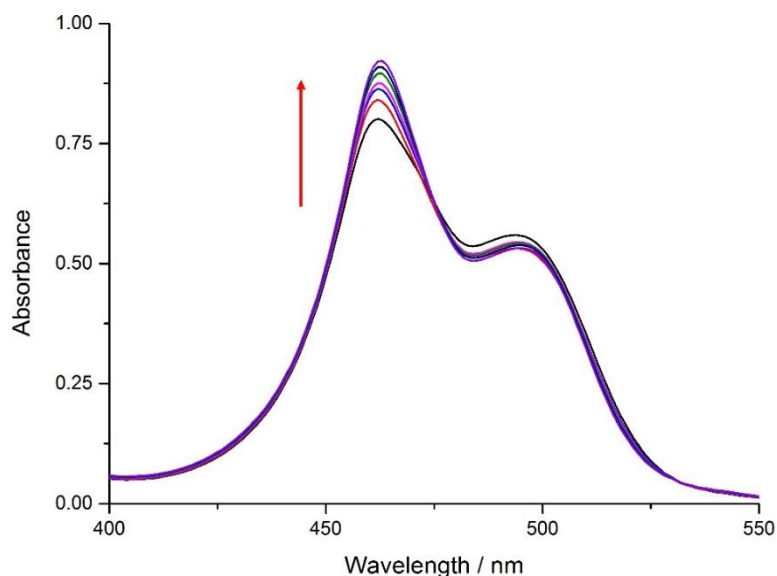


Figure 3.7 UV-vis spectra of buffered aqueous solutions (10 mM MOPS, pH 7.0) containing dye **3** (30 μ M) and different amounts of dye **2** (0-30 μ M). The red arrow indicates the changes with increasing concentration of dye **2**.

Next, we have examined whether a mixture of dye **2** and **3** would be suited for the pattern-based analysis of the aminoglycoside antibiotics amikacin, kanamycin A and B, paromomycin, neomycin, apramycin, and gentamicin (Figure 3.1).^{234, 326} These analytes were selected because of their biological significance, and because they are polycationic compounds at neutral pH. The positive charges of the analytes were expected to induce a multivalent interaction with the polyanionic micellar aggregates.³²⁷

A concentration of 4 μ M was chosen for dye **2**. This value is slightly lower than the cmc of **2**, allowing an analyte-induced aggregation process to occur. The concentration of dye **3** was set higher (30 μ M) because of its lower fluorescence compared to that of **2**. Solutions containing a mixture of **2**, **3** and the respective aminoglycoside (10 μ M) were analyzed by fluorescence spectroscopy. The results for five analytes are shown in Figure 3.8, and the remaining two spectra are depicted in Annex, Figure A 10 and A 11. In all cases, we observed two main emission maxima around 375 and 540 nm. The emission at 375 nm can be attributed to dye **2**, whereas the emission at 540 nm is caused by the BODIPY fluorophore of dye **3**. Compared to the emission of the mixture in the absence of aminoglycosides, one can observe an analyte-induced quenching effect for the band of **2**, and a shift towards longer wavelengths for the band of **3**. These observations suggest that the analytes promote micellization. Importantly, all seven analytes give rise to a characteristic fluorescence spectrum. The differences are apparent when comparing the results obtained for paromomycin, kanamycin

B, neomycin, and gentamicin. The sample containing neomycin (Figure 3.8, blue curve) and gentamicin (Figure 3.8, pink curve) show a very similar emission at 375 nm, but the curves are well separated in the region around 540 nm. The opposite trend is observed for paromomycin (Figure 3.8, black curve) and kanamycin B (Figure 3.8, red curve). In addition, there are more subtle differences in the shape of the curves of the different analytes.

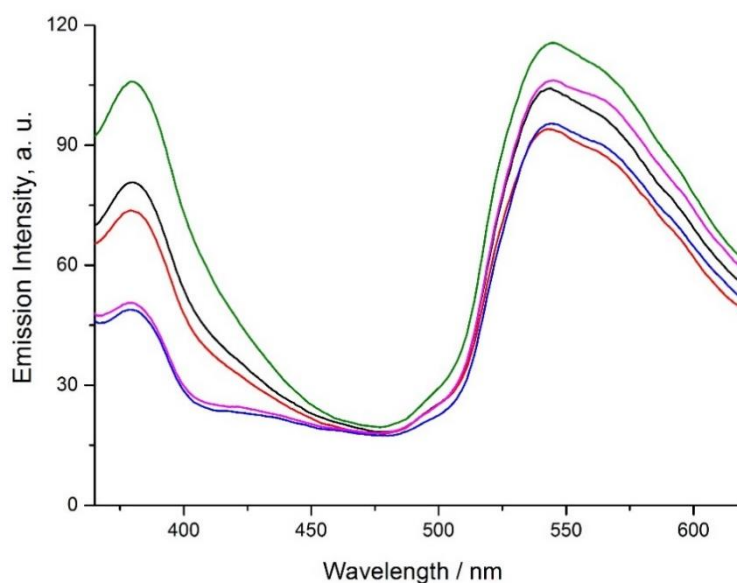


Figure 3.8 Fluorescence spectra (λ_{ex} : 335 nm) of solutions containing a mixture of dye **2** and **3** ($[\mathbf{2}] = 4 \mu\text{M}$; $[\mathbf{3}] = 30 \mu\text{M}$) and the analytes paromomycin (black line), kanamycin B (red line), neomycin (blue line), gentamicin (pink line), or apramycin (green) ($[\text{analyte}] = 10 \mu\text{M}$; 10 mM MOPS, pH 7.0).

Five independent measurements were performed for each analyte. The fluorescence data were then analyzed using the statistics software SYSTAT 11. A stepwise variable selection algorithm was used to select a sub-set of four relevant wavelengths (380, 515, 545, and 615 nm). The emission values at these wavelengths (Figure 3.9) were used as an input for a principal component analysis (PCA). The corresponding score plot shows that the sensing system is able to distinguish the seven aminoglycosides at a concentration of 10 μM (Figure 3.10). The same data set was used to perform a linear discriminant analysis (LDA) in combination with a jack knife validation procedure. When 50 % of data set was randomly omitted and the remaining data set was used as a training set for the LDA, the omitted data was classified correctly in all cases (100%).

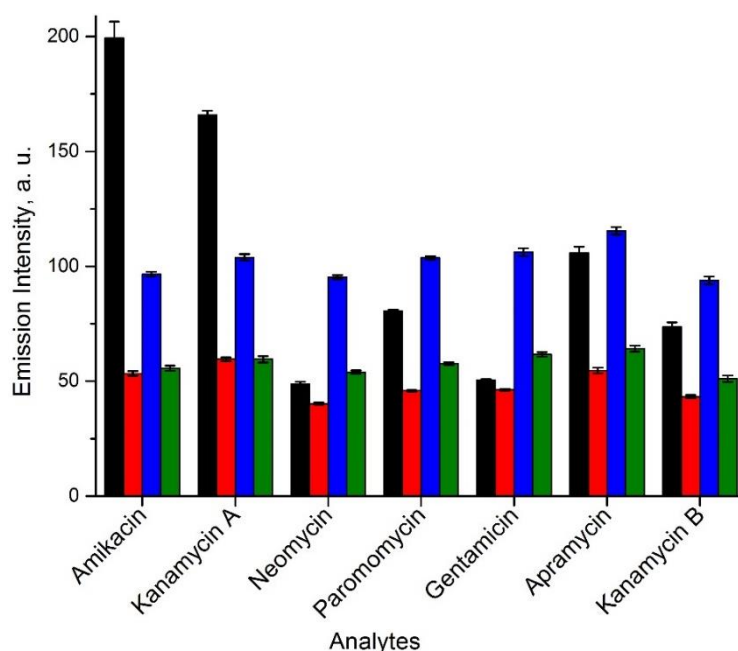


Figure 3.9 Fluorescence emission intensities (λ_{ex} : 335 nm) at 380 nm (black), 515 nm (red), 545 nm (blue), and 615 nm (green) of solutions containing a mixture of dye **2** and **3** ($[\mathbf{2}] = 4 \mu\text{M}$; $[\mathbf{3}] = 30 \mu\text{M}$) and the analytes paromomycin (black), kanamycin B (red), neomycin (blue), gentamicin (green), or apramycin (green) ($[\text{analyte}] = 10 \mu\text{M}$; 10 mM MOPS, pH 7.0). The values represent averages of five independent measurements.

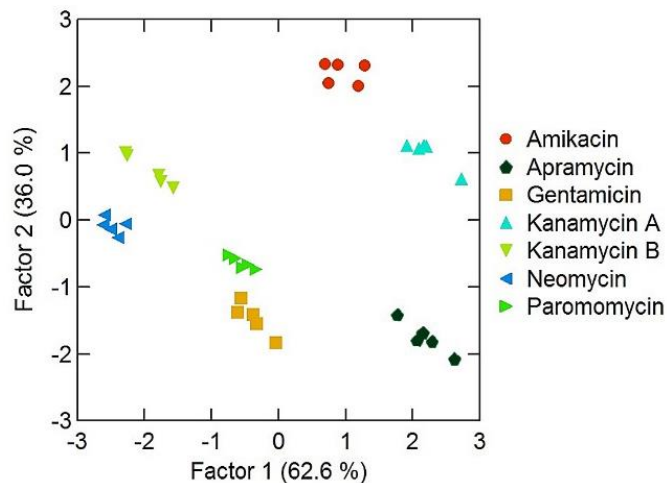


Figure 3.10 Two-dimensional PCA score plot for the analysis of seven different aminoglycosides. The data were obtained as described in the main text.

Next, we examined a more difficult analytical task: the differentiation of pure analytes from mixtures. For this study, we used the three aminoglycosides apramycin, paromomycin, and kanamycin B. In addition to samples containing the pure analytes at a concentration of 10 μM , we used samples containing equimolar mixtures of either two or all three analytes

($[\text{analyte}]_{\text{total}} = 10 \mu\text{M}$). We observed two main emission maxima around 375 and 540 nm for the mixture of analytes as in pure analyte spectra (Figure 3.11). However, there was difference in emission intensities for different analytes (Figure 3.12).

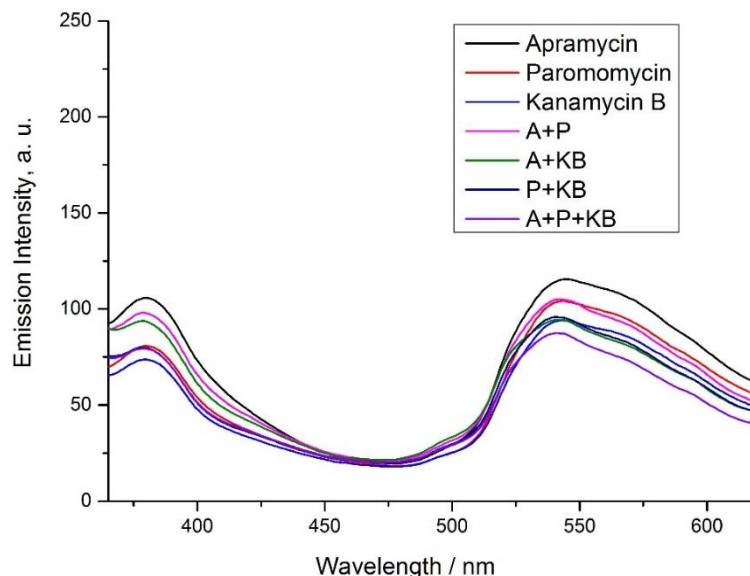


Figure 3.11 Fluorescence emission spectra (λ_{ex} : 335 nm) of solutions containing a mixture of dye **2** and **3** ($[\mathbf{2}] = 4 \mu\text{M}$; $[\mathbf{3}] = 30 \mu\text{M}$) and the analytes apramycin (A), paromomycin (P), kanamycin B (KB), or equimolar mixtures of these aminoglycosides ($[\text{analyte}]_{\text{total}} = 10 \mu\text{M}$; 10 mM MOPS, pH 7.0).

As before, we performed five independent measurements for each sample, and the data were used as an input for PCA. Well separated clusters were observed in the corresponding score plot (Figure 3.13), indicating that the sensing ensemble is able to differentiate the pure samples from the mixtures.

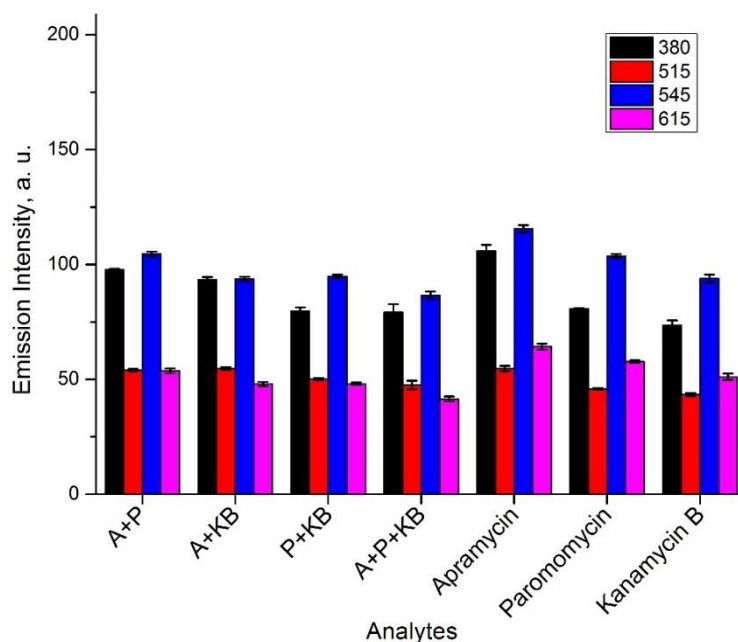


Figure 3.12 Fluorescence emission intensities (λ_{ex} : 335 nm) at 380 nm (black), 515 nm (red), 545 nm (blue), and 615 nm (pink) of solutions containing a mixture of dye **2** and **3** ($[\mathbf{2}] = 4 \mu\text{M}$; $[\mathbf{3}] = 30 \mu\text{M}$) and the analytes apramycin (A), paromomycin (P), kanamycin B (KB), or equimolar mixtures of these aminoglycosides ($[\text{analyte}]_{\text{total}} = 10 \mu\text{M}$; 10 mM MOPS, pH 7.0). The values represent averages of five independent measurements.

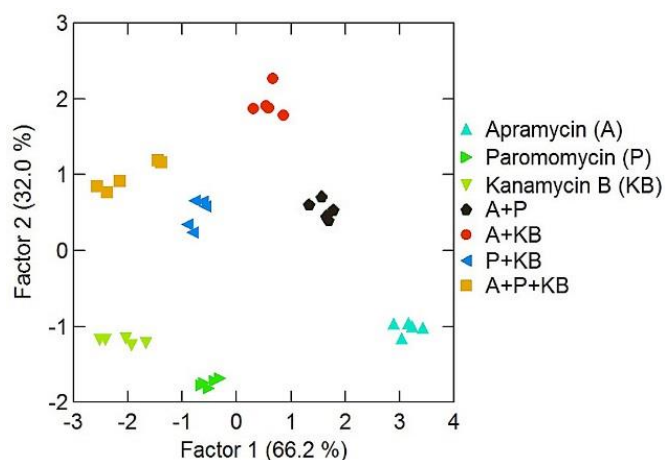


Figure 3.13 Two-dimensional PCA score plot for the analysis of apramycin (A), paromomycin (P), kanamycin B (KB), and equimolar mixtures of these aminoglycosides. The data were obtained as described in the main text.

In order to examine the benefits of using a mixture of two amphiphiles, we evaluated the ability of the individual dyes **2** and **3** to sense individual aminoglycosides and mixtures thereof. As expected, solutions containing only one amphiphilic dye (either **2** or **3**) gave also an optical response upon addition of the aminoglycoside analytes. However, the

discrimination was poor. With dye **2** alone, for example, it was not possible to differentiate paromomycin and apramycin (Figure 3.14), and it was also not possible to distinguish the mixtures from pure analytes (Figure 3.15 and 3.16).

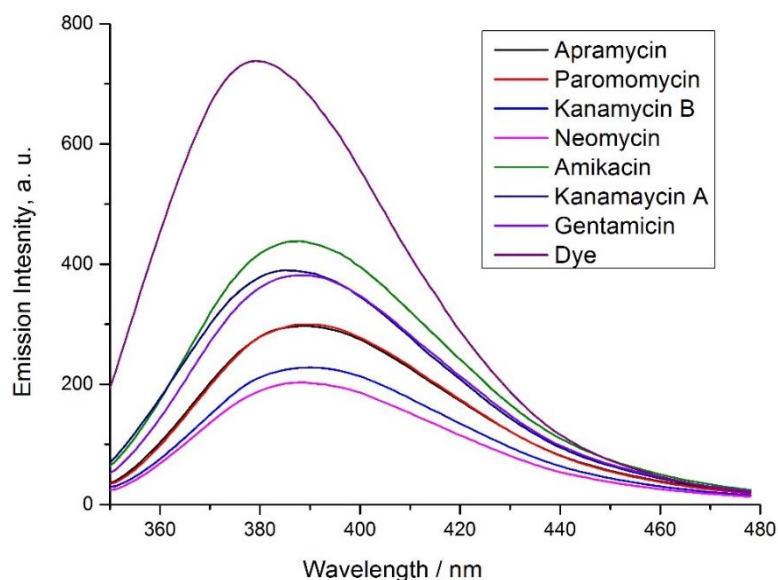


Figure 3.14 Fluorescence emission spectra (λ_{ex} : 335 nm) of solutions containing dye **2** (4 μM) and the analytes paromomycin, kanamycin B, kanamycin A, amikacin, neomycin, gentamicin, or apramycin ([analyte] = 10 μM; 10 mM MOPS, pH 7.0).

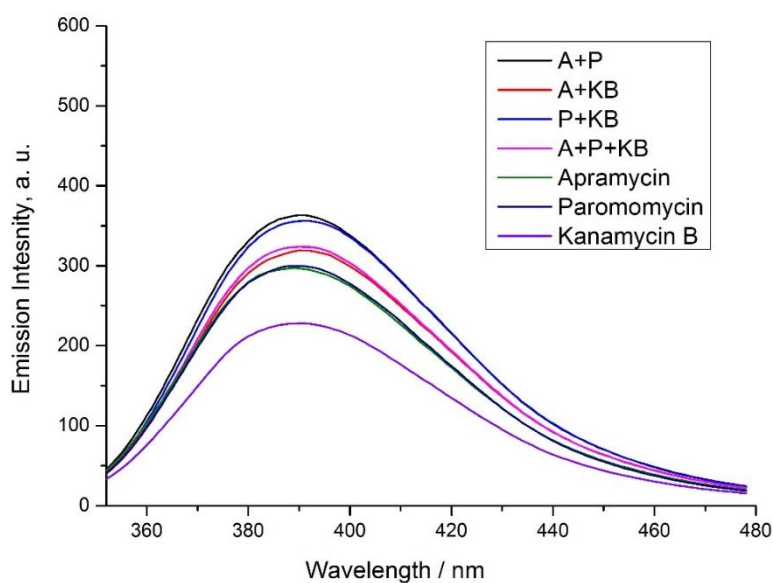


Figure 3.15 Fluorescence emission spectra (λ_{ex} : 335 nm) of solutions containing dye **2** (4 μM) and the analytes apramycin (A), paromomycin (P), kanamycin B (KB), or equimolar mixtures of these aminoglycosides ([analyte]_{total} = 10 μM; 10 mM MOPS, pH 7.0).

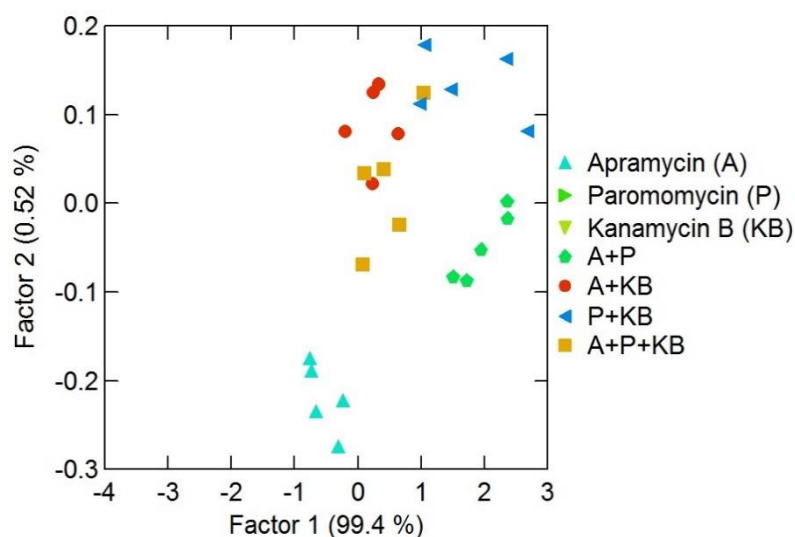


Figure 3.16 Two-dimensional PCA score plot for the analysis of apramycin (A), paromomycin (P), kanamycin B (KB), and equimolar mixtures of these aminoglycosides. The data were obtained as described above using only dye **2**.

The situation was even worse with dye **3**, which gave very similar fluorescence spectra for the seven analytes (Figure 3.17 and 3.18). Attempts to use solutions of **3** for the differentiation of mixtures from pure samples were also not successful (Figure 3.19).

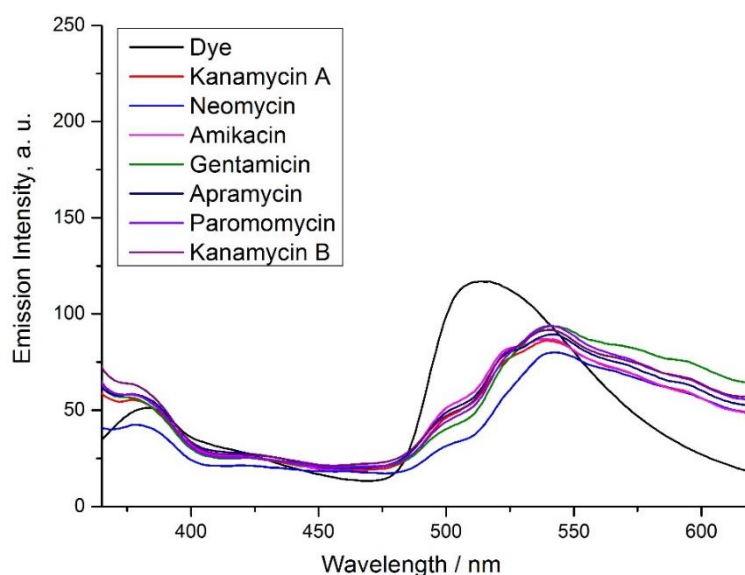


Figure 3.17 Fluorescence emission spectra (λ_{ex} : 335 nm) of solutions containing dye **3** (30 μM) and the analytes paromomycin, kanamycin B, kanamycin A, amikacin, neomycin, gentamicin, or apramycin ([analyte] = 10 μM ; 10 mM MOPS, pH 7.0)

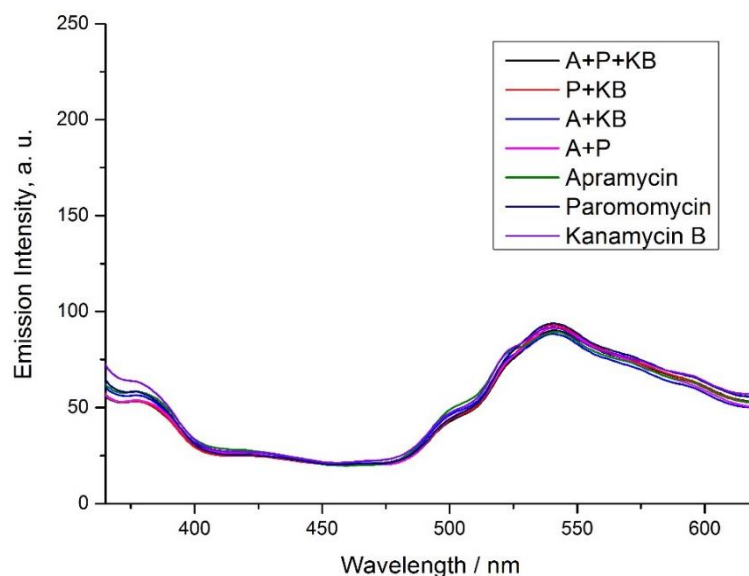


Figure 3.18 Fluorescence emission spectra (λ_{ex} : 335 nm) of solutions containing dye **3** (30 μM) and the analytes apramycin (A), paromomycin (P), kanamycin B (KB), or equimolar mixtures of these aminoglycosides ($[\text{analyte}]_{\text{total}} = 10 \mu\text{M}$; 10 mM MOPS, pH 7.0).

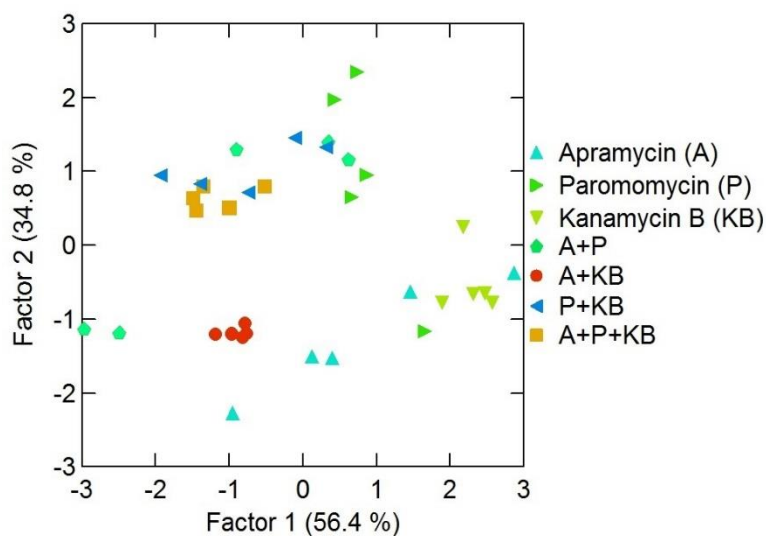


Figure 3.19 Two-dimensional PCA score plot for the analysis of apramycin (A), paromomycin (P), kanamycin B (KB), and equimolar mixtures of these aminoglycosides. The data were obtained as described above using only dye **3**.

We also tested dye **3** alone with pure analytes at a concentration below its cmc. The resulting spectra were same for five analytes in the first band and very similar in the second band (Figure 3.20). These control experiments provide evidence that the utilization of a dynamic mixture of micellar aggregates is crucial for a successful analysis.

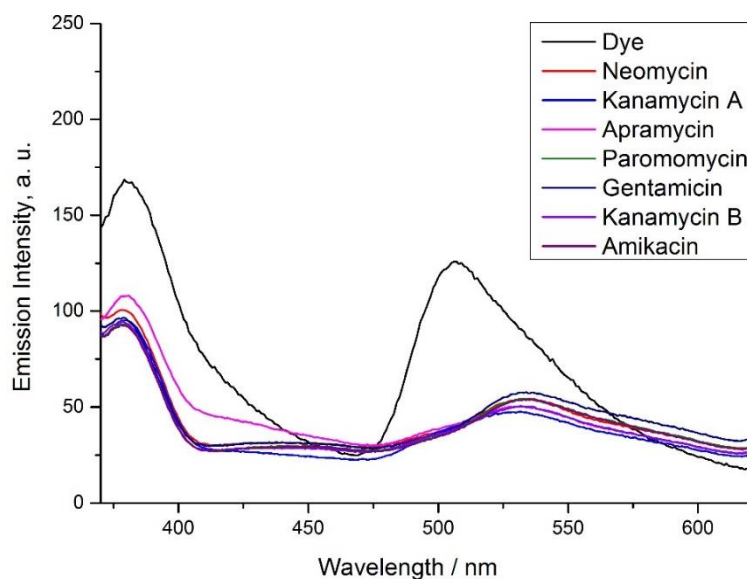


Figure 3.20 Fluorescence emission spectra (λ_{ex} : 335 nm) of solutions containing dye **3** (5 μ M) and the analytes paromomycin, kanamycin B, kanamycin A, amikacin, neomycin, gentamicin, or apramycin ([analyte] = 10 μ M; 10 mM MOPS, pH 7.0)

3.3 Conclusion

The utilization of dynamic combinatorial libraries of molecular assemblies as chemosensors has emerged as an interesting new concept in supramolecular analytical chemistry. DCLs can be used as sensors if the addition of an analyte results in a re-equilibration of the system, and if this re-equilibration is associated with a detectable signal. Due to the inherent complexity of DCLs, pattern-based recognition tools are particularly well suited for data analysis. So far, DCL sensors were often based on dynamic mixtures of metal-dye complexes, and read-out was achieved by UV-vis spectroscopy.¹⁹ Here, we have described a novel approach to create an adaptable system for pattern-based sensing. A mixture of only two compounds, the fluorescent amphiphiles **2** and **3**, was shown to constitute a sensing ensemble, which allows aminoglycosides in the low micromolar concentration range to be differentiated by fluorescence spectroscopy. The molecular basis for the sensor response is the multivalent interaction of the polycationic analytes with the polyanionic micellar aggregates formed from **2** and **3**. Overall, our results demonstrate the potential of fluorescent

amphiphiles for the creation of DCL sensors. By using different types of host-guest interactions, it should be possible to extend this approach towards other classes of analytes.

3.4 Experimental

All chemicals and solvents were purchased from standard suppliers and used without further purification. Stock solutions were prepared with bidistilled water and were stored at 4 °C. MOPS buffer (10 mM MOPS buffer, pH 7.0) was prepared by dissolving 3-(*N*-morpholino) propanesulfonic acid in bidistilled water. HCl and NaOH solutions were used to adjust the pH of the buffer. Fluorescence measurements were performed on a Varian Cary Eclipse fluorescence spectrophotometer at room temperature. Absorption spectra were measured on a Cary 50 bio spectrometer (Varian). Quartz cuvettes were used for the absorbance and fluorescence measurements. ¹H and ¹³C NMR spectra were recorded on a Bruker Advance DPX 400 and 500 instruments at 25 °C. Multiplicities of the ¹H NMR signals are assigned as following: s (singlet), d (doublet), t (triplet), dd (doublet of doublet), m (multiplet), (pp pseudo pentet). DLS measurements were performed with Zetasizer nano ZS90 (Malvern) instrument. High resolution mass spectra were recorded with a waters Q-TOF Ultima (ESI-TOF) instrument.

Stock solutions of dye **2** (2.0 mM) and **3** (50 μM) were prepared in 10 mM MOPS buffer (pH 7.0). For the fluorescence measurements, aliquots of the stock solutions were diluted with MOPS buffer (10 mM MOPS, pH 7.0). The final volume in all samples was 1.5 mL. The fluorescence spectra of the resulting solutions were recorded at room temperature (λ_{ex} : 335 nm for **2**, λ_{ex} : 460 nm for **3**). The fluorescent signal was measured 10 min after sample preparation. A mixture of dye **2** and **3** ($[\mathbf{2}]_{\text{final}} = 4 \mu\text{M}$; $[\mathbf{3}]_{\text{final}} = 30 \mu\text{M}$) in buffered aqueous solutions (10 mM MOPS, pH 7.0) was used as the sensing system. Seven different analytes (apramycin, paromomycin, neomycin, amikacin, kanamycin B, kanamycin A, and gentamicin) were employed. These analytes were also tested with dye **2** (4 μM) and dye **3** (5 and 30 μM) individually. The three aminoglycosides apramycin (A), paromomycin (P), and

kanamycin B (KB), as well as equimolar mixtures of A+KB, A+P, P+KB and A+P+KB (total conc. = 10 μ M) were selected for selectivity test.

The CMC values was calculated using the shift in the emission of the dye **2** and **3**. In detail, the fluorescence emission maxima of solutions of dye **2** shift from 378 to 390 nm upon increasing the concentration from 1 to 256 μ M (Figure 3.5, left side). Similarly, the fluorescence emission maxima for solutions of **3** shift from 503 to 529 nm upon increasing the concentrations from 1 to 45 μ M (Figure 3.5, right side). The cmc was determined by linear extrapolation as described in the literature.³²⁸

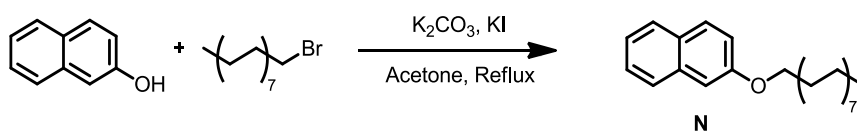
A solution of dye **3** (2.4 mM, 10 mM MOPS, pH 7.0) was measured in TEM (Figure A 35). In detail, samples were placed on a Lacey carbon coated 300 mesh copper grid. Uranyl acetate solution (2 wt%) was used for staining. A drop of the respective solution (20 μ L) was put on a parafilm sheet. The grid was placed on the top of the drop with its upper side down and kept there for 2 min. Then, an aliquot of the uranyl acetate solution (20 μ L, 2 wt%) was put on a other parafilm sheet. After 2 minutes the grid was taken and placed on the top of the drop with its upper side down and kept there for 5 min. Stained grids were dried in the fume hood at room temperature.

For DLS measurements, buffered aqueous solutions of dye **2** (1.0 mM) and dye **3** (50 μ M) were prepared (10 mM MOPS, pH 7.0) and then filtered (PTFE filter, 0.22 μ M). The solutions were found to contain polydisperse aggregates with an average size of 6 nm (**2**) and 12 nm (**3**), respectively.

Five independent fluorescence measurements were performed for each sample for the multivariate analysis. The data were analyzed with the help of the statistics software SYSTAT 11. A stepwise variable selection algorithm was used to select appropriate wavelength for the multivariate analyses. Fluorescence emission values in the region between 365 and 620 nm with incremental steps of 5 nm (365, 370, 375, etc) were used as input for the variable selection algorithm. Four wavelengths were selected: 380 nm, 515 nm, 545 nm, and 615 nm. The emission values at these four wavelengths were used as input for linear discriminant analyses (LDA) and principal component analyses (PCA).

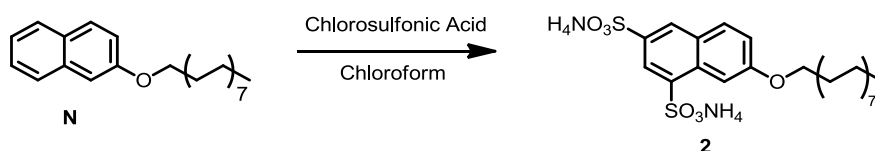
Sensing was also tested with the dye **2** and dye **3** alone. The solutions were prepared as described above. For the dye **2** alone, a stepwise variable selection algorithm was employed to select three wavelengths: 375, 390, and 410 nm. The emission values at these wavelengths were used as input for linear discriminant analyses (LDA) and principal

component analyses (PCA). For the dye **3** alone, a stepwise variable selection algorithm was employed to select three wavelengths: 380, 515, and 545 nm. The emission values at these wavelengths were used as input for linear discriminant analyses (LDA) and principal component analyses (PCA).



Compound **N** was synthesized in a similar fashion as described in the literature for a related compound:³²⁹ 1-Bromohexadecane (5.28 g, 17.3 mmol), potassium carbonate (3.59, 26.0 mmol) and potassium iodide (~ 5 mg) were added to a refluxing solution of naphthalen-2-ol (2.50g, 17.3 mmol) in acetone (200 mL). The reaction mixture was heated under reflux with stirring for 24 h. The mixture was then cooled to 4 °C, resulting in the formation of a white precipitate. The precipitate was isolated by filtration and dissolved in chloroform (50 mL). After filtration of salts, the solvent was removed under reduced pressure to give compound **N** as a white solid (5.12 g, 13.9 mmol, 81%). Compound **N** was used for the synthesis of dye **2** without further purification.

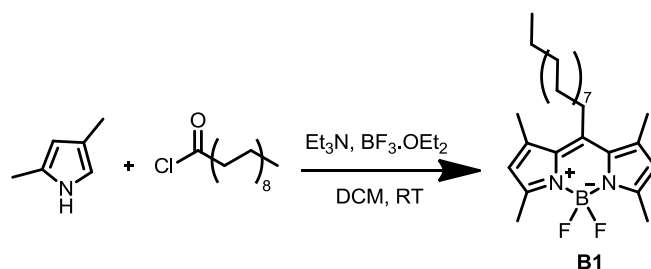
¹H NMR (400 MHz, CDCl₃): δ = 0.81 (t, J = 4.0 Hz, 3 H, CH₃), 1.17–1.34 (m, 24 H, CH₂), 1.43 (pp, J = 6.6 Hz, 2 H, CH₂), 1.77 (pp, J = 6.6 Hz, 2 H, CH₂), 4.00 (t, J = 6.6 Hz, 2 H, OCH₂), 7.03–7.08 (m, 2 H, CH_{arom}), 7.22–7.27 (m, 1 H, CH_{arom}), 7.32–7.37 (m, 1 H, CH_{arom}), 7.62–7.69 (m, 3 H, CH_{arom}). ¹³C NMR (100 MHz, CDCl₃): δ = 14.12, 22.70, 26.13, 29.27, 29.37, 29.44, 29.61, 29.62, 29.68, 29.71, 31.94, 68.05, 106.57, 119.03, 123.43, 126.25, 126.67, 127.62, 128.88, 129.28, 134.63, 157.12. ESI-MS calcd. for C₂₆H₄₀O [(M)] m/z = 369.3157 found 369.3168.



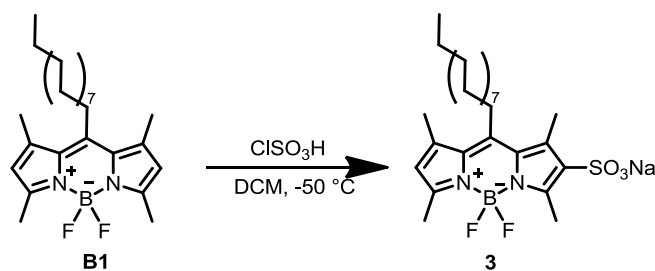
Dye **2** was synthesized in a similar fashion as described in the literature for a related compound:³²⁵ A solution of chlorosulfonic acid (3.44 mL, 51.8 mmol) in CHCl₃ (40 mL) was added dropwise over 1 h under stirring to a cooled (0 °C) solution of compound **N** (1.73 g, 4.71 mmol) in CHCl₃ (20 mL). The ice bath was then removed and the mixture was stirred for

additional 2 h at room temperature resulting in the formation of a white precipitate. The precipitate was isolated by filtration, washed with chloroform, and redissolved in water (~ 50 mL). The pH of the solution was adjusted to pH 7 by addition of aqueous NaOH (8 M), and the solution was dried under vacuum. Purification by column chromatography (SiO₂; eluent: ammonia (25 %) : isopropanol; 1 : 2) gave dye **2**, which still contained minor amounts of a second isomer. After recrystallization from methanol/hexane for three times and drying in vacuum, dye **2** was obtained as pure product (0.61 g, 1.08 mmol, 23%).

¹H NMR (400 MHz, CD₃OD): δ = 0.92 (t, J = 6.3 Hz, 3 H, CH₃), 1.28–1.50 (m, 24 H, CH₂), 1.56 (p, J = 6.6 Hz, 2 H, CH₂), 1.88 (p, J = 6.6 Hz, 2 H, CH₂), 4.21 (t, J = 6.4 Hz, 2 H, OCH₂), 7.24 (dd, J = 9.0, 2.5 Hz, 1 H, CH_{arom}), 7.90 (d, J = 9.0 Hz, 1 H, CH_{arom}), 8.26 (d, J = 2.5 Hz, 1 H, CH_{arom}), 8.35 (d, J = 1.9 Hz, 1 H, CH_{arom}), 8.62 (d, J = 1.9 Hz, 1 H, CH_{arom}).
¹³C NMR (100 MHz, CD₃OD): δ = 14.44, 23.74, 27.27, 30.38, 30.48, 30.58, 30.76, 30.80, 33.08, 69.21, 107.18, 121.04, 124.77, 129.24, 130.00, 131.59, 132.53, 139.86, 141.12, 160.20.
 ESI-MS calcd. for C₂₆H₃₈S₂O₇Na₂ [(M-2NH₄+2Na)] m/z = 573.1932 found 573.1946.



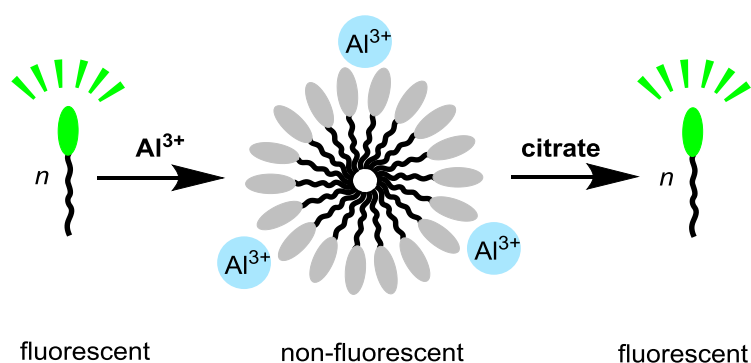
Compound **B1** was synthesized in a similar fashion as described in the literature:³²⁴ Stearoyl chloride (490 μ L, 1.46 mmol) was added under N₂ to a stirred solution of 2,4-dimethyl pyrrole (300 μ L, 2.91 mmol) in dry CH₂Cl₂ (100 mL). After 4 h, triethylamine (1.01 mL, 7.28 mmol) and BF₃·OEt₂ (1.29 mL, 10.2 mmol) were added. After stirring for 30 minutes, the mixture was washed with water (3 x 100 mL) and dried over Na₂SO₄. The solvent was removed under vacuum and the product was purified by column chromatography (SiO₂; eluent: EtOAc : Hexane, 1 : 20) to give compound **B1** as a red solid (354 mg, ~0.73 mmol, ~25%). The product contained small impurities but it was used without further purification. ¹H NMR (400 MHz, CD₃OD): δ = 0.81 (t, J = 7.0 Hz, 3 H, CH₃), 1.18–1.32 (m, 26 H, CH₂), 1.36–1.46 (m, 2 H, CH₂), 1.51–1.61 (m, 2 H, CH₂), 2.34 (s, 6 H, CH₃), 2.44 (s, 6 H, CH₃), 2.83–2.89 (m, 2 H, CH₂), 5.98 (s, 2 H, CH_{arom}). ESI-MS calcd. for C₃₀H₄₉BF₂N₂Na [(M+Na)] m/z = 509.3860 found 509.3844.



Dye **3** were synthesized in a similar fashion as described in the literature:³²⁴ A solution of chlorosulfonic acid (26.6 μL , 0.4 mmol) in CH_2Cl_2 (5 mL) was added dropwise over 20 min under stirring to a cooled ($-50\text{ }^{\circ}\text{C}$) solution of compound **B1** (100 mg, 0.20 mmol) in CH_2Cl_2 (20 mL). The ice bath was then removed and the mixture was stirred to reach room temperature resulting in the formation of a red precipitate. The precipitate was isolated by filtration, washed with CH_2Cl_2 , and redissolved in aqueous bicarbonate solution (10 mL, 40 mM). The solution was dried under vacuum. Purification by column chromatography (SiO_2 ; eluent: CHCl_3 : MeOH : H_2O - 7 : 3 : 0.5) gave **3** as a red solid (28 mg, 0.046 mmol, 24%).

^1H NMR (400 MHz, CD_3OD): δ = 0.80 (t, J = 7.0 Hz, 3 H, CH_3), 1.15-1.35 (m, 28 H, CH_2), 1.44 (p, J = 7.5 Hz, 2 H, CH_2), 1.50-1.65 (m, 2 H, CH_2), 2.38 (s, 3 H, CH_3), 2.39 (s, 3 H, CH_3), 2.62 (s, 3 H, CH_3), 2.64 (s, 3 H, CH_3), 2.98-3.04 (m, 2 H, CH_2), 6.14 (s, 1 H, CH_{arom}).
 ^{13}C NMR (125 MHz, CD_3OD): δ = 12.61, 12.92, 13.12, 15.45, 22.24, 28.02, 28.97, 29.26, 29.79, 31.50, 31.58, 122.58, 129.17, 132.59, 132.84, 137.30, 142.93, 148.61, 150.60, 156.38.
 ESI-MS calcd. for $\text{C}_{30}\text{H}_{49}\text{BF}_2\text{N}_2\text{O}_3\text{S}$ [(M-Na+H)] m/z = 565.3452 found 565.3448.

4 Selective Detection of Al^{3+} and Citric Acid with a Fluorescent Amphiphile

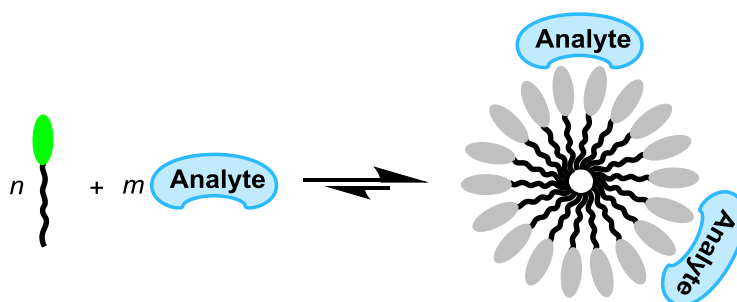


In this chapter, we present a fluorescence chemosensor based on analyte-induced aggregation/de-aggregation concept for the sensing of Al^{3+} and citric acid in buffered aqueous solution. An amphiphilic dye with a disulfonated BODIPY head group and a heptadecane side chain is used for this purpose. In buffered aqueous solution, the amphiphile can form aggregates and the aggregation of the dye is associated with a strong quenching of its fluorescence. Al^{3+} promotes aggregation, whereas other metal ions have a much smaller effect, in particular when histidine is added as masking agent. The Al^{3+} -induced aggregation process can be used to sense Al^{3+} in the low micromolar concentration range with high selectivity. Furthermore, we demonstrate that a dye- Al^{3+} mixture can be used as a sensing ensemble for the detection of citric acid. The assay allows the citric acid content of commercial beverages such as energy drinks to be quantified.

This work was published in:³³⁰ “Selective detection of Al^{3+} and citric acid with a fluorescent amphiphile” Ziya Köstereli and Kay Severin, *Org. Biomol. Chem.*, **2015**, 13, 252-257.

4.1 Introduction

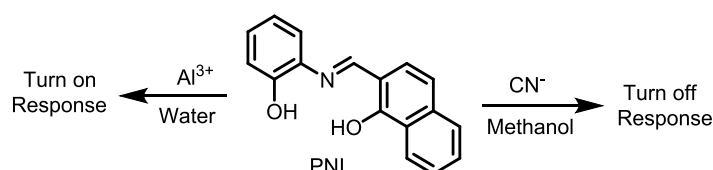
As we have discussed in previous chapters, the analyte-induced aggregation and de-aggregation (*disassembly*) of photoluminescent molecules has been used extensively for sensing purposes. In chapter 2 and 3, we have shown that amphiphiles with polysulfonated fluorescent head groups can be employed as molecular probes for the detection of spermine and aminoglycosides. In both cases, the polycationic analytes are assumed to undergo a multivalent interaction with the anionic amphiphile, thereby facilitating micellation. This process is associated with a change of the optical properties of the fluorescent head group, thereby allowing the detection of the analyte (Scheme 4.1). We hypothesized that a similar approach could be used for the detection of Al^{3+} ions.



Scheme 4.1 The analyte-induced aggregation of amphiphiles can be used for sensing purposes if aggregation induces a change in the optical properties of the amphiphile.

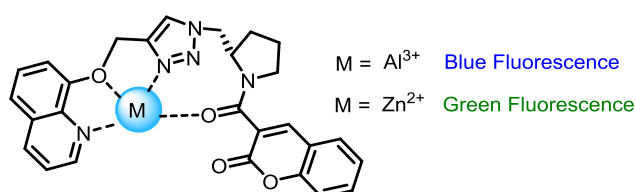
Aluminum is a ductile metal and it is the third most abundant element on the surface of the Earth.³³¹ It is not an essential element for living systems.³³²⁻³³³ In the body, it is found as a trivalent cation, Al^{3+} . Al^{3+} has pharmacological effects. At high doses, Al^{3+} can be neurotoxic.³³²⁻³³³ Furthermore, the accumulation of Al^{3+} in the human body has been associated with Alzheimer's disease.³³⁴⁻³³⁵ The world health organization (WHO) limit of Al^{3+} in safe drinking water is 7 μM .³³⁶ Given its biological relevance, it is not surprising that numerous optical probes for Al^{3+} have been reported.^{102, 108, 337-361} However, these sensing systems often require substantial amounts of organic co-solvents^{337, 340, 344, 346, 349-355, 357, 359-361} or they suffer from interference from other metal ions.^{337, 357-358} So far, there are few studies about the detection of Al^{3+} by analyte-induced aggregation of fluorophores.^{102, 343, 345}

The Kim group has published a fluorescence assay for the sensing of aluminum and cyanide ions.³⁵⁸ The probe is based on a phenol-naphthol (Figure 4.2), which has no emission in water. However, addition of Al^{3+} to the probe caused a turn-on response of the probe complexation. There was no significant change upon addition of other metal ions. However, if same probe was used in methanol, there was a turn-off response upon addition of cyanide ions. The probe was selective for cyanide over potential ions such as H_2PO_4^- , CH_3COO^- , F^- , Br^- , I^- and Cl^- .



Scheme 4.2 The structure of the PNI probe used for the detection of Al^{3+} and CN^-

Another chemosensor for Al^{3+} was published by Govindaraju *et.al.* They synthesized a quinoline-coumarin fluorescent probe based on an ICT mechanism (Figure 4.3).³⁴⁷ The probe has weak emission in mixed solvents (acetonitrile : water = 9 : 1). Addition of different metal cations caused different responses in the emission of the probe. The most pronounced difference was seen upon addition of Zn^{2+} and Al^{3+} . Zn^{2+} addition caused emission enhancement and Al^{3+} addition caused a 84 nm blue shift and a four fold enhancement in the emission of the probe. These two distinct responses of the probe for Zn^{2+} and Al^{3+} enabled two different metal ions to be monitored using the same chemosensor.



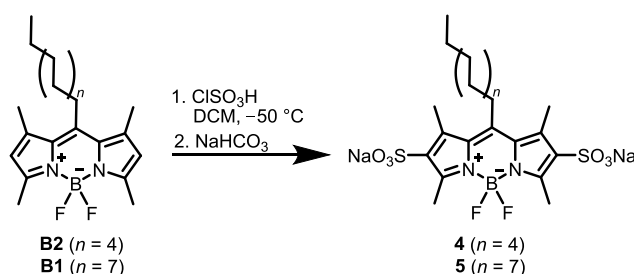
Scheme 4.3 The structure of the fluorescent probe for the detection of Al^{3+} and Zn^{2+}

Below, we show that an amphiphilic dye with a disulfonated BODIPY head group and a heptadecane side chain can be used to sense low micromolar concentrations of Al^{3+} in buffered aqueous solution with high selectivity. Furthermore, we show that an amphiphile/ Al^{3+} mixture can be used as a sensing ensemble for the detection citric acid.^{139, 362-}

³⁶⁹ The system is based on analyte-induced aggregation/de-aggregation concept which was discussed in chapter 1.2 and 1.3.

4.2 Results and Discussion

For this study, we synthesized the amphiphilic dyes **4** and **5** containing a disulfonated BODIPY head group and alkyl side chains of different lengths (**4**: undecyl; **5**: heptadecyl). The dyes were obtained by sulfonation of the easily accessible precursors **B2** and **B1** with chlorosulfonic acid in analogy to a known procedure (Scheme 4.4).³²⁴ The sulfonated BODIPY was chosen as fluorescent head group because of the high quantum yield of this fluorophore. Furthermore, we expected an emission maximum of higher than 500 nm, which would be well suited for sensing applications because of reduced interference from background fluorescence.³⁷⁰



Scheme 4.4 Synthesis of the fluorescent dyes **4** and **5**.

Both amphiphiles were characterized by NMR spectroscopy and mass spectrometry. The aggregation of the dyes in buffered aqueous solution (10 mM MOPS buffer, pH 7.0) was investigated by concentration-dependent fluorescence spectroscopy. For dye **5**, we observed a shift of the fluorescence emission maximum from 504 to 534 nm ($\lambda_{\text{ex.}} = 490\text{ nm}$) upon increasing the concentration from 0.21 to 105 μM (Figure 4.1). A critical micelle concentration (cmc) of $\sim 20\text{ }\mu\text{M}$ was determined by linear extrapolation of the relative fluorescence emission intensity at 534 and 505 nm (Figure 4.2).

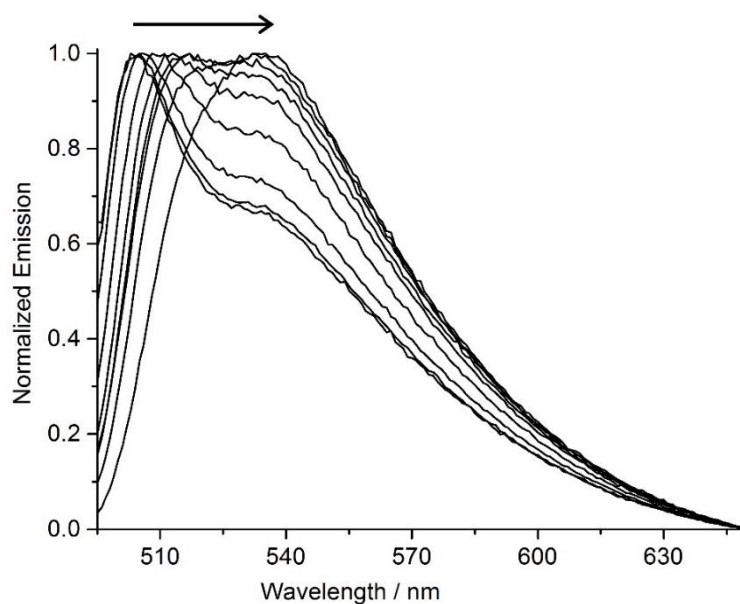


Figure 4.1 Normalized fluorescence emission spectra ($\lambda_{\text{ex}} = 490 \text{ nm}$) of buffered aqueous solutions (10 mM MOPS, pH 7.0) containing different amounts of dye **5** (0.21-105 μM).

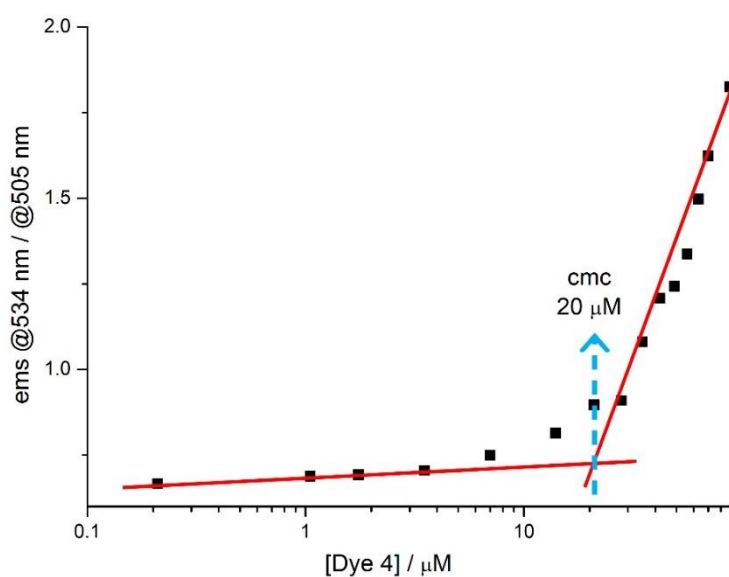


Figure 4.2 Relative fluorescence intensity at 534 and 505 nm of the buffered aqueous solutions (10 mM MOPS, pH 7.0) containing different amounts of dye **5** (0.21-105 μM).

Similar experiments were performed with dye **4**, which features a shorter undecyl side chain. No evidence for aggregation was observed in the concentration range between 1 μM and 1 mM. The formation of micellar aggregates by dye **5** at concentrations above 20 μM was substantiated by dynamic light scattering (DLS) experiments. At a concentration of $[\mathbf{5}] = 50$

μM , we were able to observe aggregates with an average hydrodynamic diameter of 13 nm (Figure 4.3).

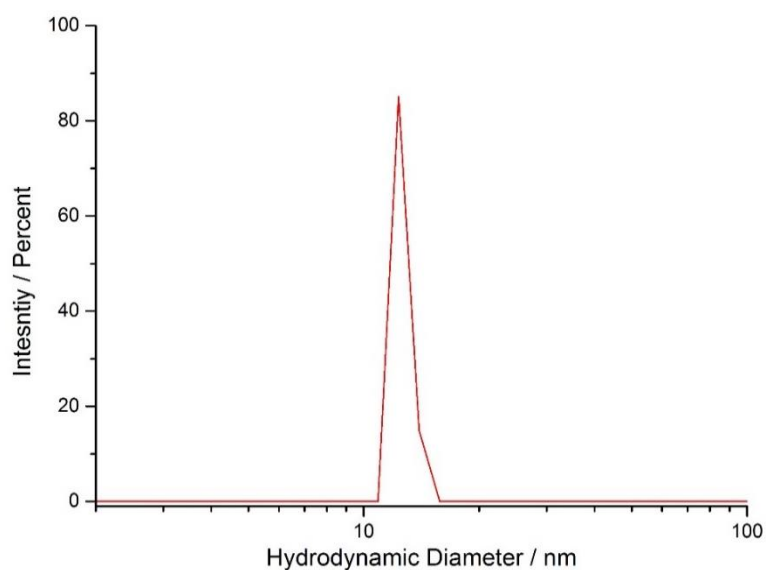


Figure 4.3 The size distribution of dye **5** aggregates as determined by DLS (average size is ~ 13 nm).

We hypothesized that metal cations could induce the aggregation of **5**. Therefore, we measured the fluorescence spectra of solutions containing dye **5** in the presence of different metal salts ($[\text{M}^{n+}] = 60 \mu\text{M}$; stock solutions in MeOH). For these studies, a dye concentration of $[\text{5}] = 4.0 \mu\text{M}$ was chosen. This value is slightly below the cmc of the amphiphile. Most metal salts had a very small effect on the fluorescence emission. For CuCl_2 and for AlCl_3 , however, substantial fluorescence quenching was observed (Figure 4.4). The most pronounced change was found for AlCl_3 , the addition of which resulted in nearly complete quenching of the fluorescence.

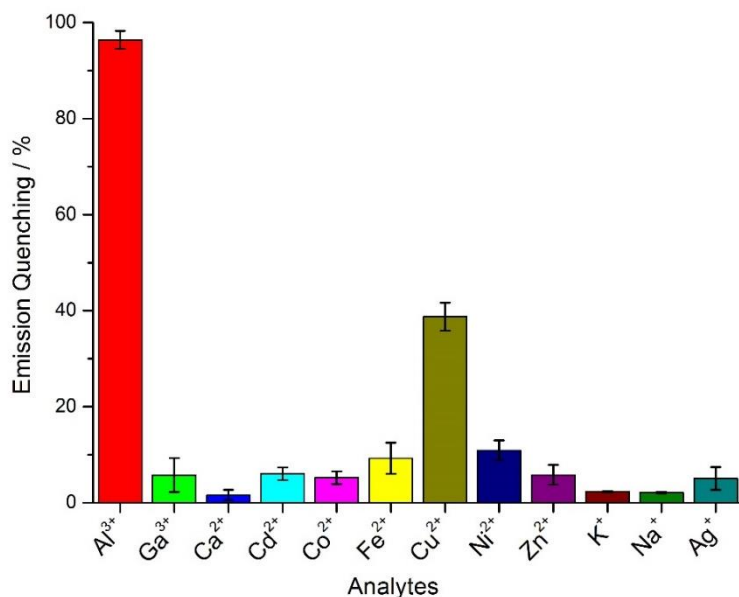


Figure 4.4 Fluorescence emission quenching ($\lambda_{\text{ex}} = 490 \text{ nm}$; $\lambda_{\text{em}} = 505 \text{ nm}$) of buffered aqueous solutions (10 mM MOPS, pH 7.0, H₂O with 0.6 vol% MeOH) of dye **5** (4.0 μM) in the presence of different metal cations (60 μM). The values are averages of three independent measurements.

Control experiments with dye **4** support the hypothesis of analyte-induced aggregation. Only minor fluorescence quenching was observed with Al³⁺ (Figure 4.5), indicating that a simple complexation between the BODIPY head group and Al³⁺ is not responsible for the optical changes observed for **5**. Experiments with the solvatochromic probe Nile Red are in line with these results. When Al³⁺ was added to solutions containing dye **5** (4.0 μM) and Nile Red (6.0 μM), an increased fluorescence at 660 nm was observed in the presence of Al³⁺ (Figure 4.6). This increase can be attributed to the encapsulation of Nile Red in a hydrophobic domain.³⁷¹ Additionally, the change in UV-vis spectrum of dye **5** upon addition of Al³⁺ indicates the formation of complex between the dye **5** and Al³⁺ (Figure 4.7). Because of the low concentration of dye **5** under sensing conditions, we were not able to confirm aggregation by DLS.

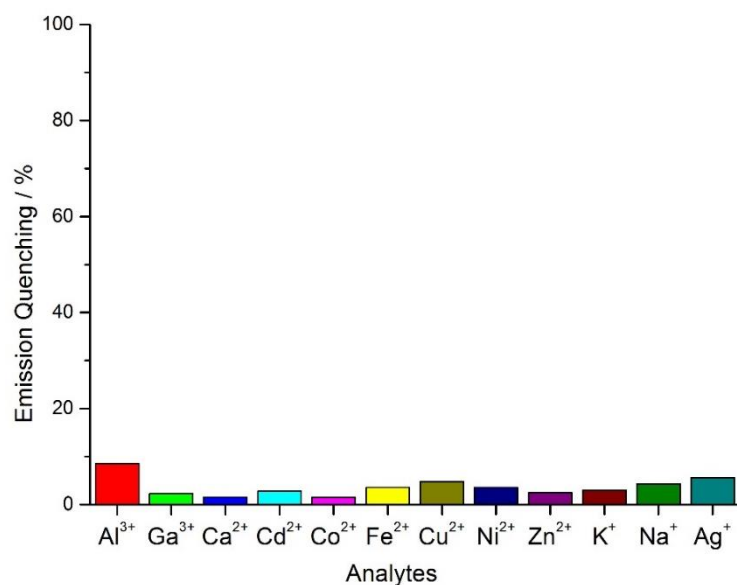


Figure 4.5 Fluorescence emission quenching ($\lambda_{\text{ex}} = 490 \text{ nm}$; $\lambda_{\text{em}} = 505 \text{ nm}$) of buffered aqueous solutions (10 mM MOPS, pH 7.0, H₂O with 0.6 vol% MeOH) of dye **4** (4.0 μM) in the presence of different metal cations (60 μM).

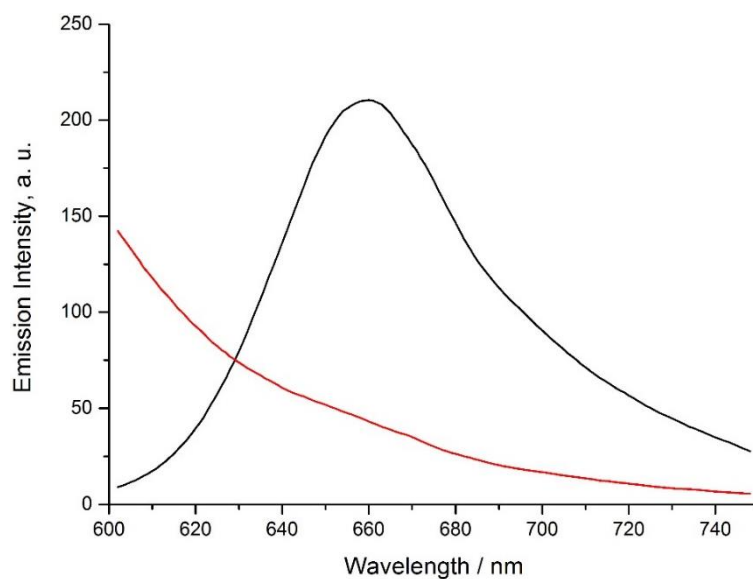


Figure 4.6 Fluorescence spectra (λ_{ex} : 520 nm) of buffered aqueous solutions (10 mM MOPS, pH 7.0) of Nile Red (6.0 μM) and dye **5** (4.0 μM) in the absence (red) and in the presence (black) of Al³⁺ (60 μM).

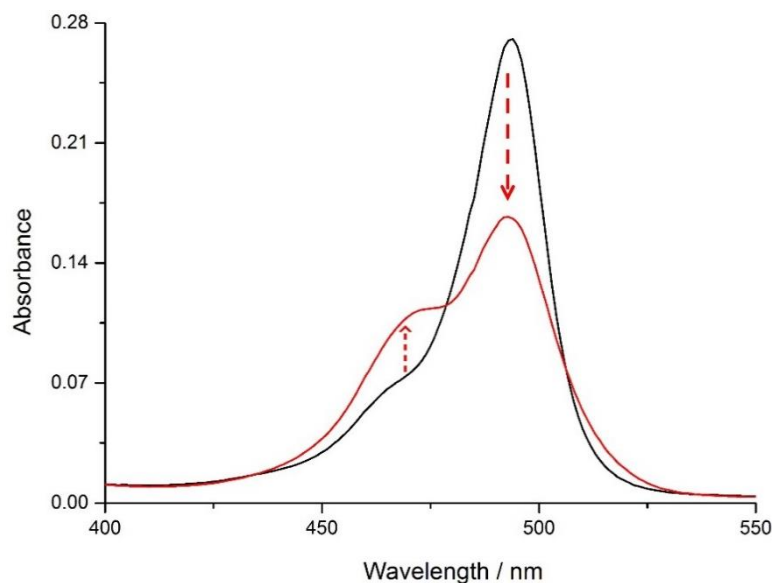


Figure 4.7 Absorption spectra of buffered aqueous solutions (10 mM MOPS, pH 7.0, H₂O with 0.6 vol% MeOH) containing dye **5** (4.0 μ M) and histidine (5.0 mM) in the absence (black) and in the presence (red) of Al³⁺ (6 μ M).

In order to enhance the selectivity for Al³⁺, we explored different masking agents. The amino acid histidine, a known chelate ligand for transition metal ions,³⁷² was found to give good results. In the presence of 5.0 mM histidine, none of the metal ions gave a significant fluorescence change apart from Al³⁺ (Figure 4.8). For the latter, an emission quenching of nearly 90% was observed.

Fluorescence titration experiments with solutions of **5** and different amounts of AlCl₃, CuCl₂, ZnCl₂, NiCl₂, and Cd(NO₃)₂ (0-135 μ M) showed that it is possible to selectively sense low micromolar concentrations of Al³⁺ with a detection limit of approximately 3 μ M (3 σ) (Figure 4.9).

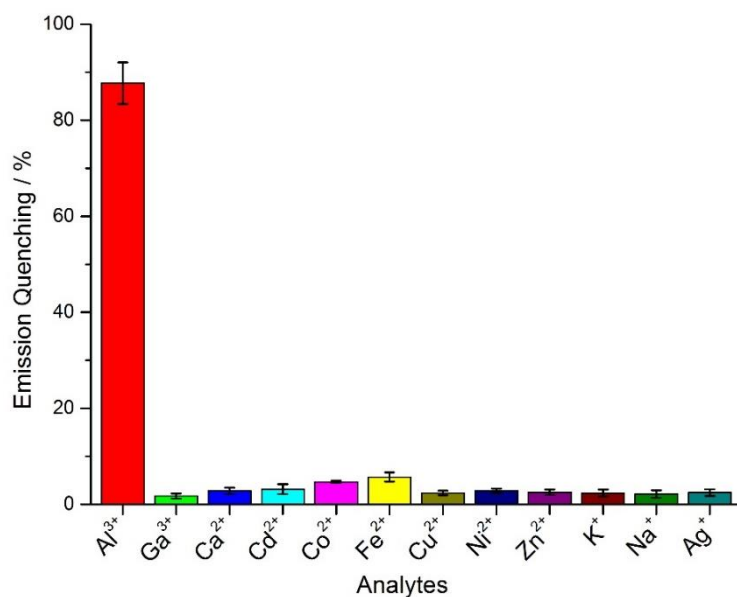


Figure 4.8 Fluorescence emission quenching ($\lambda_{\text{ex}} = 490 \text{ nm}$; $\lambda_{\text{em}} = 505 \text{ nm}$) of buffered aqueous solutions (10 mM MOPS, pH 7.0, H₂O with 0.6 vol% MeOH) of dye **5** (4.0 μM) with the masking agent histidine (5.0 mM) in the presence different metal cations (60 μM). The values are averages of three independent measurements.

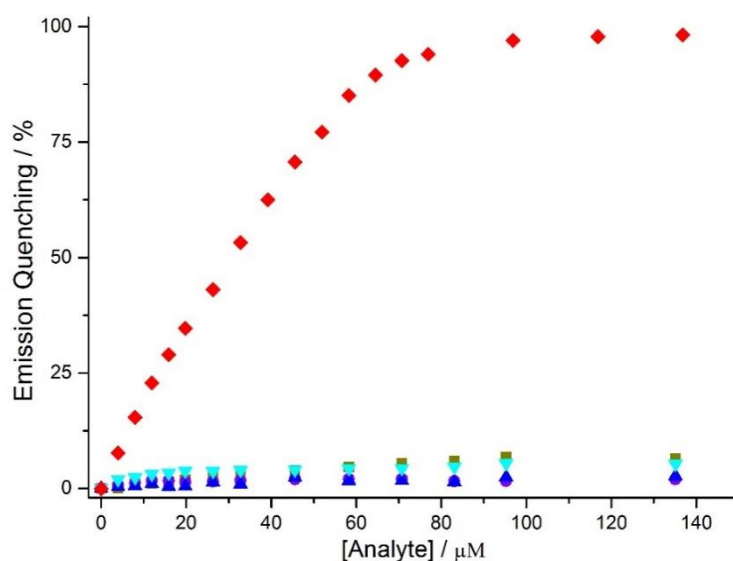


Figure 4.9 Fluorescence emission quenching ($\lambda_{\text{ex}} = 490 \text{ nm}$; $\lambda_{\text{em}} = 505 \text{ nm}$) of buffered aqueous solutions (10 mM MOPS, pH 7.0, H₂O with 0-1.3 vol% MeOH) containing dye **5** (4.0 μM), histidine (5.0 mM), and different amounts of Al³⁺(red symbols), Cd²⁺ (cyan symbols), Cu²⁺ (olive symbols), Ni²⁺ (blue symbols), or Zn²⁺ (violet symbols). The data points are averages of three independent measurements. The errors are less than 4%.

The good selectivity was further confirmed by measuring the fluorescence of solutions containing dye **5** (4.0 μM), histidine (5.0 mM), AlCl_3 (20 μM) and an additional metal salt (20 μM). In all cases a fluorescence quenching of around 40% was observed (Figure 4.10).

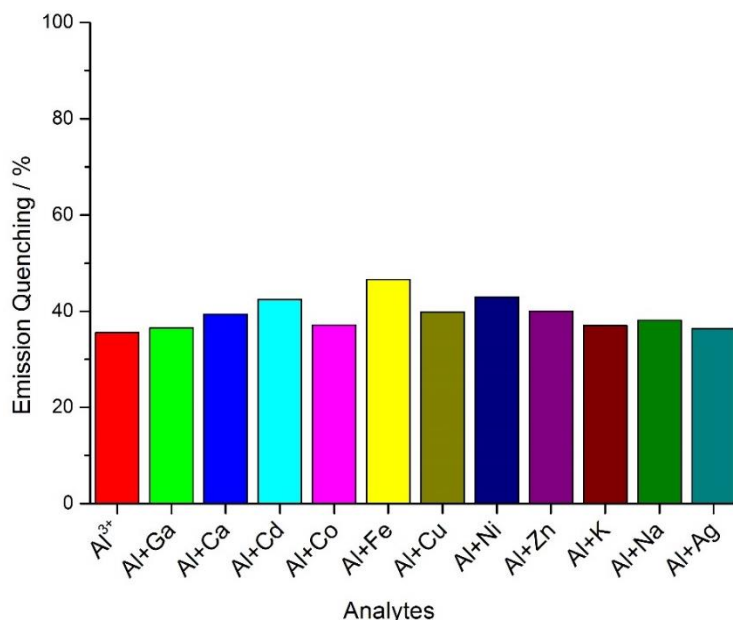


Figure 4.10 Fluorescence emission quenching ($\lambda_{\text{ex}} = 490 \text{ nm}$; $\lambda_{\text{em}} = 505 \text{ nm}$) of buffered aqueous solutions (10 mM MOPS, pH 7.0, H_2O with 0.4 vol% MeOH) containing dye **5** (4.0 μM), histidine (5.0 mM), Al^{3+} (20 μM) and different metal cations (20 μM).

Citric acid is known to bind Al^{3+} with high affinity and selectivity.^{108, 373} Therefore, it seemed possible to use citric acid for the disassembly of dye **4**- Al^{3+} aggregates. This is indeed the case. When citric acid was added to a buffered aqueous solution containing dye **5** (4.0 μM) and AlCl_3 (120 μM), an increased fluorescence emission at 505 nm was observed (Figure 4.11), suggesting the formation of monomeric **5**. It is thus possible to use a mixture of **5** and Al^{3+} as a sensing ensemble for the detection of citric acid *via* a turn-on fluorescence signal.^{108, 364-365, 367-368} The titration data depicted in Figure 4.11 and 4.12 could be used to sense citric acid in the low micromolar concentration range with a detection limit of approximately 5 μM ($3\sigma_0$).

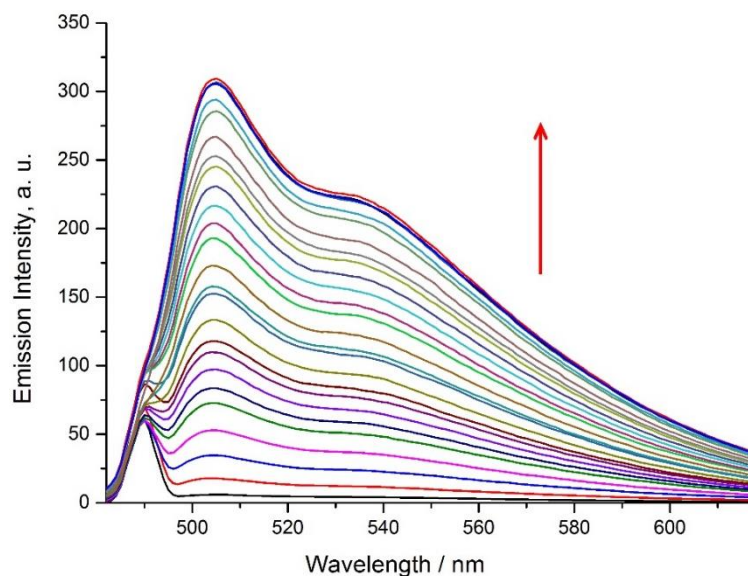


Figure 4.11 Fluorescence emission spectra ($\lambda_{\text{ex}} = 490 \text{ nm}$; $\lambda_{\text{em}} = 505 \text{ nm}$) of buffered aqueous solutions (10 mM MOPS, pH 7.0, H₂O with 1.2 vol% MeOH) containing dye **5** (4.0 μM), Al³⁺ (120 μM), and different amounts of citric acid (0–400 μM).

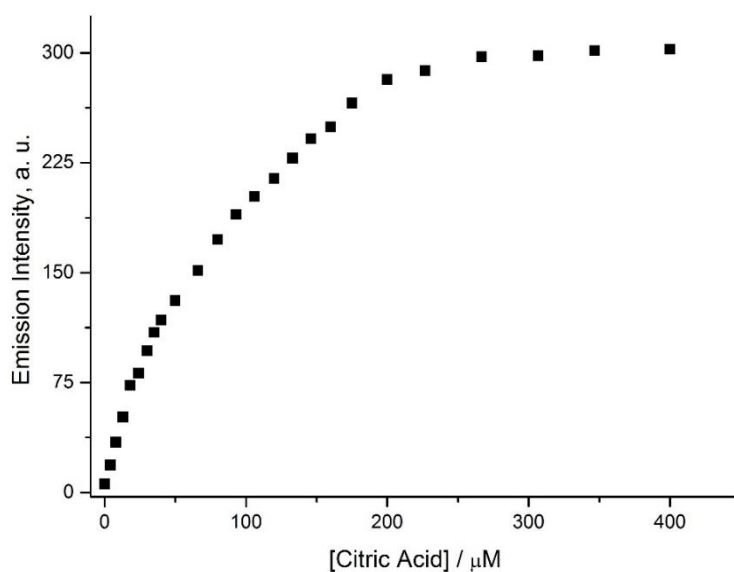


Figure 4.12 Fluorescence emission intensity ($\lambda_{\text{ex}} = 490 \text{ nm}$; $\lambda_{\text{em}} = 505 \text{ nm}$) of buffered aqueous solutions (10 mM MOPS, pH 7.0, H₂O with 1.2 vol% MeOH) containing dye **5** (4.0 μM), Al³⁺ (120 μM), and different amounts of citric acid (0–400 μM). The data points are averages of three independent measurements. The errors are less than 4%.

The selectivity of this assay turned out to be very good. Several biological relevant carboxylic acids were tested (400 μM), most of which gave a negligible optical response

(Figure 4.13). Only tartaric acid resulted in a fluorescence signal, but its intensity was only 1/3 of that of citric acid. We have also tested the influence of glucose, fructose, or sucrose (400 μ M in each case) on the sensing system. These carbohydrates gave a negligible fluorescence response.

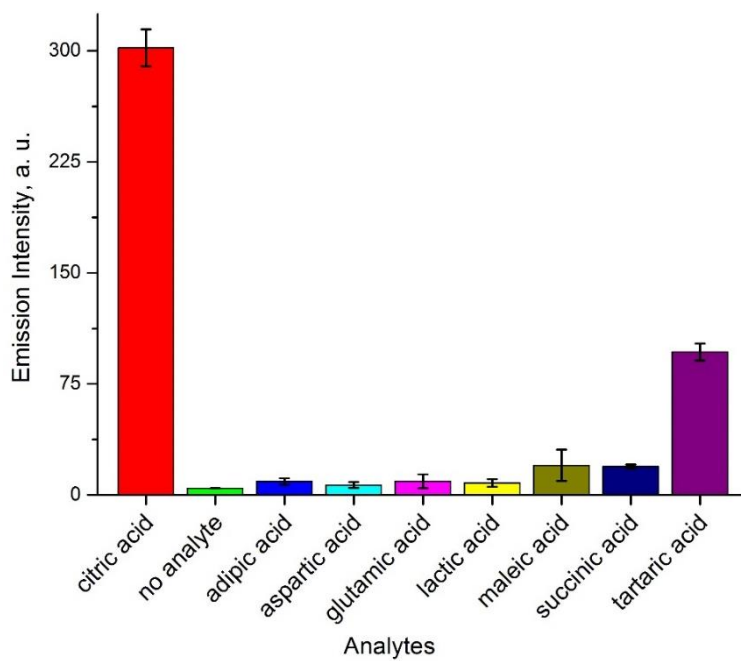


Figure 4.13 Fluorescence emission intensity ($\lambda_{\text{ex}} = 490$ nm; $\lambda_{\text{em}} = 505$ nm) of buffered aqueous solutions (10 mM MOPS, pH 7.0, H₂O with 1.2 vol% MeOH) of dye **5** (4.0 μ M) and Al³⁺ (120 μ M) in the presence different analytes (400 μ M). The values are averages of three independent measurements.

The good selectivity and sensitivity of our citric acid assay prompted us to examine the possibility of detecting and quantifying citric acid in commercial beverages. Three energy drinks, two soft drinks, and one mineral water were chosen as representative samples. First, we have determined the content of citric acid in these samples by ¹H NMR spectroscopy. This analytical technique is well suited for such an analysis because the signals of the CH₂ group of citric acid are well separated in the spectra, allowing for a reasonably precise integration (see Annex, Figure A51-A57). We then determined the citric acid concentration of the samples using a mixture of dye **5** and AlCl₃ as a sensing ensemble. The fluorescence signal was converted into a concentration value by using the calibration curve depicted in Figure 4.12. As shown in Figure 4.14, the match between the values obtained by NMR and by fluorescence spectroscopy is remarkably good.

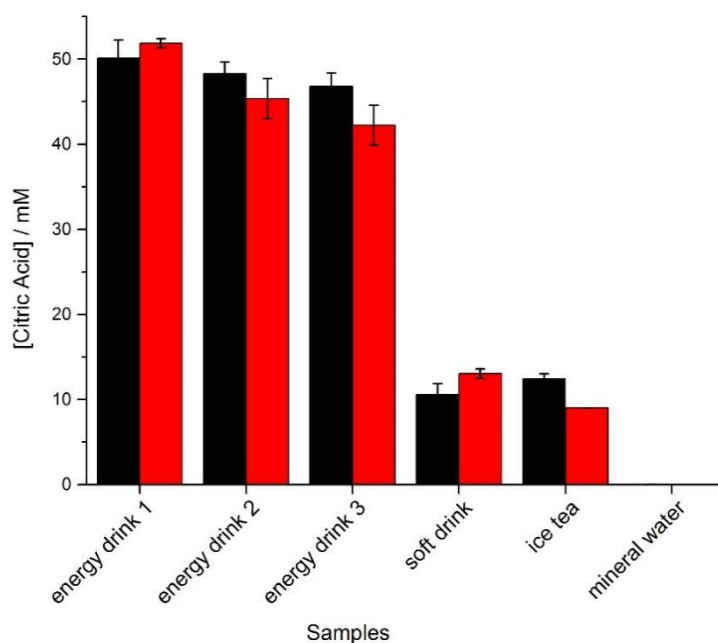


Figure 4.14 Concentration of citric acid in drinks as determined by ^1H NMR spectroscopy (black bars) and by the dye **5**- Al^{3+} sensing ensemble (red bars). Experimental details are given in the Chapter 4.4.

4.3 Conclusion

The amphiphilic fluorescent dye **5** with a disulfonated BODIPY head group and a heptadecyl side chain can be used to sense Al^{3+} in the low micromolar concentration range with high selectivity. The optical response is due to analyte-induced aggregation of the dye. From an application point of view, it is noteworthy that the assay can be performed in aqueous solution at neutral pH without the need of large amounts of organic co-solvents. Citric acid, a known chelator for Al^{3+} , can reverse the aggregation of **5**. It is thus possible to use a mixture of **5** and Al^{3+} as a turn-on fluorescence sensor for citric acid. As proof of concept, we have shown that it is possible to detect the citric acid concentration in commercial beverages. Overall, our results provide further evidence for the utility of fluorescent amphiphiles in supramolecular analytical chemistry.

4.4 Experimental

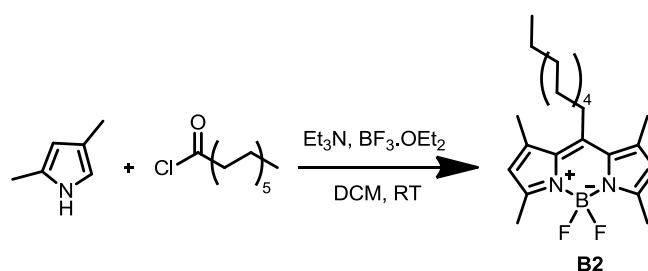
All chemicals and solvents were purchased from standard suppliers and used without further purification. Stock solutions of respective dye **4** (1 mM) and dye **5** (105 μ M) were prepared in 10 mM MOPS buffer (pH 7.0). Stock solutions of histidine (100 mM) and carboxylic acid analytes (citric acid: 20 mM; citric acid, adipic acid, aspartic acid, glutamic acid, lactic acid, maleic acid, succinic acid, tartaric acid: 100 mM) were prepared in bidistilled water. Stock solutions of metal analytes (2 mM and 10 mM) were prepared in methanol. NiCl_2 , ZnCl_2 , AlCl_3 , CuCl_2 , CaCl_2 , KCl , NaCl , AgCl , $\text{Ga}(\text{acac})_3$, $\text{Cd}(\text{NO}_3)_2$, $\text{Fe}(\text{ClO}_4)_2$, $\text{Co}(\text{C}_2\text{H}_3\text{O}_2)_2$ salts were used to prepare metal stock solutions. All solutions were stored at 4 °C. MOPS buffer (10 mM MOPS buffer, pH 7.0) was prepared by dissolving 3-(N-morpholino) propanesulfonic acid in bidistilled water. HCl and NaOH solutions were used to adjust the pH of the buffer. The samples were prepared by mixing aliquots of the corresponding stock solutions with MOPS buffer in quartz cuvettes. The final volume of all samples was 1.5 mL. The fluorescent signal was measured 3 minutes after sample preparation. Dye **4** (4.0 μ M) was used in control experiments with the same analytes. A mixture of dye **5** (4.0 μ M) and AlCl_3 (120 μ M) in buffered aqueous solutions (10 mM MOPS, pH 7.0) was used as a sensing system for citric acid detection. Fluorescence measurements were performed on a Varian Cary Eclipse fluorescence spectrophotometer at room temperature. Absorption spectra were measured on a Cary 50 bio spectrometer (Varian). Quartz cuvettes were used for the absorbance and fluorescence measurements. ^1H and ^{13}C NMR spectra were recorded on a Bruker Advance DPX 400 and 800 instruments at 25 °C. Multiplicities of the ^1H NMR signals are assigned as following: s (singlet), d (doublet), t (triplet), m (multiplet). DLS measurements were performed with Zetasizer nano ZS90 (Malvern) instrument. High resolution mass spectra were recorded with a waters Q-TOF Ultima (ESI-TOF) instrument.

For determining the cmc, a stock solution of dye **5** (105 μ M) was prepared in 10 mM MOPS buffer (pH 7.0). Aliquots of the stock solutions of dye **5** were diluted with MOPS buffer (10 mM MOPS, pH 7.0). The fluorescence spectra of the resulting solutions were recorded at room temperature (λ_{ex} : 490 nm). The fluorescence emission maxima of solutions of dye **5** shift from 504 to 534 nm upon increasing the concentration from 0.21 to 105 μ M (Figure 4.1). The cmc was determined by linear extrapolation as described in the literature.³²⁸

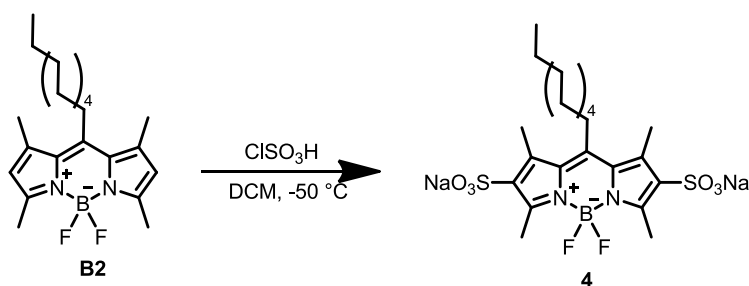
A value of $\text{cmc} = 20 \mu\text{M}$ was obtained (Figure 4.2). For dye **4**, no evidence for aggregation was observed in the concentration range between $1 \mu\text{M}$ and 1 mM .

For the DLS measurements, a solution of dye **5** ($50 \mu\text{M}$) in buffer (10 mM MOPS , $\text{pH } 7.0$) was prepared and then filtered (PTFE filter, $0.22 \mu\text{M}$). The solution contained polydisperse aggregates according to the measurements, but the results met the data quality criteria. For dye **4**, we were not able to detect aggregate by DLS. Nile Red was also used as described in section 8.3.

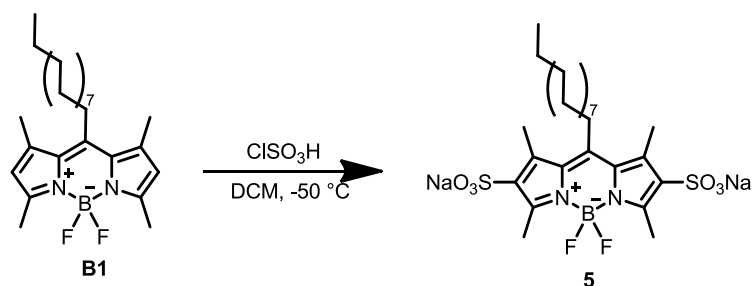
For the real world sample testing, the following commercial beverages were used: energy drink 1 (Denner energy drink), energy drink 2 (Migros energy drink, sugar free), energy drink 3 (Red Bull, sugar free), soft drink (Yedigun from Pepsi Co.), ice tea (Lipton ice tea, peach), and mineral water (Henniez drinking water). ^1H NMR spectroscopy in combination with isopropanol as internal standard was used to determine the concentration of citric acid in the samples. First, a reference sample containing 50 mM citric acid and 50 mM isopropanol in a mixture of H_2O and D_2O (9:1) was analyzed by ^1H NMR spectroscopy. The citric signals at 2.75 ppm and 2.97 ppm and the isopropanol signal at 1.10 ppm were integrated as a calibration set. For the analysis of the beverages, we have mixed 0.9 mL of the respective drink with 0.10 mL of D_2O and $3.85 \mu\text{L}$ of isopropanol ($\text{conc.}_{\text{final}} = 50 \text{ mM}$). The concentration of citric acid was then determined by integration of the citric acid and isopropanol peaks while taking into account the relative signal intensities of the reference sample. Three independent measurements were performed for each sample. A representative spectrum for each type of sample is shown in Figures A 51-A 57. For the fluorescence measurements, we have added $5 \mu\text{L}$ of the respective beverage to buffered aqueous solutions (10 mM MOPS , $\text{pH } 7.0$, H_2O with 1.2 vol\% MeOH , final volume: 1.5 mL) containing dye **5** ($4.0 \mu\text{M}$) and AlCl_3 ($120 \mu\text{M}$). After 3 minutes, a fluorescence spectrum was recorded and the emission intensity at 505 nm was determined ($\lambda_{\text{ex}} = 490 \text{ nm}$). The signal intensity was converted into a concentration value by using the calibration curve shown in Figure 4.12. Three independent measurements were performed for each sample.



Compound **B2** was synthesized in a similar fashion as described in the literature:³²⁴ Dodecanoyl chloride (231 μ L, 0.97 mmol) was added under N₂ to a stirred solution of 2,4-dimethyl pyrrole (200 μ L, 1.94 mmol) in dry CH₂Cl₂ (50 mL). After 4 h, triethylamine (0.71 mL, 6.31 mmol) and BF₃·OEt₂ (0.86 mL, 6.80 mmol) were added. After stirring for 30 minutes, the mixture was washed with water (3 x 50 mL) and dried over Na₂SO₄. The solvent was removed under vacuum and the product was purified by column chromatography (SiO₂; eluent: EtOAc : Hexane, 1 : 20) to give compound **B2** as a red solid (210 mg, ~0.52 mmol, ~27%). The product contained small impurities but it was used without further purification. ¹H NMR (400 MHz, CD₃OD): δ = 0.81 (t, J = 7.0 Hz, 3 H, CH₃), 1.16–1.30 (m, 14 H, CH₂), 1.35–1.46 (m, 2 H, CH₂), 1.49–1.59 (m, 2 H, CH₂), 2.32 (s, 6 H, CH₃), 2.43 (s, 6 H, CH₃), 2.80–2.86 (m, 2 H, CH₂), 5.96 (s, 2 H, CH_{arom}) . ESI–MS calcd. for C₂₄H₃₇BF₂N₂ [(M+H)] m/z = 403.3101 found 403.3109.

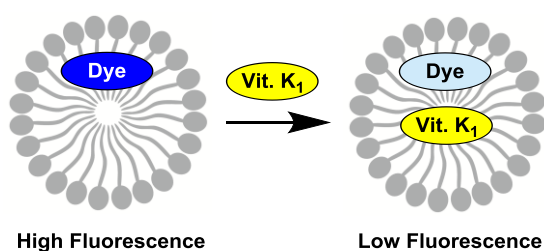


Dye **4** were synthesized in a similar fashion as described in the literature:³²⁴ A solution of chlorosulfonic acid (49.8 μ L, 0.75 mmol) in CH₂Cl₂ (5 mL) was added dropwise over 20 min under stirring to a cooled (–50 °C) solution of compound **B2** (100 mg, 0.25 mmol) in CH₂Cl₂ (30 mL). The ice bath was then removed and the stirred mixture was warmed to room temperature, resulting in the formation of a red precipitate. The precipitate was isolated by filtration, washed with CH₂Cl₂, and redissolved in aqueous bicarbonate solution (10 mL, 40 mM). The solution was dried under vacuum. Purification by column chromatography (SiO₂; eluent: CHCl₃:MeOH:H₂O; 7:3:0.5) gave **4** as a red solid (61 mg, 0.087 mmol, 35%). ¹H NMR (400 MHz, CD₃OD): δ = 0.80 (t, J = 7.0 Hz, 3 H, CH₃), 1.15–1.35 (m, 14 H, CH₂), 1.46 (p, J = 8.0 Hz, 2 H, CH₂), 1.55–1.64 (m, 2 H, CH₂), 2.65 (s, 6 H, CH₃), 2.69 (s, 6 H, CH₃), 3.09–3.13 (m, 2 H, CH₂). ¹³C NMR (100 MHz, CD₃OD): δ = 13.00, 13.03, 13.39, 22.32, 28.20, 29.06, 29.29, 29.31, 29.84, 31.55, 31.65, 130.57, 134.34, 139.61, 150.99, 153.49. ESI–MS calcd. for C₂₄H₃₅BF₂N₂O₆S₂ [(M–2Na)^{–2}] m/z = 280.1001 found 280.1006.



Dye **5** were synthesized in a similar fashion as described in the literature:³²⁴ A solution of chlorosulfonic acid (39.9 μL , 0.60 mmol) in CH_2Cl_2 (5 mL) was added dropwise over 20 min under stirring to a cooled ($-50\text{ }^{\circ}\text{C}$) solution of compound **B1** (100 mg, 0.20 mmol) in CH_2Cl_2 (30 mL). The ice bath was then removed and the stirred mixture was warmed to room temperature, resulting in the formation of a red precipitate. The precipitate was isolated by filtration, washed with CH_2Cl_2 , and redissolved in aqueous bicarbonate solution (10 mL, 40 mM). The solution was dried under vacuum. Purification by column chromatography (SiO_2 ; eluent: CHCl_3 : MeOH : H_2O ; 7:3:0.5) gave **5** as a red solid (20.7 mg, 30 μmol , 15%). ^1H NMR (800 MHz, CD_3OD): δ = 0.80 (t, J = 7.0 Hz, 3 H, CH_3), 1.15–1.35 (m, 26 H, CH_2), 1.46 (p, J = 8.0 Hz, 2 H, CH_2), 1.55–1.61 (m, 2 H, CH_2), 2.65 (s, 6 H, CH_3), 2.69 (s, 6 H, CH_3), 3.10–3.12 (m, 2 H, CH_2). ^{13}C NMR (200 MHz, CD_3OD): δ = 13.0, 13.07, 13.39, 22.36, 28.21, 29.10, 29.27, 29.35, 29.38, 29.41, 29.90, 31.56, 31.69, 130.57, 134.32, 139.62, 151.02, 153.47. ESI-MS calcd. for $\text{C}_{30}\text{H}_{47}\text{BF}_2\text{N}_2\text{O}_6\text{S}_2$ $[(\text{M}-2\text{Na})^{-2}]$ m/z = 322.1471 found 322.1469.

5 Fluorescence Sensing of Vitamin K₁ using a Simple Micelle-Based Assay



In this chapter, we describe a simple micelle-based assay for the fluorescence sensing of Vitamin K₁. It enables the detection of vitamin K₁ in the low micromolar concentration range. As a sensing ensemble, we employ a mixture of the surfactant triton X-100 and 1-aminopyrene in buffered aqueous solution. Vitamin K₁ co-localizes with the fluorescent pyrene dye in the micelle, resulting in fluorescence attenuation by dynamic quenching. The assay displays good selectivity and can be used to determine the concentration of vitamin K₁ in a commercial preparation.

5.1 Introduction

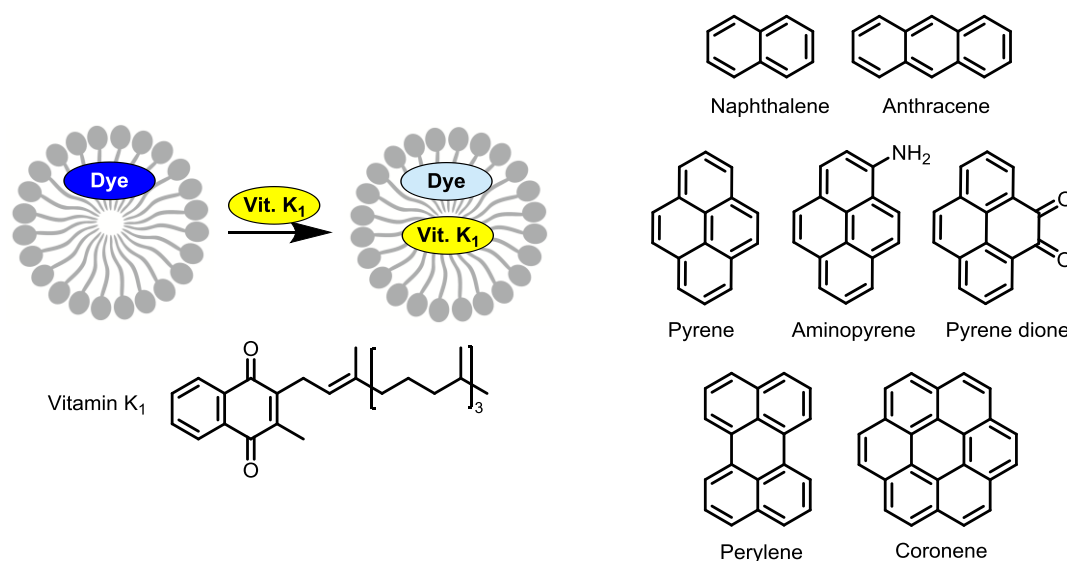
Vitamin K₁ is a fat-soluble vitamin which is needed for the production of proteins involved in blood coagulation.³⁷⁴ It is synthesized in plants, and high concentrations are found in the green leaves of vegetables such as spinach, cabbage, and kale.³⁷⁵⁻³⁷⁶ In case of vitamin K₁ deficiency, it can be supplied to the body by intramuscular injection or oral administration.³⁷⁴ Vitamin K₁ is mainly analyzed by chromatographic techniques.^{330, 374-385} The post-column detection by fluorescence spectroscopy is possible, but only after reduction of the naphthoquinone group to the highly fluorescent hydroquinone form.^{375-376, 382-385} The chemical reduction of vitamin K₁ by Ti³⁺ has also been used for the spectrophotometric detection of vitamin K₁.³⁸⁶ A sensing system based on micelles could be an alternative way of detection method for this hydrophobic analyte.

Below, we describe a simple and fast assay for the optical detection of vitamin K₁. The assay does not require a chemical reaction of the analyte. Fluorimetric detection of vitamin K₁ is achieved by combining the surfactant triton X-100 with the fluorescent dye 1-aminopyrene in buffered aqueous solution. Addition of vitamin K₁ to this sensing ensemble results in fluorescence quenching, allowing the selective detection of vitamin K₁ in the low micromolar concentration range.

5.2 Results and Discussion

Optical chemosensors typically feature a recognition unit and a sensing unit. The development of a selective recognition unit for vitamin K₁ is a challenging task because a large part of the molecule is highly flexible. Furthermore, it only features two C=O functional groups, which are difficult to exploit for molecular recognition. We therefore decided to build a fluorescent sensor based on a dynamic instead of a static quenching process. In view of the intrinsic lipophilicity of vitamin K₁, we explored mixtures of dyes and surfactants as sensing

ensembles. Our hypothesis was that the naphthoquinone part of vitamin K₁ could induce fluorescence quenching of a dye upon co-localization inside a micelle (Scheme 5.1).



Scheme 5.1 A micelle-based sensing ensemble for the detection of vitamin K₁ and the structures of the dyes used for sensitivity test.

To test our hypothesis, we used buffered aqueous solutions of the surfactant triton X-100 (0.90 mM) in combination with different lipophilic fluorophores (4.0 μ M) as potential sensing ensembles (Scheme 5.1). In order to get a first impression of the selectivity of the sensor, we used the target vitamin K₁ as well as the potential interferences vitamin E and carotene as analytes. Upon addition of the vitamin K₁ (final conc. = 4.0 μ M) to the surfactant/dye mixtures, we observed pronounced fluorescence quenching between 30 and 71 % (Figure 5.2). The potential interferences vitamin E and carotene also resulted in a reduced fluorescence, but the amount of quenching was lower than what was observed for vitamin K₁. The best selectivity was observed for 1-aminopyrene, which gave a very small response for vitamin E and a reasonably good selectivity for vitamin K₁ over carotene. Since selectivity appeared to be more crucial than small differences in sensitivity, we focused on 1-aminopyrene for further studies.

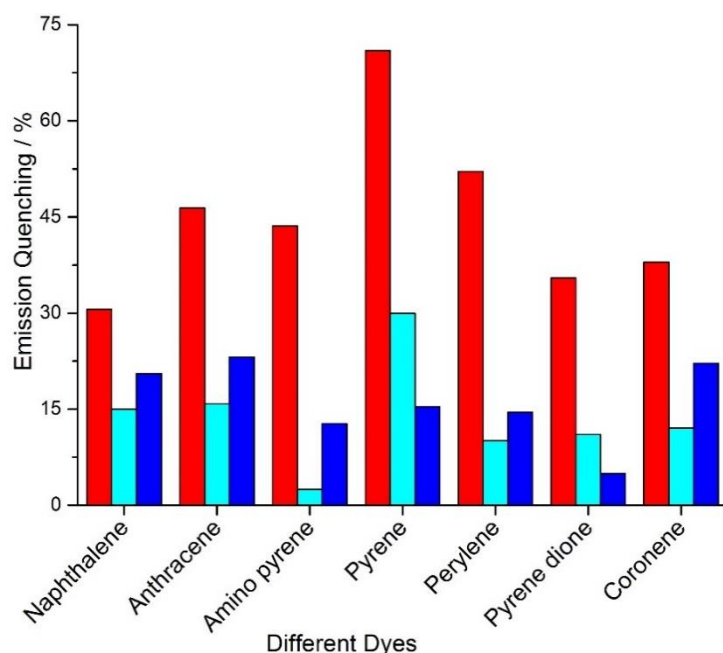


Figure 5.1 Fluorescence emission quenching of buffered aqueous solutions (100 mM MOPS, pH 7.0, H₂O with 0.8 vol% EtOH or 0.8 vol% EtOH:DMSO, 1:1) containing triton X-100 (0.90 mM), different aromatic dyes (4.0 μ M), and the analytes (4.0 μ M) vitamin K₁ (red), vitamin E (cyan) or carotene (blue).

First, we examined whether other surfactants would give better results. The amphiphiles, hexadecyltrimethylammonium bromide (C₁₆TABr), sodium dodecyl sulfate (SDS), and polysorbate 20 (Tween 20) were chosen for comparison. As in the case of triton X-100, a surfactant concentration slightly above the critical micelle concentration was employed. Out of the four surfactants, triton X-100 gave the best results (Figure 5.2).

Having identified triton X-100/1-aminopyrene as the 'best' mixture, we optimized the concentration of triton X-100 micelles to obtain good sensing condition (Figure 5.3). Then, we performed a more detailed analysis of the selectivity of the system. In addition to the analytes mentioned above, we employed the synthetic vitamin K₃, vitamin D and B, and a series of different lipophilic molecules including common fatty acids. The results are depicted in Figure 5.4. The sensor is remarkably selective for vitamin K₁, with most competing analytes resulting in less than 5% fluorescence quenching (carotene: 13%, Vitamin K₃: 9%)

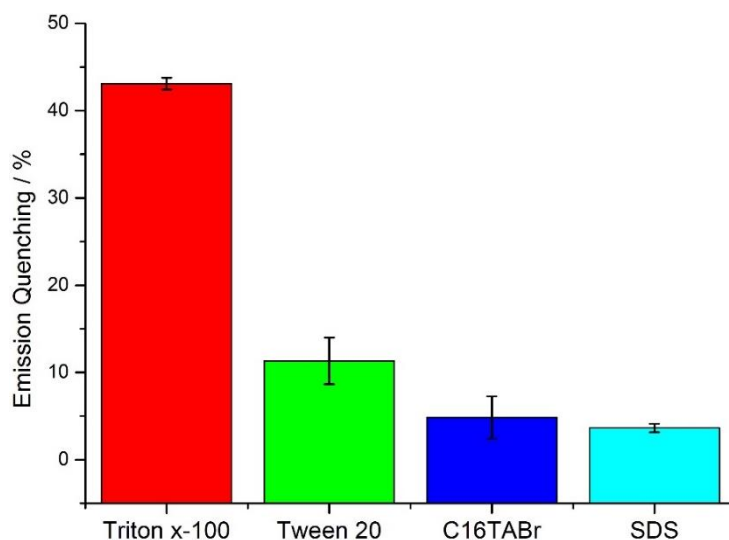


Figure 5.2 Fluorescence emission quenching ($\lambda_{\text{ex}} = 350 \text{ nm}$, $\lambda_{\text{em}} = 432 \text{ nm}$) of buffered aqueous solutions (100 mM MOPS, pH 7.0, H₂O with 0.8 vol% EtOH) containing 1-aminopyrene (4.0 μM) and the surfactant triton X-100 (0.90 mM), Tween 20 (70 μM), C₁₆TABr (1.0 mM), or SDS (9.0 mM) upon addition of vitamin K₁ (4.0 μM). The values are averages of three independent measurements.

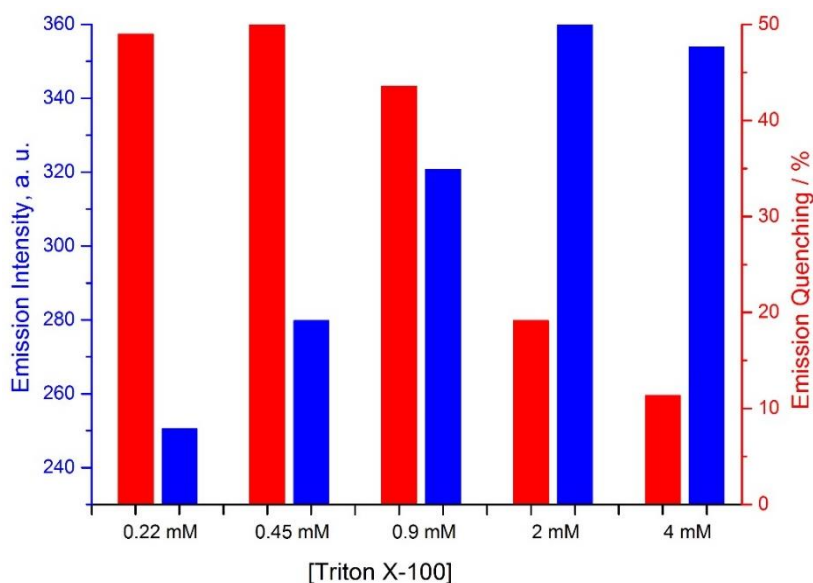


Figure 5.3 Fluorescence emission quenching and fluorescence emission intensity ($\lambda_{\text{ex}} = 350 \text{ nm}$, $\lambda_{\text{em}} = 432 \text{ nm}$) of buffered aqueous solutions (100 mM MOPS, pH 7.0, H₂O with 0.8 vol% EtOH) containing triton X-100 (0.22–4.0 mM) and 1-aminopyrene (4.0 μM) upon addition of vitamin K₁ (4.0 μM).

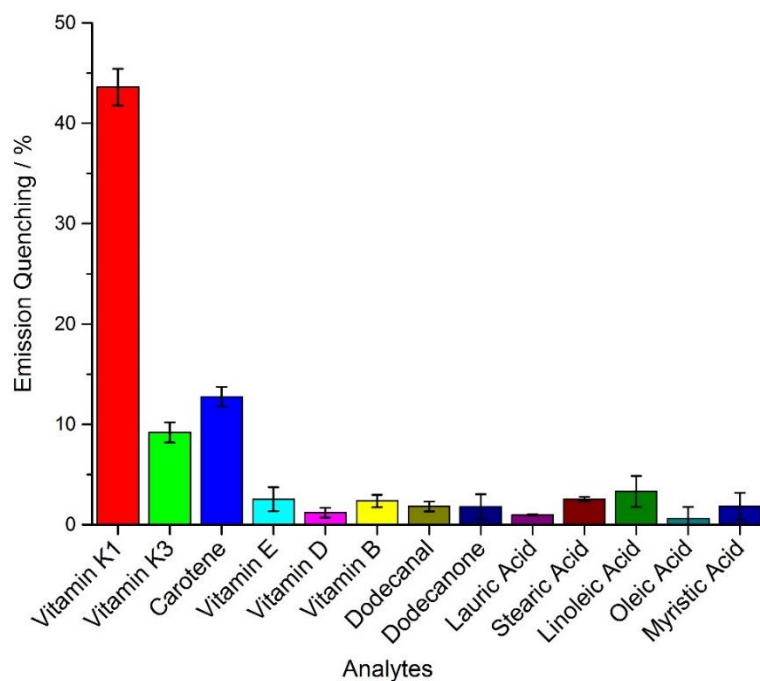


Figure 5.4 Fluorescence emission quenching ($\lambda_{\text{ex}} = 350 \text{ nm}$, $\lambda_{\text{em}} = 432 \text{ nm}$) of buffered aqueous solutions (100 mM MOPS, pH 7.0, H_2O with 0.8 vol% EtOH) containing triton X-100 (0.90 mM), 1-aminopyrene (4.0 μM) and different analytes (4.0 μM). The values are averages of three independent measurements.

Fluorescence titration experiments (Figure 5.6 and 5.7) with different amounts of vitamin K₁ show that the system allows sensing in the low micromolar concentration range with a limit of detection around 0.13 μM ($3\sigma_0$) (Figure 5.8). A Stern-Volmer plot revealed a linear relationship between I_0/I and concentration (Figure 5.8, inset). Fitting to a linear model gave a Stern-Volmer constant of $K_{\text{SV}} = 1.95 \times 10^5 \text{ M}^{-1}$.

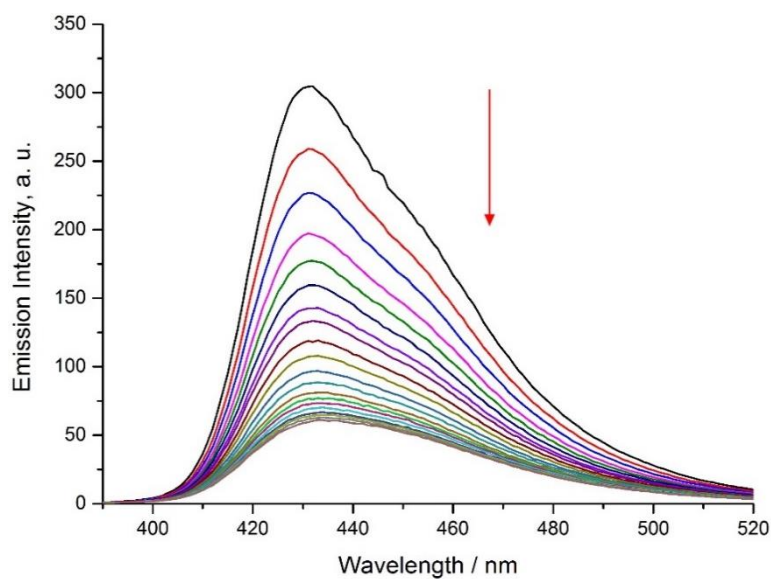


Figure 5.5 Fluorescence emission spectra (λ_{ex} : 350 nm) of buffered aqueous solutions (100 mM MOPS, pH 7.0, H₂O with 0–3.5 vol% EtOH) containing triton X-100 (0.90 mM), 1-aminopyrene (4.0 μM), and different amounts of vitamin K₁ (0–31 μM).

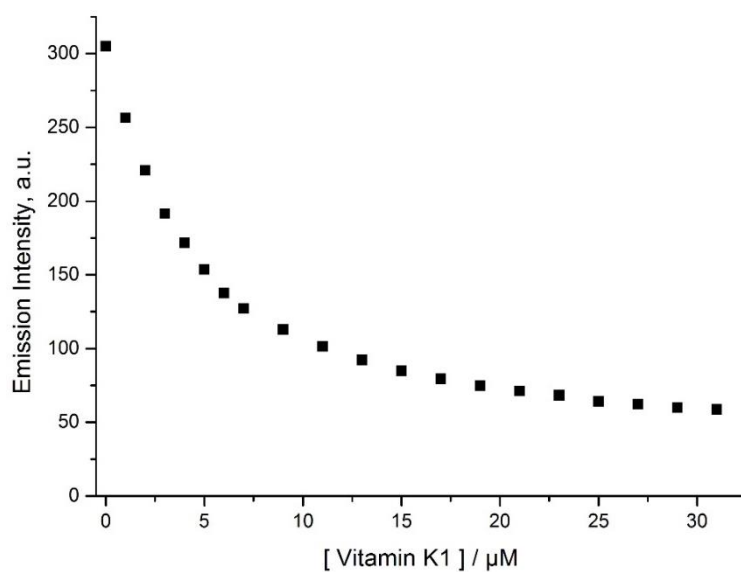


Figure 5.6 Fluorescence emission intensity ($\lambda_{\text{ex}} = 350$ nm, $\lambda_{\text{em}} = 432$ nm) of buffered aqueous solutions (100 mM MOPS, pH 7.0, H₂O with 0–3.5 vol% EtOH) containing triton X-100 (0.90 mM), 1-aminopyrene (4.0 μM), and different amounts of vitamin K₁ (0–31 μM).

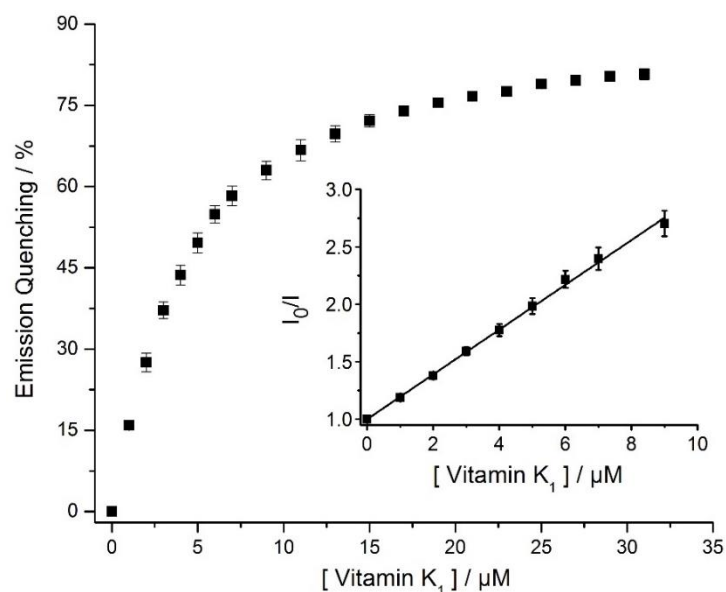


Figure 5.7 Fluorescence emission quenching ($\lambda_{\text{ex}} = 350 \text{ nm}$, $\lambda_{\text{em}} = 432 \text{ nm}$) of buffered aqueous solutions (100 mM MOPS, pH 7.0, H_2O with 0–3.5 vol% EtOH) containing triton X-100 (0.90 mM), 1-aminopyrene (4.0 μM) and different amounts of vitamin K_1 . The inset shows a Stern-Volmer plot obtained for low concentrations of vitamin K_1 . The line was obtained by fitting to a linear model. The values are averages of three independent measurements.

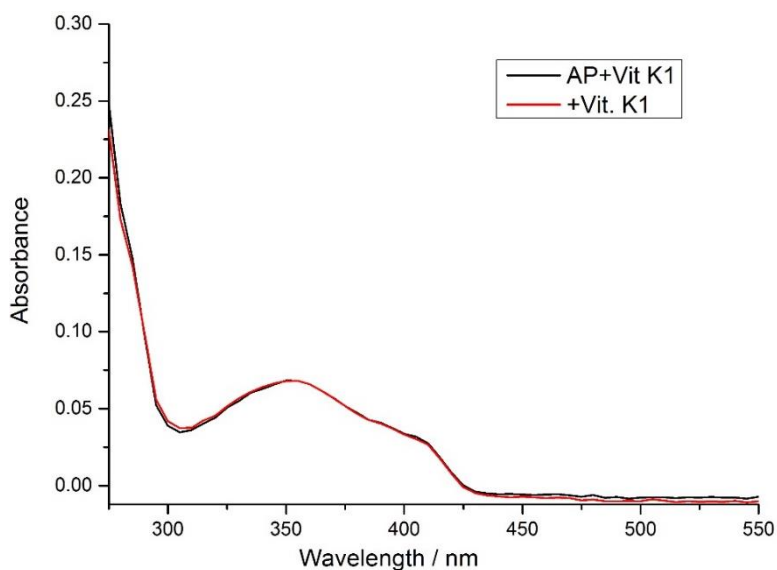


Figure 5.8 UV-vis spectra of buffered aqueous solutions (100 mM MOPS, pH 7.0, H_2O with 0.8 vol% EtOH) containing 1-aminopyrene (4.0 μM) and triton X-100 (0.90 mM) in the presence of vitamin K_1 (4.0 μM , red line), and the sum of the UV-vis spectra of 1-aminopyrene (4.0 μM) and vitamin K_1 (4.0 μM , black line) in buffered aqueous solutions (100 mM MOPS, pH 7.0, H_2O with 0.4 vol% EtOH) containing triton X-100 (0.90 mM).

Control experiments were performed to confirm that fluorescence quenching is indeed based on a dynamic encounter between dye and analyte inside the micelle (as depicted in

Scheme 5.1). Since the dye features an amino group and the analyte two carbonyl groups, the formation of a covalent connection via an imine bond appears to be a possibility. The following experiments suggest that imine bond formation is not contributing to the sensor response. The absorption spectrum of a dye/analyte mixture in a micellar solution is a superposition of the individual dye and analyte spectra (Figure 5.8). If imine bond formation would occur to a significant extent, a difference in the UV-vis spectrum should be detected. The results of ^1H NMR spectroscopy measurements at higher concentrations are in line with these data. A mixture of 1-aminopyrene (25 mM) and vitamin K₃ (a functional analogue of vitamin K₁, 25 mM) in CD_2Cl_2 (simulating the lipophilic micelle interior) showed no signs of imine bond formation after an equilibration time of 2 h (Figure 5.9).

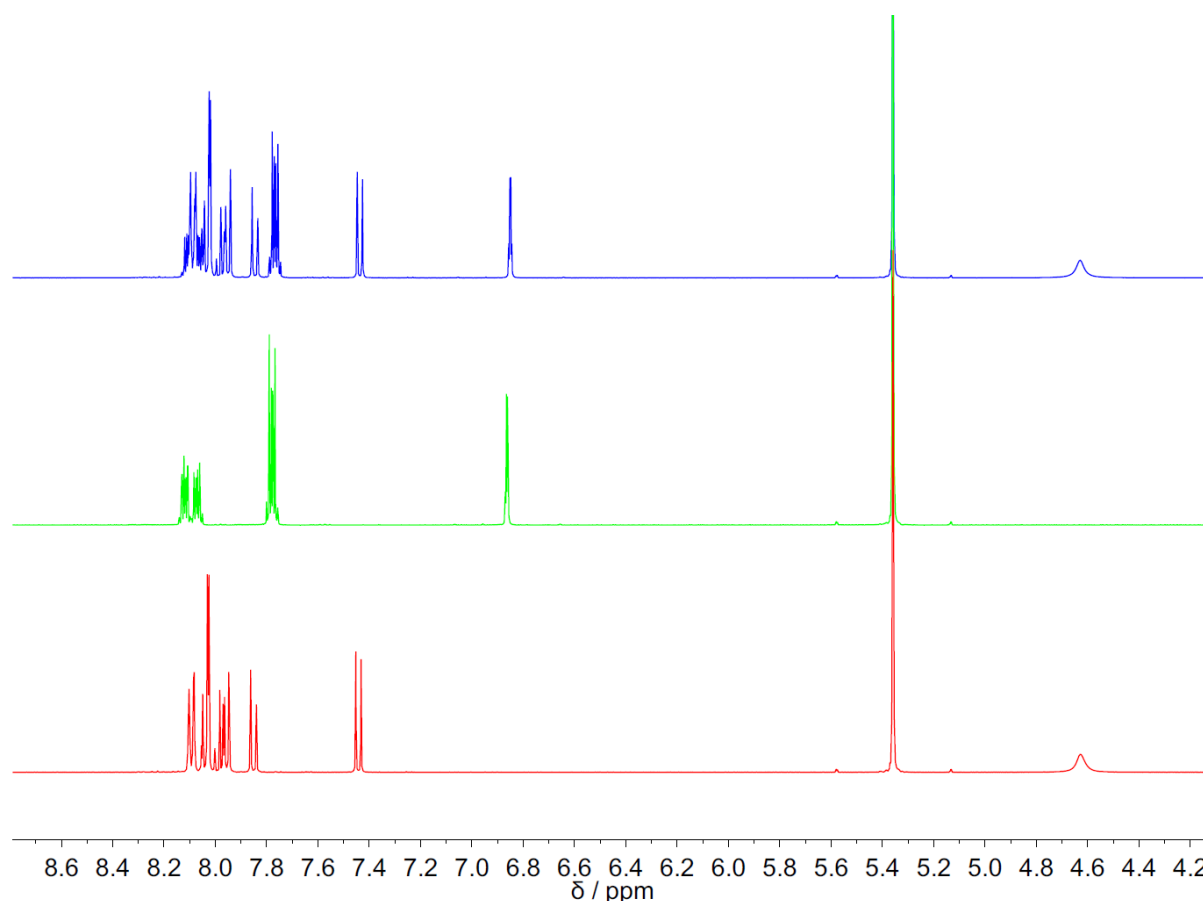


Figure 5.9 ^1H NMR spectra of 1-aminopyrene (bottom, 25 mM), vitamin K₃ (middle, 25 mM), and of a mixture of 1-aminopyrene and vitamin K₃ (top, 25 mM 1-aminopyrene + 25 mM vitamin K₃) in CD_2Cl_2 .

The importance of the co-localization inside the micelle was substantiated by control experiments with the dye **6** (trisodium 8-aminopyrene-1,3,6-trisulfonate, Figure 5.10). The

three sulfonate groups render the aminopyrene derivative highly water soluble, preventing a partitioning inside the micelle. As expected, no significant fluorescence quenching was observed when this dye was employed instead of 1-aminopyrene (Figure 5.11).

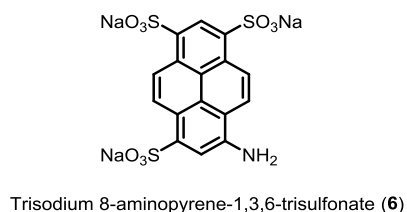


Figure 5.10 The structure of the dye **6** (trisodium 8-aminopyrene-1,3,6-trisulfonate)

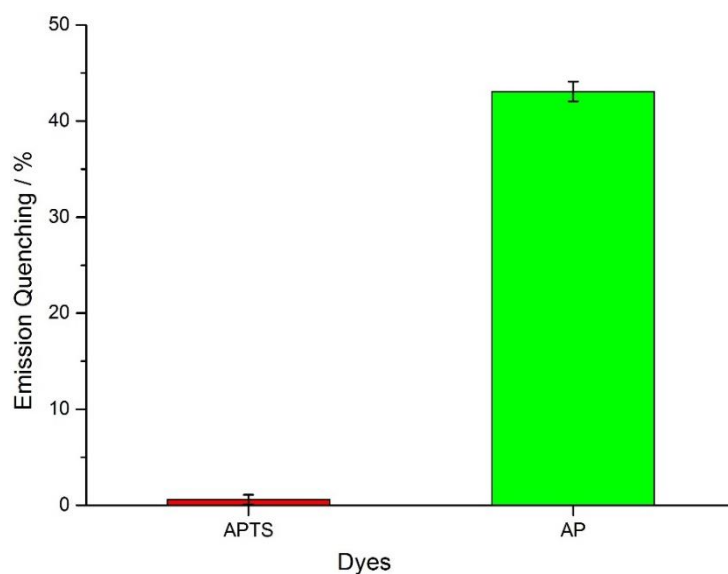


Figure 5.11 Fluorescence emission quenching of buffered aqueous solutions (100 mM MOPS, pH 7.0, H₂O with 0.8 vol% EtOH) containing triton X-100 (0.90 mM) and 1-aminopyrene (4.0 μM) or APTS (4.0 μM, λ_{ex} : 410 nm, λ_{em} : 502 nm) upon addition of vitamin K₁ (4.0 μM). Excitation and emission wavelengths: APTS: λ_{ex} : 410 nm, λ_{em} : 502 nm, 1-aminopyrene: λ_{ex} = 350 nm, λ_{em} = 432 nm. The values are averages of three independent measurements.

The co-localization of 1-aminopyrene and vitamin K₁ inside the micelle is expected to result in a high local concentration. Such an increase in apparent concentration would not be expected for mixtures of 1-aminopyrene and vitamin K₁ in bulk organic solvents. Accordingly, less quenching was observed when the dye and the analyte were mixed in normal organic solvents (Figure 5.13, fluorescence emission intensities of 1-aminopyrene in different organic solvents is given in appendix, Figure A19).

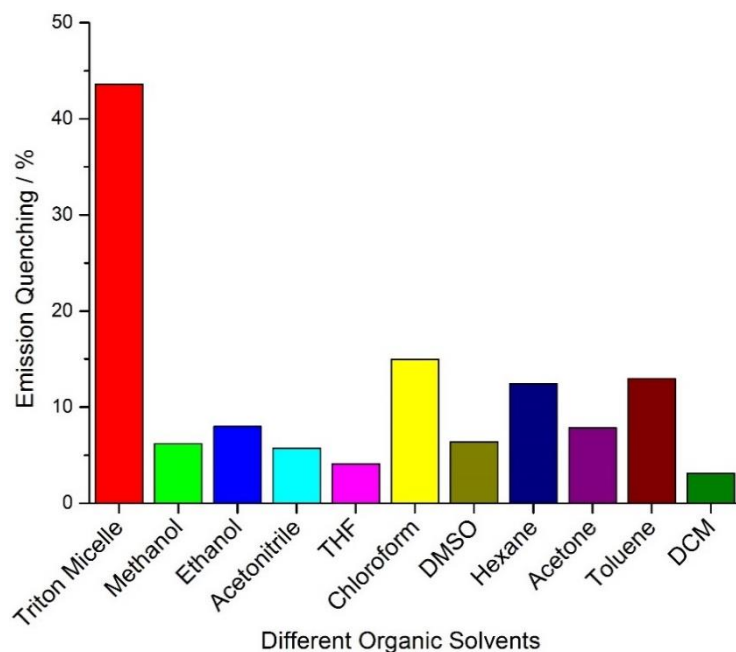


Figure 5.12 Fluorescence emission quenching ($\lambda_{\text{ex}} = 350 \text{ nm}$) of 1-aminopyrene ($4.0 \text{ } \mu\text{M}$) upon addition of vitamin K_1 ($4.0 \text{ } \mu\text{M}$) in different organic solvents.

In order to evaluate if our sensing system could be used to quantify vitamin K_1 in a 'real world' sample, we have performed an analysis of a vitamin K_1 preparation. Phytomenadione is a solution of synthetic vitamin K_1 sold by *Roche*. It is used for the treatment of hypoprothrombinemia and vitamin K deficiency. According to the vendor, the phytomenadione ampoule contains $2 \text{ mg}/0.2 \text{ mL}$ of vitamin K_1 mixed with N-cholyglycine and lecithin, among others. For the analysis of phytomenadione, an aliquot was diluted with ethanol to give a solution with a concentration of 0.50 mM . Parts of this solution were then added to the sensing ensemble of triton X-100 and 1-aminopyrene and a fluorescence spectrum was recorded. The concentration of vitamin K_1 was calculated using the Stern-Volmer constant determined before. The measurements suggest a concentration of $1.91 \pm 0.09 \text{ mg}/0.2 \text{ mL}$ for the phytomenadione solution. This value is in close agreement with what is given on the package, indicating that we can use our system to sense vitamin K_1 in a moderately complex matrix.

5.3 Conclusion

We have described a simple assay for the detection of vitamin K₁ in the low micromolar concentration range by fluorescence spectroscopy. The assay is based on the dye 1-aminopyrene, which is solubilized in buffered aqueous solution with the help of the surfactant triton X-100. The addition of vitamin K₁ to this sensing ensemble results in co-localization of the dye and the analyte in the micellar sub-phase. This confinement induces dynamic quenching of the fluorescence of 1-aminopyrene. The assay displays good selectivity for vitamin K₁ over other lipophilic compounds. As proof of principle for the applicability of our assay, we have shown that it can be used to determine vitamin K₁ in a commercial preparation.

5.4 Experimental

All chemicals and solvents were purchased from standard suppliers and used without further purification. MOPS buffer (100 mM MOPS buffer, pH 7.0) was prepared by dissolving 3-(N-morpholino) propanesulfonic acid in bidistilled water. Surfactant stock solutions were prepared by dissolving an appropriate amount of the surfactant in 100 mM MOPS buffer, pH 7.0. HCl and NaOH solutions were used to adjust the pH of the buffers. Due to the light sensitivity of vitamin K₁, the solutions were handled in subdued light. Fluorescence measurements were performed on a Varian Cary Eclipse fluorescence spectrophotometer at room temperature. Absorption spectra were measured on a Cary 50 bio spectrometer (Varian). Quartz cuvettes were used for the absorbance and fluorescence measurements. ¹H NMR spectra were recorded on a Bruker Avance DPX 400 instrument. Multiplicities of the ¹H NMR signals are assigned as following: s (singlet) and d (doublet). High resolution mass spectra were recorded with a waters Q-TOF Ultima (ESI-TOF) instrument.

Stock solutions (1.0 mM) of the different dyes were prepared in ethanol (naphthalene, 1-aminopyrene, and pyrene dione) or DMSO (anthracene, pyrene, perylene, and coronene). Stock solutions of the three test analytes (1.0 mM) vitamin K₁, vitamin E, and carotene were prepared in ethanol. An aliquot of the respective dye stock solution (6 μ L) was added to a quartz cuvette containing a buffered aqueous solution of triton X-100. After 15 min, a fluorescence spectrum was recorded (λ_{ex} : 350 nm, λ_{em} : 432 nm). Subsequently, an aliquot (6 μ L) of the respective analyte stock solution was added to the mixture, and a second fluorescence spectrum was recorded after 5 min. The emission quenching was calculated by comparing the emission intensity at 432 nm with and without the analyte. Final concentrations: MOPS (100 mM, pH 7.0), triton X-100 (0.90 mM), [analyte] = 4.0 μ M, [dye] = 4.0 μ M, V_{total} = 1.5 mL, 0.8 vol% EtOH or 0.4 vol% EtOH and 0.4 vol% DMSO. Due to the light sensitivity of vitamin K₁, the solutions were handled in subdued light.

For the selectivity test, stock solutions of the analytes (1.0 mM) including vitamin B, vitamin E, vitamin D, vitamin K₃, carotene, dodecanal, dodecanone, lauric acid, stearic acid, linoleic acid, oleic acid, and myristic acid were prepared in ethanol. An aliquot (6 μ L) of the respective analyte stock solution was added to a buffered aqueous solution of 1-aminopyrene and triton X-100. Final concentrations: MOPS (100 mM, pH 7.0), triton X-100 (0.90 mM), [analyte] = 4.0 μ M, [dye] = 4.0 μ M, V_{total} = 1.5 mL, 0.8 vol% EtOH.

Fluorescence titration was also done using a buffered aqueous solution containing 1-aminopyrene and triton X-100 as a sensing system for vitamin K₁ at different concentrations. For the low concentrations of vitamin K₁, a second stock solution with a concentration of 250 μ M was prepared (in EtOH). Aliquots of the two vitamin K₁ stock solutions were added to the sensor solution and fluorescence spectra were recorded. Final concentrations: MOPS (100 mM, pH 7.0), triton X-100 (0.90 mM), [vit. K₁] = 0–31 μ M, [dye] = 4.0 μ M, V_{total} = 1.5 mL, 0–3.5 vol% EtOH.

Control experiments were done using UV-vis spectra of a mixture of 1-aminopyrene and vitamin K₁ and of 1-aminopyrene and vitamin K₁ which were taken under same condition. The sum of the individual 1-aminopyrene and vitamin K₁ spectra is a superposition of the spectrum of the mixture (Figure 5.8).

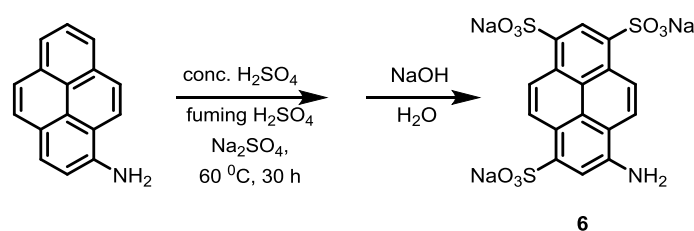
NMR experiments were performed to evidence that there is no imine formation between the dye and analyte. For the NMR study, 25 mM of 1-aminopyrene, 25 mM of

vitamin K₃ and their equimolar mixtures were prepared in CD₂Cl₂ and ¹H NMR spectra of all samples were recorded (Figure 5.9).

Phytomenadione was analyzed in one commercial product using our sensing system. The fluorescence of 1-aminopyrene/triton X-100 solutions is quenched upon addition of vitamin K₁. A Stern-Volmer plot revealed a linear relationship between I_0/I and concentration (Figure 5.4). Fitting to a linear model gave a Stern-Volmer constant of $K_{SV} = 1.95 \times 10^5 \text{ M}^{-1}$. This value was used to determine the vitamin K₁ concentration in phytomenadione, a solution of synthetic vitamin K₁ sold by *Roche*. The sample contains potential interferents such as N-cholyglycine and lecithin, among others. For the analysis, a stock solution of phytomenadione (0.5 mM) was prepared by dissolving the liquid content of an ampule from *Roche* (according to the package: 2 mg/0.2 mL) in ethanol (8.87 mL). An aliquot of this stock solution (15 µL) was then added to a quartz cuvette containing a buffered aqueous solution of triton X-100 (0.9 mM) and 1-aminopyrene (4.0 µM). After 5 min, a fluorescence measurement was performed (λ_{ex} : 350 nm), and the fluorescence intensity I at 432 nm was used to calculate the concentration of vitamin K₁ in solution using the Stern-Volmer equation.

$$\left(\frac{I_0}{I}\right) = 1 + K_{SV}[\text{Vitamin K}_1]$$

By taking the dilution into account, the concentration of the liquid in the ampule was then calculated. Three independent measurements were performed using aliquots from the three phytomenadione stock solutions. An averaged value of $1.91 \pm 0.09 \text{ mg/0.2 mL}$ was obtained, in close agreement with what is stated on the package (2 mg/0.2 mL).

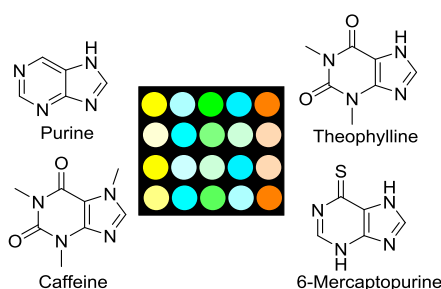


Trisodium 8-aminopyrene-1,3,6-trisulfonate (**6**) was synthesized in a similar fashion as described in the literature:³⁸⁷ Na₂SO₄ (4.00 mmol, 565 mg) and conc. H₂SO₄ (2.5 mL) were added to a 100 mL round bottom flask equipped with a drying tube (charged with drierite and NaOH pellets). 1-Aminopyrene (1.00 mmol, 217 mg) was then added, followed by the addition of fuming H₂SO₄ (20%, 3.0 mL). The reaction mixture was stirred at 60 °C for 30 h. The mixture was then carefully poured into 50 mL of water, neutralized with 50% NaOH

solution to pH 7.0, and concentrated under reduced pressure. The resulting slurry was extracted with MeOH (*via* sonication) and filtered. Further purification was achieved by column chromatography (SiO₂; eluent: NH₄OH : IPA - 1 : 2) to give the trisulfonated dye **6** as an orange powder (378 mg, 0.722 mmol, 72 %).

¹H NMR (CD₃OD, 400 MHz) δ = 8.07 (s, 1H, CH_{arom}), 8.31 (d, J = 9.63 Hz, 1H, CH_{arom}), 8.81 (d, J = 9.73 Hz, 1H, CH_{arom}), 8.94 (d, J = 9.66 Hz, 1H, CH_{arom}), 9.05 (d, J = 9.72 Hz, 1H, CH_{arom}), 9.20 (s, 1H, CH_{arom}). ¹³C NMR (100 MHz, CDCl₃): δ = 113.44, 116.29, 118.03, 120.66, 122.72, 123.52, 124.69, 126.35, 126.60, 127.45, 130.02, 130.50, 134.75, 135.15, 140.98, 144.43. ESI-MS calculated for C₁₆H₉NS₃O₉ [(M-3Na+H)⁻²] m/z = 227.4725 found 227.4720.

6 Array-Based Sensing of Purine Derivatives with Fluorescent Dyes



In this chapter, we describe a sensor array which can be used to differentiate pharmacologically important purine derivatives with good accuracy. The array is composed of four polysulfonated fluorescent dyes, all of which can bind purines via π -stacking interactions. The complexation of the analytes resulting in partial quenching of the fluorescence. The fluorescence response of the four dyes provides a characteristic signal pattern, enabling the identification of thirteen purine derivatives at low millimolar concentration. Furthermore, it is possible to use the array for obtaining information about the quantity and purity of purine samples.

This work was published in:³⁸⁸ “Array-based sensing of purine derivatives with fluorescent dyes” Ziya Köstereli and Kay Severin, *Org. Biomol. Chem.*, 2015, **13**, 9231-9235.

6.1 Introduction

Naturally occurring purine alkaloids are pharmacologically important compounds. Caffeine is a stimulus of the central nervous system (CNS) and “the world’s most popular drug”.³⁸⁹ The structurally related theophylline is a bronchodilator which is used by people suffering from respiratory problems such as asthma.³⁹⁰⁻³⁹¹ The isomers theobromine and paraxanthine are – like caffeine – stimulants of the CNS.³⁹²⁻³⁹³ Some synthetic purine derivatives have also gained importance as drugs. 8-Chlorotheophylline, for example is given in combination with the antihistamine diphenhydramine as a drug against motion sickness.³⁹⁴⁻³⁹⁵ The simple 6-mercaptopurine is an immunosuppressive drug which is used during the treatment of leukemia and inflammatory bowel disease, among others.³⁹⁶ The N9-alkylated purine derivatives cladribine and penciclovir are important drugs as well, the former being used against hairy cell leukemia and multiple sclerosis,³⁹⁷ whereas the latter is a key component for the treatment of herpesvirus.³⁹⁸⁻³⁹⁹

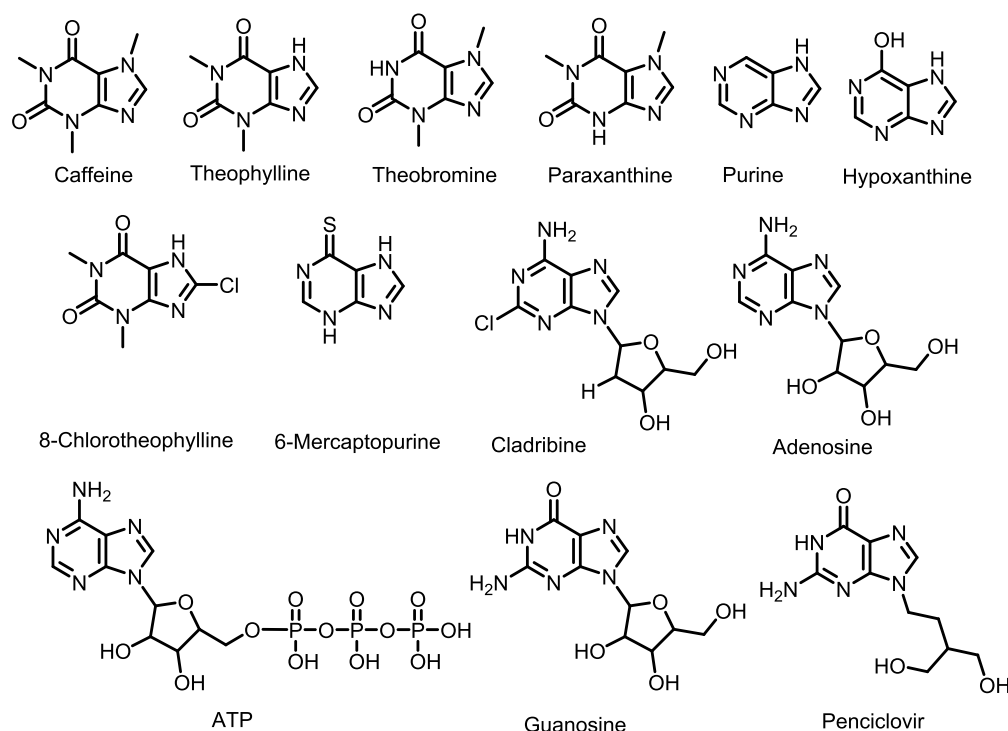


Figure 6.1 Purine and some biological and pharmacological important derivatives

Given the biological and pharmacological importance of purine derivatives, it is not surprising that substantial efforts have been devoted to create synthetic receptors and optical

sensors for these compounds.⁴⁰⁰ Caffeine has been a particularly popular target, and numerous studies about the selective recognition⁴⁰¹⁻⁴⁰⁶ and/or sensing^{407-412,413-414} of this drug have appeared over the last years. Other investigations have focused on the binding of natural methylxanthines (caffeine, theophylline and theobromine) to RNA⁴¹⁵⁻⁴¹⁶ or DNA,⁴¹⁷ on the complexation and the fluorescence sensing of theobromine via hydrogen bonds,⁴¹⁸⁻⁴¹⁹ and on the binding of purine derivatives by molecularly imprinted polymers.⁴²⁰⁻⁴²⁴

A key difficulty in the preparation of selective receptors or chemosensors for purine derivatives is the structural similarity of these compounds. This is nicely illustrated by the published chemosensors for caffeine, which typically show a poor selectivity for caffeine over theophylline.^{407-412,413-414} However, the selectivity of caffeine over theophylline was improved over the last years as discussed below with an example.

The Chang group has published a turn-on caffeine sensor, namely, “Caffeine Orange” based on fluorescence.⁴¹⁰ The poorly-fluorescent BODIPY-based dye was used to selectively detect caffeine in aqueous solution as well as in commercial drinks (Figure 6.2). Addition of caffeine results in 250-fold enhancement in fluorescence emission. Poorly water soluble dyes aggregates in water resulting in self-quenching. Addition of caffeine de-assembles the dye aggregates and triggers the formation of larger fluorescent aggregates. As a result, fluorescence of dye molecules shows up. They also described a non-toxic kit for the detection of caffeine in commercial beverages. It was possible to detect various concentrations of caffeine by naked-eye using a laser pointer. Lastly, they set up a microfluidic device for automated and quick detection of caffeine.

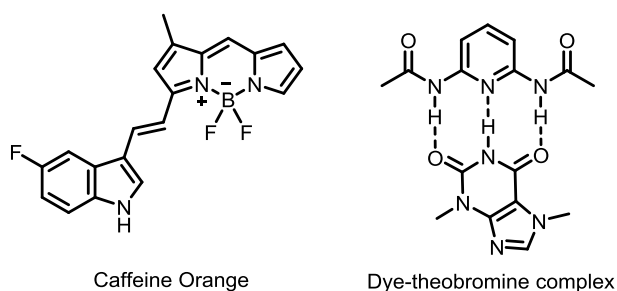


Figure 6.2 The structures of the caffeine and theobromine sensor.

The selectivity for the detection of other purine derivatives such as theophylline, theobromine is still a challenging task in the literature examples. For example, in a fluorescent theobromine sensor developed by the Fun group, a simple 2,6-diaminopyridine modified dye

was used to detect theobromine in acetonitrile solution (Figure 6.2).⁴⁰⁵ The dye binds theobromine *via* hydrogen bonding resulting in fluorescence quenching. Quantification of theobromine was possible by using UV-vis or fluorescence spectroscopy. The selectivity of the sensor over xanthine alkaloids was good except for caffeine.

In this chapter, we demonstrate that a small set of polysulfonated fluorescent dyes can be used to create a powerful sensor array for purine derivatives. The array allows the identification of a series of important purines with good precision in the low millimolar concentration range. Furthermore, we show that it is possible to differentiate samples containing different amounts of caffeine or theophylline and samples containing mixtures of these compounds.

6.2 Results and Discussion

In 2011, the Severin group has reported that the commercially available fluorescent dyes trisodium 8-hydroxypyrene-1,3,6-trisulfonate (HPTS) and tetrasodium pyrene-1,3,6,8-tetrasulfonate (PTS) can be used as molecular probes for the detection of caffeine in water (Figure 6.3).⁴¹⁴ The recognition of caffeine occurs via π -stacking interactions, which lead to partial quenching of the fluorescence. Both dyes display a moderate selectivity for caffeine over the dimethylxanthine derivatives theophylline and theobromine. In line with these results, it was found that the apparent binding constant of HPTS for caffeine ($K_a \sim 250 \text{ M}^{-1}$) is approximately twice as high as those for theophylline and theobromine. Guided by computational chemistry,⁴²⁵ the fluorescent dye disodium 3,4:3',4'-bibenzo[*b*]thiophene-2,2'-disulfonate (TDS, Figure 6.3) was subsequently synthesized. This dye was found to display a unique fluorescence response upon addition of caffeine, which was attributed to non-covalent interactions of caffeine with the dye in the ground state and in the excited state.⁴²⁶ As a consequence, it was possible to use the dye for ratiometric measurements, thereby increasing the selectivity for caffeine over theophylline.

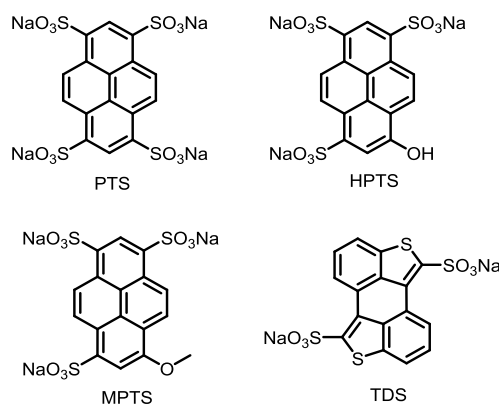


Figure 6.3 The polysulfonated fluorescent dyes used in this study.

Following these first investigations, we have examined the optical response of trisodium 8-methoxypyrene-1,3,6-trisulfonate (MPTS) upon addition of caffeine and theophylline (20 mM MOPS buffer, pH 7.0). These investigations were performed merely as control experiments, because we expected very similar results as observed for the structurally related dyes HPTS and PTS. Surprisingly, however, the selectivity profile of MPTS was inverted: a stronger fluorescence quenching was observed for theophylline than for caffeine (Figure 6.4). These results were corroborated by NMR titration experiments in D₂O, which showed that MPTS binds theophylline stronger than caffeine (Figure 6.5 and 6.6).

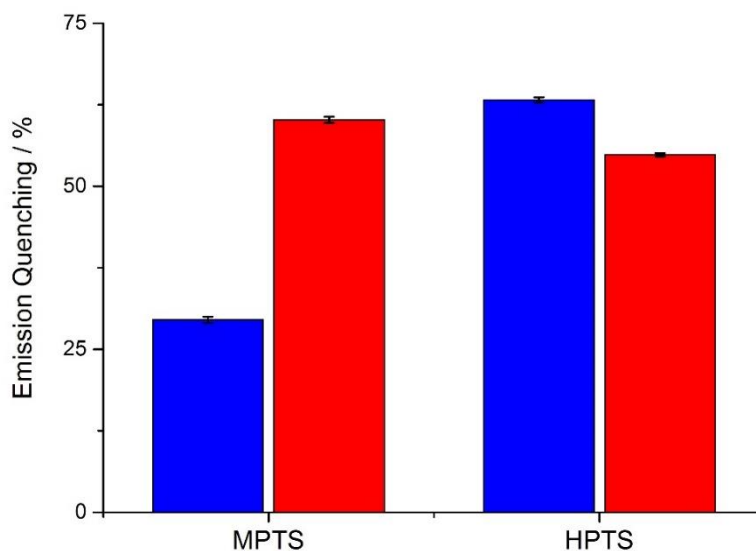


Figure 6.4 Fluorescence emission quenching of buffered aqueous solutions (20 mM MOPS, pH 7.0) containing MPTS (λ_{ex} : 350 nm, λ_{em} : 430 nm) or HPTS (λ_{ex} : 460 nm, λ_{em} : 511 nm) upon addition of caffeine (blue) or theophylline (red) ([dye]_{final} = 2.0 μ M, [analyte]_{final} = 5.0 mM). The values represent averages of 3 independent measurements.

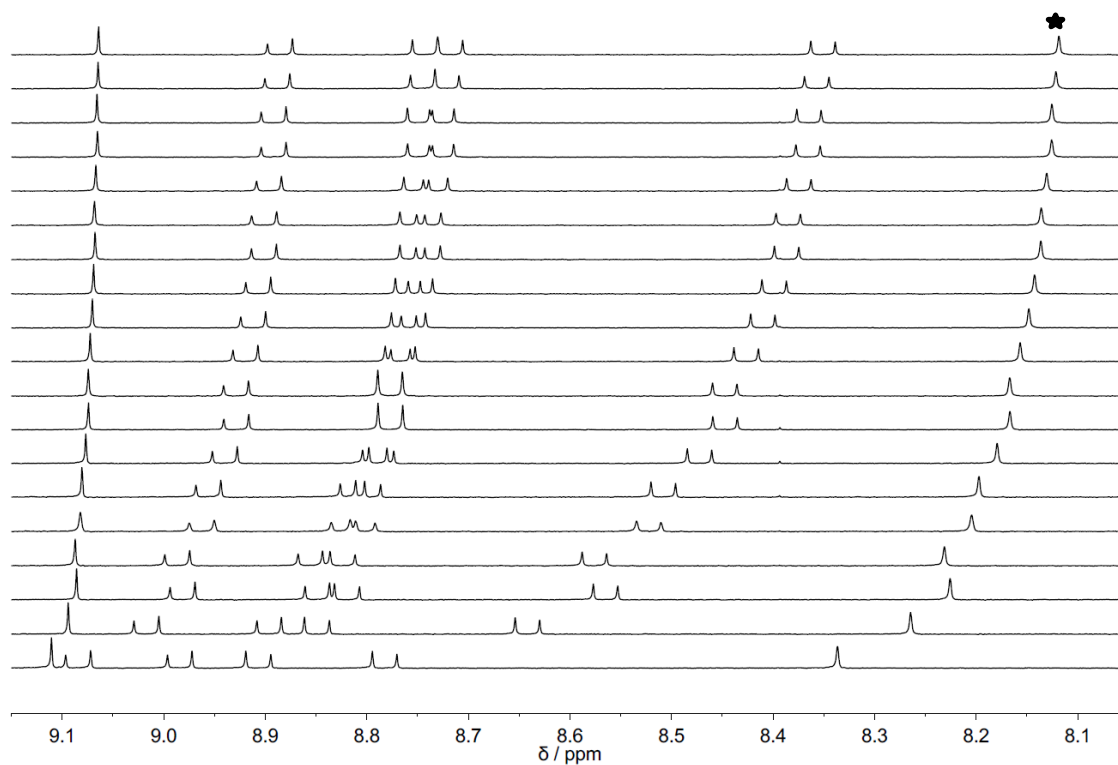


Figure 6.5 ^1H NMR spectra of solutions containing MPTS (1.0 mM) and different amounts of caffeine (1.0 - 20.0 mM) in D_2O . The derived binding is $K_a : 98 \text{ M}^{-1}$.

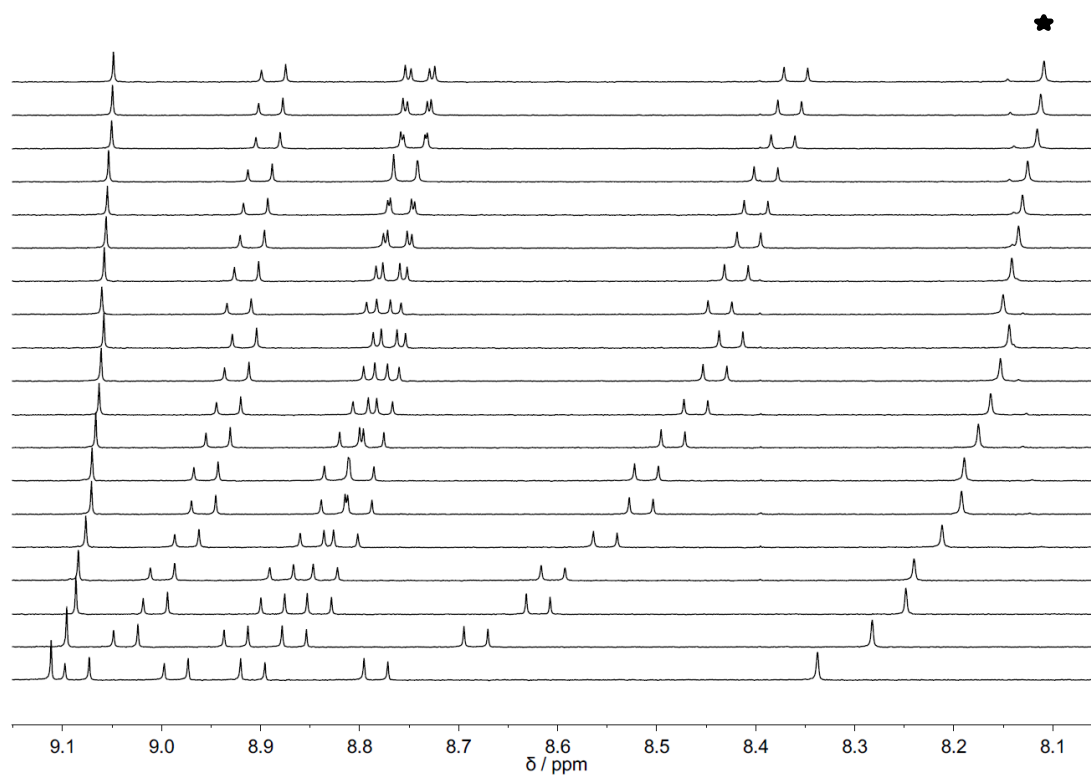


Figure 6.6 ^1H NMR spectra of solutions containing MPTS (1.0 mM) and different amounts of theophylline (1.0 - 20.0 mM) in D_2O . The derived binding is $K_a : 120 \text{ M}^{-1}$.

The different selectivity of MPTS when compared to HPTS or PTS, and the unique optical response of TDS suggested to us that it might be possible to use a sensor array approach for the differentiation of structurally related purine derivatives. To test this hypothesis, we analyzed the ten purine derivatives shown in Figure 6.1 using the dyes HPTS, PTS, MPTS and TDS (Figure 6.7). This small array of four fluorescent dyes was used to generate a five-dimensional signal output, with TDS fluorescence being recorded at two different wavelengths (424 and 546 nm). The fluorescence measurements were performed in buffered aqueous solution (20 mM MOPS, pH 7.0) with a dye concentration of 2.0 μ M and an analyte concentration of 1.0 mM. For each analyte, five independent measurements were performed.

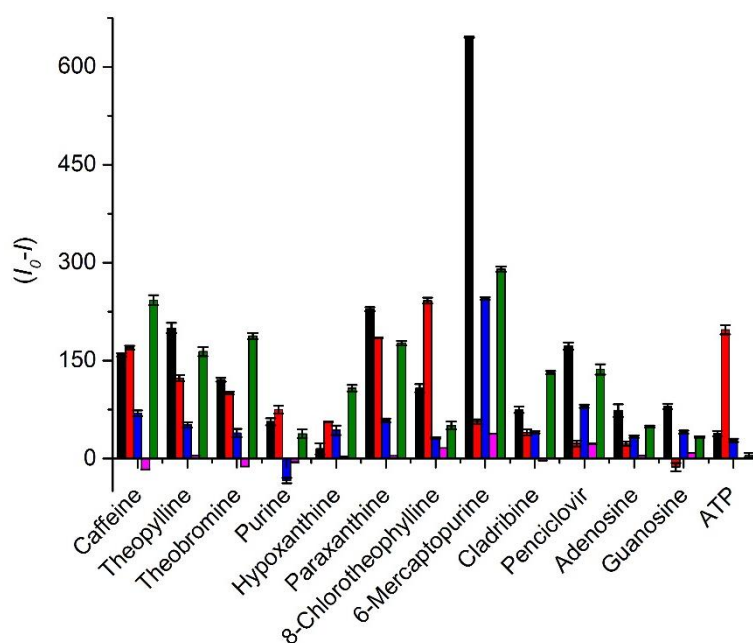


Figure 6.7 Changes of the fluorescence emission intensities of buffered aqueous solutions (20 mM MOPS, pH 7.0) containing the dyes MPTS (λ_{ex} : 350 nm, λ_{em} : 430 nm, black), HPTS (λ_{ex} : 460 nm, λ_{em} : 511 nm, red), TDS (λ_{ex} : 350 nm, λ_{em} : 424 nm, blue; λ_{em} : 546 nm, pink) or PTS (λ_{ex} : 364 nm, λ_{em} : 384 nm, green) upon addition of caffeine, theophylline, theobromine, purine, hypoxanthine, paraxanthine, 8-chlorotheophylline, 6-mercaptopurine, cladribine or penciclovir ($[\text{dye}]_{\text{final}} = 2.0 \mu\text{M}$, $[\text{analyte}]_{\text{final}} = 1.0 \text{ mM}$). The values represent averages of five independent measurements.

A characteristic signal pattern was obtained for each of the thirteen analytes (Figure 6.7). As expected, the signal pattern is rather similar for the isomers theophylline, theobromine and paraxanthine, but on close inspection one can clearly detect differences in relative and absolute signal intensity. However, other analytes clearly stand out. 8-

Chlorotheophylline, for example, leads to a rather selective quenching of HPTS fluorescence, and 6-mercaptapurine is an efficient and selective quencher for MPTS.

The array data was then processed by using a principal component analysis (PCA).⁴²⁷ The corresponding two-dimensional score plot shows well separated data clusters (Figure 6.8), confirming that the individual purine analytes can be identified correctly. It is worth to point out that the two main principal components combined account for only 82.2% of the variance of the system. Factor 3 contributes 14.6% and factor 4 still 1.3%. These values indicate a rather high dimensionality, even though we have only used a small array.

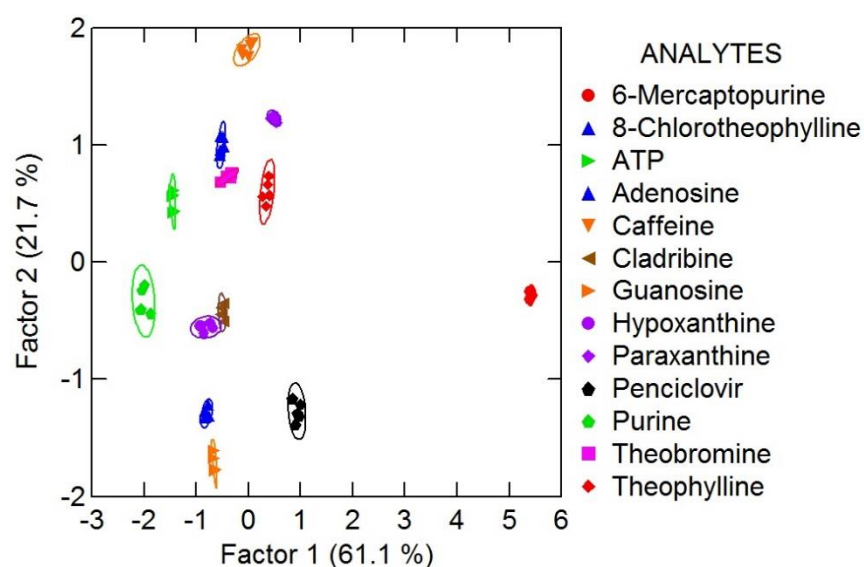


Figure 6.8 Two-dimensional PCA score plot for the analysis of samples containing different purine derivatives ($[\text{dye}]_{\text{final}} = 2.0 \mu\text{M}$, $[\text{analyte}]_{\text{final}} = 1.0 \text{ mM}$). The data were obtained as described above.

To quantify the similarity of the signal patterns, we have used a hierarchical cluster analysis (HCA). The resulting HCA dendrogram confirms the similarity of the data from the isomers theophylline, theobromine and paraxanthine, and the unique position of the analyte 6-mercaptapurine (Figure 6.9).

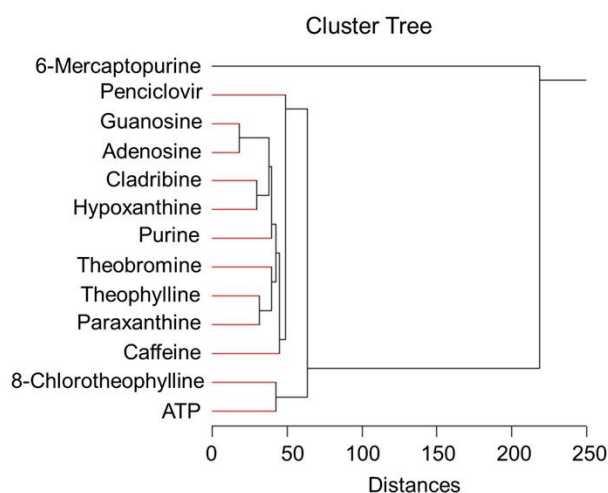


Figure 6.9 HCA dendrogram derived from the array data.

To demonstrate the scope of the sensor array, we examined a more difficult analytical task: the differentiation of samples containing either caffeine or theophylline at different concentrations (1.0 - 5.0 mM). In addition, we have used five samples containing mixtures of caffeine and theophylline with a fixed total concentration of 5.0 mM. The entire set of 19 samples was then subjected to a sensor array analysis as described above and the fluorescence data is depicted in Figure 6.10. The PCA score plot indicates that it is possible to identify the samples containing pure caffeine or theophylline at a given concentration and to distinguish the samples which contain different caffeine-theophylline ratios (Figure 6.11).

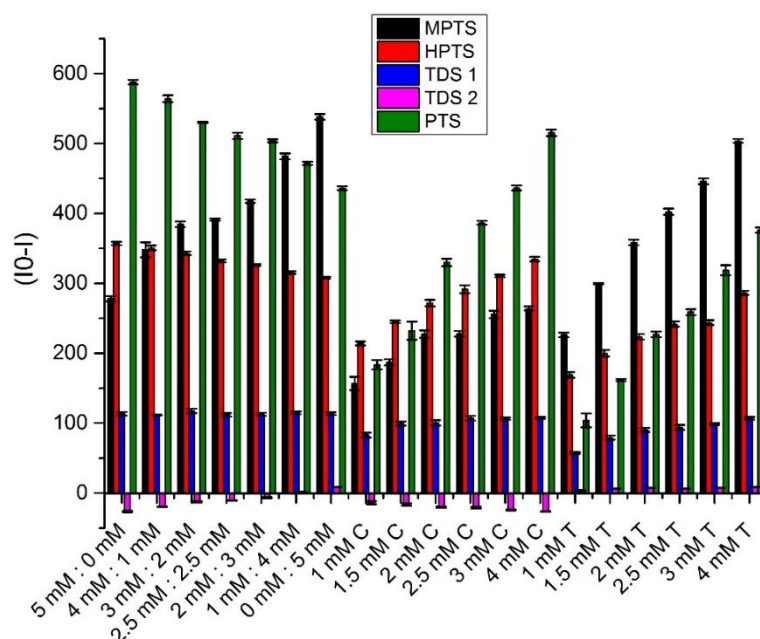


Figure 6.10 Fluorescence emission intensities of the dyes ($[\text{dye}]_{\text{final}} = 2.0 \mu\text{M}$) including MPTS ($\lambda_{\text{exc}}: 350 \text{ nm}$, $\lambda_{\text{ems}}: 430 \text{ nm}$, black), HPTS ($\lambda_{\text{exc}}: 460 \text{ nm}$, $\lambda_{\text{ems}}: 511 \text{ nm}$, red), TDS ($\lambda_{\text{exc}}: 350 \text{ nm}$, $\lambda_{\text{ems}}: 424 \text{ nm}$ (blue) and 546 nm , pink) and PTS ($\lambda_{\text{exc}}: 364 \text{ nm}$, $\lambda_{\text{ems}}: 384 \text{ nm}$) in the presence of the analytes ($[\text{caffeine}]_{\text{final}} = 1.0 - 5.0 \text{ mM}$; $[\text{theophylline}]_{\text{final}} = 1.0 - 5.0 \text{ mM}$; $[\text{caffeine} - \text{theophylline}]_{\text{final}} = 5.0 : 0.5 \text{ mM}$ in 20 mM MOPS , $\text{pH } 7.0$). The values represent averages of five independent measurements.

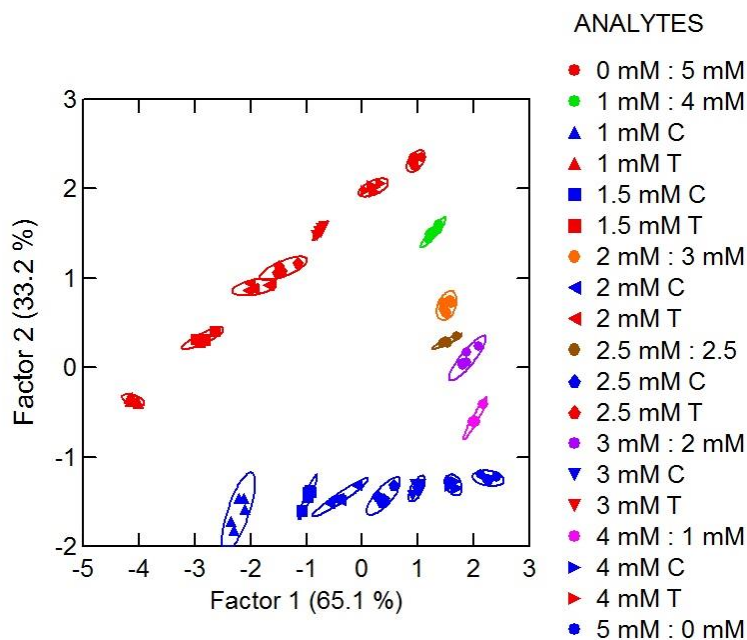


Figure 6.11 Two-dimensional PCA score plot for the analysis of samples containing caffeine and/or theophylline at different concentrations and ratios ($[\text{dye}] = 2.0 \mu\text{M}$, $[\text{caffeine}] = 1.0 - 5.0 \text{ mM}$; $[\text{theophylline}] = 1.0 - 5.0 \text{ mM}$; $[\text{caffeine}:\text{theophylline mix}] = 5.0:0 \text{ mM} - 0:5.0 \text{ mM}$). The data were obtained as described in the main text.

In addition to the PCA, we have used the same data set to perform a linear discriminant analysis (LDA). A “Jack-knifed matrix” validation procedure was then performed, randomly omitting one measurement at a time. The remaining data were used as the training set for the LDA, and the omitted observation was classified. This procedure resulted in a correct classification in 98% of all cases. For a real application (e.g. simultaneous quantification of caffeine and theophylline in a sample of unknown composition), it would be necessary to record a more comprehensive data set using additional test samples. The data could then be used to train an artificial neural network. The trained network would be able to make a prediction regarding the composition of unknown samples.

In order to estimate the limit of detection for a quantitative analysis, we have examined the response of the four dyes with theophylline samples of 0.50 and 0.25 mM. A good signal-to-noise ratio was observed for 0.50 mM, but the 0.25 mM sample provided a too weak response with the dyes HPTS and TDS. It is thus recommended to use sample concentration of 0.50 mM or higher.

6.3 Conclusion

A small sensor array composed of four polysulfonated fluorescence dyes was used for the optical analysis of purine derivatives. The discriminatory power of the system is remarkably high, allowing the differentiation of thirteen different purines at a concentration of 1.0 mM with good precision. Furthermore, we have shown that it is possible to obtain information about the quantity and the purity of samples. This point was demonstrated by the analysis of samples containing different amounts of caffeine and/or theophylline. In terms of potential applications, one should note that an array approach with cross-reactive receptors is prone to interference from a complex matrix. However, it could be a well suited method to achieve a fast and cheap quality control of synthetic samples. From a more fundamental point of view, it is noteworthy that an intrinsically non-specific interaction such as π -stacking can be used to differentiate structurally closely related compounds.

6.4 Experimental

All chemicals and solvents were purchased from standard suppliers and used without further purification. Stock solutions were prepared with bi-distilled water and were stored at 4 °C. MOPS buffer (20 mM MOPS buffer, pH 7.0) was prepared by dissolving 3-(N-morpholino) propanesulfonic acid in bidistilled water. HCl and NaOH solutions were used to adjust the pH of the buffer. The dyes MPTS, HPTS, and PTS were obtained from commercial sources, and TDS was synthesized as described earlier.⁴²⁶ Fluorescence measurements were performed on a Varian Cary Eclipse fluorescence spectrophotometer at room temperature.

Stock solutions of dyes (0.20 mM) including MPTS, HPTS, TDS, PTS and the analytes (1.0 - 5.0 mM) were prepared in 20 mM MOPS buffer (pH 7.0). The dye solution is added to the corresponding analyte containing buffered aqueous solutions ($V_{\text{total}} = 1.5$ mL, in 20 mM MOPS buffer, pH 7.0). The fluorescent signal was measured 5 min after sample preparation. Ten different analytes (caffeine, theophylline, theobromine, xanthine, hypoxanthine, paraxanthine, 8-chlorotheophylline, 6-mercaptopurine, cladribine, ATP, adenosine, guanosine and penciclovir) were employed ($[\text{dye}]_{\text{final}} = 2.0 \mu\text{M}$; $[\text{analyte}]_{\text{final}} = 1.0$ mM in 20 mM MOPS buffer, pH 7.0). Also, the two analytes, caffeine and theophylline, were analyzed at different concentrations ($[\text{dye}]_{\text{final}} = 2.0 \mu\text{M}$; $[\text{analyte}]_{\text{final}} = 0.25 - 5.0$ mM) and the mixtures of caffeine and theophylline at different ratio ($[\text{dye}]_{\text{final}} = 2.0 \mu\text{M}$; $[\text{caffeine} : \text{theophylline}]_{\text{final}} = 5:0 - 0:5$ mM in 20 mM MOPS, pH 7.0).

Five independent fluorescence measurements were performed for each sample with four different dyes (MPTS, HPTS, TDS, PTS) for multivariate analysis. The data were analyzed with the help of the statistics software SYSTAT 11. The wavelength of the emission maxima of the dyes (λ_{exc} , MPTS: 350 nm, λ_{ems} , MPTS: 430 nm, λ_{exc} , HPTS: 460 nm, λ_{ems} , HPTS: 511 nm, λ_{exc} , TDS: 350 nm, λ_{ems} , TDS: 424 nm and 546 nm (excimer), λ_{exc} , PTS: 364 nm, λ_{ems} , PTS: 384 nm) were used for the multivariate analyses. The emission values at these wavelengths were used as input for principal component analyses (PCA), linear discriminant analyses (LDA), and hierarchical cluster analysis (HCA).

¹H NMR titration experiments were performed to calculate the binding constant of MPTS-caffeine complex and MPTS-theophylline complex. The first titration experiment (Figure 6.5) was performed with MPTS in the presence of different amount of caffeine ($[\text{MPTS}] = 1.0$ mM; $[\text{caffeine}] = 1.0 - 20.0$ mM) and the second titration (Figure 6.6) was

performed with MPTS in the presence of theophylline ($[MPTS] = 1.0 \text{ mM}$; $[theophylline] = 1.0 - 20.0 \text{ mM}$). The labelled signals were used to calculate binding constant using Wineqnmr software assuming a 1:1 complexation. The derived binding was 98 M^{-1} for MPTS-caffeine complex and MPTS-theophylline 120 M^{-1}

7 General Conclusion

In this thesis, different approaches of fluorescent-based chemosensors are presented for the detection of important analytes in buffer solutions. These approaches include analyte-induced aggregation/de-aggregation, pattern-based sensing and micelled-based sensing.

In chapter 2, we have described a conceptually new chemosensor for the biogenic amine spermine. A charge-frustrated amphiphile (dye **1**) composed of a highly fluorescent head group and an eicosane side chain was used as a chemosensor. Addition of spermine causes analyte-induced aggregation and it results in pronounced fluorescence quenching. The sensor showed a very good selectivity over closely related biogenic amines such as spermidine. It was also very sensitive. Low nanomolar concentration of spermine could be detected. The sensing of spermine was also achieved in a complex matrix (in artificial urine) using same sensing system.

We have presented a conceptually new ‘one-cuvette’ sensing system for the pattern-based analysis of seven aminoglycosides in the following chapter 3. It is a novel approach to create an adaptable system for pattern-based sensing. We used a mixture of two fluorescent amphiphiles **2** and **3**, to constitute a sensing ensemble. The amphiphiles form a dynamic mixture of micellar aggregates. Addition of aminoglycosides modifies the relative amount and the composition of the micelles. The re-equilibration of the system is analyte-specific, and characteristic fluorescence spectra are obtained for different aminoglycosides. Likely, there is a multivalent interaction of the polycationic analytes with the polyanionic micellar aggregates formed from **2** and **3**. These interactions affects the optical response of the system. The sensing system allowed accurate differentiation in the low micromolar concentration range. It was also possible to distinguish pure aminoglycosides from their mixtures. Overall, our results demonstrate the potential of fluorescent amphiphiles for the creation of DCL sensors.

In chapter 4, we used the amphiphilic fluorescent dye **5** for the sensing of Al^{3+} in the low micromolar concentration range. In the presence of Al^{3+} , there was analyte-induced aggregation of the dye **5**, and the aggregation of the dye resulted in a strong quenching of its fluorescence. From an application point of view, it is noteworthy that the assay can be performed in aqueous solution at neutral pH without the need of large amounts of organic co-solvents. It displays remarkable selectivity when histidine is added as masking agent. The nonfluorescent dye- Al^{3+} complex was used as a sensing ensemble for the detection of citric acid, a known chelator for Al^{3+} . It reversed the aggregation of **5** resulting in an increase in the fluorescence emission (turn-on response). The sensing ensemble was used to detect the citric acid concentration in commercial beverages.

In chapter 5, we have described a simple micelle-based assay for the detection of vitamin K₁ in the low micromolar concentration range by fluorescence spectroscopy in chapter 5. A mixture of the surfactant triton X-100 and 1-aminopyrene was used as a sensing assay in buffered aqueous solution. Vitamin K₁ co-localizes with the fluorescent pyrene dye in the micelle and it results in fluorescence emission decrease *via* dynamic quenching. The assay is selective for vitamin K₁ over other potential analytes. We have shown that the sensing assay can also be used to detect the concentration of vitamin K₁ in a commercial preparation.

In chapter 6, a small sensor array was described for the optical analysis of ten purine derivatives. The array is based on fluorescence response of the four dyes, which provides a characteristic signal pattern. The array enables the differentiation of thirteen different purines at a concentration of 1.0 mM with good precision. It was also possible to obtain information about the quantity and the purity of samples using same array.

8 Annex

8.1 UV and Fluorescence Spectra

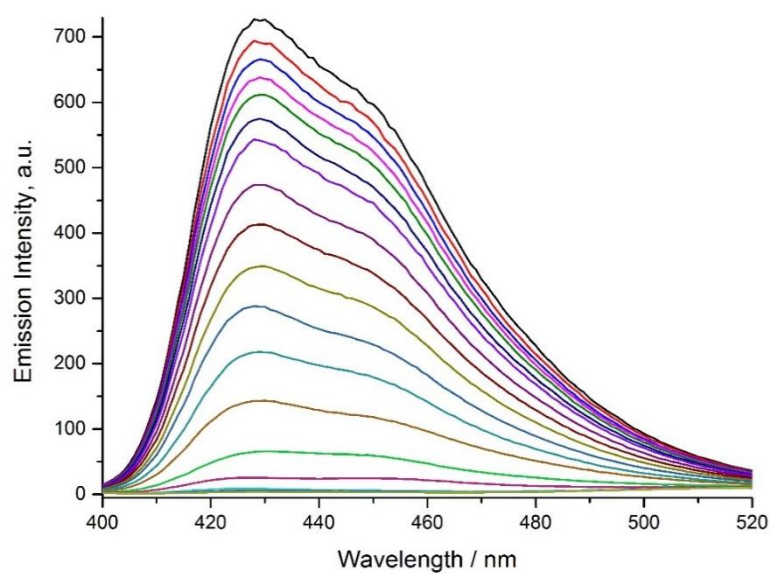


Figure A1 Fluorescence emission spectra (λ_{ex} : 350 nm) of buffered aqueous solutions (0.8 mM MOPS, pH 7) containing dye **1** (2.0 μM) and different amounts of spermine (0-1.44 μM).

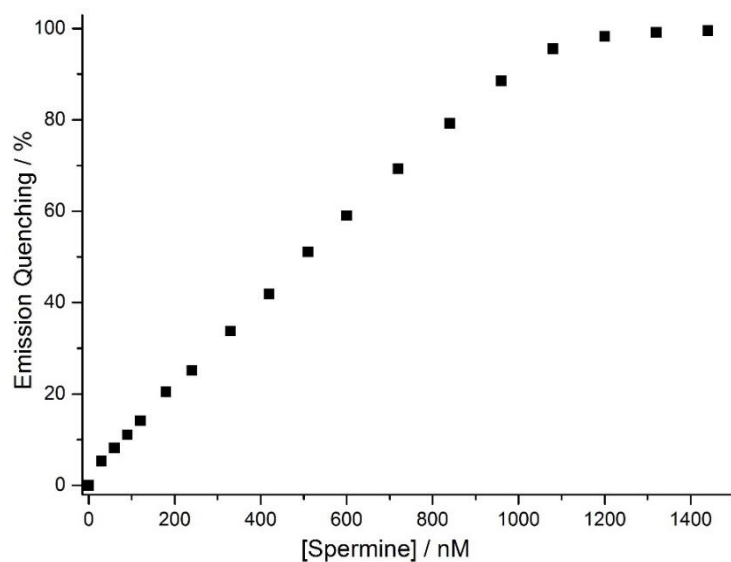


Figure A2 Fluorescence emission quenching ($\lambda_{\text{ex}} = 350$ nm, $\lambda_{\text{em}} = 430$ nm) of buffered aqueous solutions (0.8 mM MOPS, pH 7.0) containing dye **1** (2.0 μM) and different amounts of spermine (0-1.44 μM).

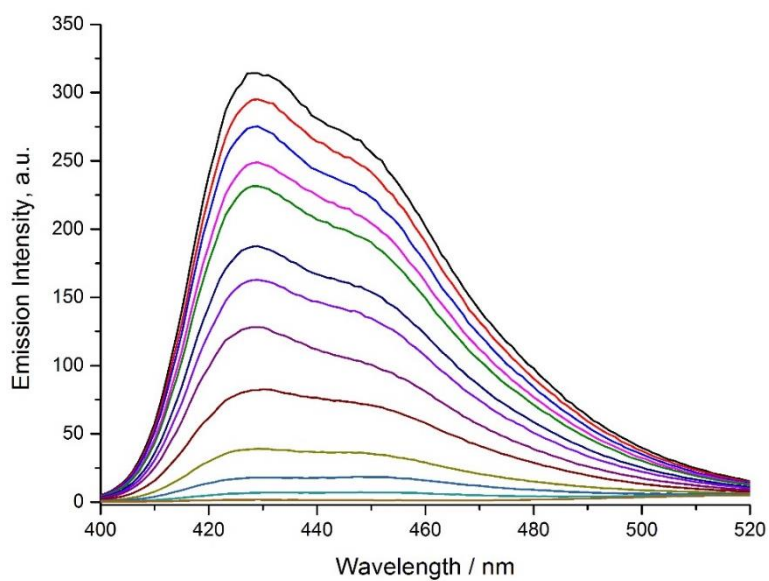


Figure A3 Fluorescence emission spectra (λ_{ex} : 350 nm) of buffered aqueous solutions (0.8 mM MOPS, pH 7) containing dye **1** (5.0 μM) and different amounts of spermine (0-3.20 μM).

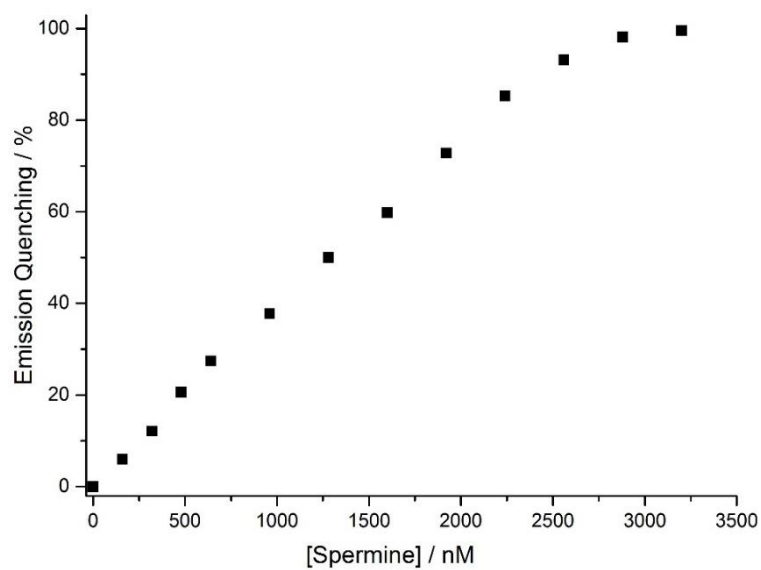


Figure A4 Fluorescence emission quenching ($\lambda_{\text{ex}} = 350$ nm, $\lambda_{\text{em}} = 430$ nm) of buffered aqueous solutions (0.8 mM MOPS, pH 7.0) containing dye **1** (5.0 μM) and different amounts of spermine (0-3.20 μM).

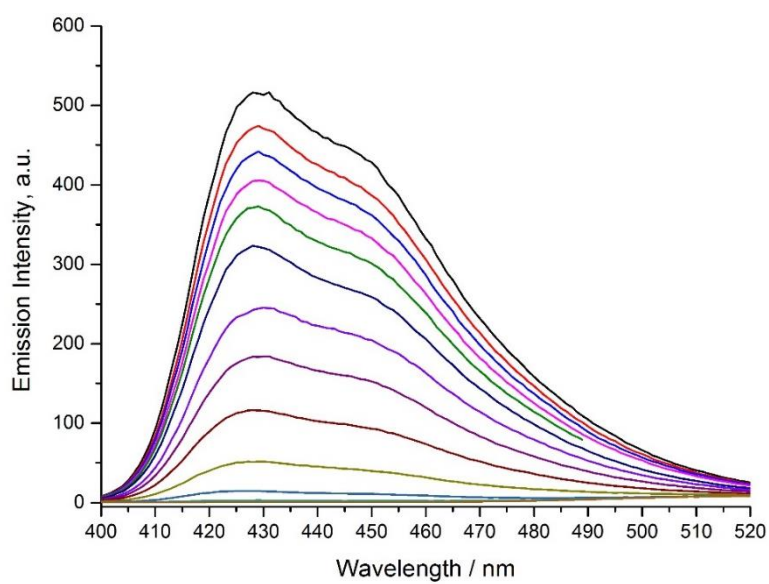


Figure A5 Fluorescence emission spectra ($\lambda_{\text{ex}}: 350$ nm) of buffered aqueous solutions (0.8 mM MOPS, pH 7) containing dye **1** (8.0 μM) and different amounts of spermine (0-5.36 μM).

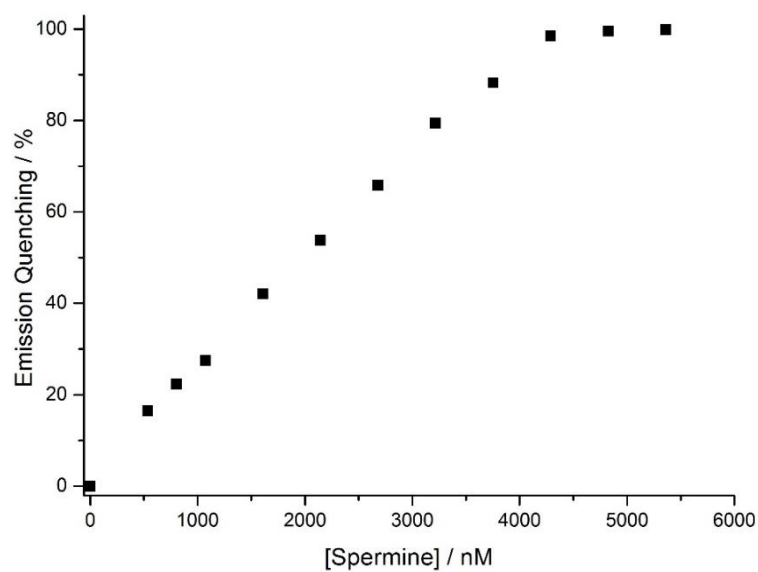


Figure A6 Fluorescence emission quenching ($\lambda_{\text{ex}} = 350$ nm, $\lambda_{\text{em}} = 430$ nm) of buffered aqueous solutions (0.8 mM MOPS, pH 7.0) containing dye **1** (8.0 μM) and different amounts of spermine (0-5.36 μM).

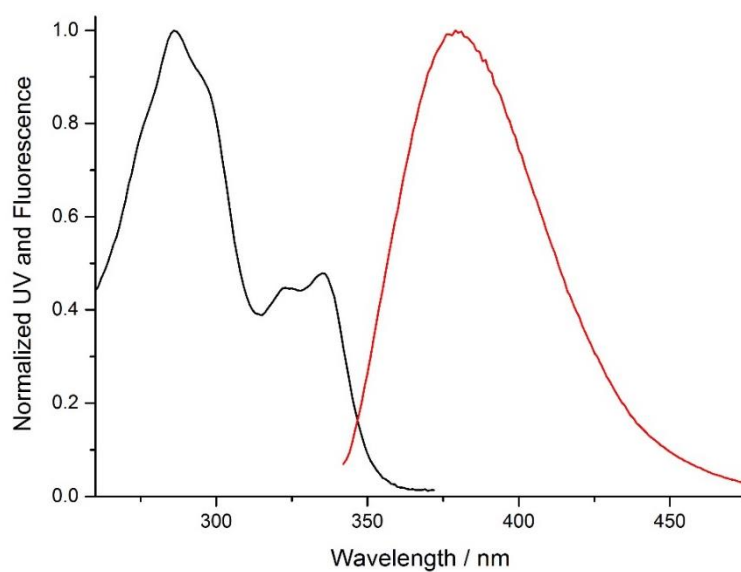


Figure A7 Normalized UV-vis (black) and fluorescence (red) spectra ($\lambda_{\text{ex}}: 335$ nm) of buffered aqueous solutions (10 mM MOPS, pH 7.0) containing dye **2** (10 μM).

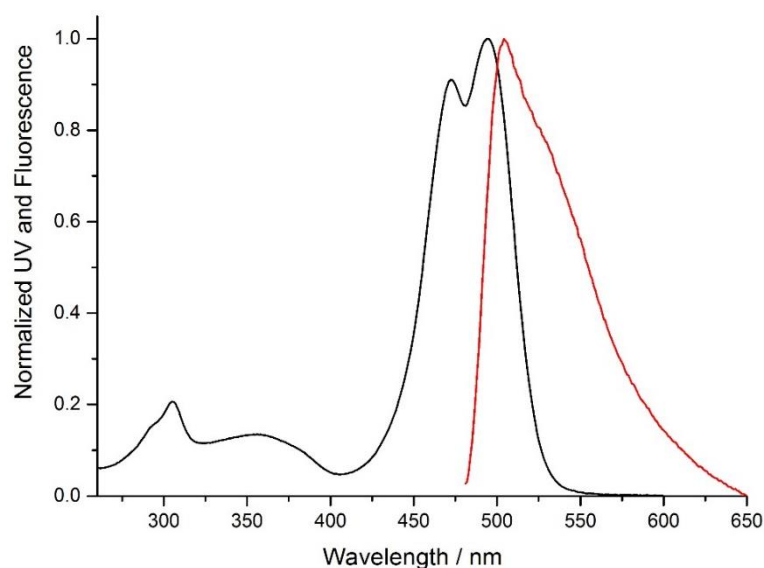


Figure A8 Normalized UV-vis (black) and fluorescence (red) spectra (λ_{ex} : 470 nm) of buffered aqueous solutions (10 mM MOPS, pH 7.0) containing dye **3** (10 μM).

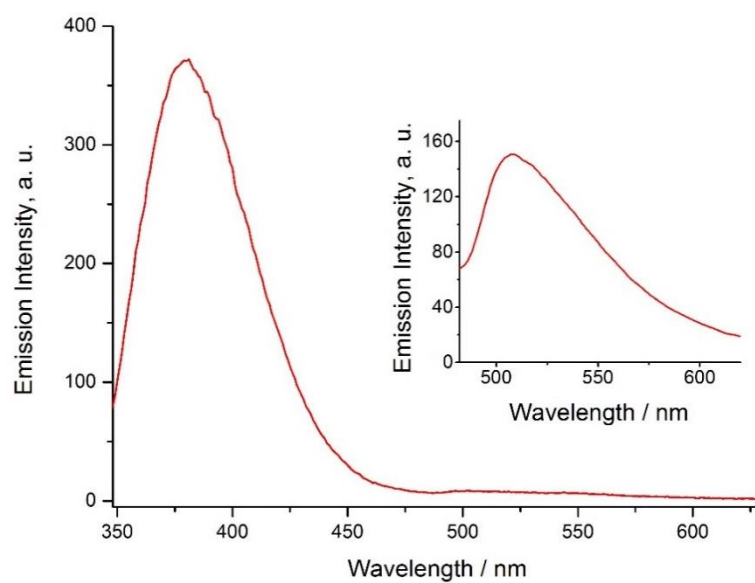


Figure A9 Fluorescence emission spectra (λ_{ex} : 335 nm) of solutions containing a mixture of dye **2** and **3** ($[\mathbf{2}] = 4 \mu\text{M}$; $[\mathbf{3}] = 30 \mu\text{M}$) in MOPS buffer (10 mM, pH 7.0). The inset shows the fluorescence emission of dye **3**. This spectrum was obtained using a slightly larger slit width on the spectrometer.

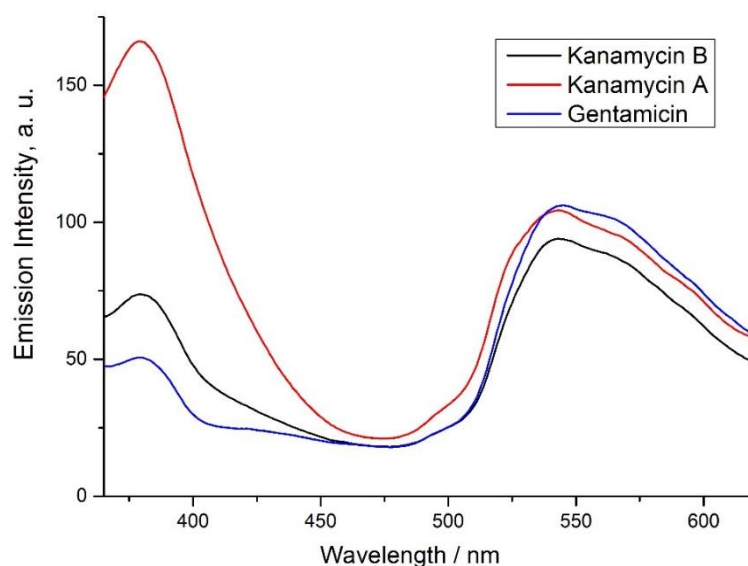


Figure A10 Fluorescence emission spectra (λ_{ex} : 335 nm) of solutions containing a mixture of dye **2** and **3** ($[\mathbf{2}] = 4 \mu\text{M}$; $[\mathbf{3}] = 30 \mu\text{M}$) and the analytes gentamicin (blue line), kanamycin A (red line), or kanamycin B (black line) ($[\text{analyte}] = 10 \mu\text{M}$; 10 mM MOPS, pH 7.0).

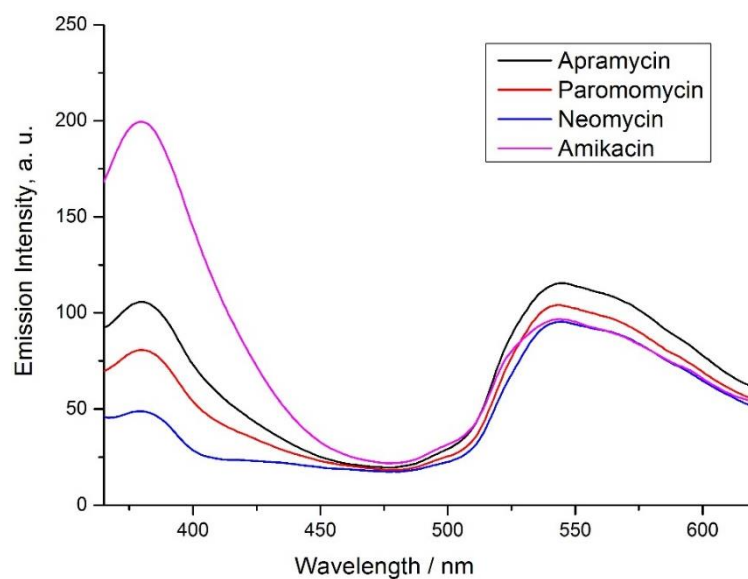


Figure A11 Fluorescence emission spectra (λ_{ex} : 335 nm) of solutions containing a mixture of dye **2** and **3** ($[\mathbf{2}] = 4 \mu\text{M}$; $[\mathbf{3}] = 30 \mu\text{M}$) and the analytes neomycin (blue line), paromomycin (red line), apramycin (black line), or amikacin (pink line) ($[\text{analyte}] = 10 \mu\text{M}$; 10 mM MOPS, pH 7.0).

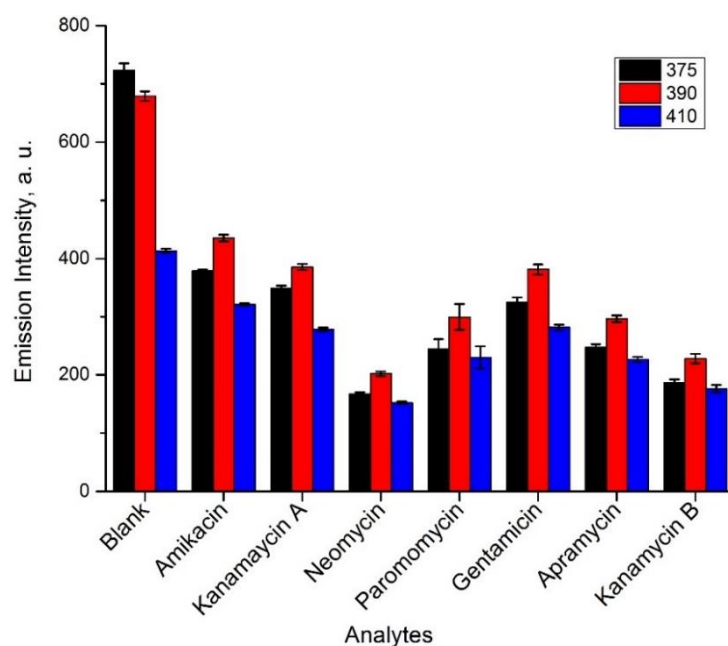


Figure A12 Fluorescence emission intensities (λ_{ex} : 335 nm) at 375 nm (black), 390 nm (red), and 410 nm (blue) of solutions containing dye **2** (4 μM) and the analytes paromomycin, kanamycin B, kanamycin A, amikacin, neomycin, gentamicin, or apramycin ([analyte] = 10 μM ; 10 mM MOPS, pH 7.0). The values represent averages of five independent measurements.

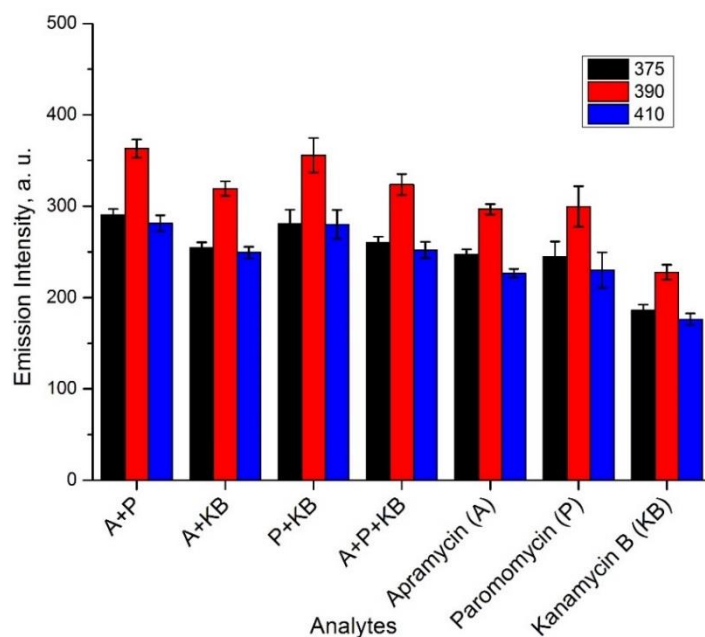


Figure A13 Fluorescence emission intensities (λ_{ex} : 335 nm) at 375 nm (black), 390 nm (red), and 410 nm (blue) of solutions containing dye **2** ([**2**] = 4 μM) and the analytes apramycin (A), paromomycin (P), kanamycin B (KB), or equimolar mixtures of these aminoglycosides ([analyte]_{total} = 10 μM ; 10 mM MOPS, pH 7.0). The values represent averages of five independent measurements.

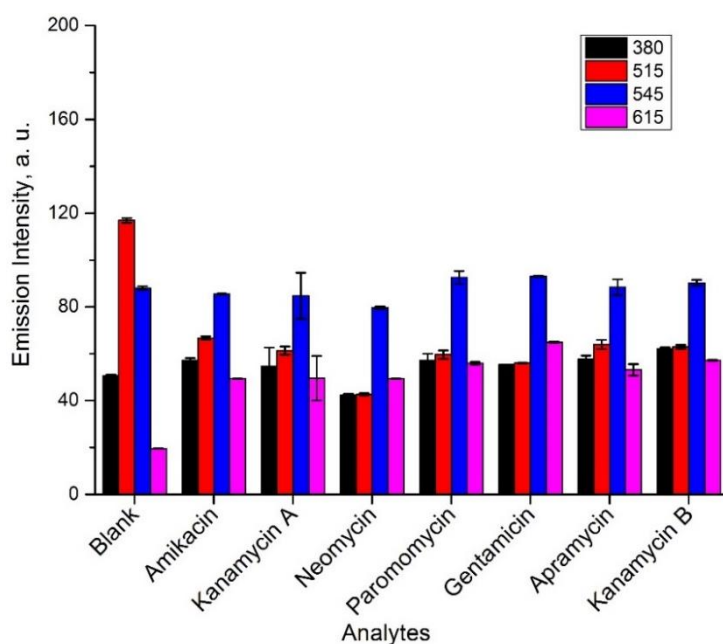


Figure A14 Fluorescence emission intensities (λ_{ex} : 335 nm) at 380 nm (black), 515 nm (red), 545 nm (blue), and 615 nm (pink) of solutions containing dye **3** (30 μM) and the analytes paromomycin, kanamycin B, kanamycin A, amikacin, neomycin, gentamicin, or apramycin ($[\text{analyte}] = 10 \mu\text{M}$; 10 mM MOPS, pH 7.0). The values represent averages of five independent measurements.

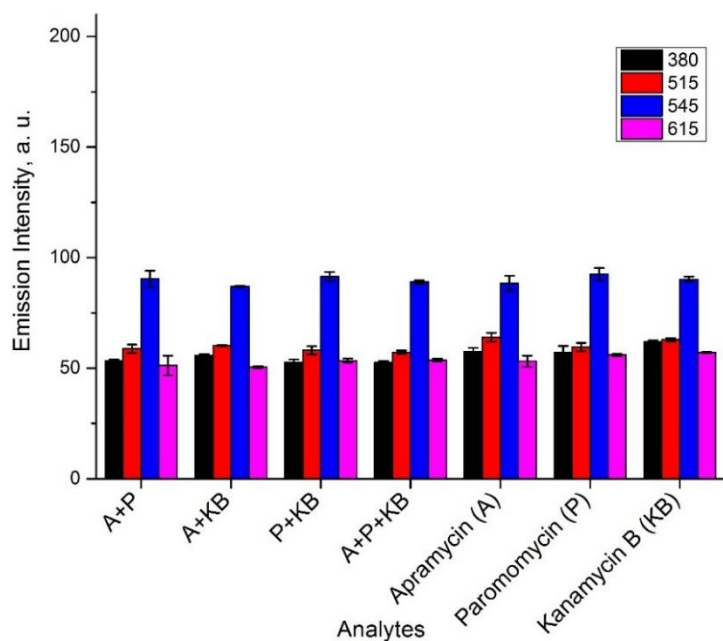


Figure A15 Fluorescence emission intensities (λ_{ex} : 335 nm) at 380 nm (black), 515 nm (red), 545 nm (blue), and 615 nm (pink) of solutions containing dye **3** (30 μM) and the analytes apramycin (A), paromomycin (P), kanamycin B (KB), or equimolar mixtures of these aminoglycosides ($[\text{analyte}]_{\text{total}} = 10 \mu\text{M}$; 10 mM MOPS, pH 7.0). The values represent averages of five independent measurements.

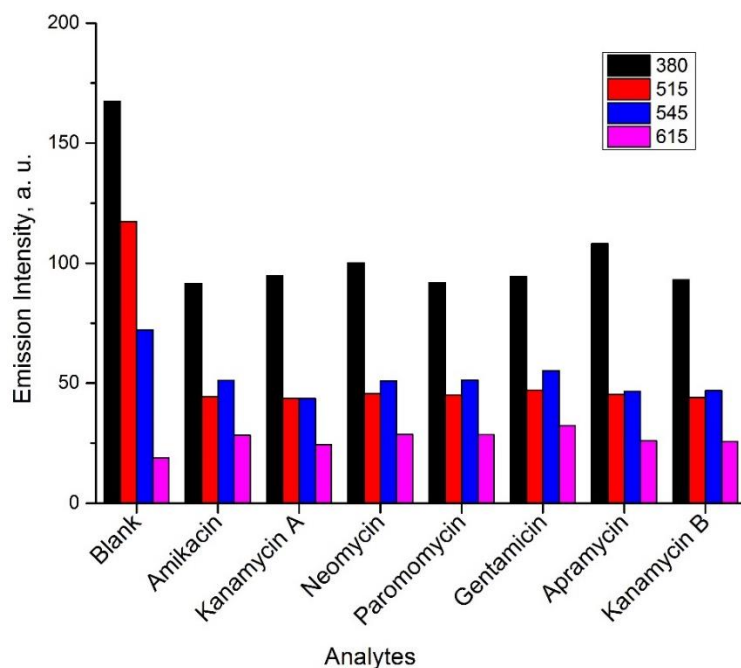


Figure A16 Fluorescence emission intensities (λ_{ex} : 335 nm) at 380 nm (black), 515 nm (red), 545 nm (blue), and 615 nm (pink) of solutions containing dye **3** (5 μM) and the analytes paromomycin, kanamycin B, kanamycin A, amikacin, neomycin, gentamicin, or apramycin ([analyte] = 10 μM ; 10 mM MOPS, pH 7.0).

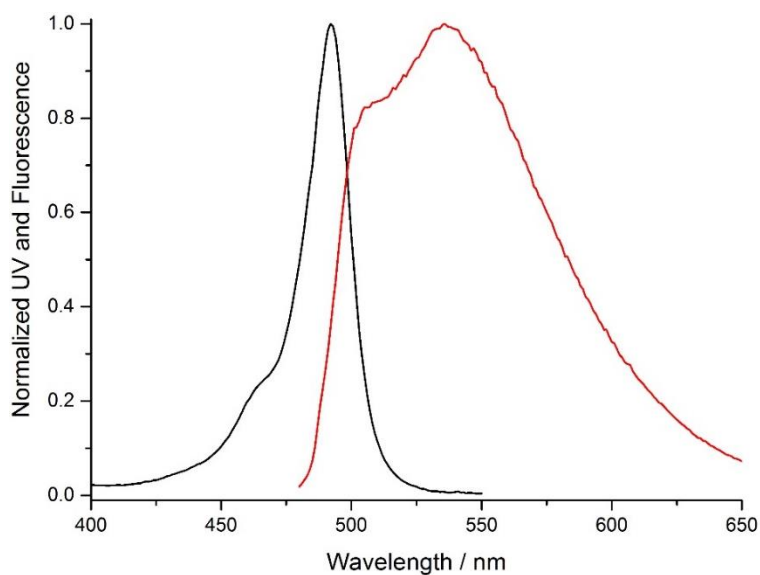


Figure A17 Normalized UV-vis (black) and fluorescence (red) spectra (λ_{ex} : 490 nm) of buffered aqueous solutions (10 mM MOPS, pH 7.0) containing dye **4** (4.0 μM).

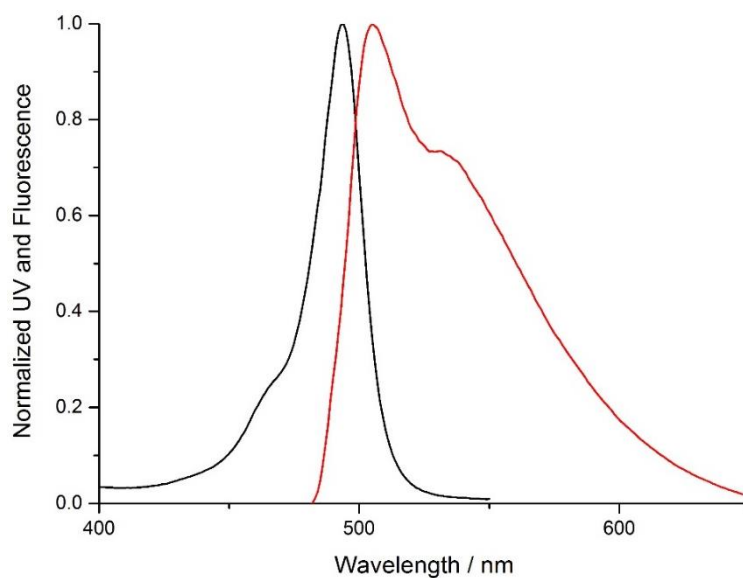


Figure A18 Normalized UV-vis (black) and fluorescence (red) spectra (λ_{ex} : 490 nm) of buffered aqueous solutions (10 mM MOPS, pH 7.0) containing dye **5** (4.0 μ M).

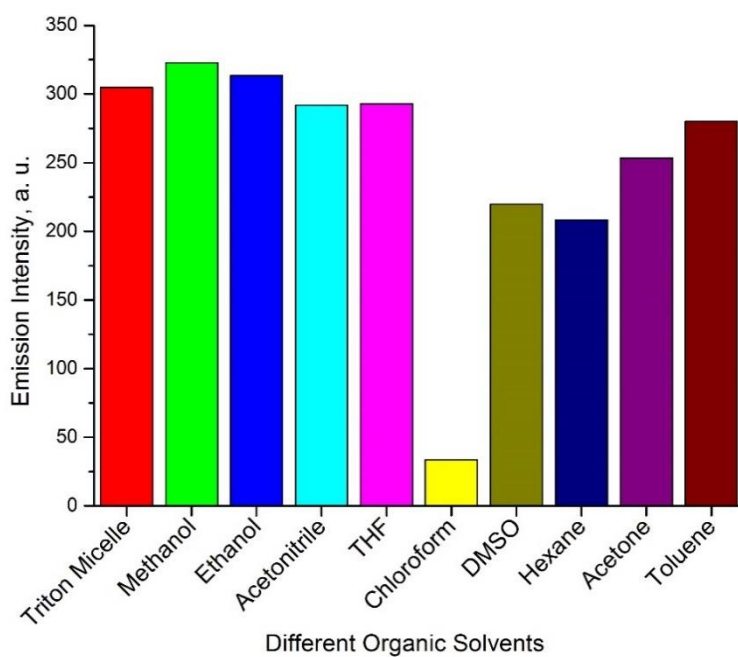


Figure A19 Fluorescence emission intensity (λ_{ex} = 350 nm) in different organic solvents containing 1-aminopyrene (4.0 μ M).

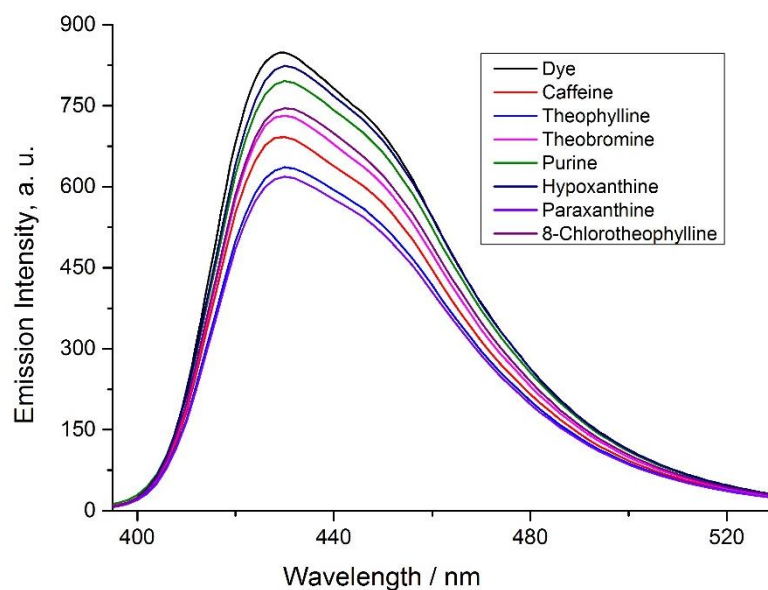


Figure A20 Fluorescence emission spectra (λ_{ex} : 350 nm) of solutions containing a mixture of MPTS ([MPTS] = 2.0 μM) and the analytes dye (black line), caffeine (red line), theophylline (blue line), theobromine (pink line), purine (green line) and paraxanthine (violet line) ([analyte] = 1.0 mM; 20 mM MOPS, pH 7.0).

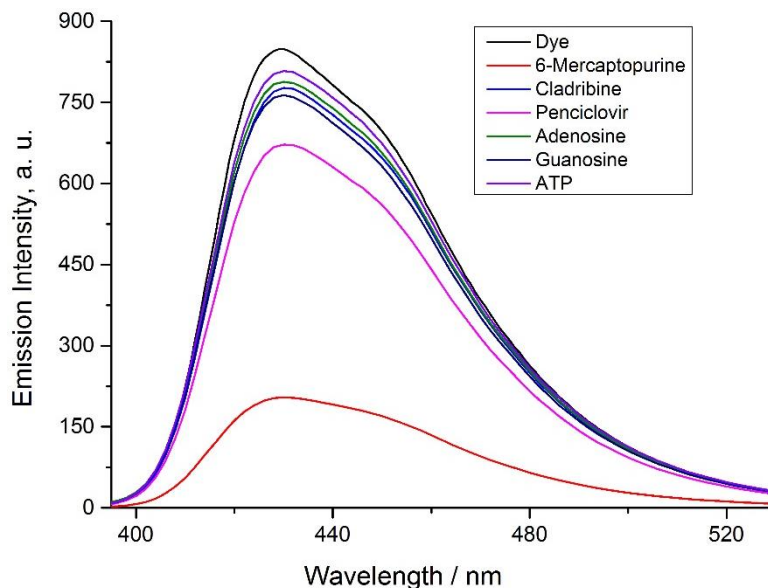


Figure A21 Fluorescence emission spectra (λ_{ex} : 350 nm) of solutions containing a mixture of MPTS ([MPTS] = 2.0 μM) and the analytes dye (black line), hypoxanthine (red line), 8-chlorotheophylline (blue line), 6-mercaptopurine (pink line), cladribine (green line) and penciclovir (violet line) ([analyte] = 1.0 mM; 20 mM MOPS, pH 7.0).

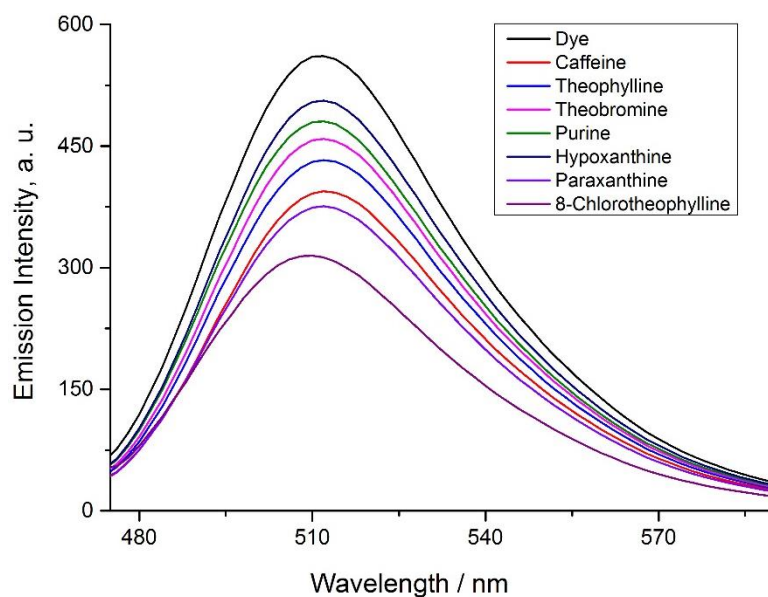


Figure A22 Fluorescence emission spectra (λ_{ex} : 460 nm) of solutions containing a mixture of HPTS ([HPTS] = 2.0 μM) and the analytes dye (black line), caffeine (red line), theophylline (blue line), theobromine (pink line), purine (green line) and paraxanthine (violet line) ([analyte] = 1.0 mM; 20 mM MOPS, pH 7.0).

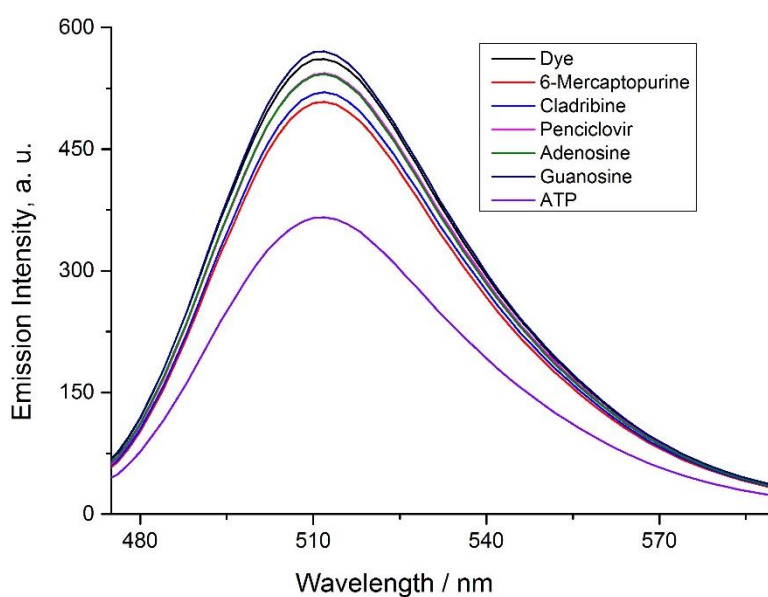


Figure A23 Fluorescence emission spectra (λ_{ex} : 460 nm) of solutions containing a mixture of HPTS ([HPTS] = 2.0 μM) and the analytes dye (black line), hypoxanthine (red line), 8-chlorotheophylline (blue line), 6-mercaptopurine (pink line), cladribine (green line) and penciclovir (violet line) ([analyte] = 1.0 mM; 20 mM MOPS, pH 7.0).

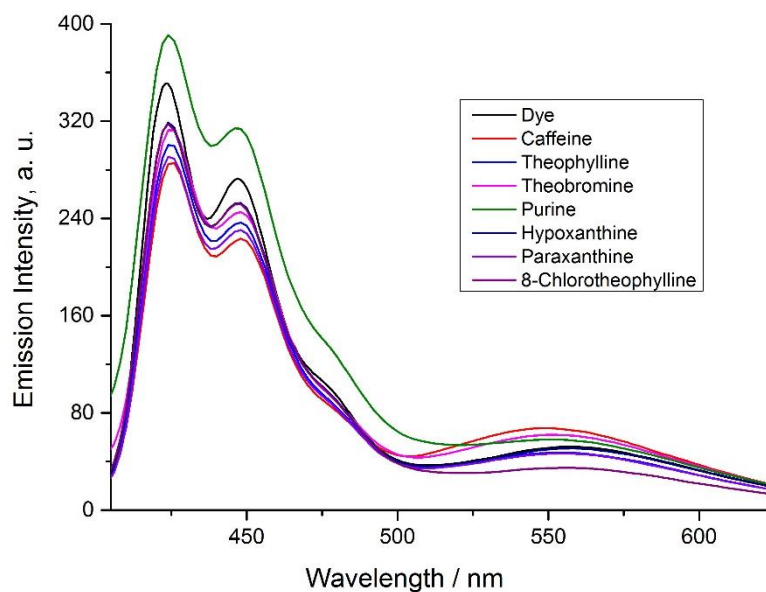


Figure A24 Fluorescence emission spectra (λ_{ex} : 350 nm) of solutions containing a mixture of TDS ([TDS] = 2.0 μM) and the analytes dye (black line), caffeine (red line), theophylline (blue line), theobromine (pink line), purine (green line) and paraxanthine (violet line) ([analyte] = 1.0 mM; 20 mM MOPS, pH 7.0).

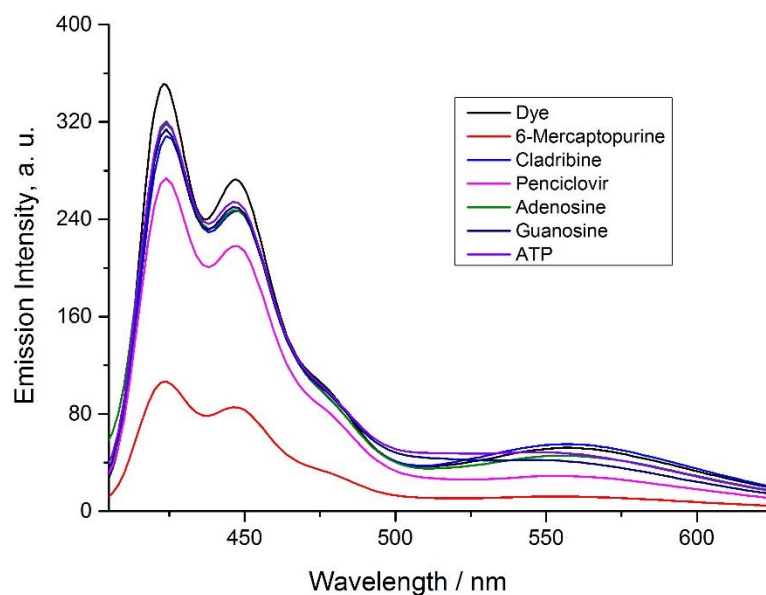


Figure A25 Fluorescence emission spectra (λ_{ex} : 350 nm) of solutions containing a mixture of TDS ([TDS] = 2.0 μM) and the analytes dye (black line), hypoxanthine (red line), 8-chlorotheophylline (blue line), 6-mercaptopurine (pink line), cladribine (green line) and penciclovir (violet line) ([analyte] = 1.0 mM; 20 mM MOPS, pH 7.0).

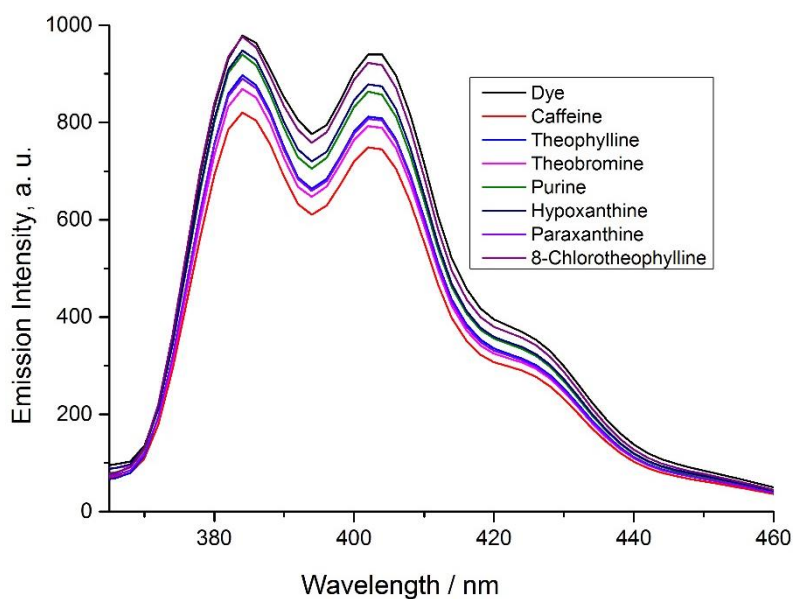


Figure A26 Fluorescence emission spectra (λ_{ex} : 364 nm) of solutions containing a mixture of PTS ([PTS] = 2.0 μM) and the analytes dye (black line), caffeine (red line), theophylline (blue line), theobromine (pink line), purine (green line) and paraxanthine (violet line) ([analyte] = 1.0 mM; 20 mM MOPS, pH 7.0).

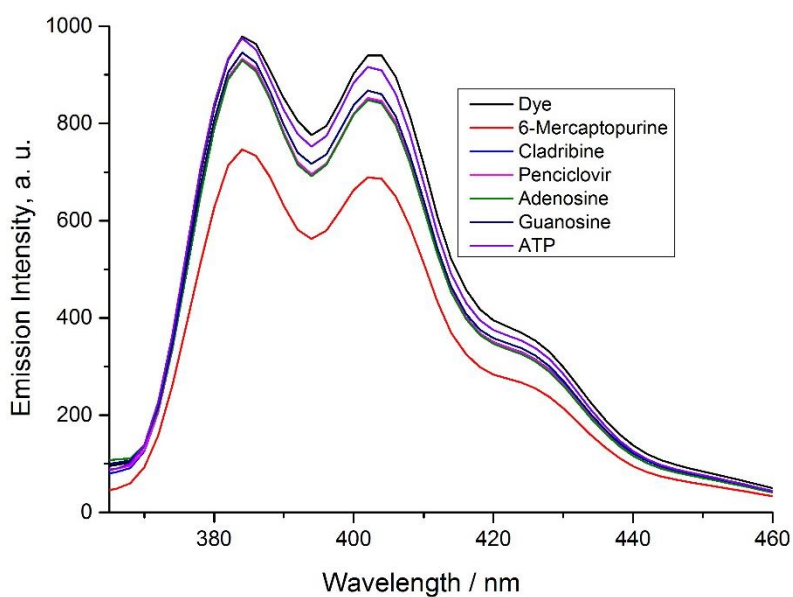


Figure A27 Fluorescence emission spectra (λ_{ex} : 364 nm) of solutions containing a mixture of PTS ([PTS] = 2.0 μM) and the analytes dye (black line), hypoxanthine (red line), 8-chlorotheophylline (blue line), 6-mercaptopurine (pink line), cladribine (green line) and penciclovir (violet line) ([analyte] = 1.0 mM; 20 mM MOPS, pH 7.0).

8.2 LDA Plots

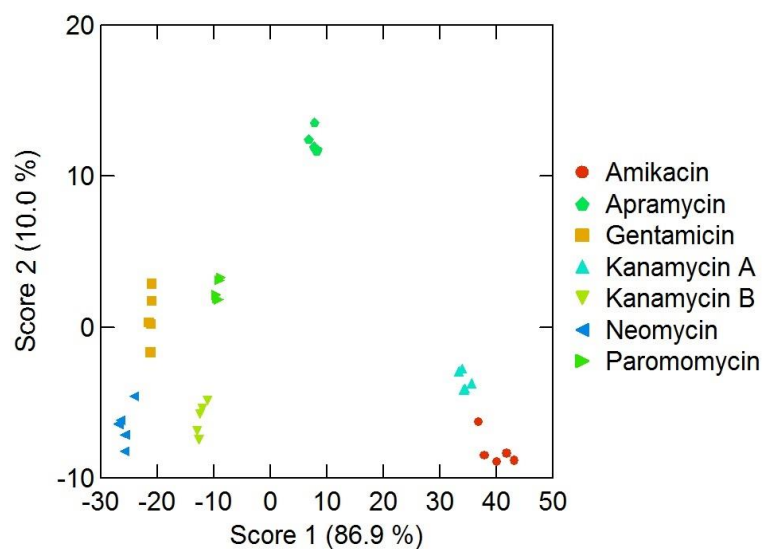


Figure A28 Two-dimensional LDA score plot for the analysis of seven different aminoglycosides. The data were obtained as described in experimental part of chapter 3 using the solutions containing a mixture of dye **2** and **3** (**[2]** = 4 μ M; **[3]** = 30 μ M)

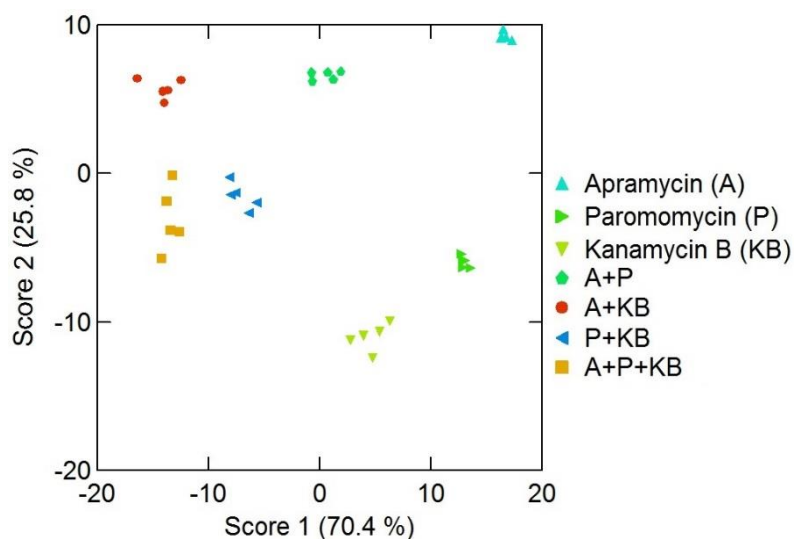


Figure A29 Two-dimensional LDA score plot for the analysis of apramycin (A), paromomycin (P), kanamycin B (KB), and equimolar mixtures of these aminoglycosides. The data were obtained as described in experimental part of chapter 3 using the solutions containing a mixture of dye **2** and **3** (**[2]** = 4 μ M; **[3]** = 30 μ M).

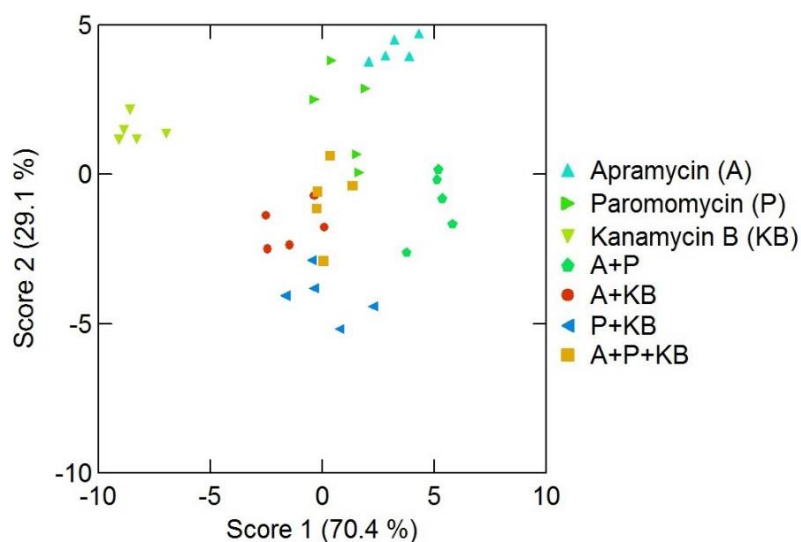


Figure A30 Two-dimensional LDA score plot for the analysis of apramycin (A), paromomycin (P), kanamycin B (KB), and equimolar mixtures of these aminoglycosides. The data were obtained as described in experimental part of chapter 3 using only dye **2**.

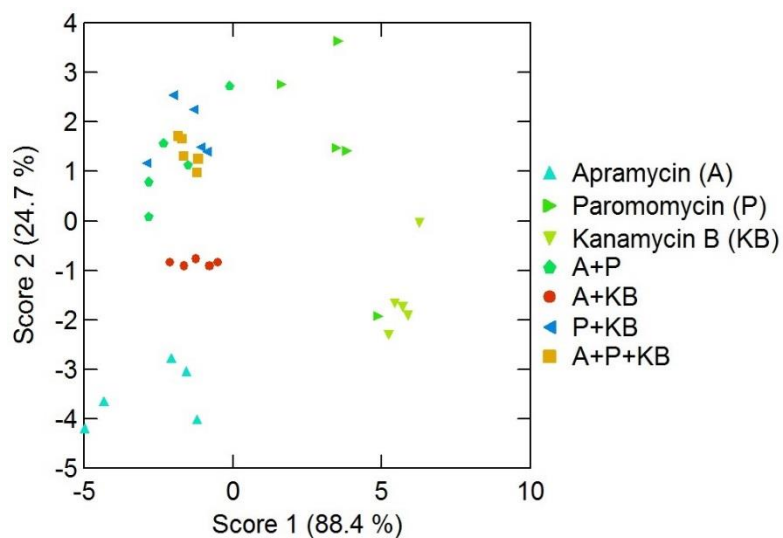


Figure A31 Two-dimensional LDA score plot for the analysis of apramycin (A), paromomycin (P), kanamycin B (KB), and equimolar mixtures of these aminoglycosides. The data were obtained as described in experimental part of chapter 3 using only dye **3**.

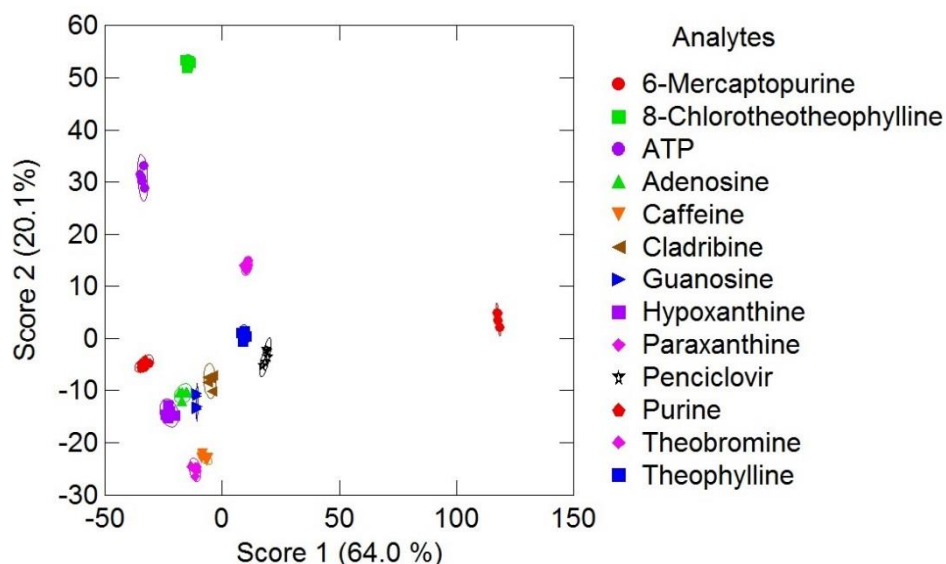


Figure A32 Two-dimensional LDA score plot for the analysis of six different purine derivatives ($[\text{dye}]_{\text{final}} = 2.0 \mu\text{M}$; $[\text{analyte}]_{\text{final}} = 1.0 \text{ mM}$). The data were obtained as described in experimental part of chapter 6.

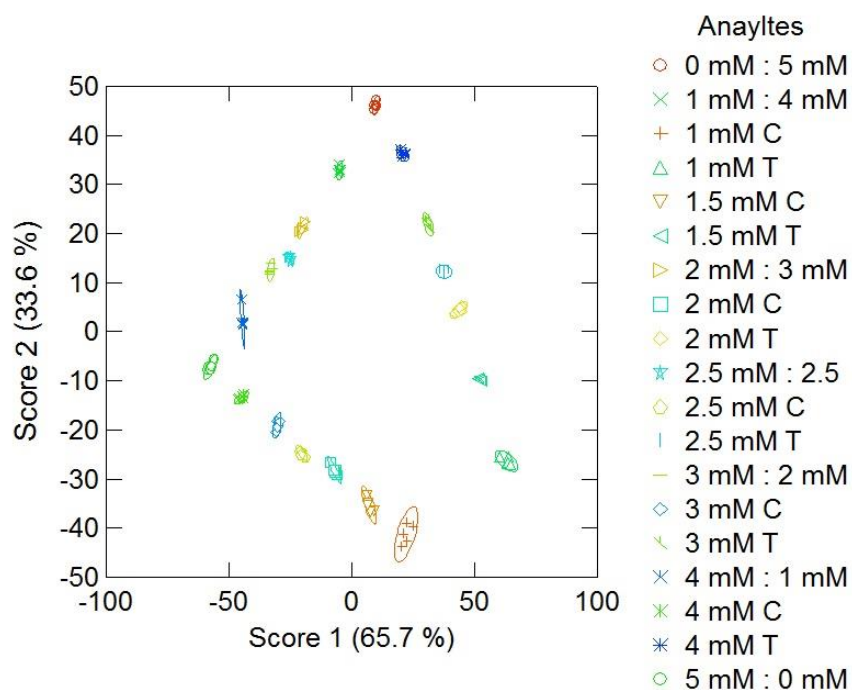


Figure A33 Two-dimensional LDA score plot for the analysis of samples containing caffeine and/or theophylline at different concentrations and ratios ($[\text{dye}] = 2.0 \mu\text{M}$, $[\text{caffeine}] = 1.0 - 5.0 \text{ mM}$; $[\text{theophylline}] = 1.0 - 5.0 \text{ mM}$; $[\text{caffeine:theophylline mix}] = 5.0:0 \text{ mM} - 0:5.0 \text{ mM}$). The data were obtained as described in experimental part of chapter 6.

8.3 TEM and DLS images

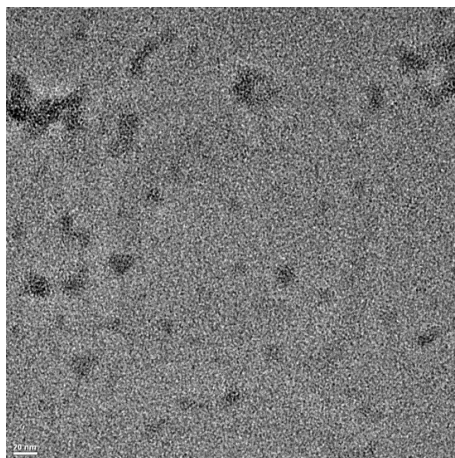


Figure A34 TEM image of a sample containing amphiphile **1** and spermine. The image reveals aggregates with a size of ~ 15 nm and larger (scale bar = 20 nm).

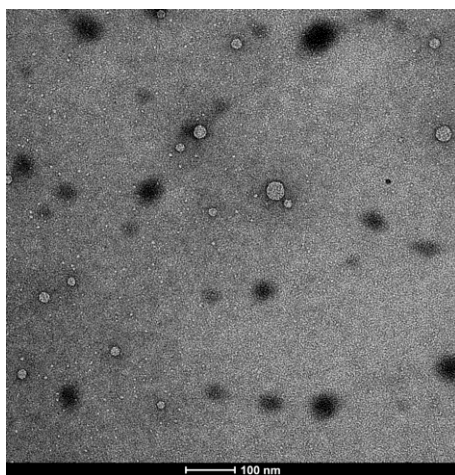


Figure A35 TEM image of a sample containing dye **2** (for sample preparation see text above). The image reveals inhomogeneous spherical aggregates with the size between 8–30 nm (scale bar = 100 nm). The black spots are due to accumulation of the staining agent.

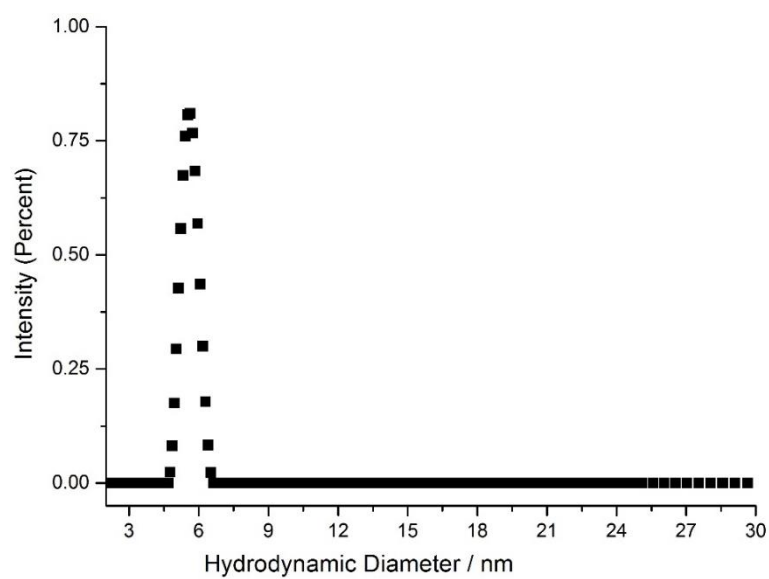


Figure A36 Typical DLS size distribution for solutions of dye **2** (1.0 mM)

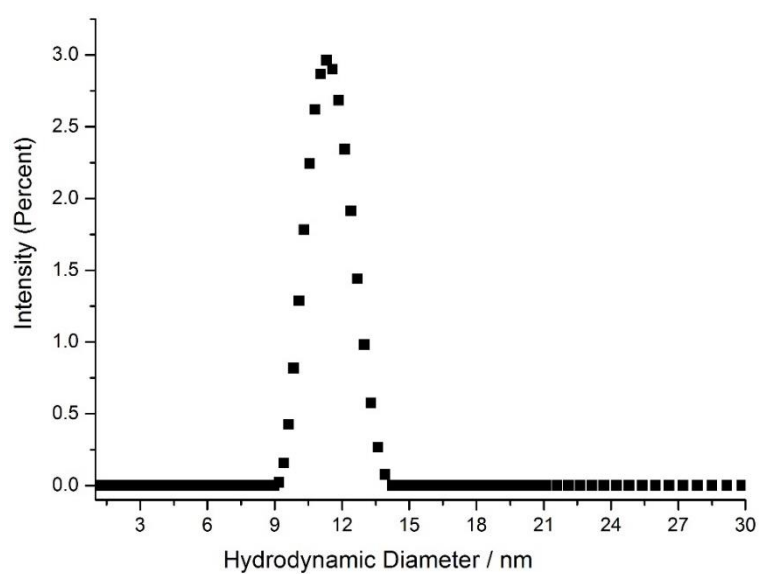


Figure A37 Typical DLS size distribution for solutions of dye **3** (50 μM).

8.4 NMR Data

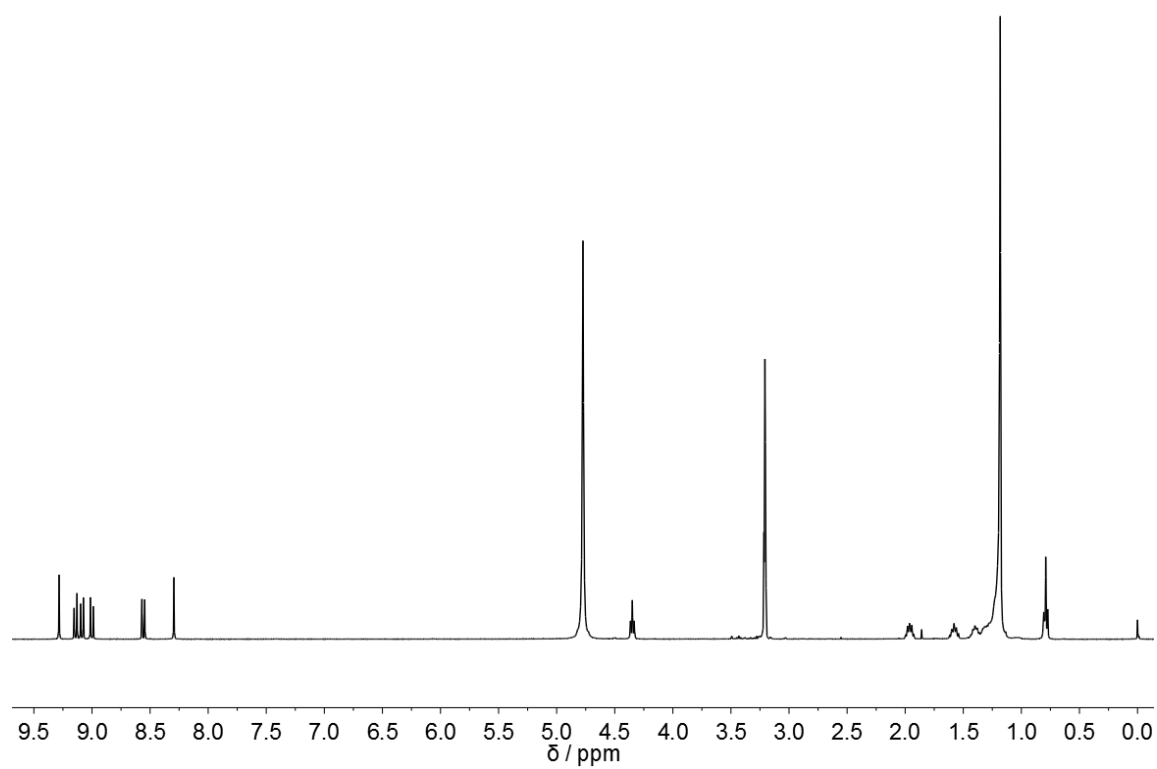


Figure A38 ^1H NMR spectrum of dye **1** (400 MHz, CDCl_3).

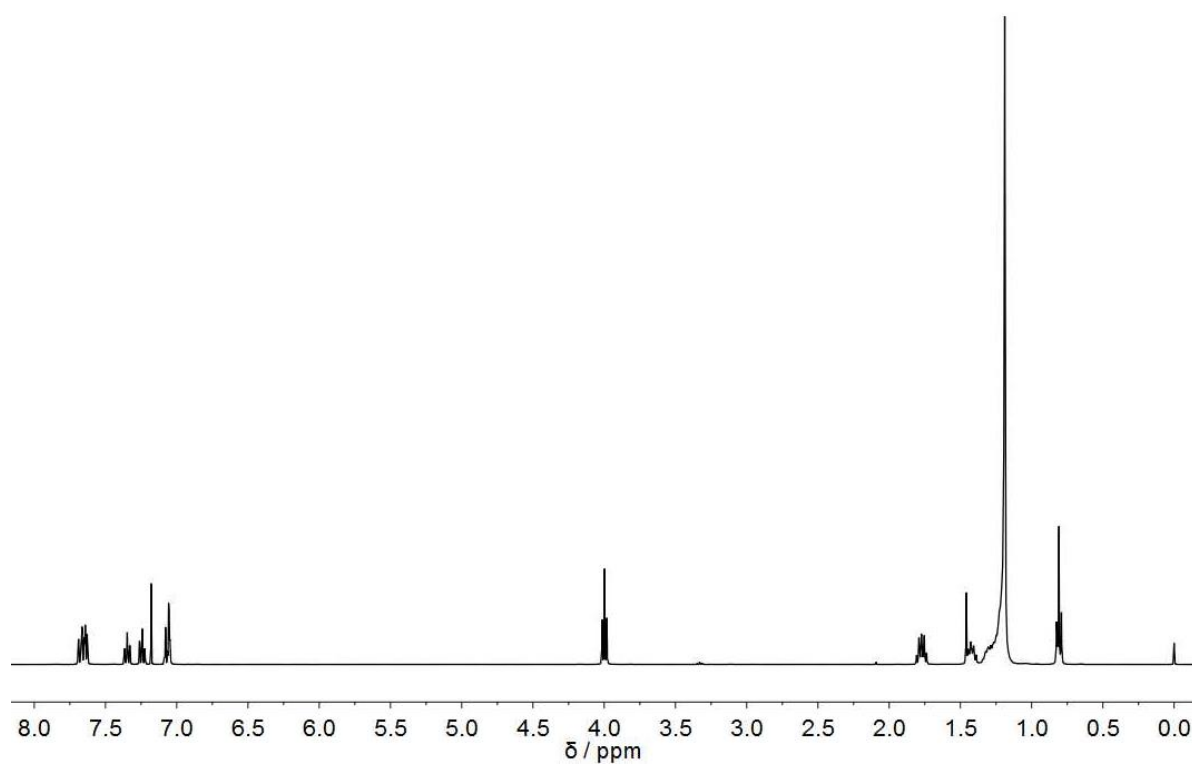


Figure A39 ^1H NMR spectrum of compound N (400 MHz, CDCl_3).

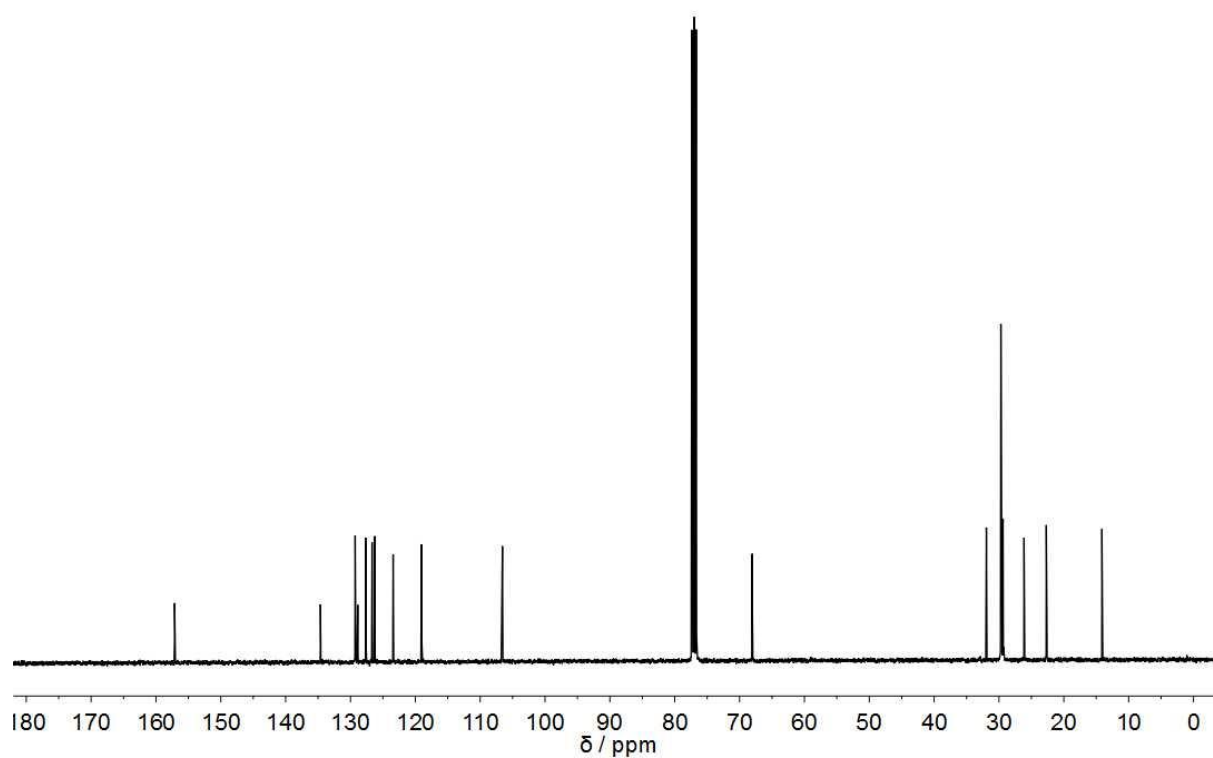


Figure A40 ^{13}C NMR spectrum of compound N (100 MHz, CDCl_3).

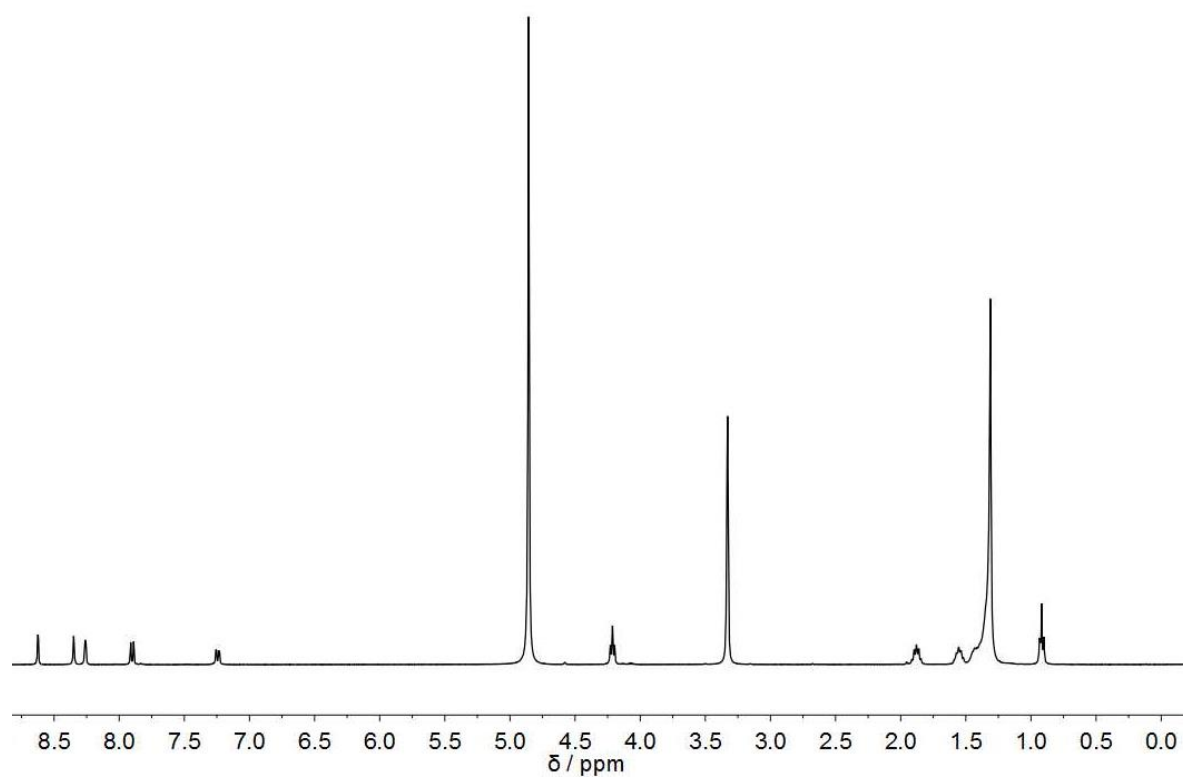


Figure A41 ^1H NMR spectrum of dye **2** (400 MHz, CD_3OD).

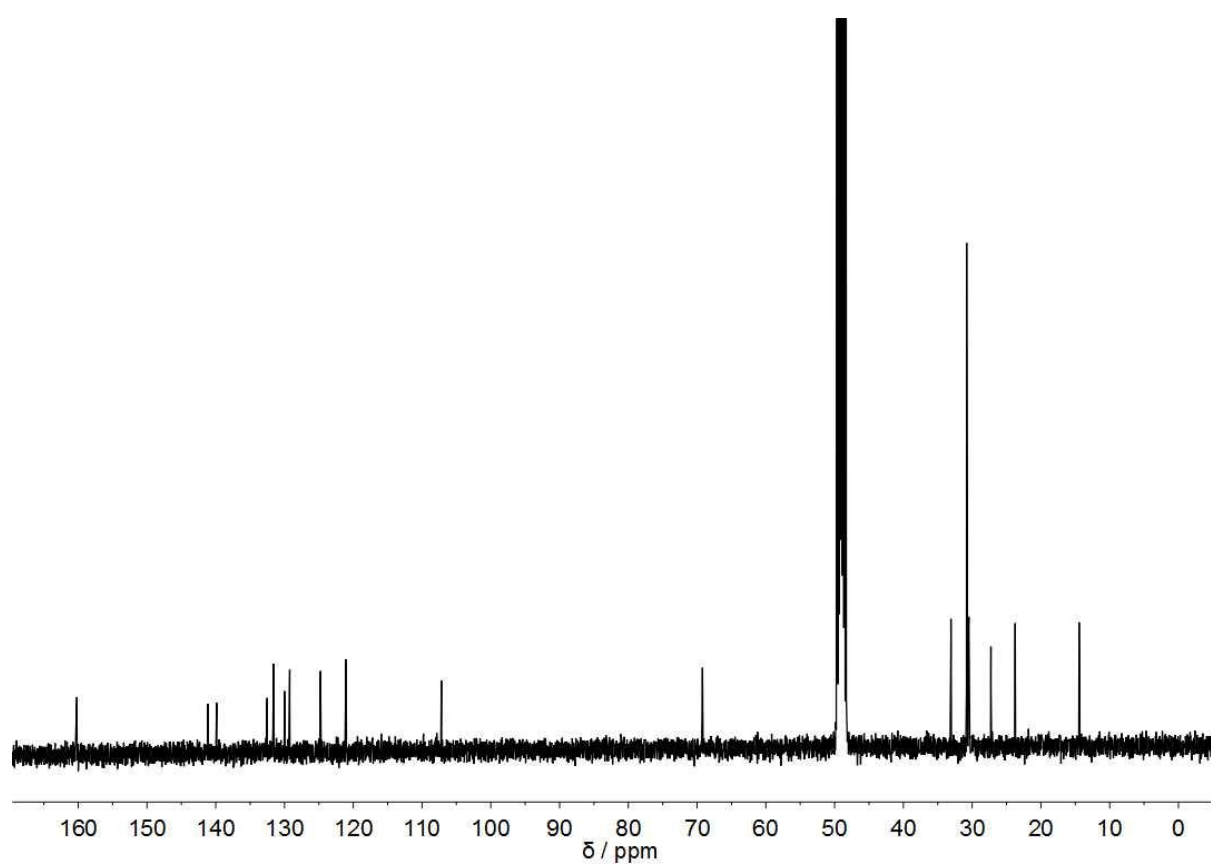


Figure A42 ^{13}C NMR spectrum of dye **2** (100 MHz, CD_3OD).

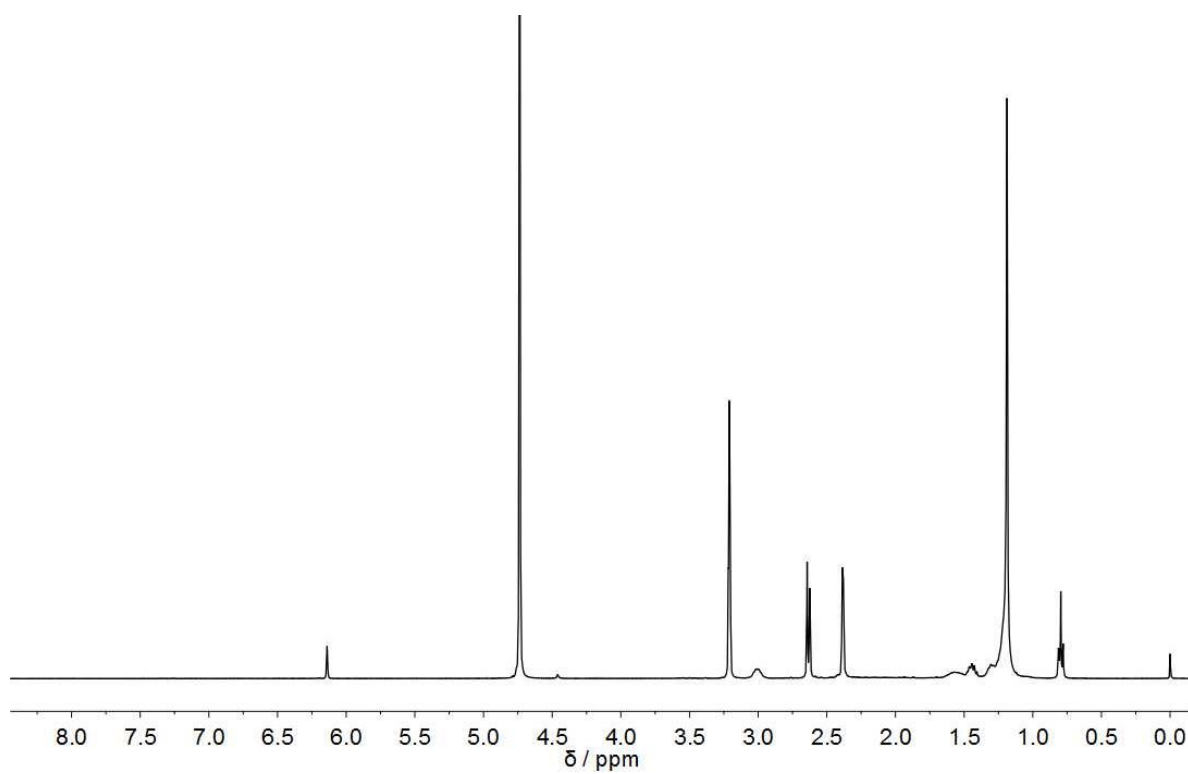


Figure A43 ^1H NMR spectrum of dye **3** (400 MHz, CD_3OD).

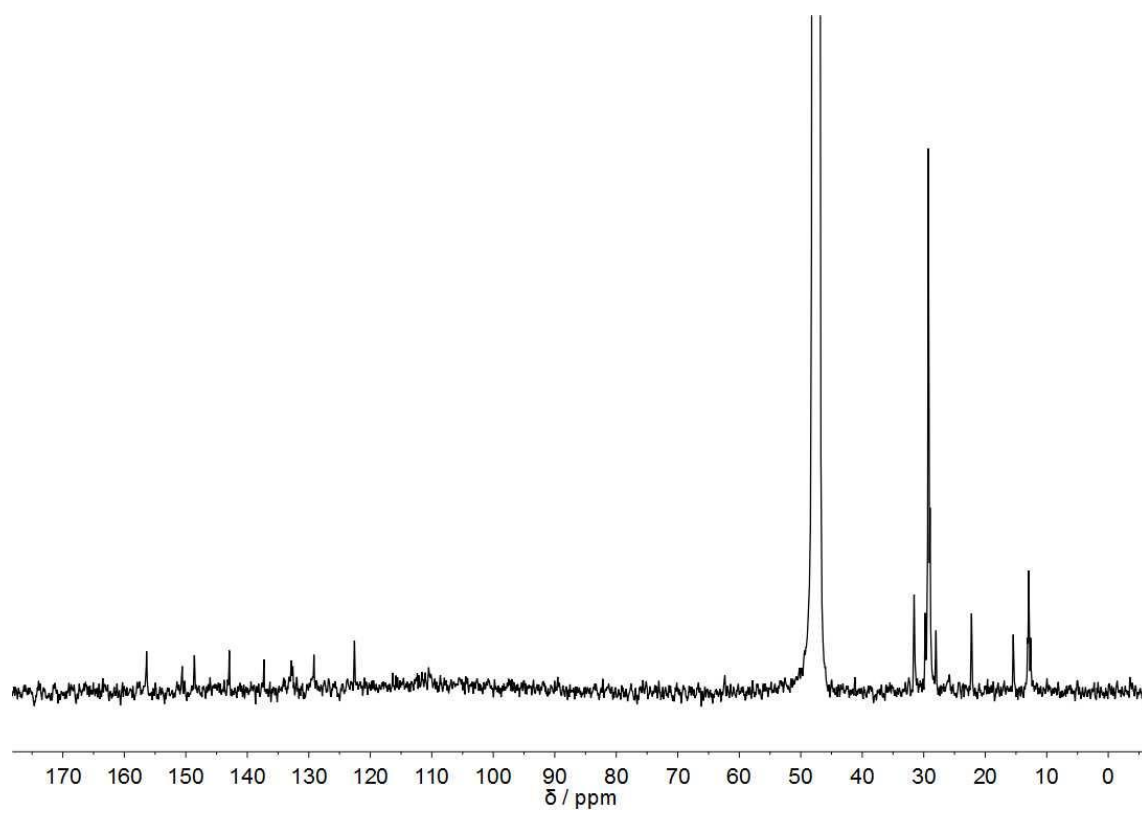


Figure A44 ^{13}C NMR spectrum of dye **3** (125 MHz, CD_3OD). The quality of the spectrum is not very good because of the poor solubility of **3**.

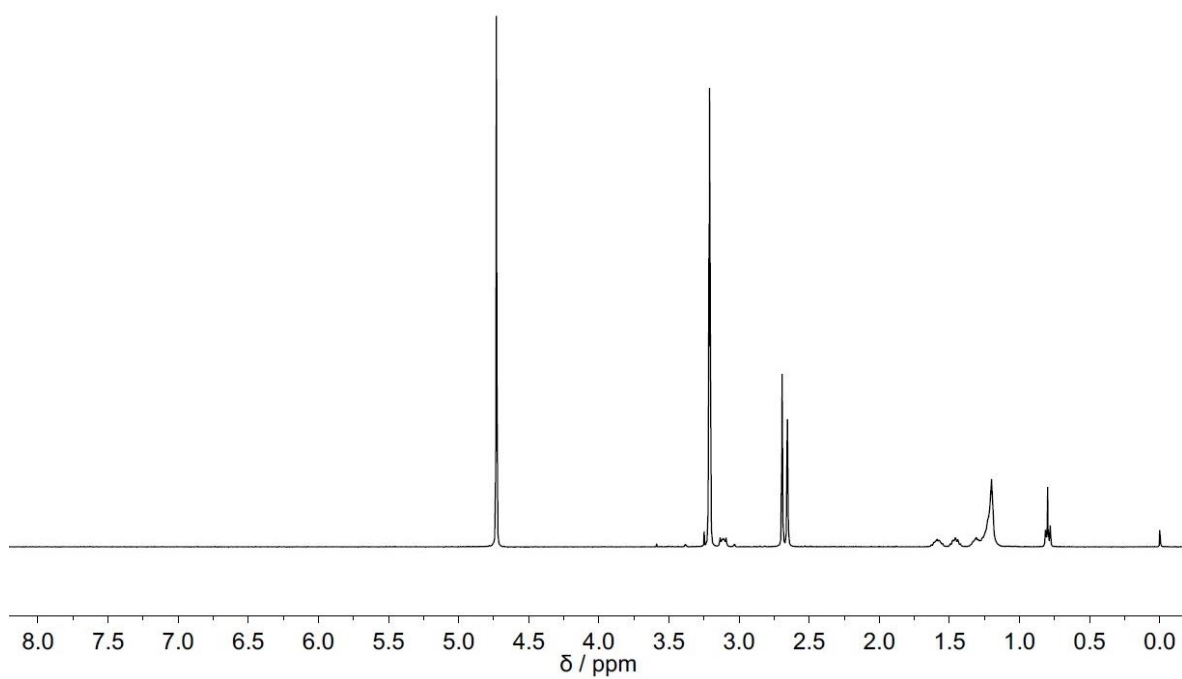


Figure A45 ¹H NMR (400 MHz, CD₃OD) spectrum of dye **4**.

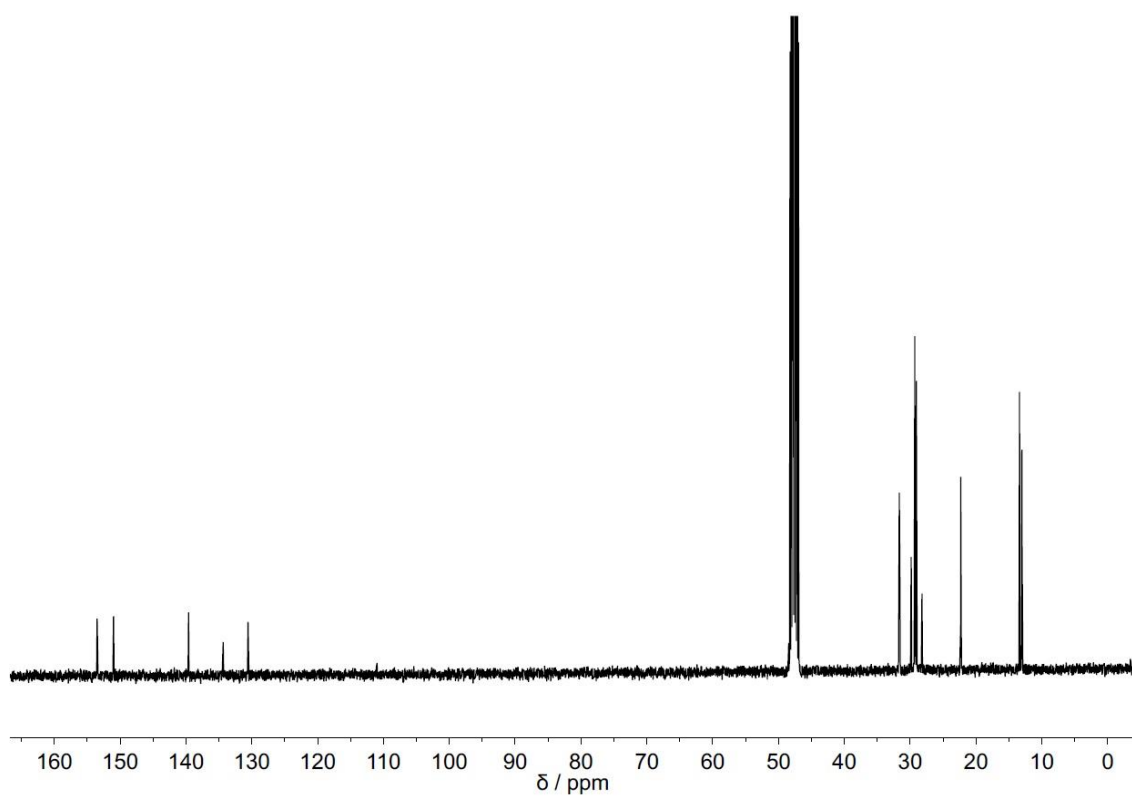


Figure A46 ¹³C NMR (100 MHz, CDCl₃) spectrum of dye **4**.

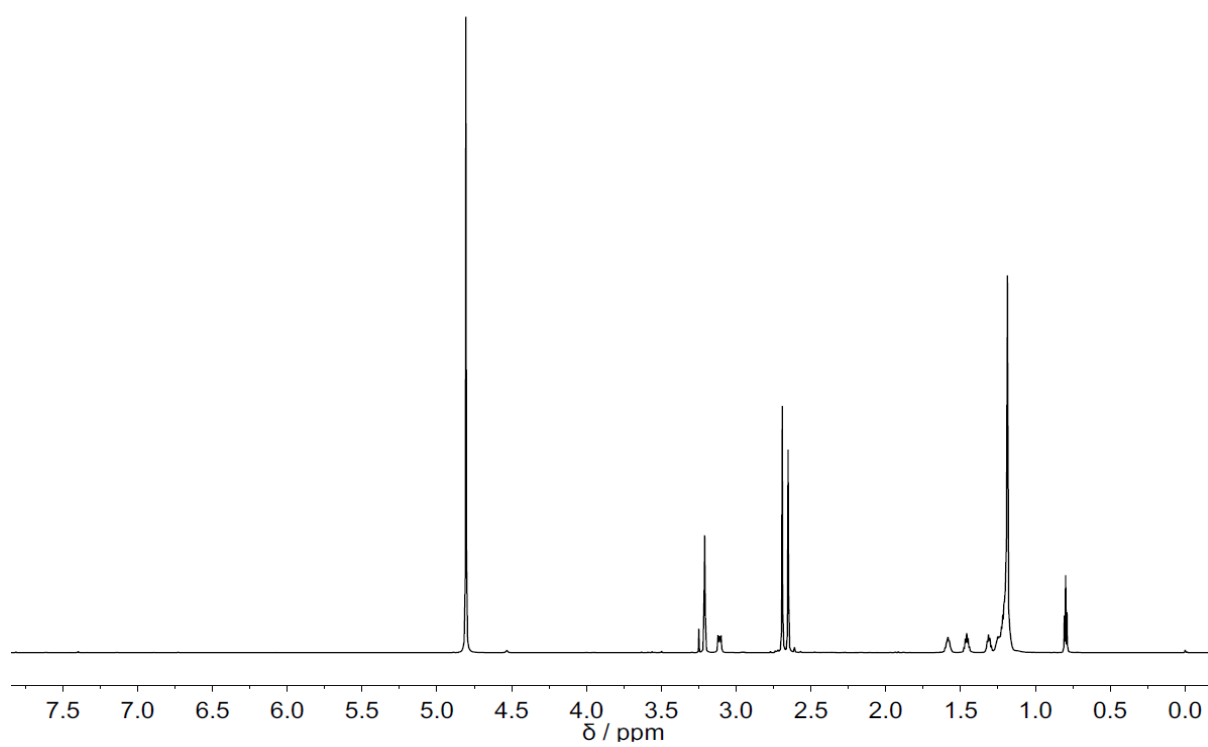


Figure A47 ^1H NMR (800 MHz, CD_3OD) spectrum of dye **5**.

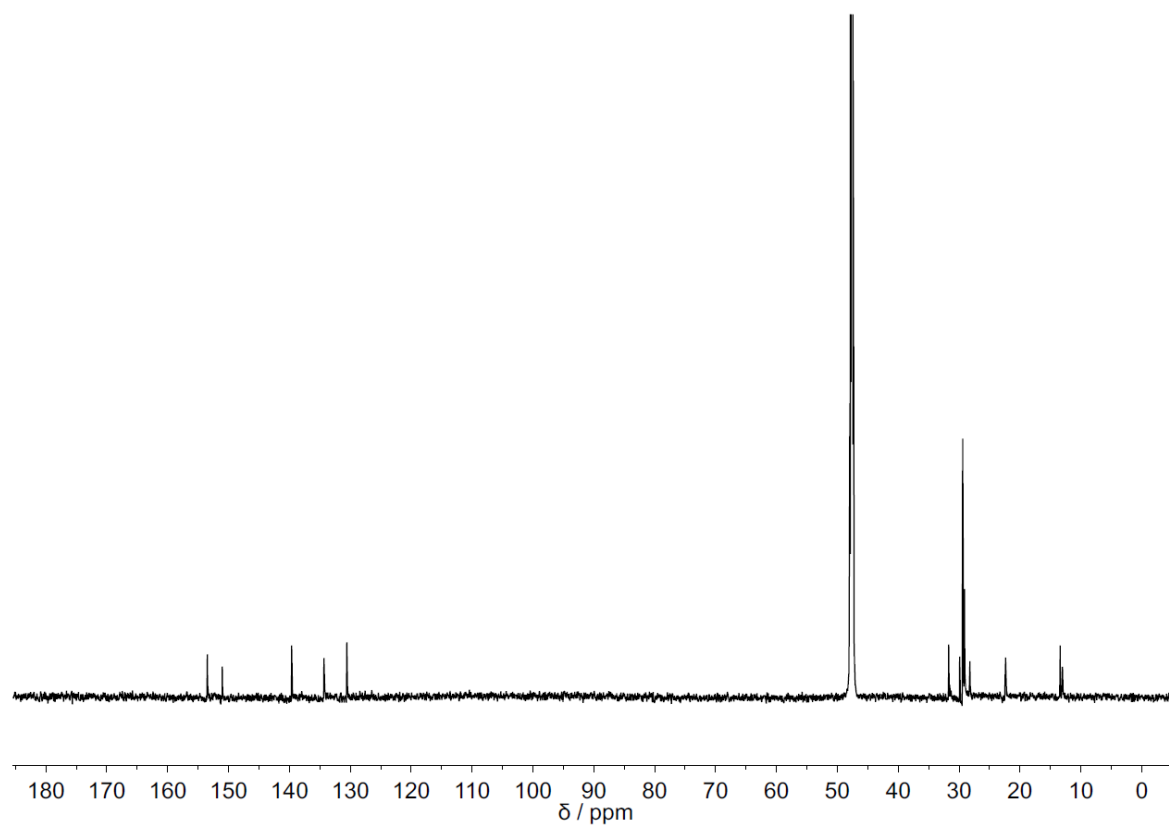


Figure A48 ^{13}C NMR (200 MHz, CDCl_3) spectrum of dye **5**.

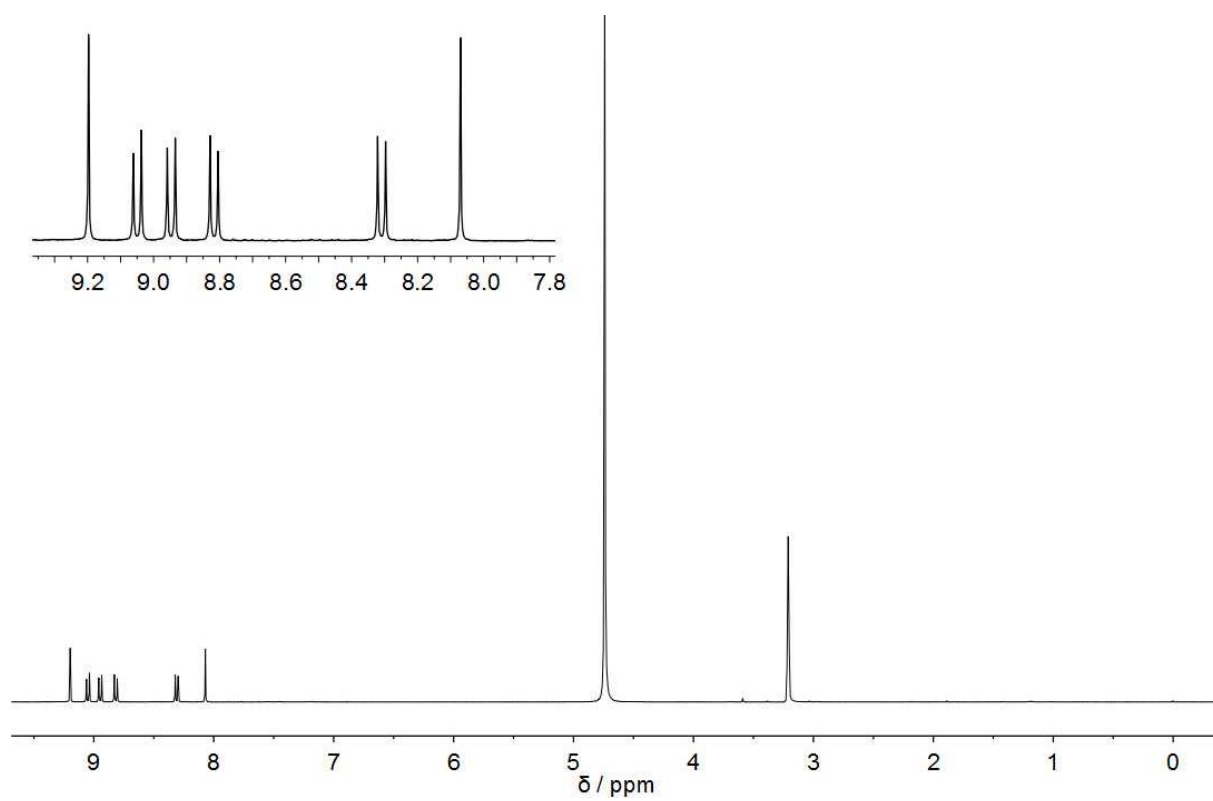


Figure A49 ^1H NMR spectrum of dye 6 in CD_3OD .

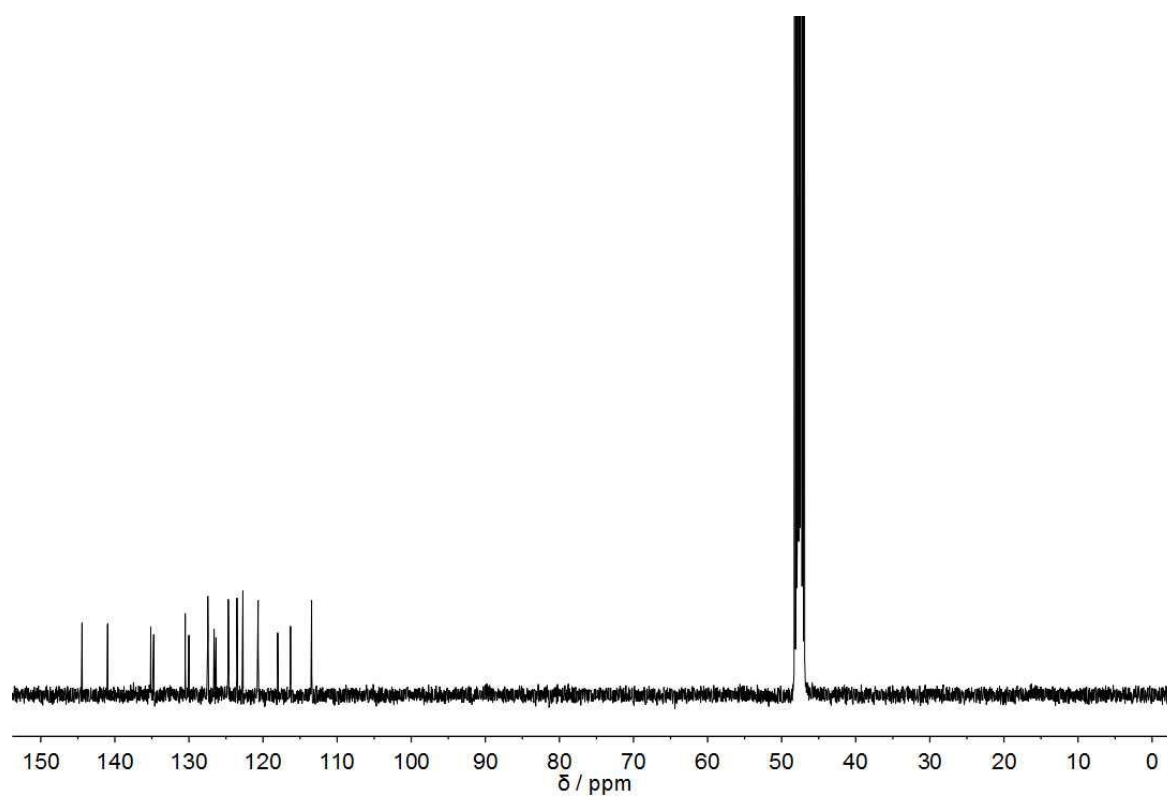


Figure A50 ^{13}C NMR spectrum of trisodium 8-aminopyrene-1,3,6-trisulfonate (**6**) in CD_3OD

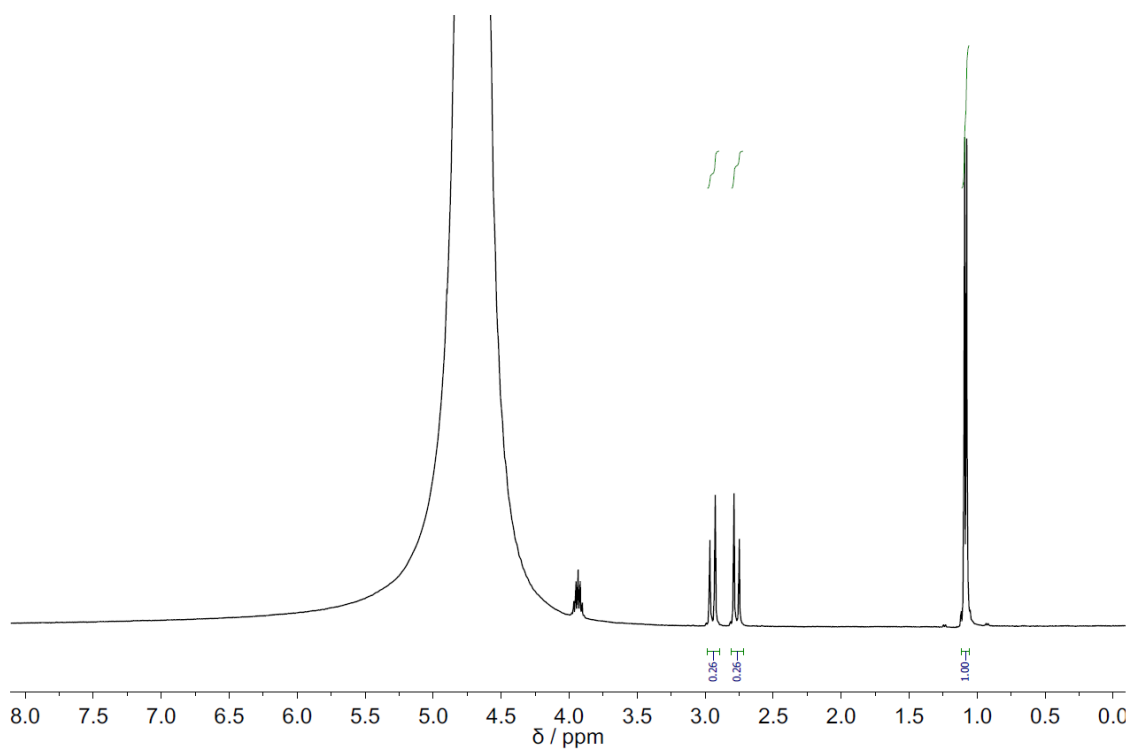


Figure A51 ^1H NMR (400 MHz, 90% H_2O : 10% D_2O) spectrum of citric acid (50 mM) and isopropanol (50 mM, 3.85 μL). The peak at 4.75 ppm corresponds to the solvent.

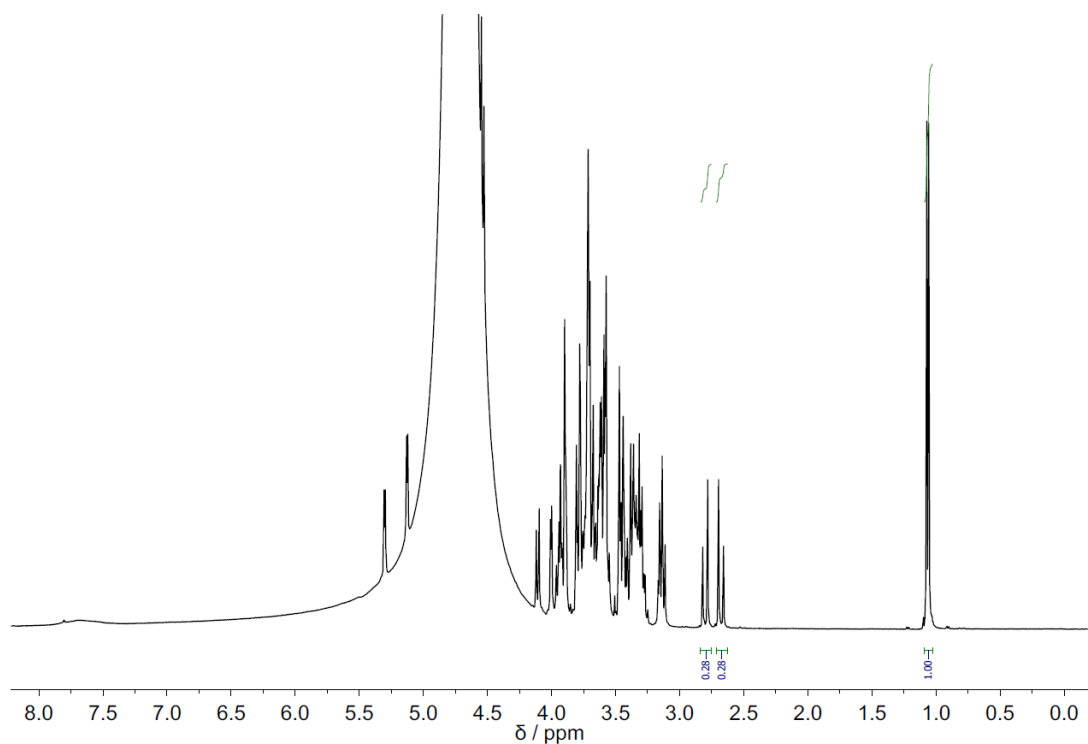


Figure A52 ^1H NMR (400 MHz) spectrum of a solution containing energy drink 1 (90%), D_2O (10%) and isopropanol (50 mM, 3.85 μL). The peak at 4.75 ppm corresponds to the solvent.

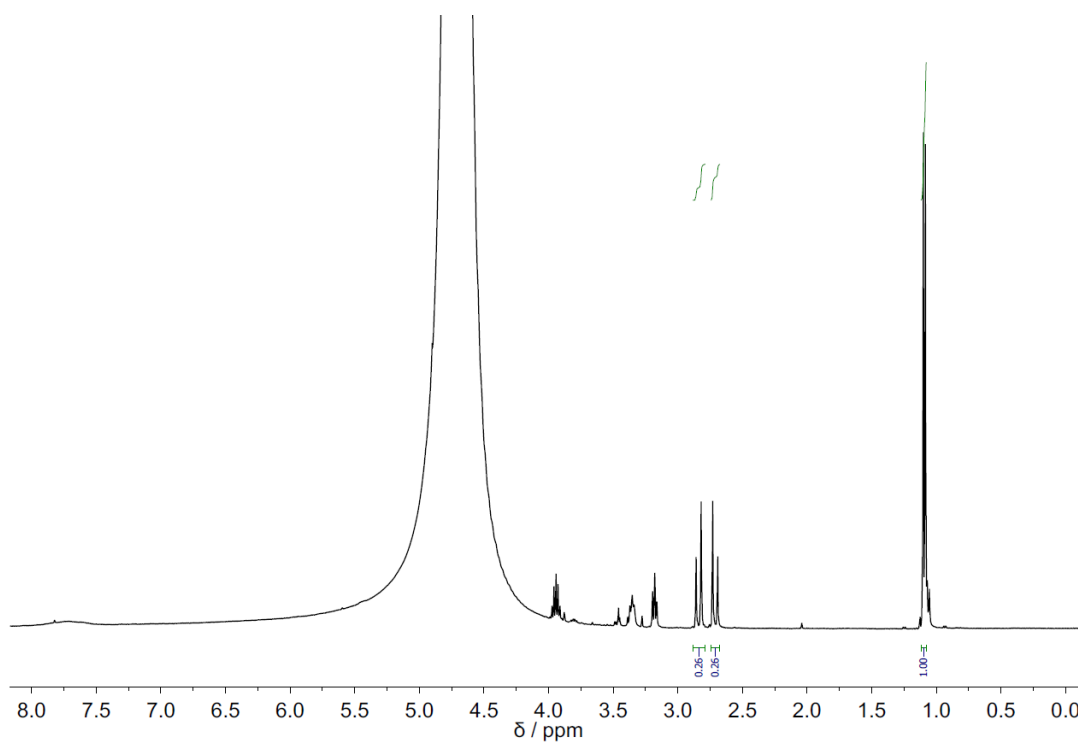


Figure A53 ^1H NMR (400 MHz) spectrum of a solution containing energy drink 2 (90%), D_2O (10%) and isopropanol (50 mM, 3.85 μL). The peak at 4.75 ppm corresponds to the solvent.

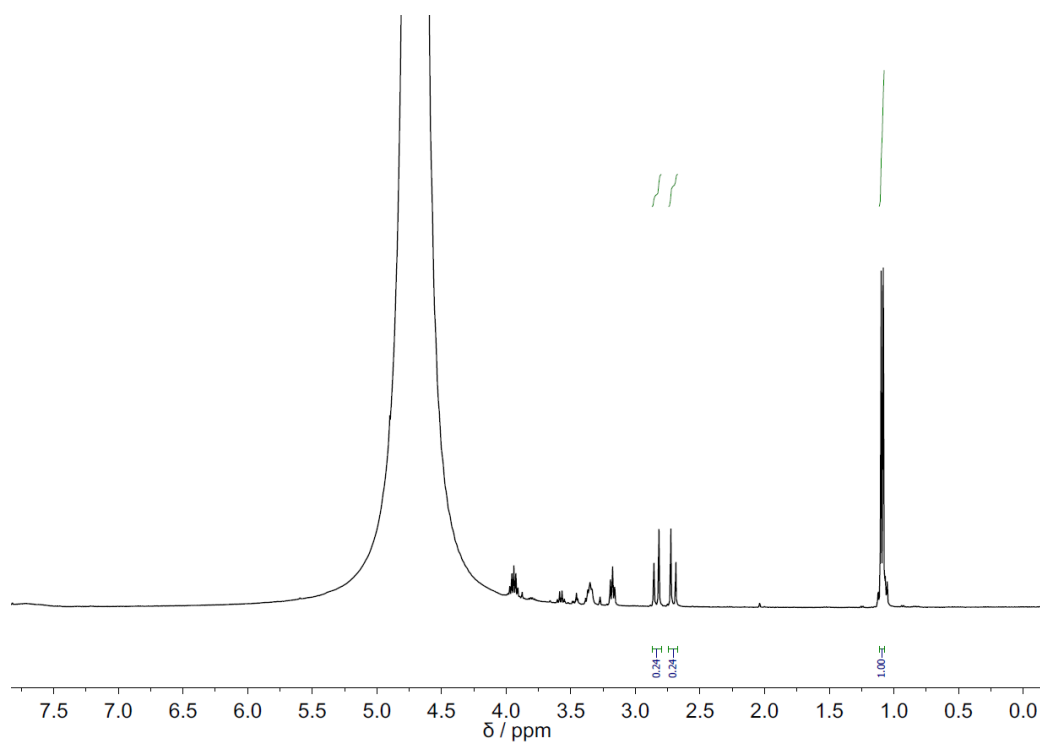


Figure A54 ^1H NMR (400 MHz) spectrum of a solution containing energy drink 3 (90%), D_2O (10%) and isopropanol (50 mM, 3.85 μL). The peak at 4.75 ppm corresponds to the solvent.

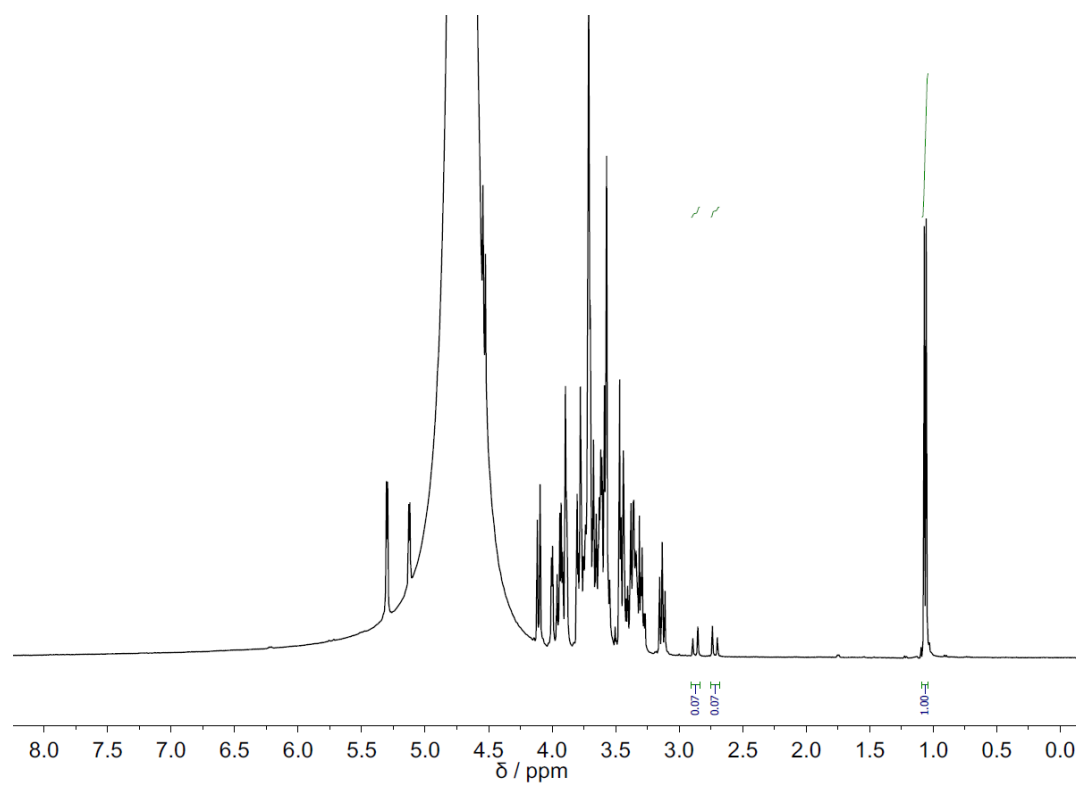


Figure A55 ^1H NMR (400 MHz) spectrum of a solution containing soft drink (90%), D_2O (10%) and isopropanol (50 mM, 3.85 μL). The peak at 4.75 ppm corresponds to the solvent.

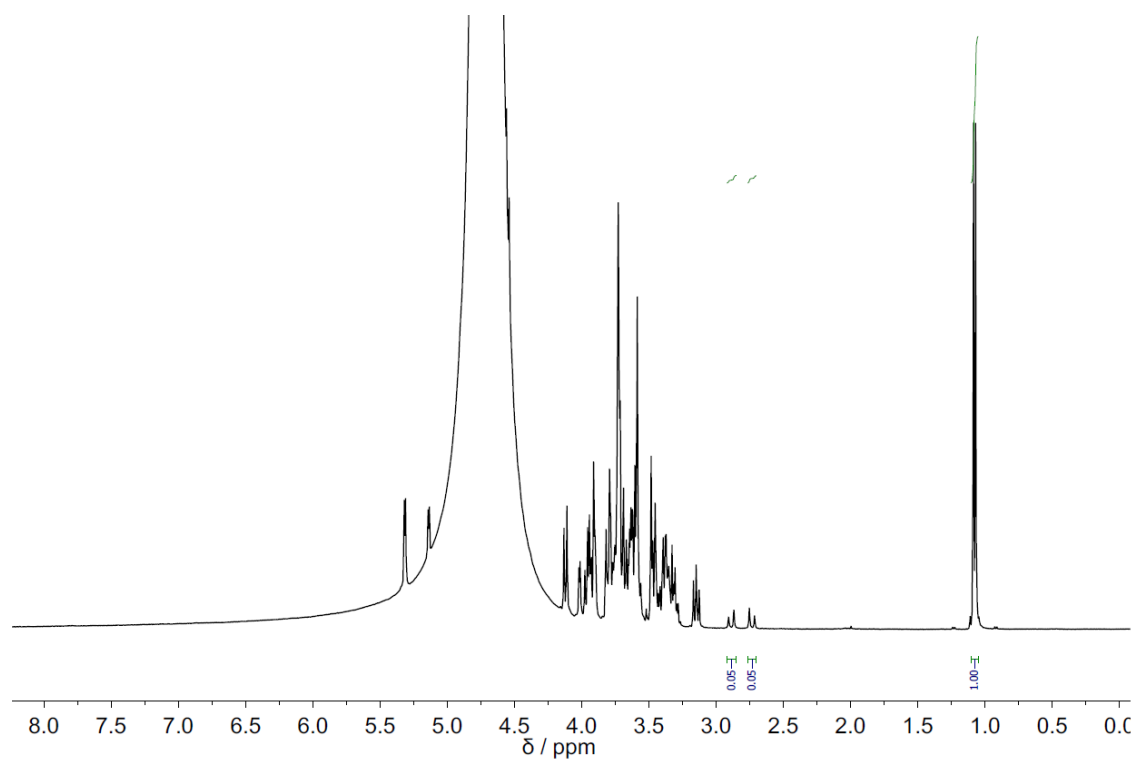


Figure A56 ^1H NMR (400 MHz) spectrum of a solution containing ice tea (90%), D_2O (10%) and isopropanol (50 mM, 3.85 μL). The peak at 4.75 ppm corresponds to the solvent.

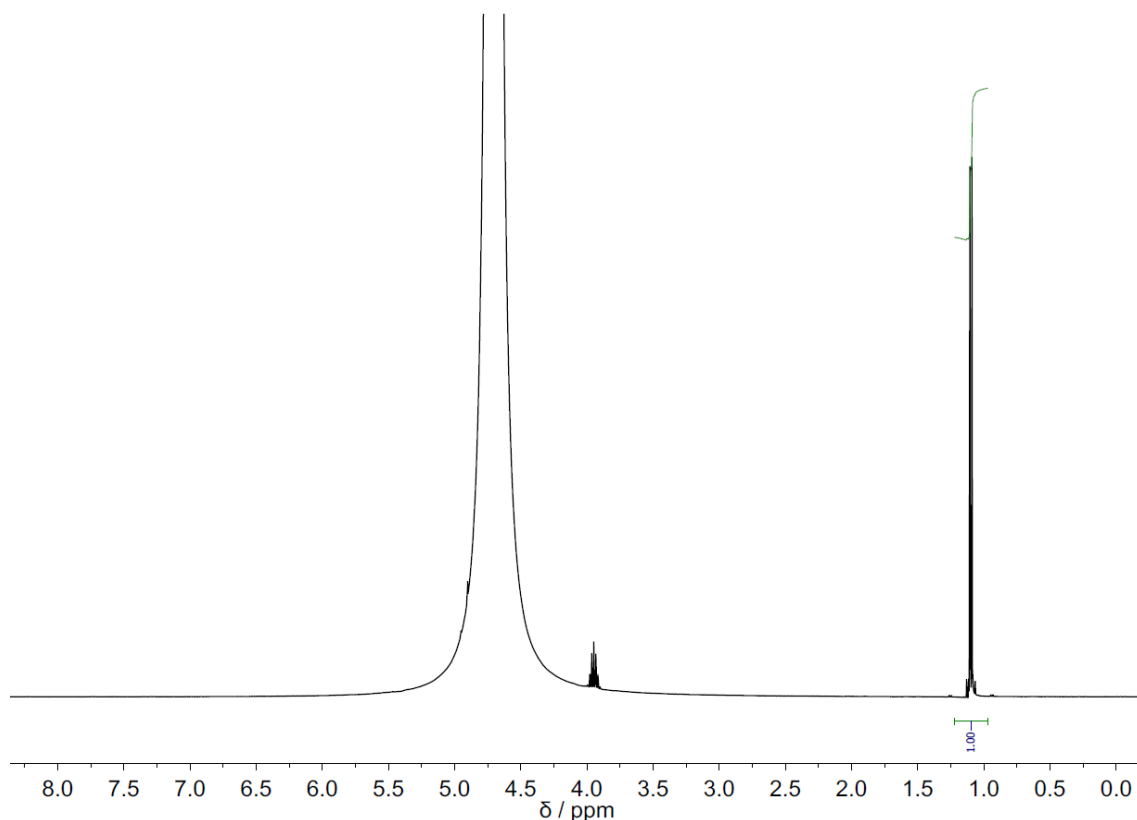


Figure A57 ¹H NMR (400 MHz) spectrum of a solution containing mineral water (90%), D₂O (10%) and isopropanol (50 mM, 3.85 μL). The peak at 4.75 ppm corresponds to the solvent.

8.5 Crystallographic data

Single crystals of dye **3** were obtained by liquid-liquid diffusion in a test tube (upper layer: hexane, lower layer: methanol). The data collection of compound dye **3** was measured at room temperature using Cu K_{α} radiation on an Agilent Technologies SuperNova dual system in combination with an Atlas CCD detector. Data reduction was carried out with CrysAlis PRO. The solution and refinement were performed by SHELX.⁴²⁸ The crystal structure was refined using full-matrix least-squares based on F^2 with all non hydrogen atoms anisotropically defined. Hydrogen atoms were placed in calculated positions by means of the “riding” model. In the final stages of the refinement, some restraints (SHELX cards: SIMU and SADI) were applied to disordered solvent (CH₃OH) and to the geometry of cations

(NH₄⁺). The crystallographic data have been deposited at the Cambridge Crystallographic Data Center (CCDC 991057).

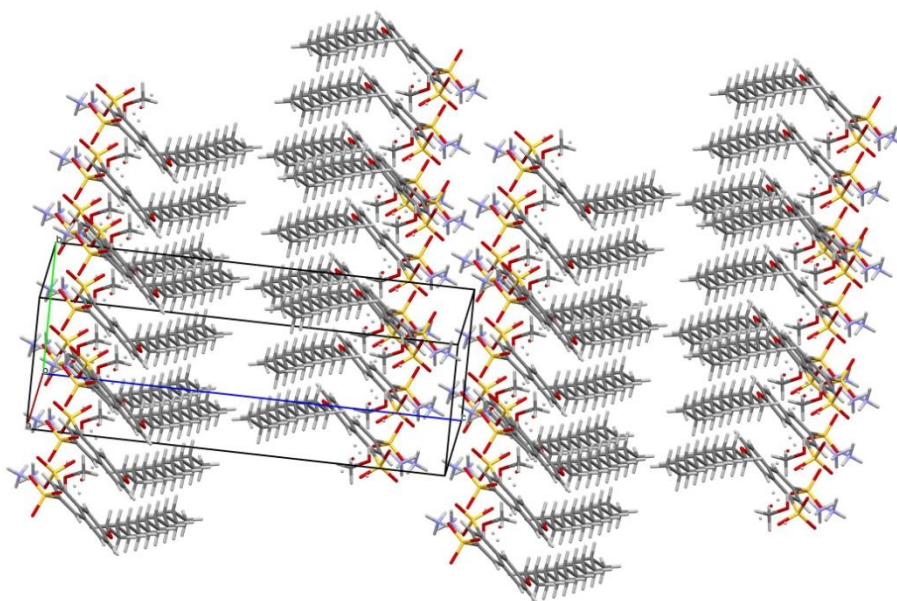


Figure A58 Packing of dye 3 in the crystal.

Table A1. Crystal data and structure refinement for dye 3.

Identification code	Dye 3	
Empirical formula	C ₂₇ H ₅₀ N ₂ O ₈ S ₂	
Formula weight	594.81	
Temperature	293(2) K	
Wavelength	1.54178 Å	
Crystal system	Triclinic	
Space group	<i>P</i> -1	
Unit cell dimensions	<i>a</i> = 6.53547(18) Å	α = 83.956(3)°.
	<i>b</i> = 9.4651(4) Å	β = 84.790(3)°.
	<i>c</i> = 26.1930(10) Å	γ = 89.716(3)°.
Volume	1604.59(10) Å ³ <i>Z</i>	2
Density (calculated)	1.231 Mg/m ³	

Absorption coefficient	1.892 mm ⁻¹ F(000) 644
Crystal size	0.49 x 0.10 x 0.06 mm ³
Theta range for data collection	3.41 to 73.28°.
Index ranges	-4 ≤ h ≤ 7, -11 ≤ k ≤ 11, -30 ≤ l ≤ 32
Reflections collected	10534
Independent reflections	6205 [<i>R</i> (int) = 0.0164]
Completeness to theta = 67.00°	99.6 %
Absorption correction	Analytical
Max. and min. transmission	0.909 and 0.568
Refinement method	Full-matrix least-squares on <i>F</i> ²
Data / restraints / parameters	6205 / 79 / 396
Goodness-of-fit on <i>F</i> ²	1.037
Final <i>R</i> indices [<i>I</i> > 2σ(<i>I</i>)]	<i>R</i> ₁ = 0.0335, <i>wR</i> ₂ = 0.0935
<i>R</i> indices (all data)	<i>R</i> ₁ = 0.0375, <i>wR</i> ₂ = 0.0980
Extinction coefficient	0.0012(2)
Largest diff. peak and hole	0.408 and -0.349 e.Å ⁻³

References

1. B. Wang and E. V. Anslyn, *Chemosensors, Principles, Strategies and Applications* Wiley, 2011.
2. H. G. Loehr and F. Voegtler, *Acc. Chem. Res.*, **1985**, *18*, 65-72.
3. E. V. Anslyn, *J. Org. Chem.*, **2007**, *72*, 687-699.
4. A. P. Demchenko, *Introduction to Fluorescence Sensing*, Springer, 2009.
5. L. Fabbrizzi and A. Poggi, *Chem. Soc. Rev.*, **1995**, *24*, 197-202.
6. A. P. de Silva and D. C. Magri, *CHIMIA International Journal for Chemistry*, **2005**, *59*, 218-221.
7. J. F. Callan, A. P. de Silva and D. C. Magri, *Tetrahedron*, **2005**, *61*, 8551-8588.
8. M. Li, B. Wu, C. Jia, X. Huang, Q. Zhao, S. Shao and X.-J. Yang, *Chem. Eur. J.*, **2011**, *17*, 2272-2280.
9. P. D. Beer and J. Cadman, *Coord. Chem. Rev.*, **2000**, *205*, 131-155.
10. H. Lu, W. Xu, D. Zhang, C. Chen and D. Zhu, *Org. Lett.*, **2005**, *7*, 4629-4632.
11. H. Sharma, N. Singh and D. O. Jang, *RSC Adv.*, **2015**, *5*, 6962-6969.
12. H. OuYang, Y. Gao and Y. Yuan, *Tetrahedron Lett.*, **2013**, *54*, 2964-2966.
13. H. N. Kim, M. H. Lee, H. J. Kim, J. S. Kim and J. Yoon, *Chem. Soc. Rev.*, **2008**, *37*, 1465-1472.
14. H. N. Kim, W. X. Ren, J. S. Kim and J. Yoon, *Chem. Soc. Rev.*, **2012**, *41*, 3210-3244.
15. J. F. Zhang, Y. Zhou, J. Yoon and J. S. Kim, *Chem. Soc. Rev.*, **2011**, *40*, 3416-3429.
16. E. S. Cho, T. Yokoyama, E. Ertem and F. Stellacci, *Israel Journal of Chemistry*, **2014**, *54*, 708-711.
17. S. K. Kim, D. H. Lee, J.-I. Hong and J. Yoon, *Acc. Chem. Res.*, **2009**, *42*, 23-31.
18. C. Zhang, K. Ji, X. Wang, H. Wu and C. Liu, *Chem. Commun.*, **2015**, *51*, 8173-8176.
19. R. Martínez-Máñez and F. Sancenón, *Chem. Rev.*, **2003**, *103*, 4419-4476.
20. Y. Zhou, J. F. Zhang and J. Yoon, *Chem. Rev.*, **2014**, *114*, 5511-5571.
21. R. M. Duke, E. B. Veale, F. M. Pfeffer, P. E. Kruger and T. Gunnlaugsson, *Chem. Soc. Rev.*, **2010**, *39*, 3936-3953.
22. C. Suksai and T. Tuntulani, *Chem. Soc. Rev.*, **2003**, *32*, 192-202.
23. F. Wang, L. Wang, X. Chen and J. Yoon, *Chem. Soc. Rev.*, **2014**, *43*, 4312-4324.
24. L. Gai, J. Mack, H. Lu, T. Nyokong, Z. Li, N. Kobayashi and Z. Shen, *Coord. Chem. Rev.*, **2015**, *285*, 24-51.
25. L. E. Santos-Figueroa, M. E. Moragues, E. Climent, A. Agostini, R. Martinez-Manez and F. Sancenon, *Chem. Soc. Rev.*, **2013**, *42*, 3489-3613.

26. A. Dalla Cort, P. De Bernardin, G. Forte and F. Yafteh Mihan, *Chem. Soc. Rev.*, **2010**, 39, 3863-3874.
27. X. Chen, Y. Zhou, X. Peng and J. Yoon, *Chem. Soc. Rev.*, **2010**, 39, 2120-2135.
28. H. S. Jung, X. Chen, J. S. Kim and J. Yoon, *Chem. Soc. Rev.*, **2013**, 42, 6019-6031.
29. Y. Zhou, Z. Xu and J. Yoon, *Chem. Soc. Rev.*, **2011**, 40, 2222-2235.
30. Y. Zhou and J. Yoon, *Chem. Soc. Rev.*, **2012**, 41, 52-67.
31. X. Zhou, S. Lee, Z. Xu and J. Yoon, *Chem. Rev.*, **2015**, 10.1021/cr500567r.
32. S. O. Obare, C. De, W. Guo, T. L. Haywood, T. A. Samuels, C. P. Adams, N. O. Masika, D. H. Murray, G. A. Anderson, K. Campbell and K. Fletcher, *Sensors*, **2010**, 10, 7018-7043.
33. B. Valeur and I. Leray, *Coord. Chem. Rev.*, **2000**, 205, 3-40.
34. N. Kumar, V. Bhalla and M. Kumar, *Coord. Chem. Rev.*, **2013**, 257, 2335-2347.
35. Z. Xu, J. Yoon and D. R. Spring, *Chem. Soc. Rev.*, **2010**, 39, 1996-2006.
36. K. Rurack and U. Resch-Genger, *Chem. Soc. Rev.*, **2002**, 31, 116-127.
37. S. Lee, K. K. Y. Yuen, K. A. Jolliffe and J. Yoon, *Chem. Soc. Rev.*, **2015**, 44, 1749-1762.
38. H. N. Kim, Z. Guo, W. Zhu, J. Yoon and H. Tian, *Chem. Soc. Rev.*, **2011**, 40, 79-93.
39. Z. Guo, S. Park, J. Yoon and I. Shin, *Chem. Soc. Rev.*, **2014**, 43, 16-29.
40. R. A. Bissell, A. P. de Silva, H. Q. N. Gunaratne, P. L. M. Lynch, G. E. M. Maguire and K. R. A. S. Sandanayake, *Chem. Soc. Rev.*, **1992**, 21, 187-195.
41. J. S. Kim and D. T. Quang, *Chem. Rev.*, **2007**, 107, 3780-3799.
42. A. P. de Silva, H. Q. N. Gunaratne, T. Gunnlaugsson, A. J. M. Huxley, C. P. McCoy, J. T. Rademacher and T. E. Rice, *Chem. Rev.*, **1997**, 97, 1515-1566.
43. S. T. Manjare, Y. Kim and D. G. Churchill, *Acc. Chem. Res.*, **2014**, 47, 2985-2998.
44. Z. Lou, P. Li and K. Han, *Acc. Chem. Res.*, **2015**, 10.1021/acs.accounts.5b00009.
45. A. W. Czarnik, *Acc. Chem. Res.*, **1994**, 27, 302-308.
46. A. R. Longstreet, M. Jo, R. R. Chandler, K. Hanson, N. Zhan, J. J. Hrudka, H. Mattoussi, M. Shatruk and D. T. McQuade, *J. Am. Chem. Soc.*, **2014**, 136, 15493-15496.
47. L.-Y. Niu, Y.-S. Guan, Y.-Z. Chen, L.-Z. Wu, C.-H. Tung and Q.-Z. Yang, *J. Am. Chem. Soc.*, **2012**, 134, 18928-18931.
48. T. W. Bell and N. M. Hext, *Chem. Soc. Rev.*, **2004**, 33, 589-598.
49. X. Cheng, Q. Li, J. Qin and Z. Li, *ACS Appl. Mater. Interfaces*, **2010**, 2, 1066-1072.
50. L. Fabbrizzi, M. Licchelli, P. Pallavicini, A. Perotti and D. Sacchi, *Angew. Chem. Int. Ed.*, **1994**, 33, 1975-1977.
51. X. Xu, C. O. Trindle, G. Zhang and L. Pu, *Chem. Commun.*, **2015**, 51, 8469-8472.
52. H. Y. Au-Yeung, J. Chan, T. Chantarojsiri and C. J. Chang, *J. Am. Chem. Soc.*, **2013**, 135, 15165-15173.
53. H.-H. Wang, L. Xue, Y.-Y. Qian and H. Jiang, *Org. Lett.*, **2010**, 12, 292-295.
54. Z. Xu, X. Chen, H. N. Kim and J. Yoon, *Chem. Soc. Rev.*, **2010**, 39, 127-137.
55. Y. Salinas, R. Martinez-Manez, M. D. Marcos, F. Sancenon, A. M. Costero, M. Parra and S. Gil, *Chem. Soc. Rev.*, **2012**, 41, 1261-1296.
56. A. P. de Silva and S. A. de Silva, *J. Chem. Soc., Chem. Commun.*, **1986**, 10.1039/C39860001709, 1709-1710.

57. X. Gao, X. Li, L. Li, J. Zhou and H. Ma, *Chem. Commun.*, **2015**, 10.1039/C5CC02788H.
58. Y. Chen, C. Zhu, Z. Yang, J. Chen, Y. He, Y. Jiao, W. He, L. Qiu, J. Cen and Z. Guo, *Angew. Chem. Int. Ed.*, **2013**, *52*, 1688-1691.
59. M. A. Cardona and D. C. Magri, *Tetrahedron Lett.*, **2014**, *55*, 4559-4563.
60. A. A. Frick, F. Busetti, A. Cross and S. W. Lewis, *Chem. Commun.*, **2014**, *50*, 3341-3343.
61. K. Y. Kim, S. H. Jung, J.-H. Lee, S. S. Lee and J. H. Jung, *Chem. Commun.*, **2014**, *50*, 15243-15246.
62. D. C. Magri, J. Callan, A. P. de Silva, D. Fox, N. McClenaghan and K. R. A. S. Sandanayake, *J Fluoresc.*, **2005**, *15*, 769-775.
63. A. P. de Silva, H. Q. N. Gunaratne and K. R. A. S. Sandanayake, *Tetrahedron Lett.*, **1990**, *31*, 5193-5196.
64. Y. Wu, X. Peng, B. Guo, J. Fan, Z. Zhang, J. Wang, A. Cui and Y. Gao, *Org. Biomol. Chem.*, **2005**, *3*, 1387-1392.
65. B. Turfan and E. U. Akkaya, *Org. Lett.*, **2002**, *4*, 2857-2859.
66. J. Guan, P. Zhang, T.-b. Wei, Q. Lin, H. Yao and Y.-m. Zhang, *RSC Adv.*, **2014**, *4*, 35797-35802.
67. B. Wardle, *Principles and Applications of Photochemistry*, Wiley, 2009.
68. E. Deniz, G. C. Isbasar, Ö. A. Bozdemir, L. T. Yildirim, A. Siemiarczuk and E. U. Akkaya, *Org. Lett.*, **2008**, *10*, 3401-3403.
69. N. Jiang, J. Fan, F. Xu, X. Peng, H. Mu, J. Wang and X. Xiong, *Angew. Chem. Int. Ed.*, **2015**, *54*, 2510-2514.
70. J. Kim, D. T. McQuade, S. K. McHugh and T. M. Swager, *Angew. Chem.*, **2000**, *112*, 4026-4030.
71. D. T. McQuade, A. E. Pullen and T. M. Swager, *Chem. Rev.*, **2000**, *100*, 2537-2574.
72. T. L. Nelson, C. O'Sullivan, N. T. Greene, M. S. Maynor and J. J. Lavigne, *J. Am. Chem. Soc.*, **2006**, *128*, 5640-5641.
73. Z. Yao, H. Bai, C. Li and G. Shi, *Chem. Commun.*, **2010**, *46*, 5094-5096.
74. L. You, D. Zha and E. V. Anslyn, *Chem. Rev.*, **2015**, 10.1021/cr5005524.
75. M. S. Maynor, T. L. Nelson, C. O'Sullivan and J. J. Lavigne, *Org. Lett.*, **2007**, *9*, 3217-3220.
76. P. K. Jain, X. Huang, I. H. El-Sayed and M. A. El-Sayed, *Acc. Chem. Res.*, **2008**, *41*, 1578-1586.
77. E. Hutter and J. H. Fendler, *Adv. Mater.*, **2004**, *16*, 1685-1706.
78. C. J. Murphy, A. M. Gole, S. E. Hunyadi, J. W. Stone, P. N. Sisco, A. Alkilany, B. E. Kinard and P. Hankins, *Chem. Commun.*, **2008**, 10.1039/B711069C, 544-557.
79. S. K. Ghosh and T. Pal, *Chem. Rev.*, **2007**, *107*, 4797-4862.
80. J. Wang, L. Wang, X. Liu, Z. Liang, S. Song, W. Li, G. Li and C. Fan, *Adv. Mater.*, **2007**, *19*, 3943-3946.
81. L. Polavarapu, J. Perez-Juste, Q.-H. Xu and L. M. Liz-Marzan, *J. Mater. Chem. C*, **2014**, *2*, 7460-7476.
82. Y. W. Lingxin Chen, Xiuli Fu, Ling Chen, *Novel Optical Nanoprobes*, Springer, 2014.

83. J. W. Hong, W. L. Hemme, G. E. Keller, M. T. Rinke and G. C. Bazan, *Adv. Mater.*, **2006**, *18*, 878-882.
84. X. Zhao and K. S. Schanze, *Chem. Commun.*, **2010**, *46*, 6075-6077.
85. A. Satrijo and T. M. Swager, *J. Am. Chem. Soc.*, **2007**, *129*, 16020-16028.
86. H. Sun, F. Feng, M. Yu and S. Wang, *Macromol. Rapid Commun.*, **2007**, *28*, 1905-1911.
87. Y. Tang, F. He, M. Yu, F. Feng, L. An, H. Sun, S. Wang, Y. Li and D. Zhu, *Macromol. Rapid Commun.*, **2006**, *27*, 389-392.
88. C. Y.-S. Chung, S. P.-Y. Li, M.-W. Louie, K. K.-W. Lo and V. W.-W. Yam, *Chem. Sci.*, **2013**, *4*, 2453-2462.
89. M. C.-L. Yeung and V. W.-W. Yam, *Chem. Sci.*, **2013**, *4*, 2928-2935.
90. P. K. Sukul, D. C. Santra, P. K. Singh, S. K. Maji and S. Malik, *New J. Chem.*, **2015**, 10.1039/C5NJ00608B.
91. D. Zhai, B. K. Agrawalla, P. S. F. Eng, S.-C. Lee, W. Xu and Y.-T. Chang, *Chem. Commun.*, **2013**, *49*, 6170-6172.
92. X. Li, X. Guo, L. Cao, Z. Xun, S. Wang, S. Li, Y. Li and G. Yang, *Angew. Chem. Int. Ed.*, **2014**, *53*, 7809-7813.
93. Y.-J. Huang, W.-J. Ouyang, X. Wu, Z. Li, J. S. Fossey, T. D. James and Y.-B. Jiang, *J. Am. Chem. Soc.*, **2013**, *135*, 1700-1703.
94. G. Zhang, F. Hu and D. Zhang, *Langmuir*, **2015**, *31*, 4593-4604.
95. Y. Wang, L. Zhang, R.-P. Liang, J.-M. Bai and J.-D. Qiu, *Anal. Chem.*, **2013**, *85*, 9148-9155.
96. A. Fermi, G. Bergamini, M. Roy, M. Gingras and P. Ceroni, *J. Am. Chem. Soc.*, **2014**, *136*, 6395-6400.
97. A. Centrone, E. Penzo, M. Sharma, J. W. Myerson, A. M. Jackson, N. Marzari and F. Stellacci, *Proc. Natl. Acad. Sci. U.S.A.*, **2008**, *105*, 9886-9891.
98. J.-S. Lee, M. S. Han and C. A. Mirkin, *Angew. Chem. Int. Ed.*, **2007**, *119*, 4171-4174.
99. K. Ai, Y. Liu and L. Lu, *J. Am. Chem. Soc.*, **2009**, *131*, 9496-9497.
100. N. Kanayama, T. Takarada and M. Maeda, *Chem. Commun.*, **2011**, *47*, 2077-2079.
101. S. Gui, Y. Huang, F. Hu, Y. Jin, G. Zhang, L. Yan, D. Zhang and R. Zhao, *Anal. Chem.*, **2015**, *87*, 1470-1474.
102. Y.-B. Ruan, A. Depauw and I. Leray, *Org. Biomol. Chem.*, **2014**, *12*, 4335-4341.
103. M. M. Watt, J. M. Engle, K. C. Fairley, T. E. Robitshek, M. M. Haley and D. W. Johnson, *Org. Biomol. Chem.*, **2015**, *13*, 4266-4270.
104. N. Jornet-Martínez, M. González-Béjar, Y. Moliner-Martínez, P. Campíns-Falcó and J. Pérez-Prieto, *Anal. Chem.*, **2014**, *86*, 1347-1351.
105. D. Cheng, Y. Li, J. Wang, Y. Sun, L. Jin, C. Li and Y. Lu, *Chem. Commun.*, **2015**, *51*, 8544-8546.
106. M. C.-L. Yeung and V. W.-W. Yam, *Chem. Eur. J.*, **2011**, *17*, 11987-11990.
107. V. Bhalla, S. Pramanik and M. Kumar, *Chem. Commun.*, **2013**, *49*, 895-897.
108. H. Wang, F. He, R. Yan, X. Wang, X. Zhu and L. Li, *ACS Appl. Mater. Interfaces*, **2013**, *5*, 8254-8259.
109. Y. Hong, J. W. Y. Lam and B. Z. Tang, *Chem. Soc. Rev.*, **2011**, *40*, 5361-5388.

110. Y.-T. Wu, M.-Y. Kuo, Y.-T. Chang, C.-C. Shin, T.-C. Wu, C.-C. Tai, T.-H. Cheng and W.-S. Liu, *Angew. Chem. Int. Ed.*, **2008**, *47*, 9891-9894.
111. G. Huang, G. Zhang and D. Zhang, *Chem. Commun.*, **2012**, *48*, 7504-7506.
112. N. Bian, Q. Chen, X.-L. Qiu, A.-D. Qi and B.-H. Han, *New J. Chem.*, **2011**, *35*, 1667-1671.
113. M. Wang, D. Zhang, G. Zhang, Y. Tang, S. Wang and D. Zhu, *Anal. Chem.*, **2008**, *80*, 6443-6448.
114. F. Hu, Y. Huang, G. Zhang, R. Zhao, H. Yang and D. Zhang, *Anal. Chem.*, **2014**, *86*, 7987-7995.
115. Y. Huang, F. Hu, R. Zhao, G. Zhang, H. Yang and D. Zhang, *Chem. Eur. J.*, **2014**, *20*, 158-164.
116. T. Sanji, K. Shiraishi and M. Tanaka, *ACS Appl. Mater. Interfaces*, **2009**, *1*, 270-273.
117. H. Shi, J. Liu, J. Geng, B. Z. Tang and B. Liu, *J. Am. Chem. Soc.*, **2012**, *134*, 9569-9572.
118. Y. Liu, Y. Yu, J. W. Y. Lam, Y. Hong, M. Faisal, W. Z. Yuan and B. Z. Tang, *Chem. Eur. J.*, **2010**, *16*, 8433-8438.
119. M. Zhao, M. Wang, H. Liu, D. Liu, G. Zhang, D. Zhang and D. Zhu, *Langmuir*, **2009**, *25*, 676-678.
120. Y. Liu, Y. Tang, N. N. Barashkov, I. S. Irgibaeva, J. W. Y. Lam, R. Hu, D. Birimzhanova, Y. Yu and B. Z. Tang, *J. Am. Chem. Soc.*, **2010**, *132*, 13951-13953.
121. T. L. Andrew and T. M. Swager, *J. Am. Chem. Soc.*, **2007**, *129*, 7254-7255.
122. S. J. Toal, K. A. Jones, D. Magde and W. C. Trogler, *J. Am. Chem. Soc.*, **2005**, *127*, 11661-11665.
123. V. Vij, V. Bhalla and M. Kumar, *ACS Appl. Mater. Interfaces*, **2013**, *5*, 5373-5380.
124. K. Mizusawa, Y. Ishida, Y. Takaoka, M. Miyagawa, S. Tsukiji and I. Hamachi, *J. Am. Chem. Soc.*, **2010**, *132*, 7291-7293.
125. K. Mizusawa, Y. Takaoka and I. Hamachi, *J. Am. Chem. Soc.*, **2012**, *134*, 13386-13395.
126. Y. Xu, B. Li, L. Xiao, W. Li, C. Zhang, S. Sun and Y. Pang, *Chem. Commun.*, **2013**, *49*, 7732-7734.
127. B. T. Nguyen and E. V. Anslyn, *Coord. Chem. Rev.*, **2006**, *250*, 3118-3127.
128. X. Lou, D. Ou, Q. Li and Z. Li, *Chem. Commun.*, **2012**, *48*, 8462-8477.
129. G. Ghale and W. M. Nau, *Acc. Chem. Res.*, **2014**, *47*, 2150-2159.
130. S. Wang, J. Sun and F. Gao, *Analyst*, **2015**, 10.1039/C5AN00320B.
131. T. Lou, L. Chen, C. Zhang, Q. Kang, H. You, D. Shen and L. Chen, *Anal. Methods*, **2012**, *4*, 488-491.
132. X. He, H. Liu, Y. Li, S. Wang, Y. Li, N. Wang, J. Xiao, X. Xu and D. Zhu, *Adv. Mater.*, **2005**, *17*, 2811-2815.
133. J. Chen, A. Zheng, A. Chen, Y. Gao, C. He, X. Kai, G. Wu and Y. Chen, *Anal. Chim. Acta*, **2007**, *599*, 134-142.
134. L. Shang, L. Jin and S. Dong, *Chem. Commun.*, **2009**, 10.1039/B902216C, 3077-3079.
135. I.-B. Kim, M. H. Han, R. L. Phillips, B. Samanta, V. M. Rotello, Z. J. Zhang and U. H. F. Bunz, *Chem. Eur. J.*, **2009**, *15*, 449-456.
136. D. J. Oh, K. M. Kim and K. H. Ahn, *Chem. Asian J.*, **2011**, *6*, 2034-2039.

137. L. Shang, C. Qin, T. Wang, M. Wang, L. Wang and S. Dong, *J. Phys. Chem. C*, **2007**, *111*, 13414-13417.
138. M. Maue and T. Schrader, *Angew. Chem. Int. Ed.*, **2005**, *44*, 2265-2270.
139. A. Metzger and E. V. Anslyn, *Angew. Chem. Int. Ed.*, **1998**, *37*, 649-652.
140. P. P. Neelakandan, M. Hariharan and D. Ramaiah, *J. Am. Chem. Soc.*, **2006**, *128*, 11334-11335.
141. A. Hennig, H. Bakirci and W. M. Nau, *Nat Meth*, **2007**, *4*, 629-632.
142. J. J. Lavigne and E. V. Anslyn, *Angew. Chem. Int. Ed.*, **1999**, *38*, 3666-3669.
143. M. Hu and G. Feng, *Chem. Commun.*, **2012**, *48*, 6951-6953.
144. A. Buryak and K. Severin, *Angew. Chem. Int. Ed.*, **2004**, *43*, 4771-4774.
145. M. H. Lim and S. J. Lippard, *Acc. Chem. Res.*, **2007**, *40*, 41-51.
146. M. Boiocchi, M. Bonizzoni, L. Fabbri, G. Piovan, and A. Taglietti, *Angew. Chem.*, **2004**, *116*, 3935-3940.
147. D. Knapton, M. Burnworth, S. J. Rowan and C. Weder, *Angew. Chem. Int. Ed.*, **2006**, *45*, 5825-5829.
148. L. Fabbri, M. Licchelli and A. Taglietti, *Dalton Trans.*, **2003**, 10.1039/B304172G, 3471-3479.
149. J. F. Folmer-Andersen, V. M. Lynch and E. V. Anslyn, *J. Am. Chem. Soc.*, **2005**, *127*, 7986-7987.
150. A. M. Piątek, Y. J. Bomble, S. L. Wiskur and E. V. Anslyn, *J. Am. Chem. Soc.*, **2004**, *126*, 6072-6077.
151. S. L. Tobey, B. D. Jones and E. V. Anslyn, *J. Am. Chem. Soc.*, **2003**, *125*, 4026-4027.
152. A. Norouzy, Z. Azizi and W. M. Nau, *Angew. Chem. Int. Ed.*, **2015**, *54*, 792-795.
153. J. T. K. Milton and J. Rosen, *Surfactants and Interfacial Phenomena*, John Wiley & Sons., 2012; Vol. 4th ed.
154. C. Wang, Z. Wang and X. Zhang, *Acc. Chem. Res.*, **2012**, *45*, 608-618.
155. Y. Nakahara, T. Kida, Y. Nakatsuji and M. Akashi, *Chem. Commun.*, **2004**, 10.1039/B311613A, 224-225.
156. T. Riis-Johannessen and K. Severin, *Chem. Eur. J.*, **2010**, *16*, 8291-8295.
157. M. Cametti, A. Dalla Cort and K. Bartik, *ChemPhysChem*, **2008**, *9*, 2168-2171.
158. K. Niikura and E. V. Anslyn, *J. Org. Chem.*, **2003**, *68*, 10156-10157.
159. O. Jurcek, M. Cametti, M. Pontini, E. Kolehmainen and K. Rissanen, *Org. Biomol. Chem.*, **2013**, *11*, 4585-4590.
160. F. Keymeulen, P. De Bernardin, I. Giannicchi, L. Galantini, K. Bartik and A. Dalla Cort, *Org. Biomol. Chem.*, **2015**, *13*, 2437-2443.
161. H. Tian, J. Qian, H. Bai, Q. Sun, L. Zhang and W. Zhang, *Anal. Chim. Acta*, **2013**, *768*, 136-142.
162. C. R. Nicoletti, L. G. Nandi and V. G. Machado, *Anal. Chem.*, **2015**, *87*, 362-366.
163. G. Li, D. Zhu, Q. Liu, L. Xue and H. Jiang, *Org. Lett.*, **2013**, *15*, 924-927.
164. N. Kumari, N. Dey, S. Jha and S. Bhattacharya, *ACS Appl. Mater. Interfaces*, **2013**, *5*, 2438-2445.
165. L. Ding, Y. Bai, Y. Cao, G. Ren, G. J. Blanchard and Y. Fang, *Langmuir*, **2014**, *30*, 7645-7653.

166. Y. Nakahara, T. Kida, Y. Nakatsuji and M. Akashi, *Org. Biomol. Chem.*, **2005**, *3*, 1787-1794.
167. P. Pallavicini, Y. A. Diaz-Fernandez and L. Pasotti, *Coord. Chem. Rev.*, **2009**, *253*, 2226-2240.
168. P. G. Bandyopadhyay, Amit K., *Sensor Letters*, **2011**, *9*, 1249-1264.
169. F. Mancin, P. Scrimin, P. Tecilla and U. Tonellato, *Coord. Chem. Rev.*, **2009**, *253*, 2150-2165.
170. P. Grandini, F. Mancin, P. Tecilla, P. Scrimin and U. Tonellato, *Angew. Chem. Int. Ed.*, **1999**, *38*, 3061-3064.
171. Y. Diaz Fernandez, A. Perez Gramatges, V. Amendola, F. Foti, C. Mangano, P. Pallavicini and S. Patroni, *Chem. Commun.*, **2004**, 10.1039/B404543B, 1650-1651.
172. Y. Díaz-Fernández, A. Pérez-Gramatges, S. Rodríguez-Calvo, C. Mangano and P. Pallavicini, *Chem. Phys. Lett.*, **2004**, *398*, 245-249.
173. P. Pallavicini, Y. A. Diaz-Fernandez, F. Foti, C. Mangano and S. Patroni, *Chem. Eur. J.*, **2007**, *13*, 178-187.
174. P. Pallavicini, L. Pasotti and S. Patroni, *Dalton Trans.*, **2007**, 10.1039/B710765J, 5670-5677.
175. M. Berton, F. Mancin, G. Stocchero, P. Tecilla and U. Tonellato, *Langmuir*, **2001**, *17*, 7521-7528.
176. C. Y.-S. Chung and V. W.-W. Yam, *Chem. Eur. J.*, **2014**, *20*, 13016-13027.
177. D. C. González, E. N. Savariar and S. Thayumanavan, *J. Am. Chem. Soc.*, **2009**, *131*, 7708-7716.
178. P. K. Hopke, *Anal. Chim. Acta*, **2003**, *500*, 365-377.
179. B. Lavine and J. Workman, *Anal. Chem.*, **2006**, *78*, 4137-4145.
180. P. C. Jurs, G. A. Bakken and H. E. McClelland, *Chem. Rev.*, **2000**, *100*, 2649-2678.
181. L. Rokach, Oded Maimon, *Data Mining and Knowledge Discovery Handbook*, Springer US, 2005.
182. C.-Y. Su, K. Menuz and J. R. Carlson, *Cell*, **2009**, *139*, 45-59.
183. A. K. Deisingh, D. C. Stone and M. Thompson, *Int. J. Food Sci. Technol.*, **2004**, *39*, 587-604.
184. U. B. Kaupp, *Nat Rev Neurosci*, **2010**, *11*, 188-200.
185. P.-M. Lledo, G. Gheusi and J.-D. Vincent, *Information Processing in the Mammalian Olfactory System*, 2005; Vol. 85, p 281-317.
186. I. Gaillard, S. Rouquier and D. Giorgi, *Cell. Mol. Life Sci.*, **2004**, *61*, 456-469.
187. M. Laska and G. M. Shepherd, *Neuroscience*, **2007**, *144*, 295-301.
188. M. Laska, C. G. Galizia, M. Giurfa and R. Menzel, *Chem Senses*, **1999**, *24*, 429-438.
189. G. V. Zyryanov, M. A. Palacios and P. Anzenbacher, *Angew. Chem. Int. Ed.*, **2007**, *46*, 7849-7852.
190. B. Garcia-Acosta, X. Albiach-Marti, E. Garcia, L. Gil, R. Martinez-Manez, K. Rurack, F. Sancenon and J. Soto, *Chem. Commun.*, **2004**, 10.1039/B314997H, 774-775.
191. L. A. Joyce, S. H. Shabbir and E. V. Anslyn, *Chem. Soc. Rev.*, **2010**, *39*, 3621-3632.
192. P. Anzenbacher, Jr., Y. Liu, M. A. Palacios, T. Minami, Z. Wang and R. Nishiyabu, *Chemistry*, **2013**, *19*, 8497-8506.

193. B. García-Acosta, R. Martínez-Máñez, F. Sancenón, J. Soto, K. Rurack, M. Spieles, E. García-Breijo and L. Gil, *Inorg. Chem.*, **2007**, *46*, 3123-3135.
194. M. A. Palacios, R. Nishiyabu, M. Marquez and P. Anzenbacher, *J. Am. Chem. Soc.*, **2007**, *129*, 7538-7544.
195. S. Yamaguchi, I. Yoshimura, T. Kohira, S.-i. Tamaru and I. Hamachi, *J. Am. Chem. Soc.*, **2005**, *127*, 11835-11841.
196. T. Ema, K. Okuda, S. Watanabe, T. Yamasaki, T. Minami, N. A. Esipenko and P. Anzenbacher, *Org. Lett.*, **2014**, *16*, 1302-1305.
197. T. Mayr, C. Igel, G. Liebsch, I. Klimant and O. S. Wolfbeis, *Anal. Chem.*, **2003**, *75*, 4389-4396.
198. D. Mikami, T. Ohki, K. Yamaji, S. Ishihara, D. Citterio, M. Hagiwara and K. Suzuki, *Anal. Chem.*, **2004**, *76*, 5726-5733.
199. Z. Wang, M. A. Palacios and P. Anzenbacher, *Anal. Chem.*, **2008**, *80*, 7451-7459.
200. W. Xu, C. Ren, C. L. Teoh, J. Peng, S. H. Gadre, H.-W. Rhee, C.-L. K. Lee and Y.-T. Chang, *Anal. Chem.*, **2014**, *86*, 8763-8769.
201. J. W. Lee, J.-S. Lee, M. Kang, A. I. Su and Y.-T. Chang, *Chem. Eur. J.*, **2006**, *12*, 5691-5696.
202. R. Zimmerman, L. Basabe-Desmonts, F. van der Baan, D. N. Reinhoudt and M. Crego-Calama, *J. Mater. Chem.*, **2005**, *15*, 2772-2777.
203. A. Goodey, J. J. Lavigne, S. M. Savoy, M. D. Rodriguez, T. Curey, A. Tsao, G. Simmons, J. Wright, S.-J. Yoo, Y. Sohn, E. V. Anslyn, J. B. Shear, D. P. Neikirk and J. T. McDevitt, *J. Am. Chem. Soc.*, **2001**, *123*, 2559-2570.
204. A. P. Goodey and J. T. McDevitt, *J. Am. Chem. Soc.*, **2003**, *125*, 2870-2871.
205. J. J. Lavigne, S. Savoy, M. B. Clevenger, J. E. Ritchie, B. McDoniel, S.-J. Yoo, E. V. Anslyn, J. T. McDevitt, J. B. Shear and D. Neikirk, *J. Am. Chem. Soc.*, **1998**, *120*, 6429-6430.
206. M. A. Palacios, Z. Wang, V. A. Montes, G. V. Zyryanov and P. Anzenbacher, *J. Am. Chem. Soc.*, **2008**, *130*, 10307-10314.
207. I. Yoshimura, Y. Miyahara, N. Kasagi, H. Yamane, A. Ojida and I. Hamachi, *J. Am. Chem. Soc.*, **2004**, *126*, 12204-12205.
208. M. S. Maynor, T. K. Deason, T. L. Nelson and J. J. Lavigne, *Supramol. Chem.*, **2009**, *21*, 310-315.
209. T. L. Nelson, I. Tran, T. G. Ingallinera, M. S. Maynor and J. J. Lavigne, *Analyst*, **2007**, *132*, 1024-1030.
210. N. T. Greene, S. L. Morgan and K. D. Shimizu, *Chem. Commun.*, **2004**, 10.1039/B401677G, 1172-1173.
211. N. T. Greene and K. D. Shimizu, *J. Am. Chem. Soc.*, **2005**, *127*, 5695-5700.
212. C. Zhang and K. S. Suslick, *J. Am. Chem. Soc.*, **2005**, *127*, 11548-11549.
213. J. Kumpf, J. Freudenberg, S. T. Schwaebel and U. H. F. Bunz, *Macromolecules*, **2014**, *47*, 2569-2573.
214. P. Montes-Navajas, L. A. Baumes, A. Corma and H. Garcia, *Tetrahedron Lett.*, **2009**, *50*, 2301-2304.
215. R. K. Pathak, J. Dessingou and C. P. Rao, *Anal. Chem.*, **2012**, *84*, 8294-8300.
216. A. Buryak and K. Severin, *J. Am. Chem. Soc.*, **2005**, *127*, 3700-3701.

217. J. F. Folmer-Andersen, M. Kitamura and E. V. Anslyn, *J. Am. Chem. Soc.*, **2006**, *128*, 5652-5653.
218. L. A. Baumes, M. Buaki, J. Jolly, A. Corma and H. Garcia, *Tetrahedron Lett.*, **2011**, *52*, 1418-1421.
219. S. L. Wiskur, P. N. Floriano, E. V. Anslyn and J. T. McDevitt, *Angew. Chem. Int. Ed.*, **2003**, *42*, 2070-2072.
220. J. Viljanen, J. Larsson, A. Larsson and K. S. Broo, *Bioconjugate Chem.*, **2007**, *18*, 1935-1945.
221. M. Kitamura, S. H. Shabbir and E. V. Anslyn, *J. Org. Chem.*, **2009**, *74*, 4479-4489.
222. S. L. Wiskur and E. V. Anslyn, *J. Am. Chem. Soc.*, **2001**, *123*, 10109-10110.
223. S. C. McCleskey, P. N. Floriano, S. L. Wiskur, E. V. Anslyn and J. T. McDevitt, *Tetrahedron*, **2003**, *59*, 10089-10092.
224. K. L. Diehl and E. V. Anslyn, *Chem. Soc. Rev.*, **2013**, *42*, 8596-8611.
225. Y. Liu, T. Minami, R. Nishiyabu, Z. Wang and P. Anzenbacher, *J. Am. Chem. Soc.*, **2013**, *135*, 7705-7712.
226. T. Minami, N. A. Esipenko, A. Akdeniz, B. Zhang, L. Isaacs and P. Anzenbacher, *J. Am. Chem. Soc.*, **2013**, *135*, 15238-15243.
227. A. D. Hughes, I. C. Glenn, A. D. Patrick, A. Ellington and E. V. Anslyn, *Chem. Eur. J.*, **2008**, *14*, 1822-1827.
228. M. E. Germain and M. J. Knapp, *J. Am. Chem. Soc.*, **2008**, *130*, 5422-5423.
229. A. Ponnu, N. Y. Edwards and E. V. Anslyn, *New J. Chem.*, **2008**, *32*, 848-855.
230. A. Schiller, B. Vilozny, R. A. Wessling and B. Singaram, *Anal. Chim. Acta*, **2008**, *627*, 203-211.
231. C. J. Musto, S. H. Lim and K. S. Suslick, *Anal. Chem.*, **2009**, *81*, 6526-6533.
232. J. W. Lee, J.-S. Lee and Y.-T. Chang, *Angew. Chem. Int. Ed.*, **2006**, *45*, 6485-6487.
233. A. Schiller, R. A. Wessling and B. Singaram, *Angew. Chem. Int. Ed.*, **2007**, *46*, 6457-6459.
234. F. Zaubitzer, A. Buryak and K. Severin, *Chem. Eur. J.*, **2006**, *12*, 3928-3934.
235. N. Y. Edwards, T. W. Sager, J. T. McDevitt and E. V. Anslyn, *J. Am. Chem. Soc.*, **2007**, *129*, 13575-13583.
236. Y. Koshi, E. Nakata, H. Yamane and I. Hamachi, *J. Am. Chem. Soc.*, **2006**, *128*, 10413-10422.
237. S. H. Lim, C. J. Musto, E. Park, W. Zhong and K. S. Suslick, *Org. Lett.*, **2008**, *10*, 4405-4408.
238. X. Bi, D. Li and Z. Liu, *Anal. Chem.*, **2015**, *87*, 4442-4447.
239. Y. Liu and M. Bonizzoni, *J. Am. Chem. Soc.*, **2014**, *136*, 14223-14229.
240. A. Buryak and K. Severin, *Angew. Chem. Int. Ed.*, **2005**, *44*, 7935-7938.
241. B. E. Collins and E. V. Anslyn, *Chem. Eur. J.*, **2007**, *13*, 4700-4708.
242. S. Rochat, J. Gao, X. Qian, F. Zaubitzer and K. Severin, *Chem. Eur. J.*, **2010**, *16*, 104-113.
243. A. Buryak and K. Severin, *J. Comb. Chem.*, **2006**, *8*, 540-543.
244. A. T. Wright, E. V. Anslyn and J. T. McDevitt, *J. Am. Chem. Soc.*, **2005**, *127*, 17405-17411.

245. T. Zhang, N. Y. Edwards, M. Bonizzoni and E. V. Anslyn, *J. Am. Chem. Soc.*, **2009**, *131*, 11976-11984.
246. F. Zaubitzer, T. Riis-Johannessen and K. Severin, *Org. Biomol. Chem.*, **2009**, *7*, 4598-4603.
247. L. Motiei, Z. Pode, A. Koganitsky and D. Margulies, *Angew. Chem. Int. Ed.*, **2014**, *53*, 9289-9293.
248. A. T. Wright, M. J. Griffin, Z. Zhong, S. C. McCleskey, E. V. Anslyn and J. T. McDevitt, *Angew. Chem. Int. Ed.*, **2005**, *44*, 6375-6378.
249. S. Jiwanpanich, B. S. Sandanaraj and S. Thayumanavan, *Chem. Commun.*, **2009**, 10.1039/B815263B, 806-808.
250. L. Baldini, A. J. Wilson, J. Hong and A. D. Hamilton, *J. Am. Chem. Soc.*, **2004**, *126*, 5656-5657.
251. O. R. Miranda, H.-T. Chen, C.-C. You, D. E. Mortenson, X.-C. Yang, U. H. F. Bunz and V. M. Rotello, *J. Am. Chem. Soc.*, **2010**, *132*, 5285-5289.
252. O. R. Miranda, C.-C. You, R. Phillips, I.-B. Kim, P. S. Ghosh, U. H. F. Bunz and V. M. Rotello, *J. Am. Chem. Soc.*, **2007**, *129*, 9856-9857.
253. B. S. Sandanaraj, R. Demont and S. Thayumanavan, *J. Am. Chem. Soc.*, **2007**, *129*, 3506-3507.
254. E. N. Savariar, S. Ghosh, D. C. González and S. Thayumanavan, *J. Am. Chem. Soc.*, **2008**, *130*, 5416-5417.
255. H. Zhou, L. Baldini, J. Hong, A. J. Wilson and A. D. Hamilton, *J. Am. Chem. Soc.*, **2006**, *128*, 2421-2425.
256. M. De, S. Rana, H. Akpınar, O. R. Miranda, R. R. Arvizo, U. H. F. Bunz and V. M. Rotello, *Nat Chem*, **2009**, *1*, 461-465.
257. C.-C. You, O. R. Miranda, B. Gider, P. S. Ghosh, I.-B. Kim, B. Erdogan, S. A. Krovi, U. H. F. Bunz and V. M. Rotello, *Nat Nano*, **2007**, *2*, 318-323.
258. M. De, S. Rana, H. Akpınar, O. R. Miranda, R. R. Arvizo, U. H. F. Bunz and V. M. Rotello, *Nat. Chem.*, **2009**, *1*, 461-465.
259. J. Rao and A. Khan, *Polym. Chem.*, **2015**, *6*, 686-690.
260. L. Feng, C. J. Musto, J. W. Kemling, S. H. Lim, W. Zhong and K. S. Suslick, *Anal. Chem.*, **2010**, *82*, 9433-9440.
261. L. Feng, C. J. Musto, J. W. Kemling, S. H. Lim and K. S. Suslick, *Chem. Commun.*, **2010**, *46*, 2037-2039.
262. L. Feng, C. J. Musto and K. S. Suslick, *J. Am. Chem. Soc.*, **2010**, *132*, 4046-4047.
263. S. H. Lim, L. Feng, J. W. Kemling, C. J. Musto and K. S. Suslick, *Nat Chem*, **2009**, *1*, 562-567.
264. S. H. Lim, J. W. Kemling, L. Feng and K. S. Suslick, *Analyst*, **2009**, *134*, 2453-2457.
265. S. H. Lim, L. Feng, J. W. Kemling, C. J. Musto and K. S. Suslick, *Nat. Chem.*, **2009**, *1*, 562-567.
266. Q. Ameer and S. B. Adeloju, *Sens. Actuators, B*, **2005**, *106*, 541-552.
267. C. Zhang, D. P. Bailey and K. S. Suslick, *J. Agric. Food Chem.*, **2006**, *54*, 4925-4931.
268. B. A. Suslick, L. Feng and K. S. Suslick, *Anal. Chem.*, **2010**, *82*, 2067-2073.
269. C. Zhang and K. S. Suslick, *J. Agric. Food Chem.*, **2007**, *55*, 237-242.
270. T. Takeuchi and S. Matile, *Chem. Commun.*, **2013**, *49*, 19-29.

271. J. R. Carey, K. S. Suslick, K. I. Hulkower, J. A. Imlay, K. R. C. Imlay, C. K. Ingison, J. B. Ponder, A. Sen and A. E. Wittrig, *J. Am. Chem. Soc.*, **2011**, *133*, 7571-7576.
272. Y. Zhang, J. R. Askim, W. Zhong, P. Orlean and K. S. Suslick, *Analyst*, **2014**, *139*, 1922-1928.
273. J. Gao, A. Granzhan, X. Qian and K. Severin, *Chem. Commun.*, **2010**, *46*, 5515-5517.
274. S. Rochat and K. Severin, *J. Comb. Chem.*, **2010**, *12*, 595-599.
275. S. O. J. N. H. Reek, *Dynamic Combinatorial Chemistry*, Wiley-VCH, 2010.
276. S. J. Rowan, S. J. Cantrill, G. R. Cousins, J. K. Sanders and J. F. Stoddart, *Angew. Chem. Int. Ed.*, **2002**, *41*, 898-952.
277. P. T. Corbett, J. Leclaire, L. Vial, K. R. West, J. L. Wietor, J. K. Sanders and S. Otto, *Chem Rev*, **2006**, *106*, 3652-3711.
278. R. A. R. Hunt and S. Otto, *Chem. Commun.*, **2011**, *47*, 847-858.
279. J.-M. Lehn, *Chem. Soc. Rev.*, **2007**, *36*, 151-160.
280. S. Ladame, *Org. Biomol. Chem.*, **2008**, *6*, 219-226.
281. A. Buryak, F. Zaubitzer, A. Pozdnoukhov and K. Severin, *J. Am. Chem. Soc.*, **2008**, *130*, 11260-11261.
282. B. Rout, L. Unger, G. Armony, M. A. Iron and D. Margulies, *Angew. Chem. Int. Ed.*, **2012**, *51*, 12477-12481.
283. Z. Yao, X. Feng, W. Hong, C. Li and G. Shi, *Chem. Commun.*, **2009**, 10.1039/B904975D, 4696-4698.
284. Y. Cao, L. Ding, W. Hu, J. Peng and Y. Fang, *J. Mater. Chem. A*, **2014**, *2*, 18488-18496.
285. K. K. Larson, M. He, J. F. Teichert, A. Naganawa and J. W. Bode, *Chem. Sci.*, **2012**, *3*, 1825-1828.
286. H. S. Hewage and E. V. Anslyn, *J. Am. Chem. Soc.*, **2009**, *131*, 13099-13106.
287. Z. Kostereli and K. Severin, *Chem. Commun.*, **2012**, *48*, 5841-5843.
288. S. S. Cohen, *A Guide to Polyamines*, Oxford University Press, USA, 1998.
289. E. Agostinelli, M. P. M. Marques, R. Calheiros, F. P. S. C. Gil, G. Tempera, N. Viceconte, V. Battaglia, S. Grancara and A. Toninello, *Amino Acids*, **2010**, *38*, 393-403.
290. K. Igarashi and K. Kashiwagi, *Int. J. Biochem. Cell Biol.*, **2010**, *42*, 39-51.
291. E. Larqué, M. Sabater-Molina and S. Zamora, *Nutrition*, **2007**, *23*, 87-95.
292. J. Jänne, L. Alhonen, M. Pietilä and T. A. Keinänen, *Eur. J. Biochem.*, **2004**, *271*, 877-894.
293. T. N. K Fujita, K Shinpo, K Maruta, R Teradaira and M Nakamura, *Clin. Chem.*, **1980**, *26*, 1577-1582.
294. D. H. Russell, *Clin. Chem.*, **1977**, *23*, 22-27.
295. C. Moinard, L. Cynober and J.-P. de Bandt, *Am. J. Clin. Nutr.*, **2005**, *24*, 184-197.
296. D. H. Russell, *Nat. New. Biol.*, **1971**, *233*, 144-145.
297. T.-C. Chiu, Y.-W. Lin, Y.-F. Huang and H.-T. Chang, *Electrophoresis*, **2006**, *27*, 4792-4807.
298. Y. Ma, G. Liu, M. Du and I. Stayton, *Electrophoresis*, **2004**, *25*, 1473-1484.
299. D. Teti, M. Visalli and H. McNair, *J. Chromatogr. B*, **2002**, *781*, 107-149.
300. M. Y. Khuhawar and G. A. Qureshi, *J. Chromatogr. B*, **2001**, *764*, 385-407.

301. B. Lee, R. Scopelliti and K. Severin, *Chem. Commun.*, **2011**, 47, 9639-9641.
302. T.-I. Kim, J. Park and Y. Kim, *Chem. Eur. J.*, **2011**, 17, 11978-11982.
303. M. Nakamura, T. Sanji and M. Tanaka, *Chem. Eur. J.*, **2011**, 17, 5344-5349.
304. M. Ikeda, T. Yoshii, T. Matsui, T. Tanida, H. Komatsu and I. Hamachi, *J. Am. Chem. Soc.*, **2011**, 133, 1670-1673.
305. N. L. Strutt, R. S. Forgan, J. M. Spruell, Y. Y. Botros and J. F. Stoddart, *J. Am. Chem. Soc.*, **2011**, 133, 5668-5671.
306. J. R. L. C. D. Geddes, *Glucose Sensing*, Springer US, 2006; Vol. 11.
307. M. Kriechbaum, O. S. Wolfbeis and E. Koller, *Chem. Phys. Lipids*, **1987**, 44, 19-29.
308. R. Sasaki and S. Murata, *Chem. Lett.*, **2007**, 36, 364-365.
309. R. Sasaki and S. Murata, *Langmuir*, **2008**, 24, 2387-2394.
310. P. Thordarson, *Chem. Soc. Rev.*, **2011**, 40, 1305-1323.
311. Z. Kostereli, R. Scopelliti and K. Severin, *Chem. Sci.*, **2014**, 5, 2456-2460.
312. Y. G. a. P. M. T. M. P. Mingeot-Leclercq, *Antimicrob. Agents Chemother.*, **1999**, 43, 727-737.
313. J. J. Lavigne and E. V. Anslyn, *Angew. Chem. Int. Ed.*, **2001**, 40, 3118-3130.
314. K. J. Albert, N. S. Lewis, C. L. Schauer, G. A. Sotzing, S. E. Stitzel, T. P. Vaid and D. R. Walt, *Chem. Rev.*, **2000**, 100, 2595-2626.
315. J. P. Anzenbacher, P. Lubal, P. Bucek, M. A. Palacios and M. E. Kozelkova, *Chem. Soc. Rev.*, **2010**, 39, 3954-3979.
316. A. T. Wright and E. V. Anslyn, *Chem. Soc. Rev.*, **2006**, 35, 14-28.
317. A. P. Umali and E. V. Anslyn, *Curr. Opin. Chem. Biol.*, **2010**, 14, 685-692.
318. M. M. Luca Prodi, Nelsi Zaccheroni, *Luminescence Applied in Sensor Science*, Springer, 2011; Vol. 300.
319. B. Lee, S. Chen, C. Heinis, R. Scopelliti and K. Severin, *Org Lett*, **2013**, 15, 3456-3459.
320. F. B. L. Cougnon and J. K. M. Sanders, *Acc. Chem. Res.*, **2012**, 45, 2211-2221.
321. E. Moulin, G. Cormos and N. Giuseppone, *Chem. Soc. Rev.*, **2012**, 41, 1031-1049.
322. K. Severin, *Curr. Opin. Chem. Biol.*, **2010**, 14, 737-742.
323. J. Li, P. Nowak and S. Otto, *J. Am. Chem. Soc.*, **2013**, 135, 9222-9239.
324. M. Shah, K. Thangaraj, M.-L. Soong, L. T. Wolford, J. H. Boyer, I. R. Politzer and T. G. Pavlopoulos, *Heteroat. Chem.*, **1990**, 1, 389-399.
325. L. Chen, H.-Y. Zhang and Y. Liu, *J. Org. Chem.*, **2012**, 77, 9766-9773.
326. N. J. Gutierrez-Moreno, F. Medrano and A. K. Yatsimirsky, *Org. Biomol. Chem.*, **2012**, 10, 6960-6972.
327. A. Barnard and D. K. Smith, *Angew. Chem. Int. Ed.*, **2012**, 51, 6572-6581.
328. C. B. Minkenberg, F. Li, P. van Rijn, L. Florusse, J. Boekhoven, M. C. A. Stuart, G. J. M. Koper, R. Eelkema and J. H. van Esch, *Angew. Chem. Int. Ed.*, **2011**, 50, 3421-3424.
329. H.-M. Kuo, S.-Y. Li, H.-S. Sheu and C. K. Lai, *Tetrahedron*, **2012**, 68, 7331-7337.
330. Z. Kostereli and K. Severin, *Org. Biomol. Chem.*, **2015**, 13, 252-257.
331. J. Emsley, *Nature's Building Blocks: An A-Z Guide to the Elements*, Oxford University Press, 2001.
332. V. Kumar and K. Gill, *Arch. Toxicol.*, **2009**, 83, 965-978.

333. S. C. Bondy, *Neurotoxicology*, **2010**, *31*, 575-581.
334. J. R. Walton, *J. Alzheimer's Dis.*, **2013**, *35*, 7-43.
335. L. Tomljenovic, *J. Alzheimer's Dis.*, **2011**, *23*, 567.
336. *Guidelines for drinking-water quality*, World Health Organization, 1998; Vol. 2.
337. Y.-W. Liu, C.-H. Chen and A.-T. Wu, *Analyst*, **2012**, *137*, 5201-5203.
338. S. Sen, T. Mukherjee, B. Chattopadhyay, A. Moirangthem, A. Basu, J. Marek and P. Chattopadhyay, *Analyst*, **2012**, *137*, 3975-3981.
339. T.-y. Zhou, L.-p. Lin, M.-c. Rong, Y.-q. Jiang and X. Chen, *Anal. Chem.*, **2013**, *85*, 9839-9844.
340. Y. Chen, Y. Mi, Q. Xie, J. Xiang, H. Fan, X. Luo and S. Xia, *Anal. Methods*, **2013**, *5*, 4818-4823.
341. S. Das, M. Dutta and D. Das, *Anal. Methods*, **2013**, *5*, 6262-6285.
342. S. M. Supian, T. L. Ling, L. Y. Heng and K. F. Chong, *Anal. Methods*, **2013**, *5*, 2602-2609.
343. T.-T. Wei, J. Zhang, G.-J. Mao, X.-B. Zhang, Z.-J. Ran, W. Tan and R. Yu, *Anal. Methods*, **2013**, *5*, 3909-3914.
344. A. Barba-Bon, A. M. Costero, S. Gil, M. Parra, J. Soto, R. Martinez-Manez and F. Sancenon, *Chem. Commun.*, **2012**, *48*, 3000-3002.
345. T. Han, X. Feng, B. Tong, J. Shi, L. Chen, J. Zhi and Y. Dong, *Chem. Commun.*, **2012**, *48*, 416-418.
346. F. K.-W. Hau, X. He, W. H. Lam and V. W.-W. Yam, *Chem. Commun.*, **2011**, *47*, 8778-8780.
347. D. Maity and T. Govindaraju, *Chem. Commun.*, **2012**, *48*, 1039-1041.
348. T.-H. Ma, M. Dong, Y.-M. Dong, Y.-W. Wang and Y. Peng, *Chem. Eur. J.*, **2010**, *16*, 10313-10318.
349. W.-H. Ding, W. Cao, X.-J. Zheng, W.-J. Ding, J.-P. Qiao and L.-P. Jin, *Dalton Trans.*, **2014**, *43*, 6429-6435.
350. D. Maity and T. Govindaraju, *Eur. J. Inorg. Chem.*, **2011**, *2011*, 5479-5485.
351. S. Kim, J. Y. Noh, K. Y. Kim, J. H. Kim, H. K. Kang, S.-W. Nam, S. H. Kim, S. Park, C. Kim and J. Kim, *Inorg. Chem.*, **2012**, *51*, 3597-3602.
352. D. Maity and T. Govindaraju, *Inorg. Chem.*, **2010**, *49*, 7229-7231.
353. A. Dhara, A. Jana, N. Guchhait, P. Ghosh and S. K. Kar, *New J. Chem.*, **2014**, *38*, 1627-1634.
354. A. Sahana, A. Banerjee, S. Das, S. Lohar, D. Karak, B. Sarkar, S. Kanti Mukhopadhyay, A. K. Mukherjee and D. Das, *Org. Biomol. Chem.*, **2011**, *9*, 5523-5529.
355. S. H. Kim, H. S. Choi, J. Kim, S. J. Lee, D. T. Quang and J. S. Kim, *Org. Lett.*, **2010**, *12*, 560-563.
356. X. Sun, Y.-W. Wang and Y. Peng, *Org. Lett.*, **2012**, *14*, 3420-3423.
357. A. Barba-Bon, L. Calabuig, A. M. Costero, S. Gil, R. Martinez-Manez and F. Sancenon, *RSC Adv.*, **2014**, *4*, 8962-8965.
358. S. Kim, J. Y. Noh, S. J. Park, Y. J. Na, I. H. Hwang, J. Min, C. Kim and J. Kim, *RSC Adv.*, **2014**, *4*, 18094-18099.

359. L. Cao, C. Jia, Y. Huang, Q. Zhang, N. Wang, Y. Xue and D. Du, *Tetrahedron Lett.*, **2014**, *55*, 4062-4066.
360. H. M. Park, B. N. Oh, J. H. Kim, W. Qiong, I. H. Hwang, K.-D. Jung, C. Kim and J. Kim, *Tetrahedron Lett.*, **2011**, *52*, 5581-5584.
361. Y.-W. Wang, M.-X. Yu, Y.-H. Yu, Z.-P. Bai, Z. Shen, F.-Y. Li and X.-Z. You, *Tetrahedron Lett.*, **2009**, *50*, 6169-6172.
362. C.-Y. Li, Y. Zhou, Y.-F. Li, X.-F. Kong, C.-X. Zou and C. Weng, *Anal. Chim. Acta*, **2013**, *774*, 79-84.
363. D. Parker and J. Yu, *Chem. Commun.*, **2005**, 10.1039/B502553B, 3141-3143.
364. M. I. Burguete, F. Galindo, S. V. Luis and L. Vigar, *Dalton Trans.*, **2007**, 10.1039/B711139H, 4027-4033.
365. L. A. Cabell, M. D. Best, J. J. Lavigne, S. E. Schneider, D. M. Perreault, M.-K. Monahan and E. V. Anslyn, *J. Chem. Soc., Perkin Trans. 2*, **2001**, 10.1039/B008694K, 315-323.
366. K. Ghosh and A. Ranjan Sarkar, *Org. Biomol. Chem.*, **2011**, *9*, 6551-6558.
367. C. Schmuck and M. Schwegmann, *Org. Biomol. Chem.*, **2006**, *4*, 836-838.
368. L. Fabbrizzi, F. Foti and A. Taglietti, *Org. Lett.*, **2005**, *7*, 2603-2606.
369. K. Ghosh, T. Sen and R. Fröhlich, *Tetrahedron Lett.*, **2007**, *48*, 2935-2938.
370. N. Boens, V. Leen and W. Dehaen, *Chem. Soc. Rev.*, **2012**, *41*, 1130-1172.
371. M. C. A. Stuart, J. C. van de Pas and J. B. F. N. Engberts, *J. Org. Chem.*, **2005**, *18*, 929-934.
372. R. J. Sundberg and R. B. Martin, *Chem. Rev.*, **1974**, *74*, 471-517.
373. S. Chen, Y.-M. Fang, Q. Xiao, J. Li, S.-B. Li, H.-J. Chen, J.-J. Sun and H.-H. Yang, *Analyst*, **2012**, *137*, 2021-2023.
374. R. R. Eitenmiller and W. O. Landen, *Vitamin analysis for the health and food sciences*, 2 ed., CRC Press, 2008.
375. M. Damon, N. Z. Zhang, D. B. Haytowitz and S. L. Booth, *J. Food Compos. Anal.*, **2005**, *18*, 751-758.
376. G. Ferland and J. A. Sadowski, *J. Agric. Food Chem.*, **1992**, *40*, 1874-1877.
377. G. F. M. Ball, *Fat-Soluble Vitamin Assays in Food Analysis*, Elsevier, 1988.
378. X. Fu, J. W. Peterson, M. Hdeib, S. L. Booth, M. A. Grusak, A. H. Lichtenstein and G. G. Dolnikowski, *Anal. Chem.*, **2009**, *81*, 5421-5425.
379. Y. Suhara, M. Kamao, N. Tsugawa and T. Okano, *Anal. Chem.*, **2005**, *77*, 757-763.
380. T. J. Koivu, V. I. Piironen, S. K. Henttonen and P. H. Mattila, *J. Agric. Food Chem.*, **1997**, *45*, 4644-4649.
381. J. D. Manes, H. B. Fluckiger and D. L. Schneider, *J. Agric. Food Chem.*, **1972**, *20*, 1130-1132.
382. S. L. Booth and J. A. Sadowski, *Methods Enzymol*, **1997**, *282*, 446-456.
383. D. C. Woollard, H. E. Indyk, B. Y. Fong and K. K. Cook, *J AOAC Int*, **2002**, *85*, 682-691.
384. M. Shino, *Analyst*, **1988**, *113*, 393-397.
385. J. R. Poulsen and J. W. Birks, *Anal. Chem.*, **1989**, *61*, 2267-2276.
386. J. C. Vire, G. J. Patriarche, R. J. Nowak and H. B. Mark, *Anal. Chem.*, **1977**, *49*, 1343-1346.

387. Z. Sharrett, S. Gamsey, L. Hirayama, B. Vilozny, J. T. Suri, R. A. Wessling and B. Singaram, *Org. Biomol. Chem.*, **2009**, *7*, 1461-1470.
388. K. S. Z. Köstereli, *Org. Biomol. Chem.*, **2015**, *13*, 9231-9235.
389. B. K. B. Bennett Alan Weinberg, *The World of Caffeine: The Science and Culture of the World's Most Popular Drug*, Psychology Press, 2001.
390. K. Ito, S. Lim, G. Caramori, B. Cosio, K. F. Chung, I. M. Adcock and P. J. Barnes, *Proc. Natl. Acad. Sci. U.S.A.*, **2002**, *99*, 8921-8926.
391. P. J. B. a. R. A. Pauwels, *Eur. Respir. J.*, **1994**, *7*, 579-591.
392. E. S. Mitchell, M. Slettenaar, N. vd Meer, C. Transler, L. Jans, F. Quadt and M. Berry, *Physiol Behav*, **2011**, *104*, 816-822.
393. O. S. Usmani, M. G. Belvisi, H. J. Patel, N. Crispino, M. A. Birrell, M. Korbonits, D. Korbonits and P. J. Barnes, *FASEB J*, **2005**, *19*, 231-233.
394. C. R. Gordon, A. Gonen, Z. Nachum, I. Doweck, O. Spitzer and A. Shupak, *J Psychopharmacol*, **2001**, *15*, 167-172.
395. J. Carpenter, *Pharmacology from A to Z*, Manchester University Press, 1988.
396. S. Sahasranaman, D. Howard and S. Roy, *Eur J Clin Pharmacol*, **2008**, *64*, 753-767.
397. M. Else, C. E. Dearden, E. Matutes, J. Garcia-Talavera, A. Z. Rohatiner, S. A. Johnson, N. T. O'Connor, A. Haynes, N. Osuji, F. Forconi, F. Lauria and D. Catovsky, *Br J Haematol*, **2009**, *145*, 733-740.
398. R. T. Sarisky, T. H. Bacon, R. J. Boon, K. E. Duffy, K. M. Esser, J. Leary, L. A. Locke, T. T. Nguyen, M. R. Quail and R. Saltzman, *Arch Virol*, **2003**, *148*, 1757-1769.
399. R. T. Sarisky, T. Bacon, R. Boon, L. Locke, T. T. Nguyen, J. Leary, K. Esser and R. Saltzman, *Antimicrob. Agents Chemother.*, **2002**, *46*, 2848-2853.
400. P. Talik, J. Krzek and R. J. Ekiert, *Sep. Purif. Rev.*, **2011**, *41*, 1-61.
401. M. C. Schopohl, C. Siering, O. Kataeva and S. R. Waldvogel, *Angew. Chem. Int. Ed.*, **2003**, *42*, 2620-2623.
402. S. R. Waldvogel, R. Fröhlich and C. A. Schalley, *Angew. Chem. Int. Ed.*, **2000**, *39*, 2472-2475.
403. M. Bomkamp, C. Siering, K. Landrock, H. Stephan, R. Fröhlich and S. R. Waldvogel, *Chem. Eur. J.*, **2007**, *13*, 3724-3732.
404. R. Fiammengo, M. Crego-Calama, P. Timmerman and D. N. Reinhoudt, *Chem. Eur. J.*, **2003**, *9*, 784-792.
405. N. Hayashi, T. Ujihara and S. Jin, *Tetrahedron*, **2014**, *70*, 845-851.
406. P. Ballester, M. Angel Barceló, A. Costa, P. M. Deyà, J. Morey, M. Orell and C. A. Hunter, *Tetrahedron Lett.*, **2000**, *41*, 3849-3853.
407. A. K. Mahapatra, J. Roy, P. Sahoo, S. K. Mukhopadhyay, A. R. Mukhopadhyay and D. Mandal, *Bioorg. Med. Chem. Lett.*, **2012**, *22*, 5379-5383.
408. A. Mahapatra, P. Sahoo, S. Goswami, H.-K. Fun and C. Yeap, *J. Incl. Phenom. Macrocycl. Chem.*, **2010**, *67*, 99-108.
409. C. Siering, H. Kerschbaumer, M. Nieger and S. R. Waldvogel, *Org. Lett.*, **2006**, *8*, 1471-1474.
410. W. Xu, T.-H. Kim, D. Zhai, J. C. Er, L. Zhang, A. A. Kale, B. K. Agrawalla, Y.-K. Cho and Y.-T. Chang, *Sci. Rep.*, **2013**, *3*.

411. Y. L. Wei, L. H. Ding, C. Dong, W. P. Niu and S. M. Shuang, *Spectrochimica acta. Part A, Molecular and Biomolecular Spectroscopy*, **2003**, *59*, 2697-2703.
412. C. Siering, B. Beermann and S. R. Waldvogel, *Supramol. Chem.*, **2006**, *18*, 23-27.
413. N. Luisier, A. Ruggi, S. N. Steinmann, L. Favre, N. Gaeng, C. Corminboeuf and K. Severin, *Org. Biomol. Chem.*, **2012**, *10*, 7487-7490.
414. S. Rochat, S. N. Steinmann, C. Corminboeuf and K. Severin, *Chem. Commun.*, **2011**, *47*, 10584-10586.
415. I. M. Johnson, S. G. Kumar and R. Malathi, *J. Biomol. Struct. Dyn.*, **2003**, *20*, 687-692.
416. P. C. Anderson and S. Mecozzi, *J. Am. Chem. Soc.*, **2005**, *127*, 5290-5291.
417. I. M. Johnson, H. Prakash, J. Prathiba, R. Raghunathan and R. Malathi, *PLoS ONE*, **2012**, *7*, e50019.
418. S. Goswami, A. K. Mahapatra and R. Mukherjee, *J. Chem. Soc., Perkin Trans. 1*, **2001**, 10.1039/B009319J, 2717-2726.
419. A. K. Mahapatra, P. Sahoo, S. Goswami, S. Chantrapromma and H.-K. Fun, *Tetrahedron Lett.*, **2009**, *50*, 89-92.
420. T. Hirsch, H. Kettenberger, O. S. Wolfbeis and V. M. Mirsky, *Chem. Commun.*, **2003**, 10.1039/B210554C, 432-433.
421. R. B. Pernites, R. R. Ponnappati and R. C. Advincula, *Macromolecules*, **2010**, *43*, 9724-9735.
422. G. Vlatakis, L. I. Andersson, R. Muller and K. Mosbach, *Nature*, **1993**, *361*, 645-647.
423. H. Zayas, C. I. Holdsworth, M. C. Bowyer and A. McCluskey, *Org. Biomol. Chem.*, **2014**, *12*, 6994-7003.
424. S. Rouhani and F. Nahavandifard, *Sens. Actuators, B*, **2014**, *197*, 185-192.
425. J. F. Gonthier, S. N. Steinmann, L. Roch, A. Ruggi, N. Luisier, K. Severin and C. Corminboeuf, *Chem. Commun.*, **2012**, *48*, 9239-9241.
426. N. Luisier, A. Ruggi, S. N. Steinmann, L. Favre, N. Gaeng, C. Corminboeuf and K. Severin, *Org. Biomol. Chem.*, **2012**, *10*, 7487-7490.
427. S. Stewart, M. A. Ivy and E. V. Anslyn, *Chem. Soc. Rev.*, **2014**, *43*, 70-84.
428. W. Steurer and S. Deloudi, *Acta Crystallogr. Sect. A*, **2008**, *64*, 1-11.

Curriculum Vitae

Av. du 14 Avril 1E, CH 1020
Renens, Switzerland
25.09.1986 / Turkish
zkostereli@gmail.com

Education:

2005 - 2009 B.S. in Middle East Technical University, Ankara, Turkey, Chemistry

B.Eng. in Middle East Technical University, Chemical Engineering (Double M.)

2009 - 2011 M. Sc. in Bilkent University, Ankara, Turkey, Chemistry

Laboratory of Supramolecular Chemistry, Prof. Dr. Engin Umut Akkaya

2011 - 2015 PhD in Swiss Federal Institute of Technology (EPFL), Lausanne, Switzerland

Laboratory of Supramolecular Chemistry (LCS), Prof. Dr. Kay Severin

Awards:

Fellowship : Bilkent University, fellowship for M.Sc. (with full tuition fee waiver)

Fellowship : Marie Curie fellowship for PhD studies (ITN Network, EPFL, 2012-2015)

Special award : Special Promotion Award for Teaching Assistantship (EPFL, 2014)

Language skills :

Turkish, English, French (elementary)

Technical skills :

Fortran, Origin Pro, Adobe Illustrator, MS Office and Visio

NMR, UV-vis, IR, Fluorescence, Mass Spectroscopy,
GC, ITC, TEM, Cryo - TEM, DLS, ZetaSizer, HPLC

Research Interest:

Chemometrics, Characterization, Pattern-based Sensing

Analytical / Materials / Supramolecular Chemistry, Surfactants

Organic / Fluorescent Dyes Synthesis, Chemosensors

Research Experience :

2011-2015 :

Analytical/Organic Chemistry, Chemosensors, Micelle-based Chemosensors,
Pattern-based Sensing Systems (Sensor Arrays and DCL Sensors)
Fluorescent Dyes Synthesis

2009-2011 :

Design / Synthesis of Multi-ion Chemosensors as Molecular Logic Gates

Design / Synthesis of Fluorescent Anion, Cation Sensing Systems

Design / Synthesis of Supramolecular Structures for Light Harvesting and
Efficient Energy Transfer

Teaching Experience :

2009-2011	: General Chemistry 1 Laboratory TA	(2 semesters, Bilkent University)
	General Chemistry 2 Laboratory TA	(2 semesters, Bilkent University)
2012-2015	: Biochemistry and Biophysics Laboratory TA	(1 semester, EPFL)
	General Chemistry Laboratory TA	(1 semester, EPFL)
	Inorganic Chemistry Laboratory TA	(3 semesters, EPFL)

Work Experience :

August 2007 (Intern)	POLIKOR Paint, Polyester and Resin Inc., Turkey
January 2008 (Intern)	TAMEK Food Industry Co., Turkey
June – July 2008 (Intern)	SANDOZ Pharmaceutical Co., Turkey
September 2009 – June 2011	Research and Teaching Assistant at Bilkent University
September 2011 – January 2015	Research and Teaching Assistant at EPFL

References :

Kay Severin	:	Professor of Supramolecular Inorganic Chemistry at EPFL e-mail : kay.severin@epfl.ch tel : +41 21 693 93 02
Engin U. Akkaya	:	Professor of Supramolecular Chemistry at Bilkent University e-mail : eua@fen.bilkent.edu.tr tel : +90 312 290 3570

Memberships and Social Activities :

SCS (Swiss Chemical Society) Membership

Publications :

- 1 “Designing Excited States: Theory-Guided Access to Efficient Photosensitizers for Photodynamic Action” Yusuf Cakmak, Safacan Kolemen, Selin Duman, Yavuz Dede, Yusuf Dolen, Bilal Kilic, **Ziya Kostereli**, Leyla Tatar Yildirim, Lale Dogan, Dicle Guc and Engin U. Akkaya, *Angewandte Chemie - International Edition*, **2011**, 50, 11937–11941.
- 2 “From Virtual to Physical: Integration of Chemical Logic Gates” Ruslan Guliyev, Seyma Ozturk, **Ziya Kostereli** and Engin U. Akkaya, *Angewandte Chemie - International Edition*, **2011**, 50, 9826–9831.
- 3 “Fluorescence Sensing of Spermine with a Frustrated Amphiphile” **Ziya Kostereli** and Kay Severin, *Chem. Commun.*, **2012**, 48, 5841–5843.
- 4 “Divergent synthesis of tetrastyril BODIPY energy transfer cassettes” **Ziya Kostereli**, Tugba Ozdemir, Onur Buyukcakil and Engin Umut Akkaya, *Org. Lett.*, **2012**, 14, 3636–3639.
- 5 “Ion responsive near-IR BODIPY dyes: two isomers, two different signals” Tugba Özdemir, **Ziya Köstereli**, Ruslan Guliyev, Soydan Yalçın, Yavuz Dede and Engin Umu Akkaya, *RSC Adv.*, **2014**, 4, 14915–14918.
- 6 “Atropisomeric Dyes: Axial Chirality in Orthogonal BODIPY Oligomers” Safacan Kölemen, Yusuf Çakmak, **Ziya Köstereli** and Engin Umut Akkaya *Org. Lett.*, **2014**, 16, 660–663.
- 7 “Pattern-based sensing of aminoglycosides with fluorescent amphiphiles” **Ziya Köstereli**, Rosario Scopelliti and Kay Severin, *Chem. Sci.*, **2014**, 5, 2456–2460.
- 8 “Selective detection of Al³⁺ and citric acid with a fluorescent amphiphile” **Ziya Köstereli** and Kay Severin, *Org. Biomol. Chem.*, **2015**, 13, 252–257.
- 9 “Pattern-based sensing of purine derivatives” **Ziya Köstereli** and Kay Severin, *Org. Biomol. Chem.*, **2015**, 13, 9231–9235.
- 10 “Fluorescence sensing of vitamin K₁ using a simple micelle-based assay” **Ziya Köstereli** and Kay Severin, **in preparation**.